ESTIMATING AND FORECASTING DISEASE SCENARIOS FOR COVID-19 WITH
AN SIR MODEL

Andrew Atkeson
Karen Kopecky
Tao Zha

Estimating and Forecasting Disease Scenarios for COVID-19 with an SIR Model
Andrew Atkeson, Karen Kopecky, and Tao Zha
NBER Working Paper No. 27335
June 2020
JEL No. C01,C02,C11

ABSTRACT

This paper presents a procedure for estimating and forecasting disease scenarios for COVID-19 using a structural SIR model of the pandemic. Our procedure combines the flexibility of noteworthy reduced-form approaches for estimating the progression of the COVID-19 pandemic to date with the benefits of a simple SIR structural model for interpreting these estimates and constructing forecast and counterfactual scenarios. We present forecast scenarios for a devastating second wave of the pandemic as well as for a long and slow continuation of current levels of infections and daily deaths. In our counterfactual scenarios, we find that there is no clear answer to the question of whether earlier mitigation measures would have reduced the long run cumulative death toll from this disease. In some cases, we find that it would have, but in other cases, we find the opposite — earlier mitigation would have led to a higher long-run death toll.

Andrew Atkeson
Bunche Hall 9381
Department of Economics
UCLA
Box 951477
Los Angeles, CA 90095-1477
and NBER
andy@atkeson.net

Karen Kopecky
Research Department
Federal Reserve Bank of Atlanta
1000 Peachtree ST NE
Atlanta, GA 30309
karen.kopecky@atl.frb.org

Tao Zha
Department of Economics
Emory University
Rich Memorial Building
1602 Fishburne Drive
Atlanta, GA 30322-2240
and Federal Reserve Bank of Atlanta
and also NBER
tzha@emory.edu

1 Introduction

This paper presents a procedure for estimating and forecasting disease scenarios for COVID-19 using a simple structural SIR model of the pandemic. An SIR model is a Markov model of the spread of a pandemic in a population in which the total population is divided into categories of being susceptible to the disease (S), actively infected with the disease (I), recovered and no longer contagious (R), or dead (D). How a pandemic plays out over time is determined by the transition rates at which people move between these states.

Our procedure for estimating this SIR model and constructing forecasts combines the flexibility of noteworthy reduced-form approaches for estimating the progression of the COVID-19 pandemic with the benefits of a simple structural model for interpreting these estimates and constructing scenarios for the development of the pandemic going forward. We implement our method to estimate the model using data on deaths for large states and Census regions of the United States and for a number of additional countries. We then use the estimated model to conduct counterfactuals studying how the pandemic would have progressed under alternative scenarios for mitigating the transmission of the disease and to construct forecasts under various scenarios for the transmission of the disease going forward.

Our procedure for estimating the SIR model and using it for counterfactuals and forecasting has three steps.

In step 1, for each geographic region that we consider, we estimate an empirical specification for cumulative deaths due to COVID-19 observed between an initial date t_0 at which cumulative deaths reaches a threshold of 50 and the present. The specific empirical specification we consider models the data on daily deaths in the region as derived from a mixture of Weibull functions. This specification allows for a very flexible model of the observed data on cumulative deaths, daily deaths, and the change in daily deaths over time (corresponding to the first and second derivatives of cumulative deaths with respect to time).

1

Conceptually, the estimation conducted in this first step is similar to the widely cited empirical model for cumulative deaths developed by researchers at the Institute for Health Metrics and Evaluation (IHME) at the University of Washington.[1] See also Linton (2020)[2] for a similar reduced-form approach to modeling the evolution of cases and deaths over time. Where we differ from these reduced-form approaches to estimation and forecasting is in how we then use a structural SIR model to interpret this empirical model of observed deaths due to COVID and to develop counterfactual scenarios and scenarios for forecasting the progression of the disease in the next two steps.

In step 2, we use the best available information to choose parameters for the fatality rate (the fraction of active infections that end in death) and the recovery rate (the rate per unit time at which people who are actively infected stop being infectious) of COVID-19, or a range for these parameters to be considered. Given these fatality and recovery rates, we then use the equations of the SIR model to recover the time paths of the distribution of the population across states $S(t), I(t), R(t), D(t)$ and the time path of the effective reproduction number of the disease (the ratio of the rate at which actively infected people spread the infection to the recovery rate) between the initial date t_0 and the present for which the model fits exactly the empirical specification for deaths from the initial date t_0 to the present estimated in step 1. Note that our estimates in this step of the evolution of the transmission rate of the disease over time in different geographies do not use any additional ex-ante structural assumptions beyond those imposed in our empirical estimates in step 1 and by the basic assumptions of the SIR model.

In this way, in step 2, we use the SIR model to give a structural interpretation of the empirical specification for the data on deaths estimated in step 1 in terms of a full model of the progression of the pandemic. Not only do we uncover an estimate of the current distribution of the population across states S, I, R and D, but also we

---

[1]See the working paper discussion of the IMHE forecasting model here https://www.medrxiv.org/content/10.1101/2020.04.21.20074732v1

[2]See updated forecasts at http://covid.econ.cam.ac.uk/linton-uk-covid-cases-predicted-peak

can use the model to decompose the evolution over time of the effective reproduction number of the disease in each geographic region into a component due to changes in the transmission rate of the disease (due to changes in behavior or mitigation efforts) and a component due to changes in the population of agents that continue to be susceptible to the disease.

In step 3, we use our structural model to address questions about future scenarios for the evolution of the pandemic and to conduct counterfactual exercises regarding how the pandemic would have progressed in a region if the transmission rate of the disease in that region had followed a different path due to different timing and severity of disease mitigation efforts. We construct forecast scenarios for the evolution of the pandemic going forward from the present date by positing alternative paths for the evolution of the transmission rate of the disease going forward from the present date and solving the SIR model starting from the current distribution of the population across states S, I, R and D estimated in step 2. We construct counterfactual scenarios for the evolution of the pandemic by considering alternative paths for the transmission rate of the disease both historically (corresponding to alternative initial timing of mitigation efforts) and going forward and solving the SIR model starting from the initial distribution of the population across states at date t_0. In this regard, our forecast and counterfactual scenarios are based on a structural disease model as is done by some leading epidemiological models.[3] We see the transparency of our model estimation approach as one of its key advantages in helping the reader interpret our forecast and counterfactual results.

We apply this procedure to estimate our SIR model and to construct forecast and counterfactual scenarios for ten large U.S. states and nine U.S. Census Regions as well as a number of other countries.

We model the patterns of daily deaths with a mixture of Weibull functions. We

---

[3]See, for example https://www.medrxiv.org/content/10.1101/2020.03.21.20040303v2.full.pdf for a description of the forecasting project at Columbia's Mailman School of Public Health using a structural SEIR model that estimates the impact of mitigation measures on the normalized transmission rate.

use the Bayesian procedure to fit these functions to daily deaths for each state or Census region or country. The residual term in this nonlinear regression follows a Markov-switching process with multiple regimes to capture large spikes of deaths as random events in one regime and small death fluctuations in another regime. The number of Weibull functions needed to fit death data is determined by the marginal data density (the marginal likelihood).

The Bayesian procedure allows us to characterize the uncertainty about the parameters of Weibull functions by simulating random draws of all the parameters in an estimated mixture of Weibull functions from the posterior distribution. We feed each posterior draw of these parameters into our SIR model and solve for paths of all the SIR model variables such as the transmission rate and the fraction still susceptible within the sample as well as out of the sample. We then generate the posterior distributions of these model variables, which are used to produce probability (uncertainty) bands of various variables both in and out of sample.

As of the end of May, 2020, our key findings can be summarized as follows.

First, across almost all regions and countries that we consider, the growth of the pandemic as measured by its effective reproduction number has fallen dramatically from the initial date at which cumulative deaths reached 50 and the present. In many cases, we see declines of the effective reproduction number from levels well above 3 to levels well below 1. This rapid decline in the effective reproduction number of the disease seen in the regions that we consider accounts for the observation that infections and deaths have not reached the levels that were forecast by some in mid March. At the same time, we find that the estimated fraction of the population that remains susceptible to the disease is very high in almost all regions and the fraction of the population that is actively infected, while not extraordinarily high, is substantially larger than it was in early March.

Second, we find that in most regions and countries that we consider, the current levels of susceptible and infected agents are both sufficiently large to trigger the rapid emergence of a very large second wave of the pandemic if the relaxation of

4

mitigation measures leads to transmission rate of the disease to return to levels seen in early April (consistent with an effective reproduction number close to 2). Under this scenario, the pandemic would progress very quickly through the population and would extinguish itself in 90-100 days. Under this scenario, daily deaths would rise to very high levels over the next few months — much higher levels than have been seen in the United States to date, even in New York City. This scenario corresponds to a devastating but short pandemic.

In contrast, if disease mitigation efforts going forward are successful in constraining the transmission of the disease to levels similar to those seen in late April (consistent with an effective reproduction number close to 1.3), then the number of infections and daily deaths would remain roughly constant or grow only slowly across most regions for many months going forward. In many regions, under this second scenario, the cumulative burden of the disease in terms of infections and deaths would be substantially reduced, but the pandemic would drag on for a long time.

Third, in our counterfactual exercises, we find no consistent pattern across regions regarding the answer to the question of whether earlier or later mitigation efforts would have reduced the cumulative death toll from the disease. The answer to this question regarding the impact of changes in the timing of mitigation on cumulative deaths depends on the data for each region and on the assumed scenario for the transmission of the disease going forward from the present date. We illustrate this finding with a focus on our estimates for Pennsylvania. We consider counterfactual scenarios under which the decline in the transmission rate of the disease estimated in these locations started seven days later than is estimated. We show that under one scenario, this counterfactual timing of the mitigation of the disease leads to a large increase in long-run cumulative deaths and in another scenario to a large decrease in long-run cumulative deaths. We give an intuitive explanation for this finding in terms of the key role played by the fraction of the infected population at the moment when the population reaches herd immunity in shaping the long-run cumulative deaths from the disease in an SIR model as noted in Toda (2020) and Rachel (2020).

To implement our estimation procedure, we have to obtain estimates of the fatality and recovery rates for COVID-19 from outside sources. In particular, the first two steps of our estimation procedure highlight the problem of identifying the fatality and recovery rates of the disease from time series data on deaths alone discussed in Atkeson (2020), Stock (2020), Korolev (2020), and Lourenco et al. (2020). Specifically, we obtain the following lack-of-identification result: given any empirical specification for data on cumulative deaths that is strictly increasing and twice differentiable, then, for a large set of parameters for the fatality and recovery rates of the disease, there exists a path for the transmission rate of the disease over time and an initial distribution of the population across states (at the initial date t_0) for which the SIR model with these parameters reproduces this specification for the data on deaths exactly. The only restrictions on the set of fatality and recovery rates implied by the death data are that the fractions of recovered and infected agents cannot exceed one and that the effective reproduction number can never be negative.[4]

Our procedure in step 2 for recovering an estimate of the evolution of the effective reproduction number over time from the empirical specification for deaths estimated in step 1 is related to widely cited methods for using data on the evolution of the number of active infections or deaths over time to estimate the effective reproduction number of a disease developed in Wallinga and Teunis (2004), Wallinga and Lipsitch (2006), Cori et al. (2013), and Chowell et al. (2007). Under these methodologies, the effective reproduction number of a disease at a point in time is obtained from an estimate of the growth rate of active infections at that point in time and of the recovery rate of the disease.[5] Under the assumption of a constant fatality rate, our SIR model implies that one can infer the growth rate of active infections from the growth rate of new deaths. Our empirical specification of daily deaths as following a mixture of Weibull functions with regime-switching errors allows us a very flexible

---

[4]These restrictions put lower bounds on the fatality rate and on the recovery rate.

[5]Our simple SIR model imposes an exponential distribution of recovery times. More generally, the length of time over which an infected person is contagious may follow some other distribution and then one must also estimate the distribution of serial intervals of the disease. See https://staff.math.su.se/hoehle/blog/2020/04/15/effectiveR0.html for a discussion.

model for modeling both the first and second derivatives of cumulative deaths while also allowing us to deal econometrically with the fact that the observed data on daily deaths is subject to a great deal of noise. We see the fact that we can construct Bayesian uncertainty bands for our estimates as one of the primary advantages of our specific empirical specification.

Our work is related to Fernandez-Villaverde and Jones (2020), who also use the death data to estimate a similar structural model. Both papers address some common identification issues related to the fatality and recovery rates. Our paper, however, differs from their work in several important respects. First, we use the full Bayesian procedure to characterize the uncertainty of death patterns. This approach enables us to provide probability bands of all the SIR model variables in and out of the sample. Second, we focus on the issue of how earlier or later mitigation measures would have impacted the total death toll from the disease.[6] Our estimation shows a considerable degree of heterogeneity in death impacts across geographic regions. Third, we provide a critical analysis of how such heterogeneous results are related to what we call "the IS curve," which is the phase diagram showing the relationship between the fractions of the population actively infected and still susceptible as implied by the structural model. Our estimation reveals rich model dynamics as well as complex IS relationships across geographic regions as well as forecast scenarios, an empirical finding that is absent in the literature.

This paper is organized as follows. In section 2, we present the equations of a basic SIR model and discuss the sources of data used to choose the disease parameters governing the recovery rate and fatality rate of the disease. In section 3, we present our procedure for matching the SIR model to empirical estimates of cumulative deaths outlined as step 2 of our procedure. This presentation is kept general as it can be applied to any strictly increasing and twice differentiable empirical specification for cumulative deaths. We contrast our specification to that used by the IHME

---

[6]For how this important issue bears on the public debate, see https://www.nytimes.com/2020/05/20/us/coronavirus-distancing-deaths.html and https://www.medrxiv.org/content/10.1101/2020.05.15.20103655v2.

modeling team. In section 4, we present our procedure for estimating our empirical specification for the deaths data. In section 5, we report our main findings. In section 6, we conclude.

2 A Basic SIR Model:

The SIR model we use is as follows.

The population is set to N. At each moment of time, the population is divided into four categories (states) that sum to the total population. These states are susceptible S, infected I, resistant R, and dead D. Agents that are susceptible are at risk of getting the disease. Agents that are infected are contagious and may pass it on to others through some form of interaction with susceptible agents. Agents that are resistant are not at risk of getting the disease, either because they have immunity built up from a vaccine or from previous experience with this or similar diseases. Likewise, those who have died from the disease are no longer at risk of getting the disease. In this specification of the model, we assume that immunity is permanent so that being resistant R or dead D is an absorbing state. We normalize the total population $N = 1$, so all results regarding S, I, R and D should be interpreted as fractions of the relevant population.

The initial distribution of the population across these states at time $t = 0$ is given by $S(0) > 0$, $I(0) > 0$, $R(0) \geq 0$ and $D(0) \geq 0$. For a new disease such as COVID-19, we assume that all agents are at risk of getting the disease, so that $R(0) = D(0) = 0$, $S(0)$ is very close to one, and $I(0)$ is a small number corresponding either to the initial cases of the disease transmitted to humans from some animal source (as in Wuhan) or introduced into a country or other local geography through travel.

These fractions of the population evolve over time as follows

$$dS(t)/dt = -\beta(t)\frac{S(t)}{1 - D(t)}I(t)$$

8

$$dI(t)/dt = \beta(t)\frac{S(t)}{1 - D(t)}I(t) - \gamma I(t)$$

$$dR(t)/dt = (1 - \nu)\gamma I(t)$$

$$dD(t)/dt = \nu\gamma I(t)$$

Since all of the parameters in these equations are positive, agents flow only in one direction, from the state S to the state I and then to state R or D.

We treat the evolution of the population as deterministic. This may be appropriate once the disease has infected a large number of individuals, but at the early stage of a pandemic with a small number of infected agents, it is more appropriate to think of the evolution of the number of infected agents as stochastic because of the small number of these agents. We abstract from that issue here, but it is of substantive importance if one wishes to model the dynamics of the pandemic early on or contemplates the possibility of completely eliminating the disease (driving $I(t)$ from a positive number to zero). In light of our use of a deterministic model, we focus our estimation on relatively large geographic regions and we model the pandemic starting from an initial date t_0 at which point a threshold number of 50 cumulative deaths have occurred. We then apply the model under the presumption that the Law of Large Numbers allows this deterministic model to be an accurate representation of the underlying stochastic evolution of the disease and we treat the errors in our empirical specification of deaths as reporting or measurement errors.

The parameters of the model can be interpreted as follows.

The parameter γ governs the rate at which agents who are infected stop being infectious and hence stop transmitting the disease. Here we model this as a transition from the state I to the state R or D. We refer to this parameter as the *recovery rate*. Because there is no cure for a viral disease such as COVID-19, this parameter is considered a fixed parameter determined by the biology of the disease. There is a range of estimates of this parameter γ taken from clinical observations of data such

9

as the length of time agents known to be infected shed the virus[7] as well as data from contact tracing determining who got sick from contact with whom.[8] Estimates for COVID-19 continue to be updated as new data comes in.[9]. Values of γ between 1/4 and 1/14 are considered in the literature, corresponding to an infectious period of 4 to 14 days on average. In this paper, we use $\gamma = 1/5$. We discuss sensitivity of our results to this parameter below.

We denote the fatality rate from the disease by ν. That is, ν is the fraction of infected agents who stop transmitting the disease because they died.[10] Measurement of the fatality rate of the disease is difficult because of incomplete measurement of the number of infected people and of the number of deaths from COVID-19. There is a wide range of estimates of this parameter. Early estimates of the fatality rate among infected people from the Diamond Princess cruise ship in which both infections and fatalities were well measured are in the range of 1.2%.[11] Recent estimates of the infection fatality rate obtained from trends in the case fatality rate and testing data worldwide and in the United States lie in the range of 1.0% and 1.3% respectively.[12]. The website Worldometer combines data on antibody testing and fatalities for New York City to estimate and infection fatality rate of 1.4%.[13] A number of estimates based on antibody testing (serology studies) elsewhere imply a much lower infection fatality rate in the range of 0.2%.[14] We consider values of $\nu = 0.5\%$ as our baseline value and 1% as an alternative value.

---

[7]See, for example He et al. (2020)

[8]See, for example, Zhao et al. (2020) at https://www.medrxiv.org/content/10.1101/2020.02.21. 20026559v1 and Sanche S (2020) at https://wwwnc.cdc.gov/eid/article/26/7/20-0282_article

[9]See, for example, this pre-print in *Nature* https://www.nature.com/articles/s41586-020-2196-x

[10]For the purposes of this paper, we assume that this death rate is constant and thus independent of the stress placed on the health care system at points of peak infection. That assumption is clearly incorrect. Evidence from Wuhan, Italy, and New York City all suggest that case fatality rate from COVID-19 and the overall mortality rate is much higher in periods of peak infection.

[11]See https://www.medrxiv.org/content/10.1101/2020.03.05.20031773v2

[12]See https://www.medrxiv.org/content/10.1101/2020.05.11.20098780v1.full.pdf and https://www.healthaffairs.org/doi/full/10.1377/hlthaff.2020.00455

[13]See https://www.worldometers.info/coronavirus/coronavirus-death-rate/

[14]See https://www.medrxiv.org/content/10.1101/2020.05.13.20101253v1.full.pdf for a recent summary of such studies.

The parameter $\beta(t)$ is the rate at which infected agents spread the virus to (or "shed" the virus onto) others that they encounter at date t. We refer to this parameter as the *transmission rate*. This parameter is a reduced-form parameter that is impacted by the biological disease transmission mechanism, the rate at which agents bump into each other in the course of their daily activities, and the extent to which agents use prophylactics in their meetings. This parameter can thus be impacted by mitigation measures such as social distancing, hand washing, and the use of masks, etc. This parameter is also subject to natural, or apparently random, fluctuations over time and across space due to changes in the biological disease transmission mechanism.[15]

Note in the first two equations governing the flow of agents from the state S to the state I over time, we assume that the transmission of the disease from infected to susceptible agents is mitigated through random and uniform matching of agents in the population as indicated by the term $S(t)/(1-D(t))$ in those two equations. That is, we interpret $\beta(t)$ as capturing the rate at which an infected agent interacts with and sheds virus onto agents of any kind in the population.[16] Under the assumption that the interaction of infected agents with other agents is random and uniform, then the the rate at which an infected agent meets a susceptible agent and sheds virus onto that agent is given by $\beta(t)S(t)/(1-D(t))$. This assumption that the transmission of the disease is mitigated by random and uniform matching is a very

[15]Seasonal influenza is an example of a disease whose transmission rate fluctuates regularly with the weather. The Spanish Flu of 1918-19 came and went in three big waves in the Spring and Fall of 1918 and the Spring of 1919. It is not fully understood what drove the changes over time in the transmission rate of that disease. The available data on COVID-19 indicates that the transmission rate varies tremendously across different geographies. See https://www.cidrap. umn.edu/sites/default/files/public/downloads/cidrap-covid19-viewpoint-part1_0.pdf for a careful discussion of natural fluctuation in transmission of similar diseases. See https://www.nytimes.com/2020/05/03/world/asia/coronavirus-spread-where-why.html for a discussion of geographic variation in transmission of COVID-19.

[16]Note that in this simple model, we do not differentiate between infected agents with mild and severe cases of the disease in terms of their role in spreading the disease. Clearly, the severity of the disease may impact the spread, particularly since the very sick are likely to stay at home or go to the hospital. Research is ongoing into the question of the extent to which those who are infected but asymptomatic spread the disease. See, for example this research in *Science* https://science.sciencemag.org/content/early/2020/03/24/science.abb3221

stark assumption maintained here for simplicity.

The following notation is useful in presenting our results.

We define the ratio $\beta(t)/\gamma$ to be the *normalized transmission rate*. It is standard to refer to the value of the normalized transmission rate at the start of the pandemic before any mitigation measures and use of prophylactics are undertaken as the *basic reproduction number* of the disease. We denote this basic reproduction number by $\mathcal{R}_0 \equiv \beta(0)/\gamma$. This parameter corresponds to the parameter cited in many news and academic studies.[17]

We refer to the term $\mathcal{R}(t)$ as the *effective reproduction number* of the disease at date t. This effective reproduction number is the ratio of the rate at which infected agents infect susceptible agents to the recovery rate of infected agents from the disease at date t when the the pandemic has progressed for some time. In the model, we assume that the effective reproduction number of the disease is given by the product of the normalized transmission rate and the fraction of agents who remain susceptible to the disease, $\mathcal{R}(t) = (\beta(t)/\gamma)S(t)/(1 - D(t))$. Thus, in the model, the effective reproduction number of the disease can differ from the basic reproduction number for two reasons. First, as discussed above, the normalized transmission rate $\beta(t)/\gamma$ may vary over time with changes in the transmission rate $\beta(t)$, either due to steps undertaken to mitigate the transmission rate of the disease or through naturally occurring changes in the transmission of the disease. Second, the effective reproduction number falls as the fraction of agents remaining susceptible to the disease $S(t)/(1 - D(t))$ falls.

With this notation, we can restate the equations of the model in terms of the effective reproduction number as

$$dS(t)/dt = -\mathcal{R}(t)\gamma I(t) \tag{1}$$

---

[17]The use of the notation $\mathcal{R}_0$ to denote the basic reproduction number and the letter R to denote the fraction of agents who are resistant is an unfortunate choice of notation, but it is standard. See for example https://mathworld.wolfram.com/Kermack-McKendrickModel.html

$$dI(t)/dt = (\mathcal{R}(t) - 1)\,\gamma I(t) \tag{2}$$

$$dR(t)/dt = (1 - \nu)\gamma I(t) \tag{3}$$

$$dD(t)/dt = \nu\gamma I \tag{4}$$

3 Model Estimation and Identification Strategy

In this section we provide an overview of our strategy for estimating our SIR model given an empirical specification for the data on cumulative deaths and we discuss which model parameters are identified in our procedure.

To understand our procedure for estimating our SIR model, consider the following thought experiment. Assume that we have complete data on cumulative deaths $D(t)$ in some region from dates $t = t_0$ to T, where t_0 is the calendar date on which cumulative deaths D_{t_0} are equal to some threshold (we use 50) and T represents the current period. Assume that we also have data on the first and second derivatives of cumulative deaths during this time period. These derivatives are continuous time versions of data on daily deaths and the change in daily deaths. Assume that we do not have data on the number of agents with active infections or who are resistant.

Consider the following thought experiment based on these assumptions. Imagine that we fix parameters ν and γ governing the fatality rate and recovery rate of the disease. What state of the population at date t_0, $S(t_0), I(t_0), R(t_0)$ and $D(t_0)$ and course of the time-varying normalized transmission rate $\beta(t)/\gamma$ from dates t_0 to T would allow the model to match exactly the data on deaths from t_0 to T?

We have the following equations to work with in estimating these additional parameters of the model. Note that we assume that these equations apply for all $t > 0$

but we only have data on the level and derivatives of cumulative deaths from $t \geq t_0$. From (4), we have

$$I(t) = \frac{1}{\nu\gamma}dD(t)/dt$$

Using (3) and (4) together and the assumption that $R(0) = D(0) = 0$, we have that

$$R(t) = \frac{1-\nu}{\nu}D(t)$$

Using that the states must sum to one, we have

$$S(t) = 1 - \frac{1}{\nu}D(t) - \frac{1}{\nu\gamma}\frac{dD(t)}{dt}.$$

These equations then give the full path of the state of the population from dates t_0 to T. Note that the intuition behind these equations is straightforward. To determine the number of resistant agents at time t, we simply use the observation that level of cumulative deaths together with an estimate of the fatality rate of the disease tells us how many agents are resistant to the disease. To determine the number of actively infected agents at time t, we use the observation that the level of daily deaths (the derivative of cumulative deaths) together with an estimate of the fatality and recovery rates of the disease tells us the number of active infections. The number of susceptible agents at time t is then one minus these two quantities.

One can measure the effective reproduction number from the growth rate of deaths as follows. From equation (2), the evolution of the true number of infected agents is given by

$$I(t) = I(0)\exp(\gamma \int_0^t (\mathcal{R}(s) - 1)ds)$$

From equation (4), we then have that

$$\frac{dD(t)}{dt} = \nu\gamma I(0)\exp(\gamma \int_0^t (\mathcal{R}(s) - 1)ds)$$

where this time derivative of deaths is approximated in the data by the daily number

14

of new deaths. If we differentiate this expression again, we get

$$\frac{d^2D(t)}{dt^2} = \nu\gamma^2 I(0)\exp(\gamma\int_0^t (\mathcal{R}(s) - 1)ds)(\mathcal{R}(t) - 1)$$

Thus, we can get an estimate of the effective reproduction number of the disease at time t from[18]

$$\mathcal{R}(t) = 1 + \frac{1}{\gamma}\frac{\frac{d^2D(t)}{dt^2}}{\frac{dD(t)}{dt}} \tag{5}$$

To recover the implied path of the normalized transmission rate, note that equation (5) together with the death data gives the following estimate for the path of the product of the effective reproduction between dates t_0 and T. This estimate together with the estimate of $S(t)$ above imply that the normalized transmission rate $\beta(t)/\gamma = \mathcal{R}(t)(1 - D(t))/S(t)$ needed to match the deaths data exactly for $t \in [t_0, T]$ is given by

$$\frac{\beta(t)}{\gamma} = \frac{1 + \frac{1}{\gamma}\frac{\frac{d^2D(t)}{dt^2}}{\frac{dD(t)}{dt}}}{1 - \frac{1}{\nu}D(t) - \frac{1}{\nu\gamma}dD(t)/dt}(1 - D(t))$$

This estimation procedure makes clear the identification problem in pinning down the parameters ν and γ from deaths data alone. In particular, if we start with a prior for ν and γ, we should not be able to update this prior based on deaths data alone unless the estimates above result in inadmissable values of implied $I(t)$, $R(t)$ or $S(t)$ (above 1 or negative) or some implausible path for the normalized transmission rate $\beta(t)/\gamma$ (negative).

To implement this estimation of the SIR model, one must construct an empirical estimate of the data on cumulative deaths and the first and second derivatives of cumulative deaths. It is here that our method makes contact with widely noted reduced-form approaches to estimating the progression of the COVID-19 pandemic. To illustrate this connection, we discuss the reduced form approach developed by researchers at the Institute for Health Metrics and Evaluation (IHME) at the Uni-

---

[18]Thanks to James Stock for pointing out this calculation.

15

versity of Washington.[19]

We focus on the estimation of the IHME model using data on cumulative deaths.
The simplest version of this model assumes that the path of cumulative daily deaths
from some initial calendar date t_0 on is given by

$$D(t) = \frac{p}{2}\left(1 + \frac{2}{\sqrt{\pi}}\int_0^{a(t-t_0-b)}\exp(-\tau^2)d\tau\right)$$

where the parameter p denotes the limiting number of deaths D_∞, a is a growth
parameter, and b is an inflection point. This specification produces an implication
for daily deaths (approximated by the derivative of cumulative deaths) given by

$$\frac{dD(t)}{dt} = \frac{pa}{\sqrt{\pi}}\exp(-a^2(t-t_0-b)^2)$$

that peaks at time $t = b + t_0$ and then falls thereafter. Note that the implied growth
rate of the logarithm of daily deaths is given by

$$\frac{\frac{d^2 D(t)}{dt^2}}{\frac{dD(t)}{dt}} = 2a^2(b + t_0 - t).$$

The model is fit to the available data on deaths between the initial date t_0 and the
current date, and then the assumed parametric form is used to project daily deaths
beyond the current date. This projection is based on the claim that this parametric
form fits the data for locations that are further along in disease progression. One
can incorporate measures of the extent and timing of mitigation in the estimation as
covariates for the parameters p and b based on experience across locations.

If, as our model implies with a constant fatality rate ν, observed deaths are related

to active infections by equation (4), then equation (5) implies that the path of the effective reproduction number over time implied by the parameters of this empirical specification for cumulative deaths is given by

$$\mathcal{R}(t) = 1 - \frac{2a^2}{\gamma}(t - t_0 - b)$$

That is, for our SIR model to replicate this pattern of cumulative deaths, the normalized transmission rate $\beta(t)/\gamma$ would have to vary over time so as to produce the path for the effective reproduction number $\mathcal{R}(t) = (\beta(t)/\gamma)S(t)/(1 - D(t))$ given above.

Note then that this empirical specification implies that the effective reproduction number falls linearly over time, not only in the period of estimation, but also going forward beyond the current period.[20] Thus, in the context of a structural model, unless one assumes that the current value of $S(t)/(1 - D(t))$ is substantially below one, this is equivalent to assuming that the impact of mitigation measures on disease transmission will continue to lower the transmission rate over time rather than keep it stable at current levels or even allow it to rise. It is not clear that this is a natural assumption regarding the impact of lockdowns or other disease mitigation measures — that their impact on disease transmission would grow over time.

The empirical specification for the deaths data that we use is considerably more flexible than that used in the IHME model in that it is based on Weibull functions. In the simplest version of our specification (with one regime), the data on daily deaths is modeled as

$$\frac{dD(t)}{dt} = d\left[\frac{b}{a}\left(\frac{t - t_0 - c}{a}\right)^{b-1}\exp\left(-\left(\frac{t - t_0 - c}{a}\right)^b\right)\right]$$

where the parameter $a > 0$ is the scale parameter, $b > 0$ is the slope parameter, and c is the location parameter of a Weibull density, while $d > 0$ allows us to scale this

---

[20]Clearly, at some point, this implied effective reproduction number becomes negative, which is inadmissable. This observation implies that this functional form for cumulative deaths cannot be reproduced by our SIR model with any set of parameters and time varying transmission rate $\beta(t)$.

density function up or down to integrate to d. The implied effective reproduction number is

$$\mathcal{R}(t) = 1 + \frac{1}{\gamma}\left[\frac{b-1}{t-t_0-c} - \frac{b}{a}\left(\frac{t-t_0-c}{a}\right)^{b-1}\right]$$

This prediction for the effective reproduction number given our empirical specification for daily deaths can take on various shapes parameterized by a, b, and c. In particular, with $b = 1$, the Weibull function implies a constant path for the effective reproduction number. With $b < 1$, the implied effective reproduction number rises over time. With $b > 1$ it falls over time. This critical dependence on the parameter b corresponds to the properties of the density of the Weibull distribution here representing the pattern of daily deaths itself. With $b = 1$, daily deaths start at $t = t_0$ at a constant value and decline monotonically as t increases. With $b > 1$ and $c = 0$, daily deaths approach zero as t approaches t_0, but the implied effective reproduction number approaches infinity. With a large enough value of b (say 4), this function produces a hump-shaped pattern of daily deaths. Setting $c > 0$ with $b > 1$ allows for a finite implied effective reproduction number at $t = t_0$.

4   Empirical Implementation of the Model for Daily Deaths

In this section we describe and estimate the empirical model that we use for daily deaths.

Consider a mixture of Weibull functions:

$$\frac{dD_t}{dt} = \sum_{i=1}^{\mathcal{I}} w_i(t)\left\{d_i\frac{b_i}{a_i}\left(\frac{t-t_0-c_i}{a_i}\right)^{b_i-1}\exp\left[-\left(\frac{t-t_0-c_i}{a_i}\right)^{b_i}\right]\right\}, \qquad (6)$$

where $a_i > 0$ is the scale parameter, $b_i > 0$ is the slope parameter, $c_i < t - t_0$ is the location parameter, $d_i > 0$ is the height parameter, the weight parameter

18

$w_i(t)$ is positive for all i and t, $\mathcal{I}$ is a positive integer indicating the number of mixtures, and $\sum_{i=1}^{\mathcal{I}} w_i(t) = 1$. The term in the curly bracket on the right-hand side of equation (6) is the three-parameter Weibull distribution density function scaled by d_i. In the $\mathcal{I} = 2$ case, we set, $w_1(t) = e^{-s(t-m)}/(1 + e^{-s(t-m)})$, where s is the steepness parameter and the parameter m represents the sigmoid's midpoint.

Let ΔD_t^{Data} be the measured object for dD_t/dt and denote

$$\Delta D^{t,\,\text{Data}} \equiv \left\{ \Delta D_t^{\text{Data}}, \Delta D_{t-1}^{\text{Data}}, \Delta D_{t-2}^{\text{Data}}, \dots \right\}, \ \Delta D^{\text{Data}} \equiv \left\{ \Delta D_{t_0}^{\text{Data}}, \cdots, D_T^{\text{Data}} \right\}.$$

Given the discrete-time data, we approximate continuous-time equation (6) by first estimating the non-linear regime-switching equation

$$\Delta D_t^{\text{Data}} = \sum_{i=1}^{2} w_i(t) \left\{ d_i \frac{b_i}{a_i} \left(\frac{t - t_0 - c_i}{a_i} \right)^{b_i - 1} \exp\left[-\left(\frac{t - t_0 - c_i}{a_i} \right)^{b_i} \right] \right\} + \sigma_{k_t} \varepsilon_t, \quad (7)$$

where ε_t is a state-dependent standard normal random residual. The switching state $k_t \in \{1, \dots, \mathcal{K}\}$ can accommodate both an expectedly large surge in daily deaths and a low death volatility typically associated with a low number of deaths. Since the first term on the right-hand side of equation (7) can be very large for some t, moreover, negative values of ε_t allow for actual daily deaths substantially lower than the value implied by the first term on the right-hand side of equation (7). The transition matrix $\mathcal{Q}^k = [q_{i,j}^k]$ for k_t is unrestricted except that each column of $\mathcal{Q}^k$ sums to one. For our deterministic SIR model to offer an accurate account of health consequences of the pandemic, we set t_0 at the time when the number of deaths accumulates to 50.

Denote a collection of the parameters by

$$\theta = \left\{ s, m, a_1, b_1, c_1, d_1, a_2, b_2, c_2, d_2, \sigma_1, \cdots, \sigma_{\mathcal{K}}, q_{i,j}^k \right\}.$$

From equation (7) one can derive the (log) conditional likelihood function for $\Delta D^{t,\,\text{Data}}$

19

as

$$\log \mathcal{L}\left(\Delta D_t^{\text{Data}} \mid \Delta D^{t-1,\text{Data}}, k_t, \theta\right) =$$

$$\log \mathcal{L}\left(\Delta D_t^{\text{Data}} \mid k_t, \theta\right) = -\frac{T-t_0}{2}\log(2\pi) - \sum_{t=t_0}^{T}\log(\sigma_{k_t})$$

$$-\sum_{t=t_0}^{T}\frac{\left[\Delta D_t^{\text{Data}} - \sum_{i=1}^{\mathcal{I}} w_i(t)\left\{d_i \frac{b_i}{a_i}\left(\frac{t-t_0-c_i}{a_i}\right)^{b_i-1}\exp\left[-\left(\frac{t-t_0-c_i}{a_i}\right)^{b_i}\right]\right\}\right]^2}{2\sigma_{k_t}^2}. \quad (8)$$

It follows that the likelihood function for ΔD^{Data} is

$$\mathcal{L}\left(\Delta D^{\text{Data}} \mid \theta\right) =$$

$$\prod_{t=t_0}^{T}\sum_{k_t=1}^{\mathcal{K}}\left[\mathcal{L}\left(\Delta D_t^{\text{Data}} \mid \Delta D^{t-1,\text{Data}}, k_t, \theta\right) p\left(k_t \mid \Delta D^{t-1,\text{Data}}, \theta\right)\right]. \quad (9)$$

Given the initial condition $p\left(k_{t_0-1} = 1 \mid \Delta D^{t_0-1,\text{Data}}, \theta\right) = 1/\mathcal{K}$, the predictive probability of regime, $p\left(k_t \mid \Delta D^{t-1,\text{Data}}, \theta\right)$, can be updated recursively through Hamilton (1989)'s filter as

$$p\left(k_t \mid \Delta D^{t-1,\text{Data}}, \theta\right) = \sum_{k_{t-1}=1}^{\mathcal{K}} q_{k_t,k_{t-1}} \, p\left(k_{t-1} \mid \Delta D^{t-1,\text{Data}}, \theta\right) \quad (10)$$

and

$$p\left(k_t \mid \Delta D^{t,\text{Data}}, \theta\right) =$$

$$\frac{\mathcal{L}\left(\Delta D_t^{\text{Data}} \mid \Delta D^{t-1,\text{Data}}, k_t, \theta\right) p\left(k_t \mid \Delta D^{t-1,\text{Data}}, \theta\right)}{\sum_{k_t=1}^{\mathcal{K}}\left[\mathcal{L}\left(\Delta D_t^{\text{Data}} \mid \Delta D^{t-1,\text{Data}}, k_t, \theta\right) p\left(k_t \mid \Delta D^{t-1,\text{Data}}, \theta\right)\right]}. \quad (11)$$

Let $p(\theta)$ be the prior pdf. Specifically, we take $p(\theta)$ to be the Gamma distribution for a_i, b_i, d_i, s, and m, the uniform distribution for c_i and σ_{k_t},[21] and the Dirichlet

---

[21]The linear regression literature only uses the inverse Gamma distribution for σ_{k_t} as conjugate

distribution for the elements of $\mathcal{Q}_k$. It follows that the log posterior density function of θ is

$$\log p\left(\theta \mid \Delta D^{\text{Data}}\right) = \log \mathcal{L}\left(\Delta D^{\text{Data}} \mid \theta\right) + \log p(\theta) - \log p\left(\Delta D^{\text{Data}}\right), \qquad (12)$$

where $p\left(\Delta D^{\text{Data}}\right)$ is the marginal data density (MDD). For each case (i.e., state, Census region, or country), we use the MDD to select the number of mixtures, $\mathcal{I}$.

5 Findings

The data sources for daily deaths are New York Times for U.S. states and regions and Johns Hopkins University for other countries. We do not smooth the data with a preset filter but rather estimate the death pattern using the Bayesian procedure presented in Section 4. The estimation enables us to incorporate the uncertainty about deaths into our structural model.

We present estimates, forecasts, and counterfactual exercises for ten large U.S. states, nine U.S. Census Regions, and a number of additional countries. The ten states we consider are New York, New Jersey, Massachusetts, Michigan, Pennsyvania, Illinois, California, Connecticut, Louisiana and Maryland. The Census Regions are South Atlantic, East North Central, Mountain, West North Central, West South Central, Pacific, and New England. The additional countries that we consider are the United Kingdom, Italy, France, Spain, Brazil, Belgium, Germany, Iran, Mexico, Canada, Netherlands, Sweden India, Peru, Russia, and Switzerland. The presentation is ordered from most deaths to least deaths on May 21, 2020 first for states, then for Census regions, and finally for countries.

For each region, we start the estimation at a region specific date t_0 at which

---

prior. For our nonlinear regression here, the inverse Gamma prior is no longer conjugate. Moreover, since the death data implies that the values of σ_{k_t} are far less than one, the inverse Gamma prior only with no moments can cover such small values. This makes the inverse Gamma prior not only undesirable but also unpractical.

cumulative deaths first reach 50 and let T denote the number of days in the estimation period. We then present forecast and counterfactual scenarios for an additional time period equal to twice the number of days in the estimation period ($2T$).

We consider two forecast scenarios for each state, region, or country. In the first forecast scenario, we set the normalized transmission rate to $\beta_t/\gamma = 2$ from the end of the estimation period to the end of the forecast period. In the second forecast scenario, we set the normalized transmission rate to $\beta_t/\gamma = 1.3$ from the end of the estimation period to the end of the forecast period.

To construct counterfactual scenarios, we shift the estimated/forecast path for the normalized transmission rate $\beta(t)/\gamma$ back by seven days and fill in the first seven days of this counterfactual path for the transmission rate of the disease with its initial value $\beta(0)/\gamma$. That is, the counterfactual path for the normalized transmission rate is given by $\tilde{\beta}(t+7)/\gamma = \beta(t)/\gamma$ for $t \geq 0$ and $\tilde{\beta}(s)/\gamma = \beta(0)/\gamma$ for $0 \leq s < 7$. Note that this shift is for both the estimation and forecast period. Thus, there are two counterfactual scenarios for each state, region, or country, corresponding to the two forecast scenarios outlined above. We interpret this shift as corresponding to a one-week delay in the imposition and relaxation of mitigation measures. Mechanically, given our estimation of a rapidly declining effective reproduction number early on in the estimation period in nearly all regions, this counterfactual corresponds to adding a week of rapid transmission of the disease after the region reaches 50 cumulative deaths beyond what actually occurred.

We present our results in a collection of tables and figures below.

5.1   Organization of the figures and tables

For each state, census region, and country considered, we present our estimation, forecast, and counterfactual results in a collection of four figures.

In each case, the first figure, with two panels, shows the data on daily and cumu-

lative deaths over the estimation period with the estimated Weibull specification for daily and cumulative deaths.

The second figure, also with two panels, shows our estimated and forecast paths for daily and cumulative deaths under the two forecast scenarios that we consider. The normalized transmission rate after the estimation period is set to 1.3 for the first forecast scenario (blue curve) and 2 for the second forecast scenario (red curve), except for West South Central where the normalized transmission rate is set to 1.9 for the second forecast scenario.

The third figure has six panels that shows other model outcomes for the estimation and forecast period under the two forecast scenarios. These are the effective reproduction number, the normalized transmission rate, the fraction of the population remaining susceptible, the fraction actively infected, the fraction resistant, and the change in daily deaths (the second derivative of our empirical specification for cumulative deaths). Outcomes under the forecast scenario with the normalized transmission rate set to 1.3 after the estimation period are shown in blue and with the normalized transmission rate set to 2 after the estimation period are shown in red.

The fourth figure also has six panels. These panels show six model outcomes for the estimation and forecast periods under our counterfactual scenarios. These are the effective reproduction number, the fraction remaining susceptible, daily deaths, cumulative deaths, the normalized transmission rate (the counterfactual), and the fraction of the population actively infected.

In tables 1 and 2, we summarize the results of our counterfactual experiments across states and census regions (table 1) and countries (table 2) by showing the number of cumulative deaths at the end of the forecast period for the two baseline and counterfactual scenarios (normalized transmission rates for the forecast period equal to 1.3 and 2 respectively).

In tables 3 and 4 we show how the change in the effective reproduction number

over the estimation period for New York and the United Kingdom is decomposed into a change in the normalized transmission rate and a change in the fraction of agents still susceptible to the disease.

5.2 Key Findings

Consider our key findings.

5.2.1 Decline in the transmission of the disease in the estimation period

Across almost all regions and countries that we consider, the growth of the pandemic, as measured by its effective reproduction number, has fallen dramatically from the initial date at which cumulative deaths reached 50 to the present (the end of the estimation period marked by a vertical line in the figures). In many cases, we see declines of the effective reproduction number from levels well above 3 to levels well below 1.

In almost all regions, we see that the decline in the effective reproduction number has occurred primarily through a reduction in the normalized transmission rate rather than through a decline in the fraction of the population remaining susceptible to the disease. We illustrate this point in greater detail in Tables 3 and 4.

This rapid decline in the effective reproduction number of the disease seen in the regions that we consider accounts for the observation that infections and deaths have not reached the levels that were forecast by some in mid March. In fact, across the regions that we study, we see within the estimation period a clear first wave in terms of daily deaths — these have peaked and begun to decline rather than continue to grow to very high levels.

Our estimation also indicates that in almost all states, Census regions, and countries, the fraction of the population that remains susceptible to the disease is still quite high and the fraction of the population with active infections, while not ex-

traordinarily high, is considerably higher than it was in mid-March. These findings regarding the current distribution of the population across the states S, I, R, and D then play an important role in shaping our forecast scenarios.

5.2.2   Forecast scenarios

Our two forecast scenarios for the normalized transmission rate of the disease going forward (1.3 in blue and 2 in red) correspond to normalized transmission rates seen in many states, regions, and countries late and early in the estimation period respectively. We see in our forecast scenarios in red with a normalized transmission rate of 2, the threat of a severe second wave of infections and daily deaths that in many cases is much larger than the first wave (in New York these are of roughly equal size). In this second forecast scenario, this large second wave would be over in about 100 days from the end of the estimation period. In most cases, under our forecast scenario with the normalized transmission rate set to 1.3, we also have a second wave of daily deaths and infections, but this second wave is milder and lasts longer. These forecast scenarios of a second wave are driven by our estimates that the fraction of the population that remains susceptible to the disease is very high in almost all regions and the fraction of the population that is actively infected, while not extraordinarily high, is substantially larger than it was in early March.

In terms of the cumulative burden of the disease, we see that these two forecast scenarios have dramatically different implications for cumulative deaths at the end of the forecast period. In each case, the forecast scenario with the normalized transmission rate at 2 results in substantially more daily deaths than that with the normalized transmission rate at 1.3. To see this point, compare the cumulative deaths reported in tables 1 and 2 under the columns labeled baseline scenario 1 (with normalized transmission rate 1.3) and baseline scenario 2 (with normalized transmission rate 2).

It remains to be seen whether it will be possible to keep the normalized transmission rate as low as considered in our blue scenario for the next 100 days or so. Note that the fraction of agents still susceptible under this milder scenario remains high

at the end of the forecast period in many regions. This observation implies that, under this scenario, regions that did succeed in keeping the normalized transmission rate low for the next 100 days or more would still be vulnerable to a large increase in daily deaths and infections were the transmission rate to rise substantially above 1.3 after the end of the forecast period.

5.3 Counterfactuals

Perhaps most interesting are our counterfactual results regarding the implications for changes in the timing of mitigation of disease transmission on the cumulative number of deaths from the disease over the long run. Recall that we consider a counterfactual scenario under which the path of the normalized transmission rate through time is pushed back seven days in both the estimation and forecast period. Because we have two forecast scenarios, we thus have two counterfactual scenarios as well, corresponding to the assumed path of the normalized transmission rate after the estimation period. Results on counterfactual model outcomes including active infections and daily deaths for both the estimation and forecast periods are shown in the fourth figure for each state, Census region, and country. Recall that the vertical lines in these figures mark the end of the estimation period. Results on cumulative deaths at the end of the forecast period under these two counterfactual scenarios are reported in tables 1 and 2 for each state, Census region, and country.

One can see in the lower left panel (first panel of the third row) of the fourth figure for each state, Census region, and country, the counterfactual normalized transmission rate considered, with that in the scenario corresponding to a normalized transmission rate in the forecast period of 1.3 shown in blue and that with a normalized transmission rate of 2 in the forecast period shown in red. In each of these figures, one can see the small flat portion at the start of the estimation period which is where we are assuming that rapid transmission of the disease would have continued for seven days after the region first reached the threshold of 50 deaths.

We report on the counterfactual paths of daily deaths in the first panel of the second row and on active infections in the second panel of the third row of this figure of counterfactual outcomes. In many regions, the counterfactual paths for the normalized transmission rate result in a significantly larger first peak of daily deaths and infections in the estimation period. This finding confirms the common wisdom that delayed mitigation of the disease in this early phase of the pandemic would have resulted in a more severe first wave than actually occurred. Corresponding to this observation, this counterfactual also typically results in a significantly larger number of cumulative deaths (shown in the second panel of the second row) at the end of the estimation period than actually occurred.

But what do these counterfactual scenarios imply for the cumulative number of deaths in the longer run at the end of the forecast period? Here the results can go either way — a seven day delay in the reduction (and subsequent increase) in the normalized transmission rate can result in either an increase or a decline in the number of cumulative deaths at the end of the forecast period.

This finding can be seen most clearly in tables 1 and 2. For New York, we see that the counterfactual number of cumulative deaths at the end of the forecast period is either substantially or mildly larger than that under the baseline paths for the normalized transmission rate. For California, we see that the counterfactual outcomes for cumulative deaths at the end of the forecast period hardly differ from the baseline.

But this is not always the case. For Pennsylvania, and for the aggregate for the United States, we see that the counterfactual number of cumulative deaths at the end of the forecast period under the scenario with a normalized transmission rate equal to 2 during the forecast period is actually lower than the baseline number, and for Pennsylvania in particular this difference is quite large. We see the same result that the counterfactual cumulative deaths at the end of the forecast period are lower than the baseline cumulative deaths under scenario 2 for Italy, Brazil, Iran, Canada, and Switzerland.

How should one understand this result? Here, as suggested by Rachel (2020), examination of the phase diagram of the model is quite useful for building intuition for this result. We show such a phase diagram for our two baseline and counterfactual scenarios in the case of Pennsylvania in figure 24. Each of the two panels of this figure show the model outcomes for $S(t)$ on the x-axis and $I(t)$ on the y-axis in the first scenario (with the normalized transmission rate after the estimation period set to 1.3) on the left and in the second scenario (with the normalized transmission rate set to 2) on the right. There is a vertical line in each figure marking the point of herd immunity once the normalized transmission rate reaches it long run value. For the first scenario, this is at $S = 1/1.3$. For the second scenario, this is at $S = 1/2$.

One can use this figure to understand the model dynamics as follows. The model outcomes start at $S(t_0)$ very close to one and $I(t_0)$ very small at the extreme lower right part of the panel. The long run outcome for $S(t)$ as t gets very large must occur at a point to the left of the vertical line in the panel — in the long-run, active infections do not decline unless the population has herd immunity relative to the long-run value of the normalized transmission rate marked by the vertical line in the figure.

But exactly how far to the left of the vertical line marking herd immunity the fraction of the population that is susceptible at the end of the pandemic lands when infections shrink to zero depends on what fraction of agents are actively infected at the moment in the forecast period that the population reaches that point of herd immunity. If that fraction is high, then it will take a long time for the number of active infections to decline to zero and many more susceptible agents will be infected in the long run. If that fraction is low, then, the remaining active infections will die out quickly and the fraction of agents remaining susceptible in the long run will end up close to the line marking herd immunity. Counterfactual changes in the timing of mitigation as represented by a delay in the decline of the normalized transmission rate can thus raise or lower the long run burden of the disease, measured as one minus the fraction of susceptible agents left in the long run, depending on the impact of these changes on the fraction of agents actively infected when the population reaches

28

herd immunity in the forecast period.

Consider first the left panel in figure 24 showing the evolution of $S(t)$ and $I(t)$ for Pennsylvania in our baseline and counterfactual scenarios in which the normalized transmission rate is 1.3 during the forecast period. In this case, in the baseline scenario, the early decline in the effective reproduction number as estimated implied that the fraction of agents still susceptible at the end of the estimation period is above that needed to achieve herd immunity in the forecast period (1/1.3). Thus, in the forecast period, we see a second wave in the solid black line, as infections rise, reach herd immunity, and then fall. In contrast, under the counterfactual for this scenario, the seven-day delay in initial decline in the transmission of the disease leads to a very large first wave of infections — so large that infections are very high at the point at which they start to decline in the forecast period due to herd immunity. Thus, in this counterfactual scenario as shown by the dotted pink line, the long run fraction of the population that is still susceptible is quite a bit smaller than under the baseline scenario, resulting in a substantial increase in the long-run number of deaths.

But now consider the right panel in figure 24. This panel shows the evolution of $S(t)$ and $I(t)$ for Pennsylvania in our baseline and counterfactual scenarios in which the normalized transmission rate is 2 during the forecast period. In this case, the ordering for cumulative long-run deaths is reversed. Under the baseline scenario shown in the solid black line, the first wave of the pandemic is very small. Thus, when the second wave builds during the forecast period, it builds to a high level of active infections at the point at which the population hits herd immunity, and the fraction of the population that remains susceptible in the long run is very low. In contrast, under the counterfactual scenario in this case, because the first wave of the pandemic is larger, the population actually reaches herd immunity before the end of the estimation period and active infections at the start of the forecast period are so low that the pandemic dies out very quickly once that period starts. Thus, in this case, a delay in mitigation leading to a larger first wave of infections leads, in the long run, to a smaller cumulative death toll.

One can see how these rich model dynamics make it very difficult to draw firm conclusions about the impact of changes in the timing of mitigation measures on the long run cumulative death toll by considering alternative counterfactual scenarios with a shorter delay of mitigation of 5 days (shown in figure 25) and a longer delay of mitigation of 14 days (shown in figure 27). In the left panel of figure 25, we see that a five day delay of mitigation would have had no impact on cumulative deaths if the normalized transmission rate was 1.3 in the forecast period, while in the right panel of that figure, we see that the five day delay would again have been helpful in reducing the cumulative death toll. In contrast, in figure 27, we see that a 14 day delay in mitigation would have resulted in an increase in the cumulative death toll under both scenarios for the normalized transmission rate during the forecast period.

5.4 Uncertainty bands

We simulate $100,000$ random draws from the posterior probability distribution $p\left(\theta \mid \Delta D^{\text{Data}}\right)$ and use these draws to generate 68% probability bands of various SIR model variables as they provide an informative description of the posterior shape (Sims and Zha, 1999).[22] Using Pennsylvania as an example, we report these uncertainty bands in figures 21, 22, and 23. As one can see from the left panel of figure 21, the posterior distribution is skewed. During April 22-28, for instance, the posterior mode (the solid line) is outside and above the 68% probability bands, indicating that the posterior distribution is skewed downward to reflect the sudden drops in daily deaths. During May 6-10, the posterior mode is below the 68% probability bands, indicating that the posterior distribution is skewed upward to reflect a large rise in daily deaths. For cumulative deaths, the 68% probability bands contain the actual observations (right panel of figure 21).

The left panel of figure 22 displays 68% probability bands of daily deaths under our two scenarios of the normalized transmission rate. After cumulating these daily

---

[22]On our standard modern desktop, this whole computation process takes about 192 minutes. The program is coded up in a combination of C++ and Matlab.

deaths, the right panel of the figure shows a large degree of uncertainty about the total death toll. This uncertainty can be explained by figure 23, which shows that the posterior distribution for the normalized transmission rate is skewed downward during the 25-day period around the end of the sample because the mode estimate is above the 68% probability bands for both forecast scenarios. As a result, the 68% probability bands for the effective reproduction number stay below the mode estimate during the same period, even though there is more probability assigned to larger values of $S(t)/N(t)$ than the mode estimate. A majority of the posterior probability of $\mathcal{R}_t$ below the mode estimate explains a large probability of daily and cumulative deaths that stay below the mode estimate at the beginning of the forecast period.

6   Conclusion

In this paper, we have presented a method for estimating a structural SIR model of the COVID-19 pandemic that shares the flexibility of reduced-form models of the evolution of this pandemic with a structural model for forecasting and counterfactual exercises. Our Bayesian approach allows us to not only quantify the uncertainty in our estimates, but also to model the impact of that uncertainty on our forecasts and counterfactual exercises.

We have estimated the model and used it to construct forecast and counterfactual scenarios for ten large states, nine Census regions, and a number of other countries. In further work, we plan to update, on a regular basis, our estimates and forecast and counterfactual scenarios along with uncertainty bands.

31

References

Andrew Atkeson. How deadly is COVID-19? Understanding the difficulties with estimation of its fatality rate. Staff Report 598, Federal Reserve Bank of Minneapolis, March 2020.

Gerado Chowell, Hiroshi Nishiura, and Luis M.A. Bettencourt. Comparative estimation of the reproduction number for pandemic influenza from daily case notification data. *Journal of the Royal Society Interface*, 4(2):155–166, Feb 22 2007.

Anne Cori, Neil M Ferguson, Christophe Fraser, and Simon Cauchemez. A new framework and software to estimate time-varying reproduction numbers during epidemics. *American Journal of Epidemiology*, 178(9), 2013.

Jesus Fernandez-Villaverde and Charles I. Jones. Estimating and simulating a SIRD model of COVID-19 for many countries, states, and cities. Working Paper 27128, NBER, April 2020.

James D. Hamilton. A new approach to the economic analysis of nonstationary time series and the business cycle. *Econometrica*, 57(2):357–384, 1989.

Xi He, Eric H. Y. Lau, Peng Wu, Xilong Deng, Jian Wang, Xinxin Hao, Yiu Chung Lau, Jessica Y. Wong, Yujuan Guan, Xinghua Tan, Xiaoneng Mo, Yanqing Chen, Baolin Liao, Weilie Chen, Fengyu Hu, Qing Zhang, Mingqiu Zhong, Yanrong Wu, Lingzhai Zhao, Fuchun Zhang, Benjamin J. Cowling, Fang Li, and Gabriel M. Leung. Temporal dynamics in viral shedding and transmissibility of covid-19. *Nature Medicine*, 26(5):672–675, 2020. doi: 10.1038/s41591-020-0869-5. URL https://doi.org/10.1038/s41591-020-0869-5.

Ivan Korolev. Identification and estimation of the seird epidemic model for covid-19. April 2020.

Oliver Linton. When will the COVID-19 pandemic peak? Technical Report 2020/11, Cambridge-INET Working Paper Series, April 2020.

Jose Lourenco, Robert Paton, Mahan Ghafari, Moritz Kraemer, Craig Thompson, Peter Simmonds, Paul Klenerman, and Sunetra Gupta. Fundamental principles of epidemic spread highlight the immediate need for large-scale serological surveys to assess the stage of the SARS-COV-2 epidemic. *Cold Spring Harbor Laboratory Press*, March 26 2020.

Lucasz Rachel. An analytical model of COVID-19 lockdowns. May 2020.

Xu C Romero-Severson E Hengartner N Ke R. Sanche S, Lin YT. High contagiousness and rapid spread of severe acute respiratory syndrome coronavirus 2. *Emerging Infectious Diseases*, 26, July 2020.

Christopher A. Sims and Tao Zha. Error bands for impulse responses. *Econometrica*, 67(5):1113–1155, 1999.

James H. Stock. Data gaps and the policy response to the novel coronavirus. Working Paper 26902, NBER, March 2020.

Alexis Akira Toda. Susceptible-infected-recovered (SIR) dynamics of COVID-19 and economic impact. Technical report, Cornell University, March 25 2020.

Jacco Wallinga and Marc Lipsitch. How generation intervals shape the relationship between growth rates and reproductive numbers. *Proceedings of the Royal Society London B*, (274):599–604, November 2006.

Jacco Wallinga and Peter Teunis. Different epidemic curves for severe acute respiratory syndrome reveal similar impacts of control measures. *American Journal of Epidemiology*, 160(6):509–516, September 2004.

Shi Zhao, Daozhou Gao, Zian Zhuang, Marc Chong, Yongli Cai, Jinjun Ran, Peihua Cao, Kai Wang, Yijun Lou, Weiming Wang, Lin Yang, Daihai He, and Maggie Wang. Estimating the serial interval of the novel coronavirus disease (covid-19): A statistical analysis using the public data in hong kong from january 16 to february 15, 2020. February 2020.

Table 1: Cumulative deaths at the end of the forecast period in the U.S.

	Forecast scenario 1		Forecast scenario 2	
	Baseline	Counterfactual	Baseline	Counterfactual
New York	30445	69813	65121	69820
New Jersey	13330	31665	30515	31670
Massachusetts	11012	29687	24943	29687
Michigan	12913	29253	37919	29298
Pennsylvania	24091	32129	49266	34976
Illinois	22053	34844	48792	35216
California	65520	64554	156294	153612
Connecticut	5943	11227	12652	11250
Louisiana	6500	6247	17476	16445
Maryland	9618	9282	23304	21790
South Atlantic	26493	26624	75837	75014
East North Central	33264	33430	84574	83210
Mountain	21224	19395	53254	51699
West North Central	97385	87613	235799	206431
West South Central	43001	41894	94255	92832
East South Central	46055	51710	137284	135278
Pacific	602546	1129696	1223241	1129868
New England	5644	5750	17200	15943
United States	1046592	1645000	2322605	2154219

Notes: The forecast period is twice the length of the sample. United States is the sum of all the states and Census regions in the table, which excludes Guam, Virgin Islands, and Puerto Rico.

Table 2: Cumulative deaths at the end of the forecast period in other countries

	Forecast scenario 1		Forecast scenario 2	
	Baseline	Counterfactual	Baseline	Counterfactual
U.K.	115956	286394	254075	286395
Italy	92459	148948	229217	150001
France	89300	319872	249636	319872
Spain	52443	216733	175925	216733
Brazil	405437	459211	833790	650367
Belgium	9496	57065	42731	57065
Germany	19365	376174	330263	376174
Iran	151722	255019	328282	255027
Mexico	197887	228343	505847	490486
Canada	55320	137496	146871	137513
Netherlands	20236	76655	66105	76655
Sweden	16119	36687	39429	36690
India	438907	695507	5431452	5424026
Peru	54424	74823	128451	95568
Russia	101381	207897	577874	567162
Switzerland	4404	10059	33603	29165

Notes: The forecast period is twice the length of the sample.

Table 3: Decomposition of changes in effective reproduction number $\mathcal{R}_t$: New York

Day	$\Delta_{10} \log \mathcal{R}_t$	$\Delta_{10} \log \beta_t$	$\Delta_{10} \log \frac{S(t)}{N(t)}$	β_t (%)	$\frac{S(t)}{N(t)}$ (%)
10	-0.547	-0.515	-0.0316	94.23	5.77
20	-0.576	-0.461	-0.1149	80.07	19.93
30	-0.286	-0.205	-0.0813	71.63	28.37
40	-0.104	-0.048	-0.0562	45.88	54.12
50	-0.098	-0.067	-0.0316	67.86	32.14
60	-0.099	-0.084	-0.0151	84.83	15.17

Notes: The symbol Δ_{10} denotes a change every 10 days (i.e., in a 10-day time interval). In the row for Day 30, for instance, the change is from Day 20 to Day 30. The last two columns report the percentage contributions of $\log \beta_t$ and $\log \frac{S(t)}{N(t)}$ with a 10-day interval. If the signs are opposite in the last two columns, the percentage contribution can be over 100%.

Table 4: Decomposition of changes in effective reproduction number $\mathcal{R}_t$: United Kingdom

Day	$\Delta_{10} \log \mathcal{R}_t$	$\Delta_{10} \log \beta_t$	$\Delta_{10} \log \frac{S(t)}{N(t)}$	β_t (%)	$\frac{S(t)}{N(t)}$ (%)
10	-1.194	-1.188	-0.0060	99.50	0.50
20	-0.257	-0.237	-0.0195	92.40	7.60
30	-0.340	-0.306	-0.0331	90.25	9.75
40	0.028	0.049	-0.0205	172.28	-72.28
50	-0.054	-0.032	-0.0223	58.90	41.10
60	-0.048	-0.029	-0.0194	59.52	40.48

Notes: The symbol Δ_{10} denotes a change every 10 days (i.e., in a 10-day time interval). In the row for Day 30, for instance, the change is from Day 20 to Day 30. The last two columns report the percentage contributions of $\log \beta_t$ and $\log \frac{S(t)}{N(t)}$ with a 10-day interval. If the signs are opposite in the last two columns, the percentage contribution can be over 100%.
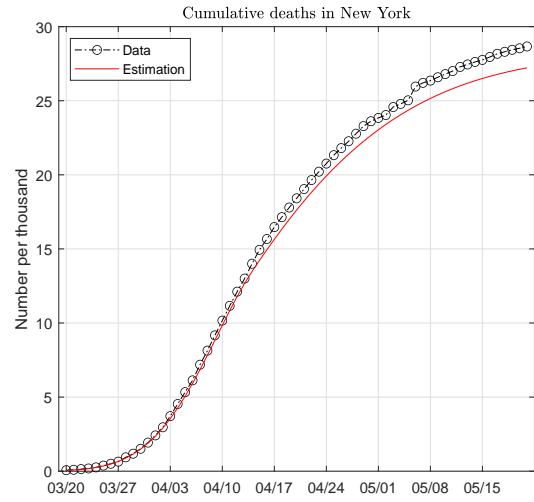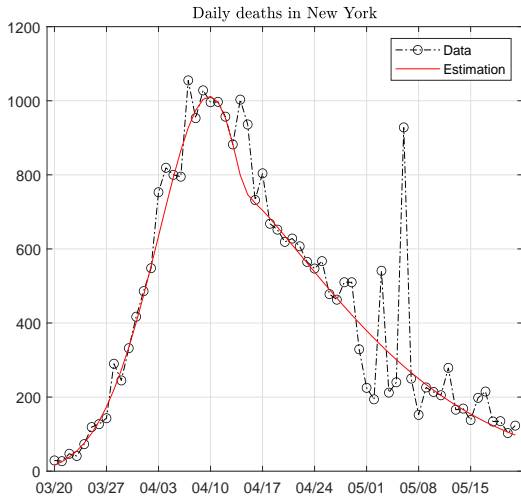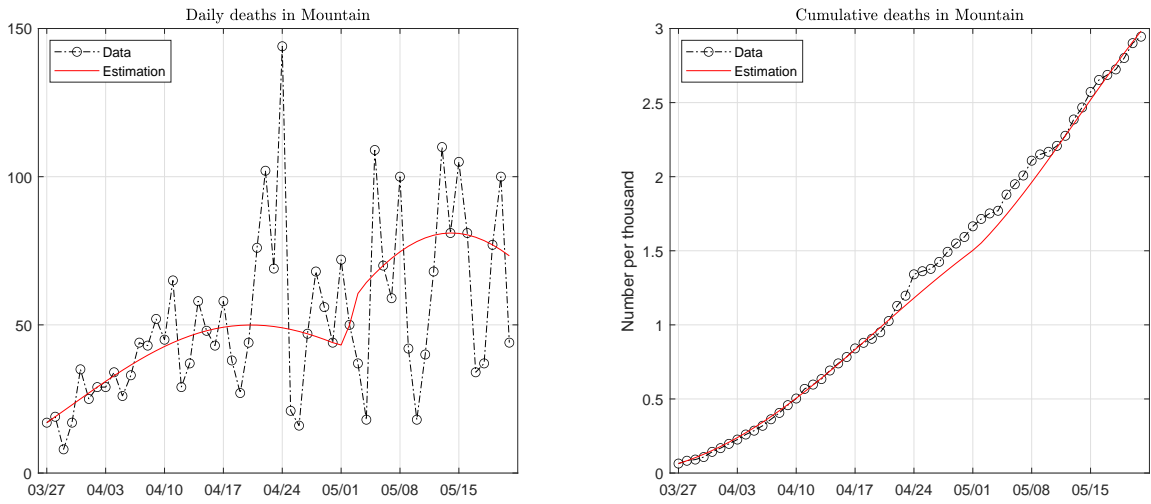
Figure 1: Data and fitted paths of deaths in New York. The death pattern is fitted with one Weibull function.
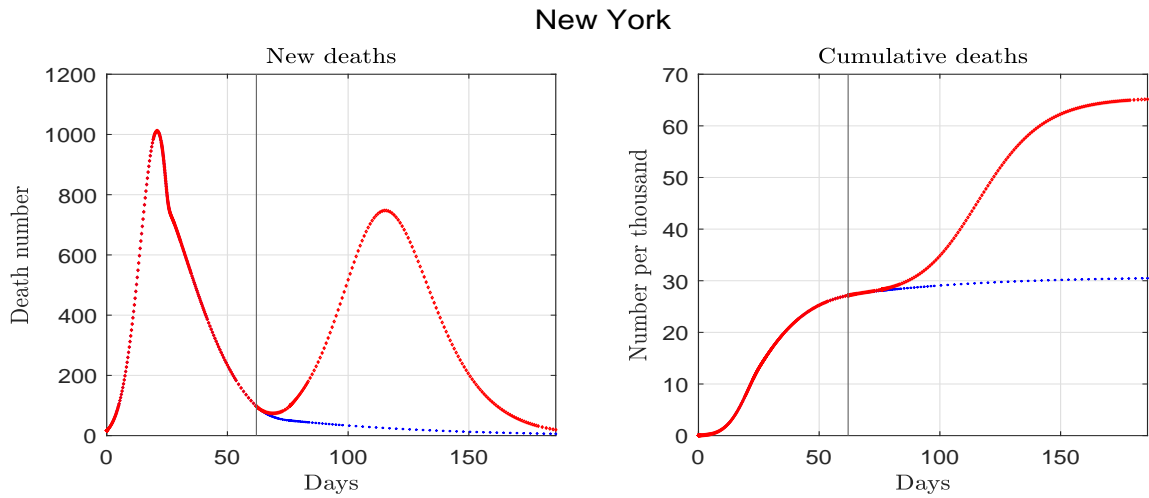
Figure 2: Estimated and forecast deaths for New York. The vertical line marks the end of the sample.
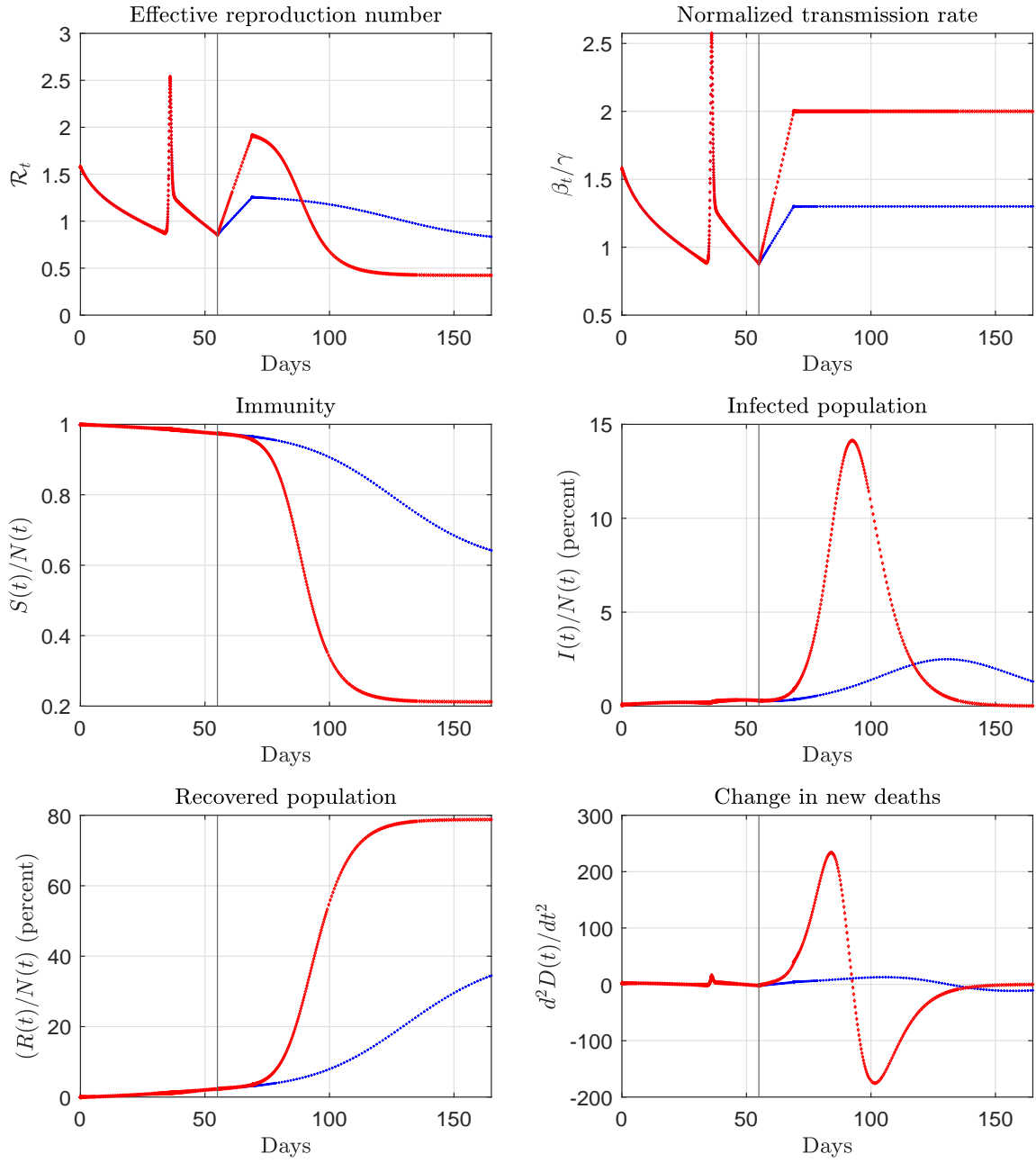
37
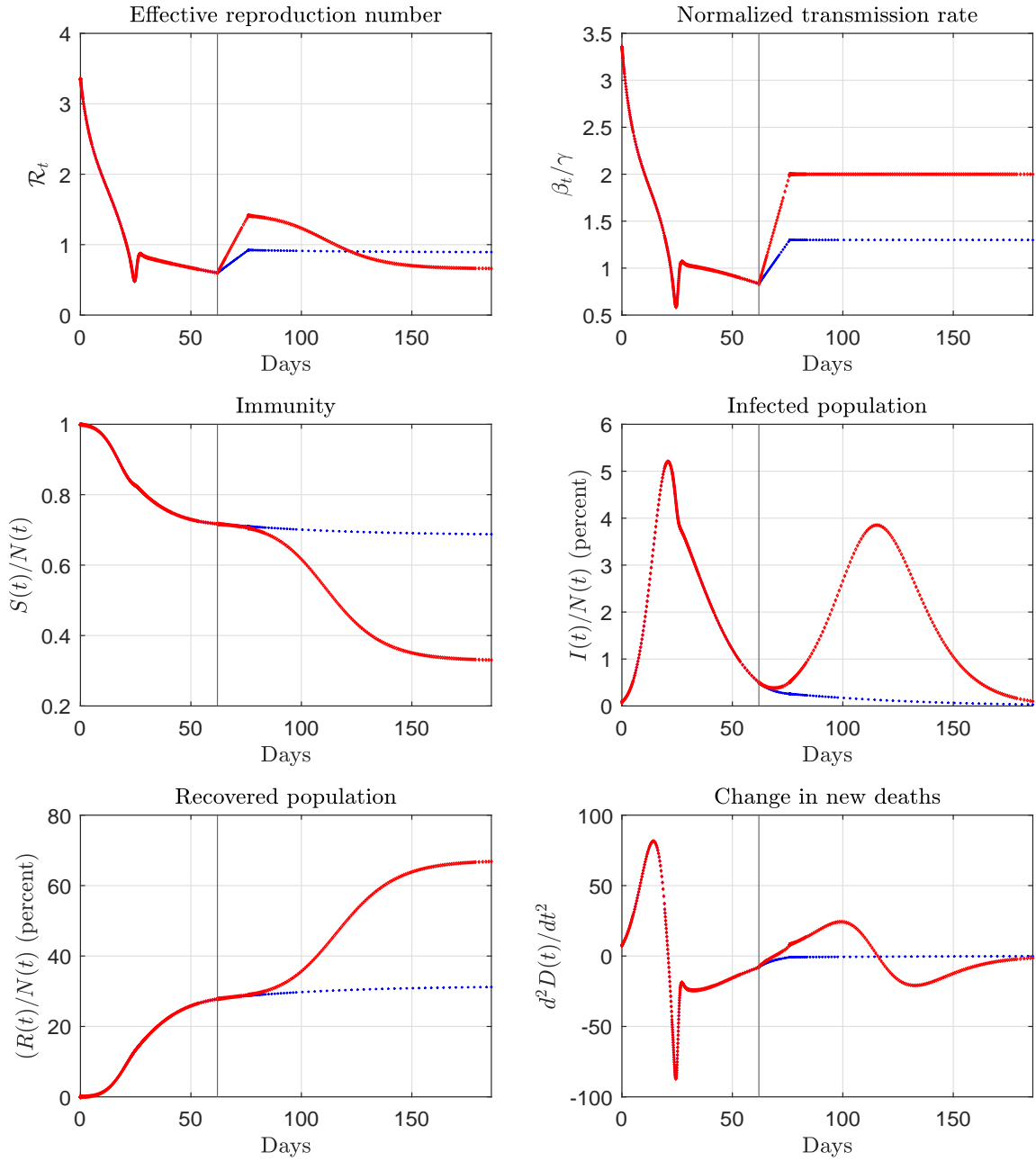
New York

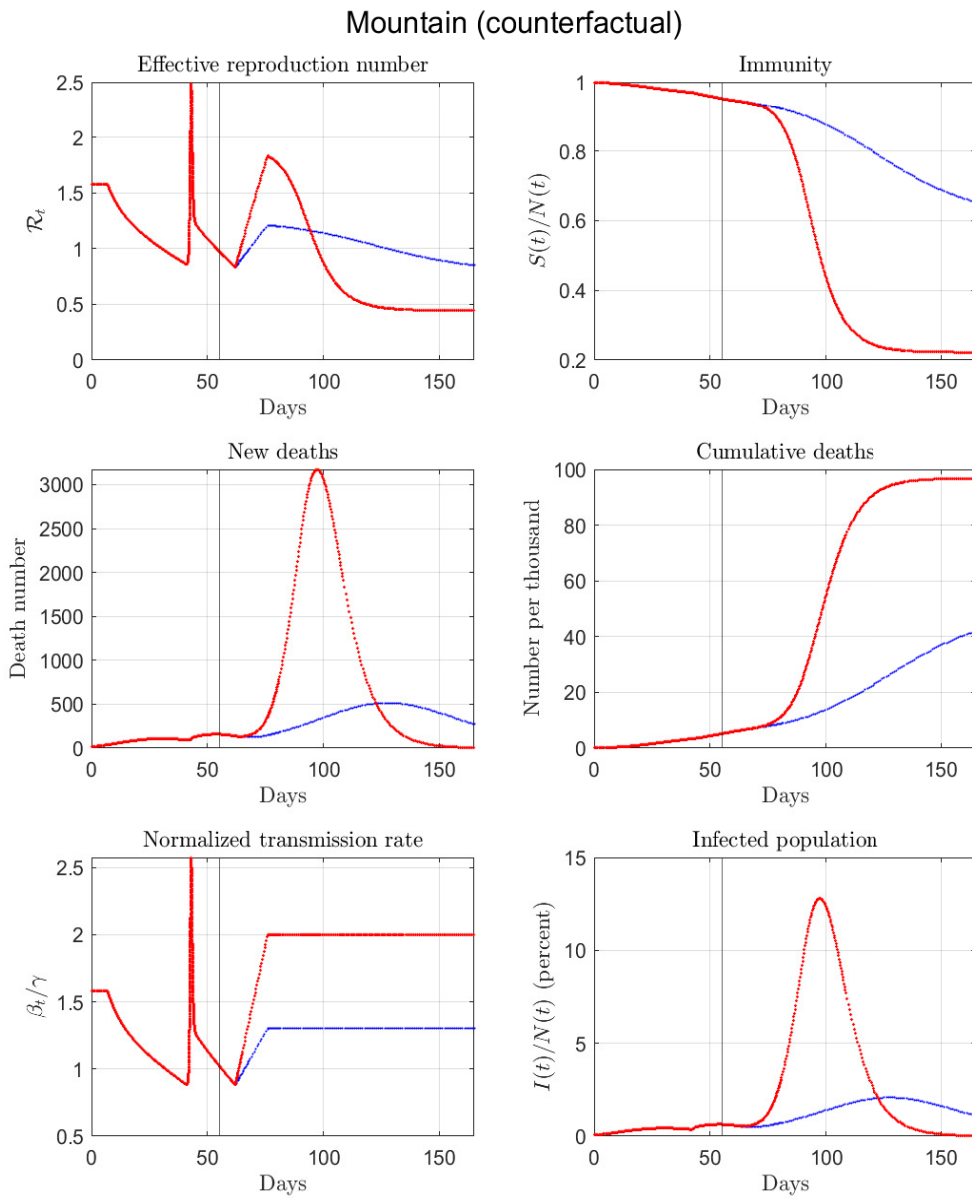**Figure 3:** Estimated and forecast paths for New York. The vertical line marks the end of the sample.
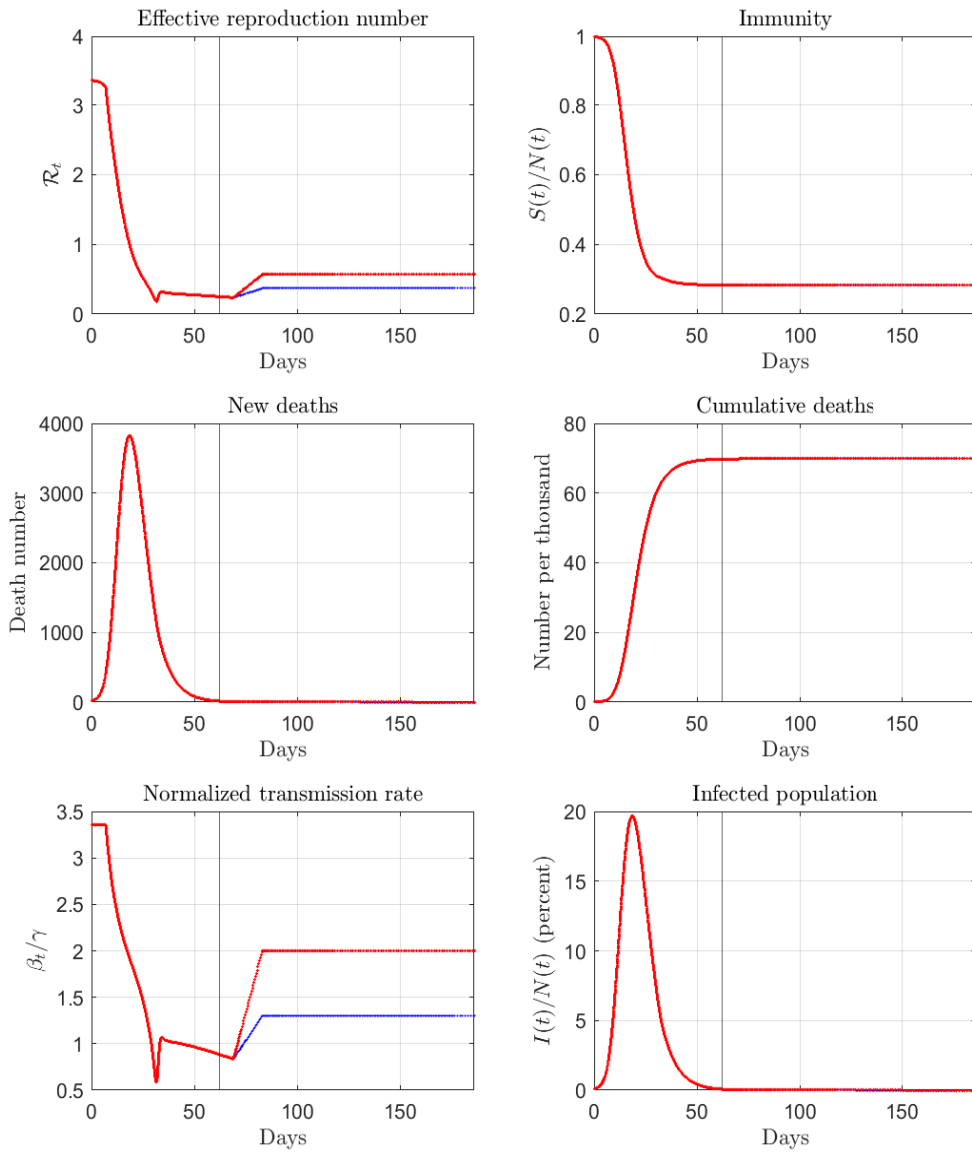
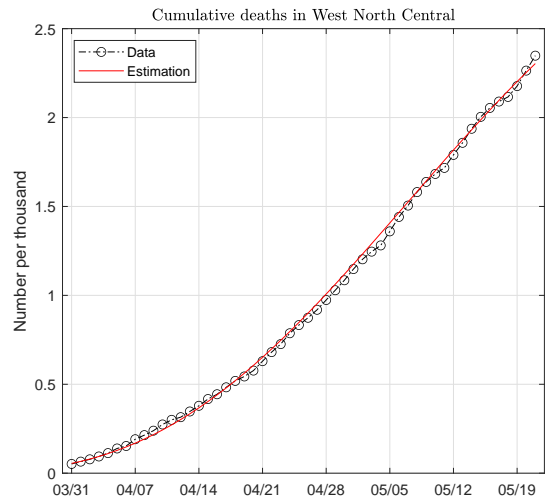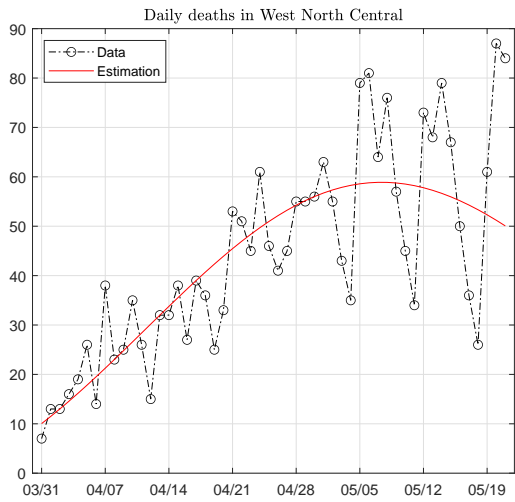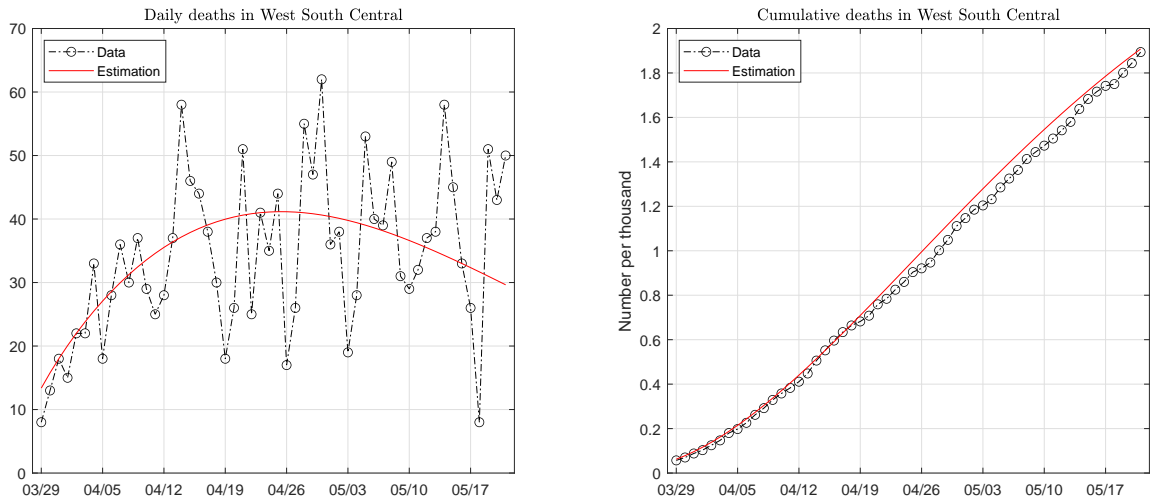**Figure 4:** Counterfactual paths for New York. The vertical line marks the end of the sample.
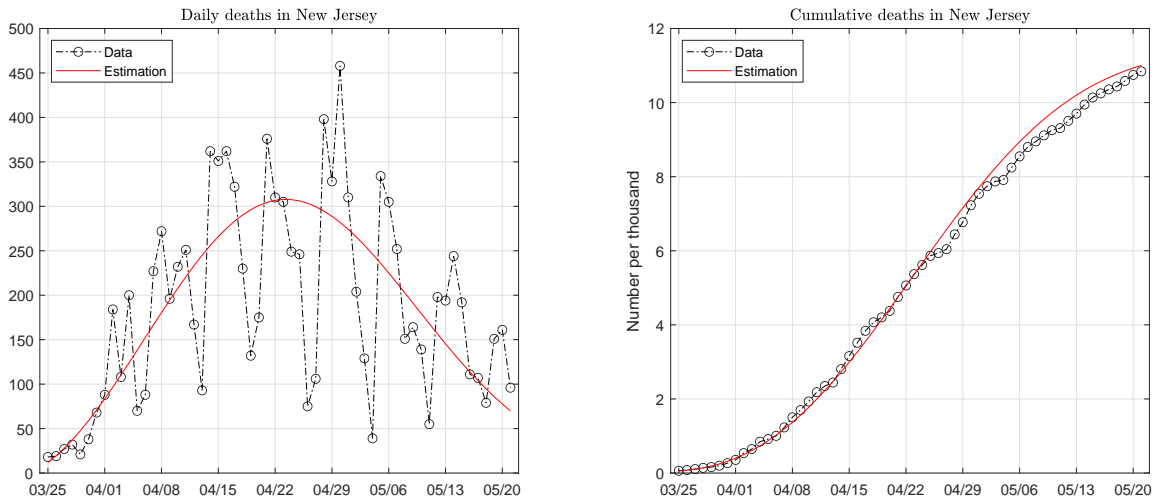
Figure 5: Data and fitted paths of deaths in New Jersey. The death pattern is fitted with one Weibull function.
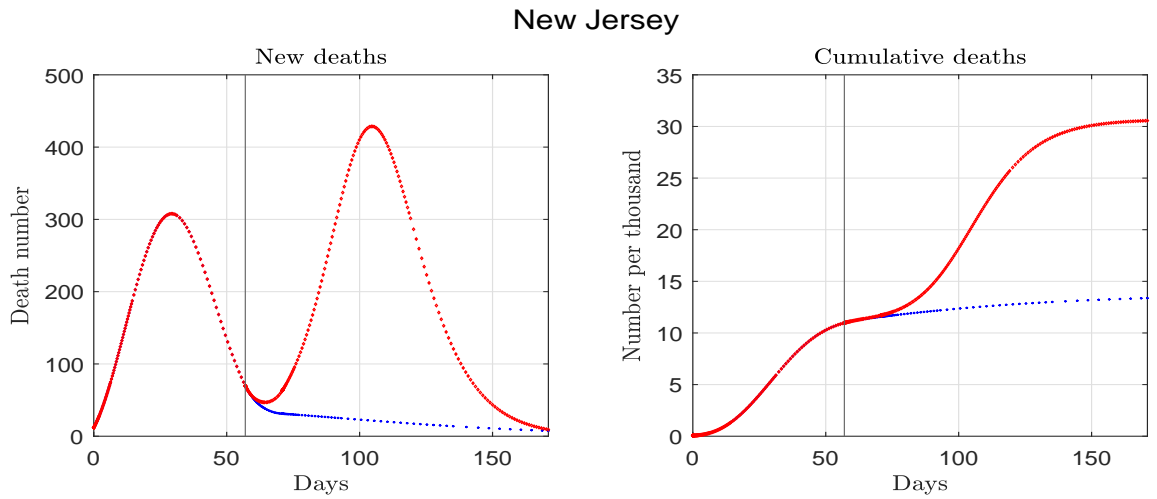
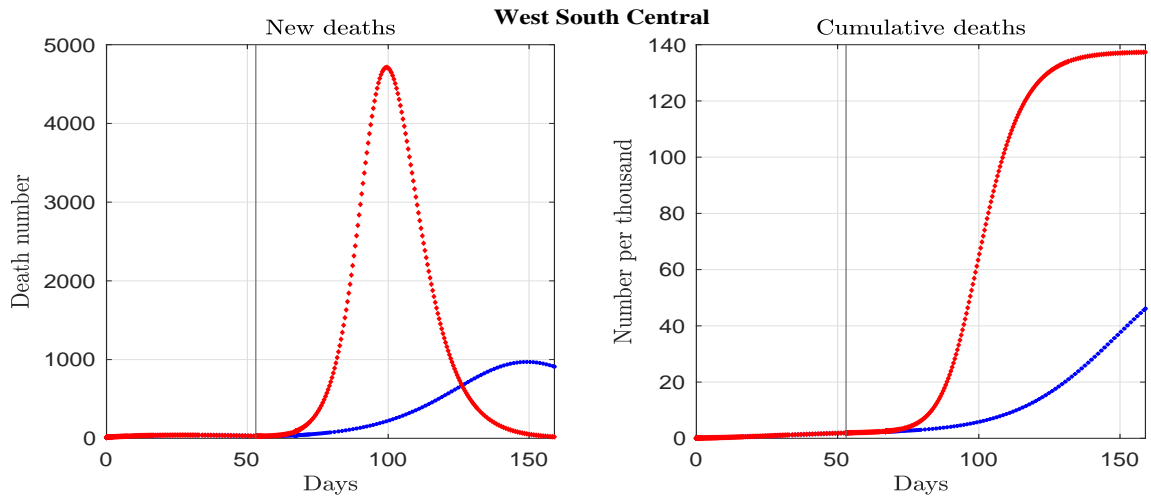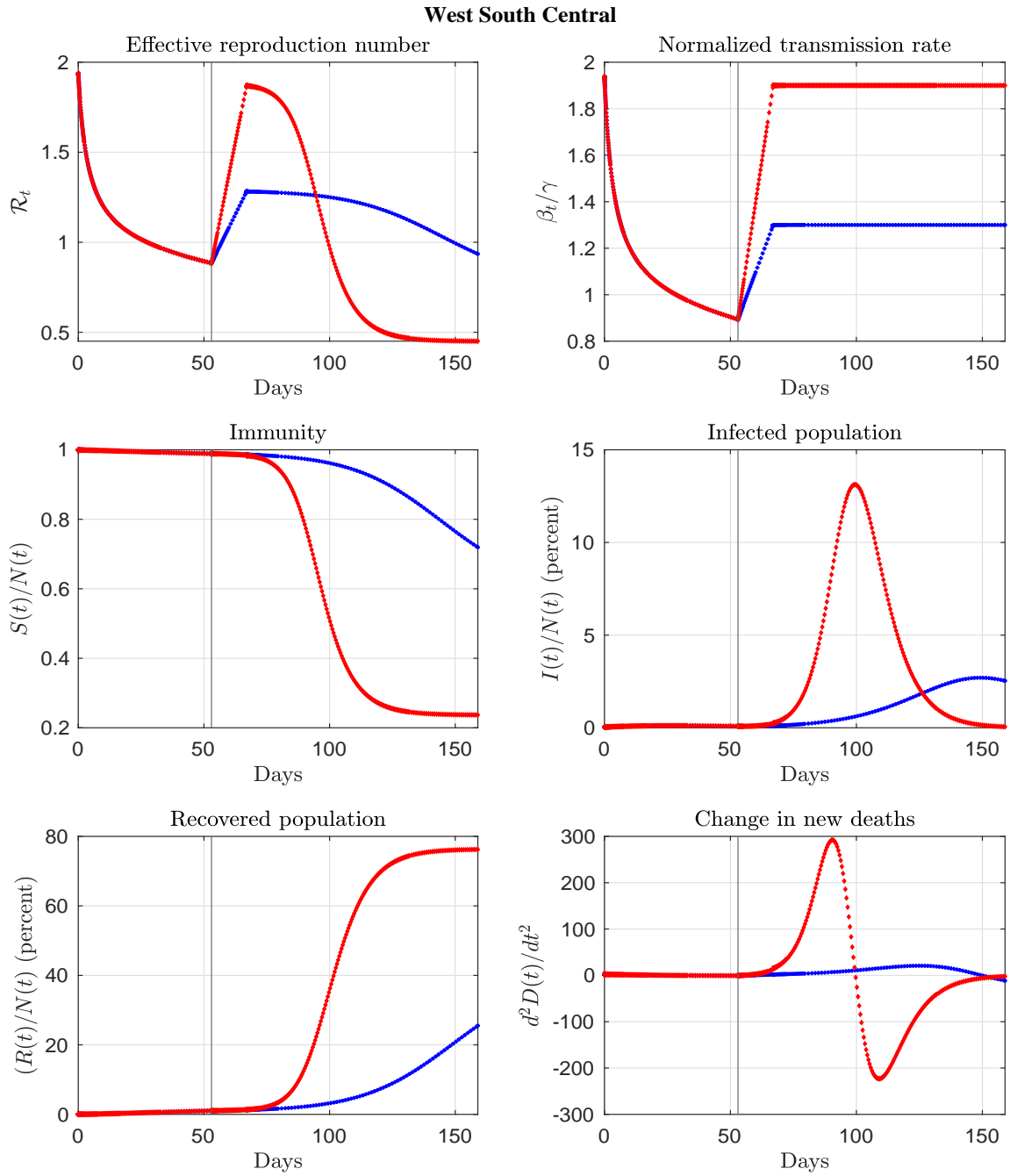**Figure 6:** Estimated and forecast deaths for New Jersey. The vertical line marks the end of the sample.
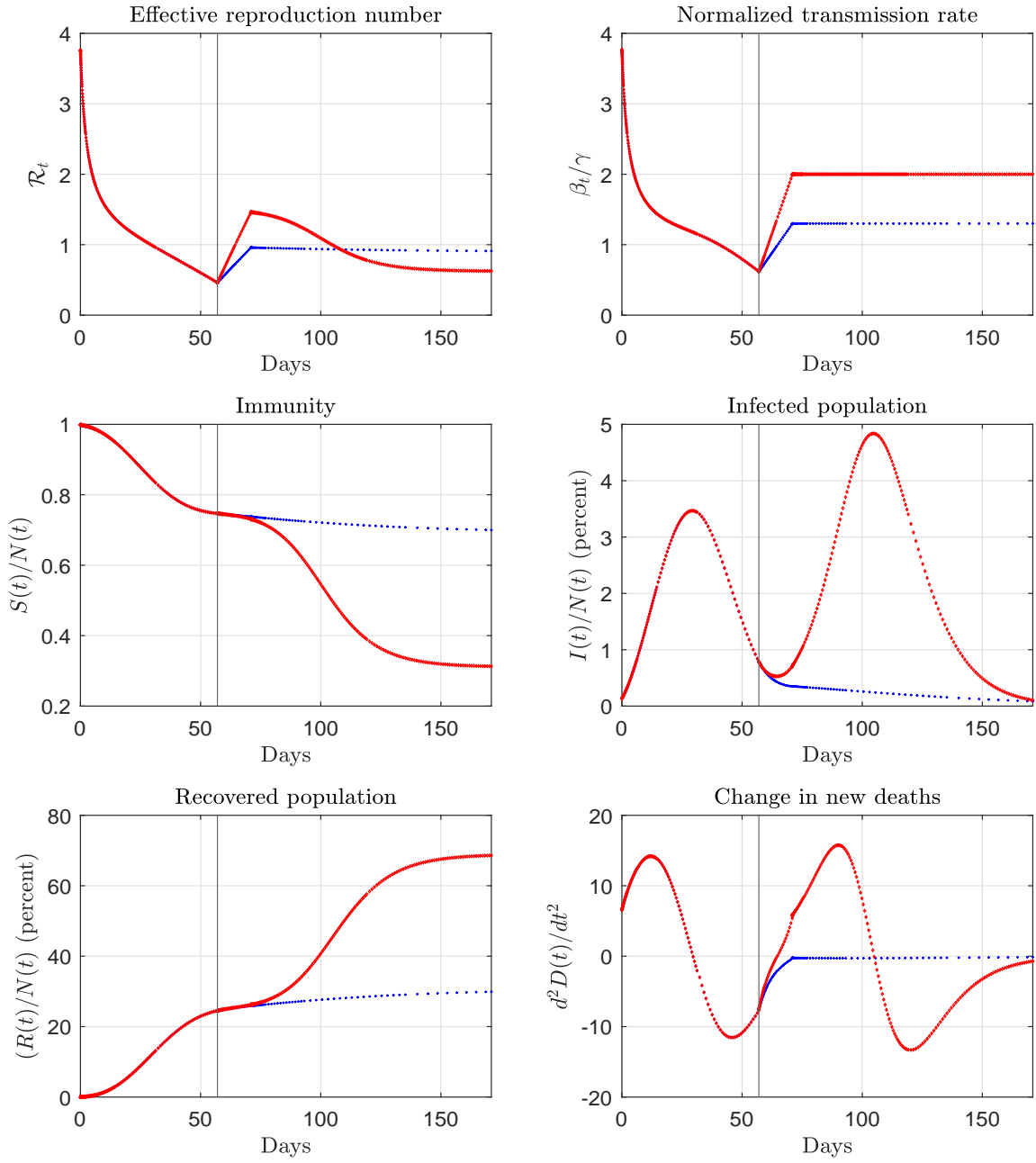
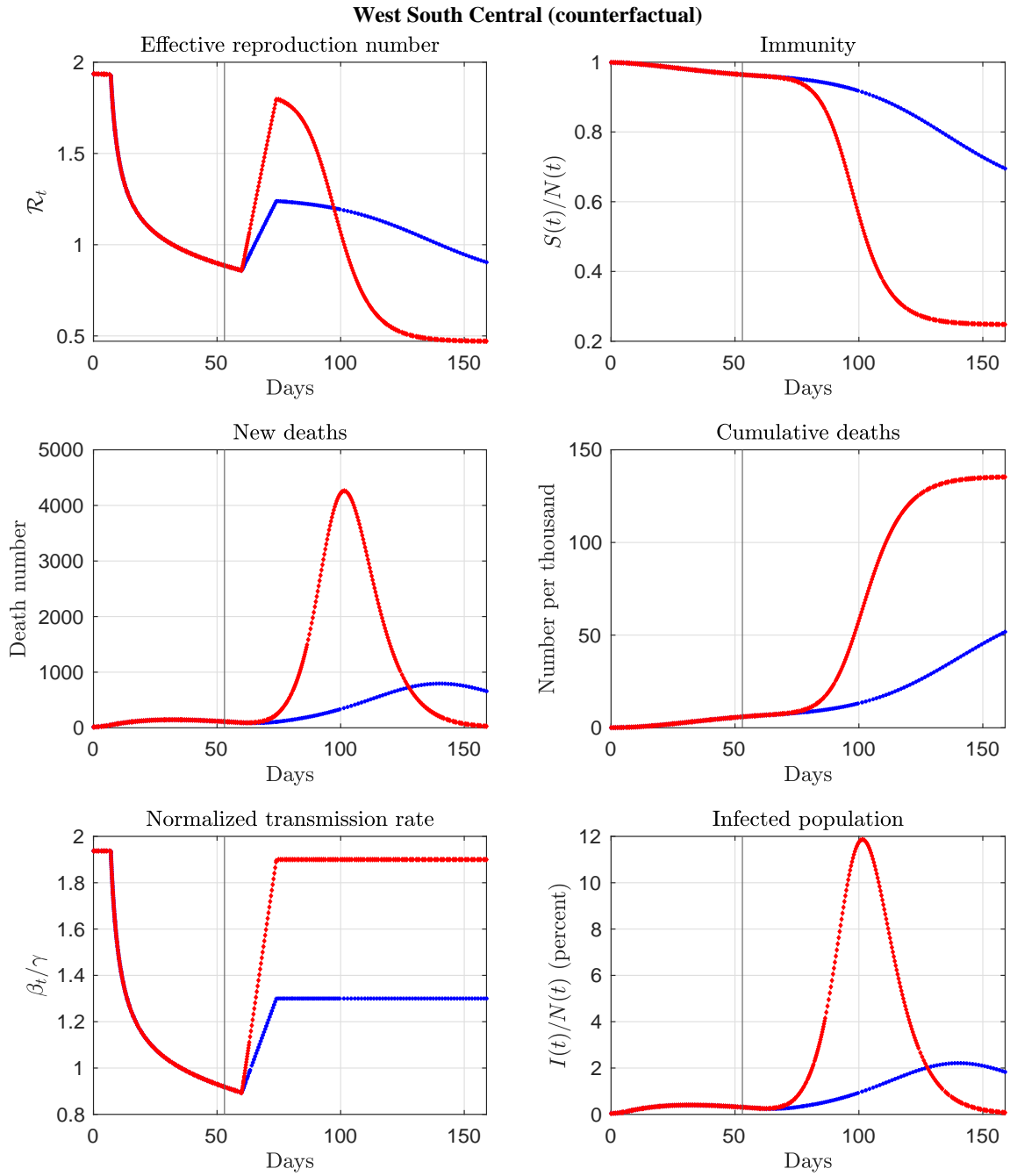**Figure 7:** Estimated and forecast paths for New Jersey. The vertical line marks the end of the sample.

41

New Jersey (counterfactual)
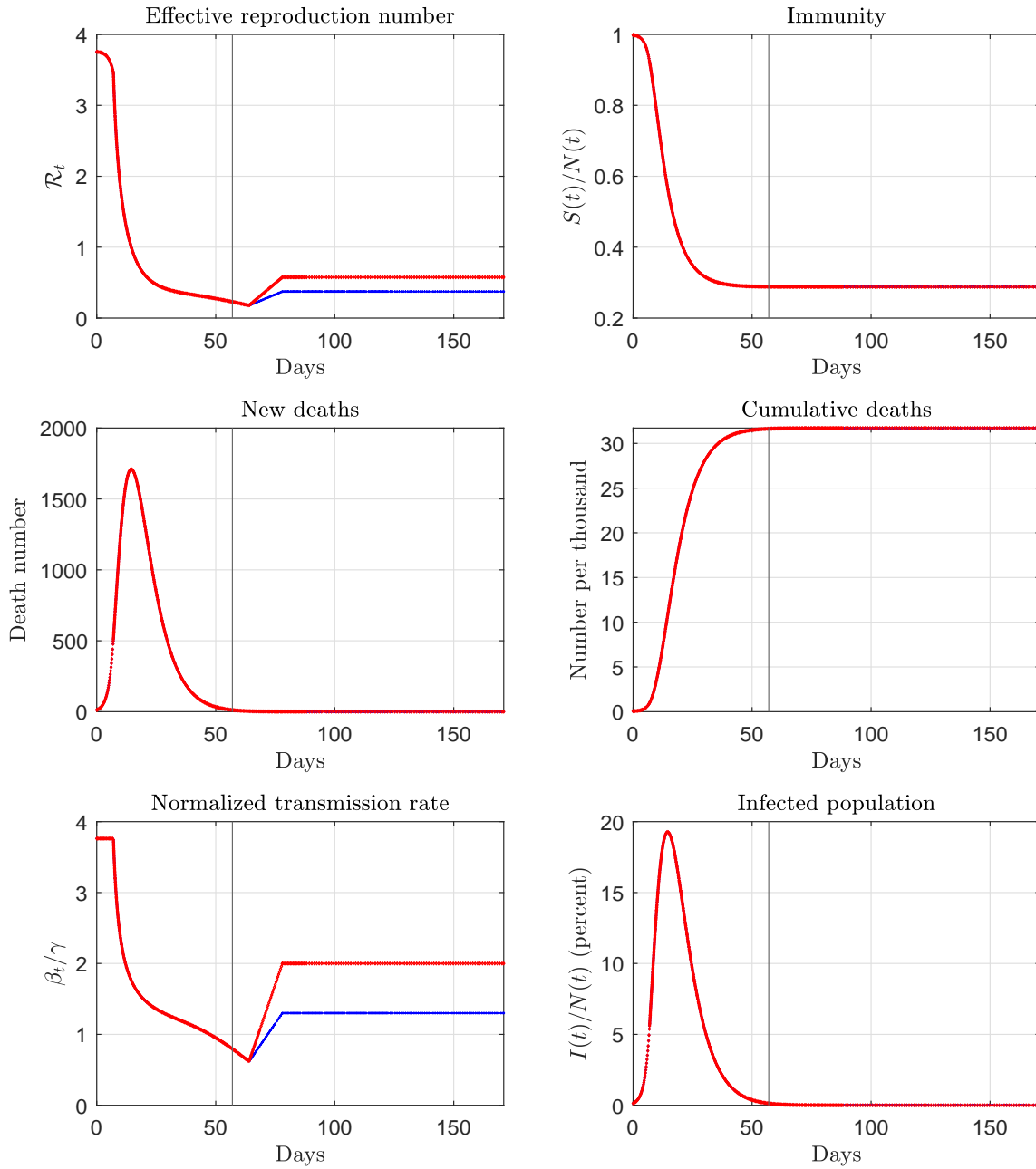
Figure 8: Counterfactual paths for New Jersey. The vertical line marks the end of the sample.
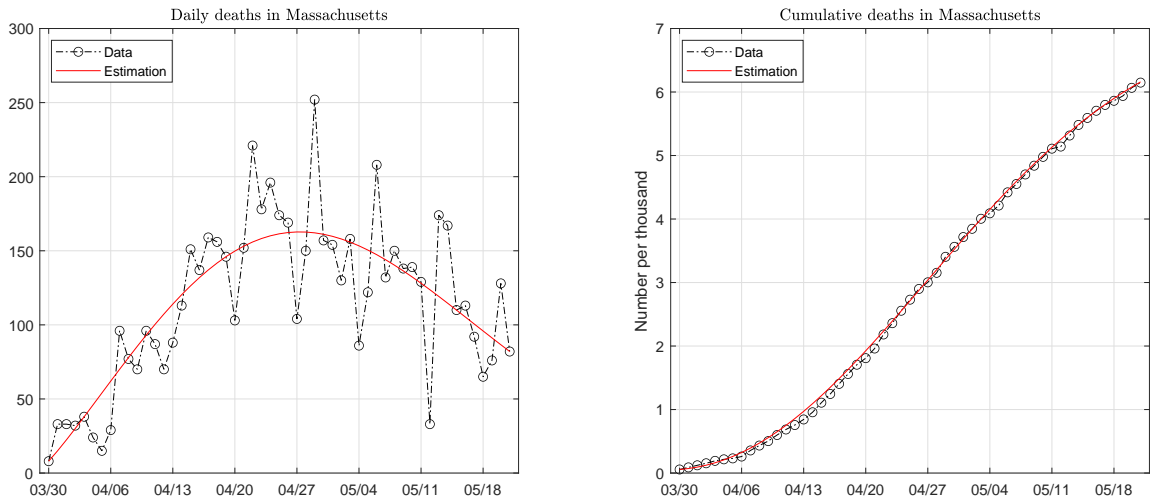
Figure 9: Data and fitted paths of deaths in Massachusetts. The death pattern is fitted with one Weibull function.
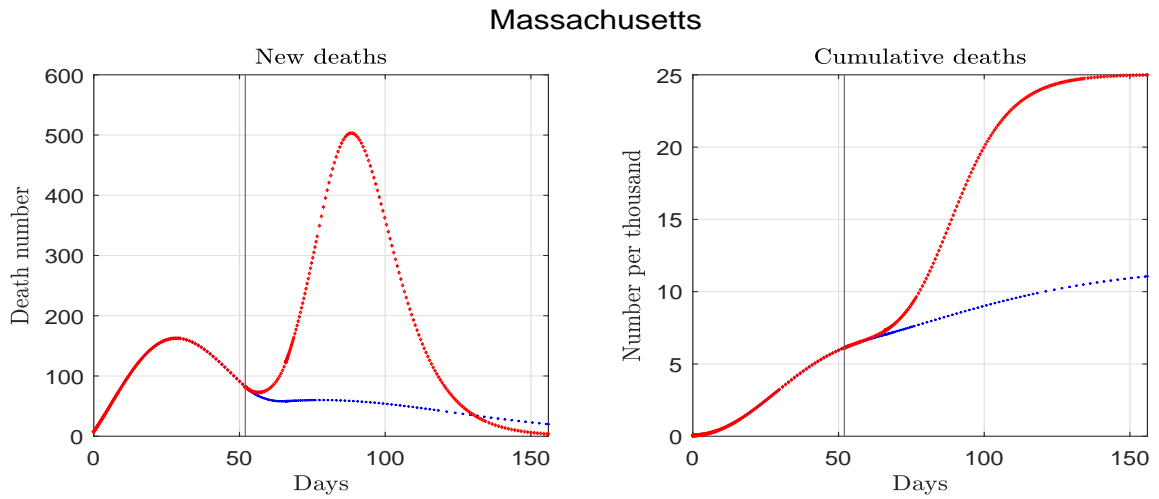
Figure 10: Estimated and forecast deaths for Massachusetts. The vertical line marks the end of the sample.

Massachusetts
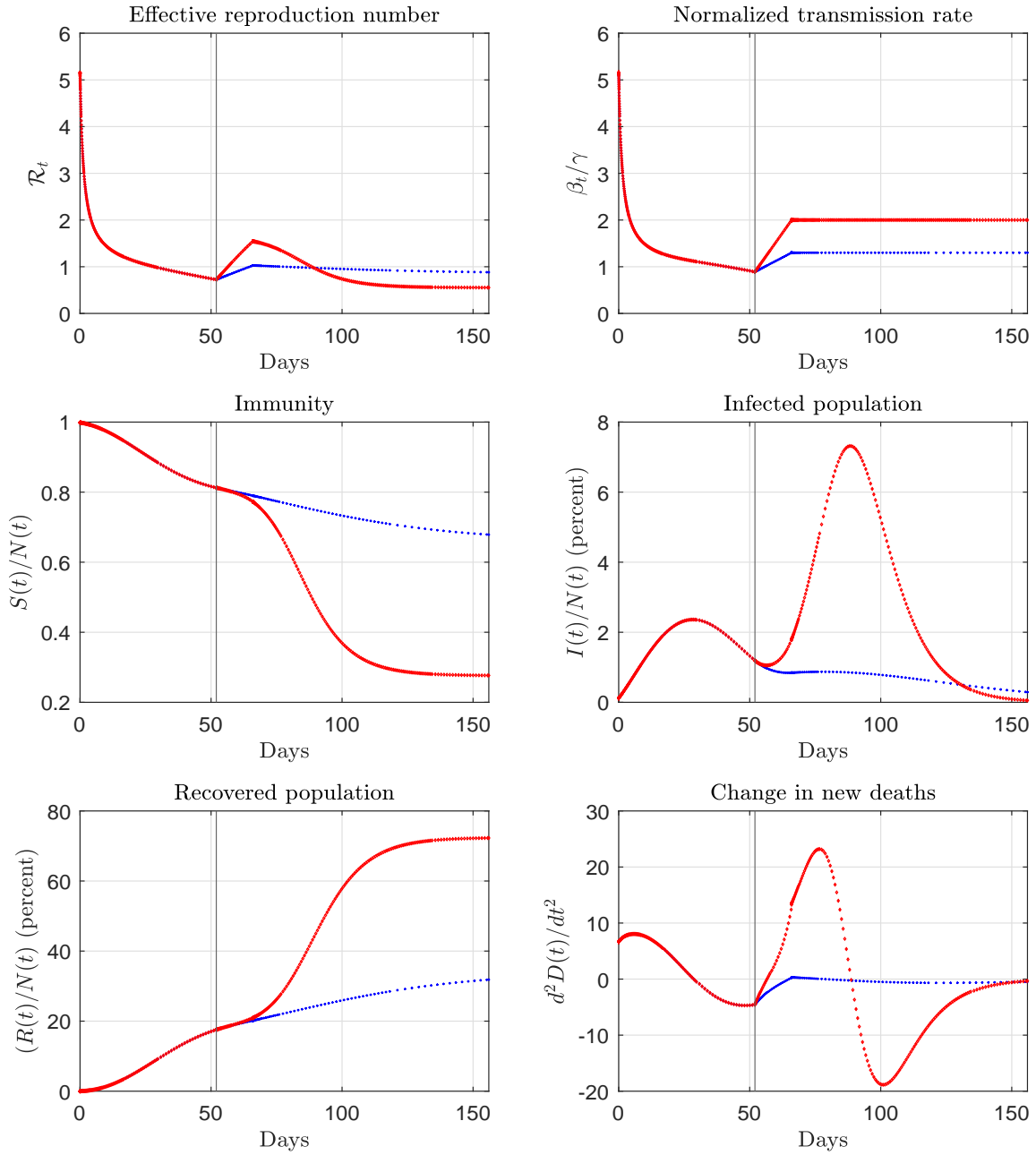
Figure 11: Estimated and forecast paths for Massachusetts. The vertical line marks the end of the sample.

44
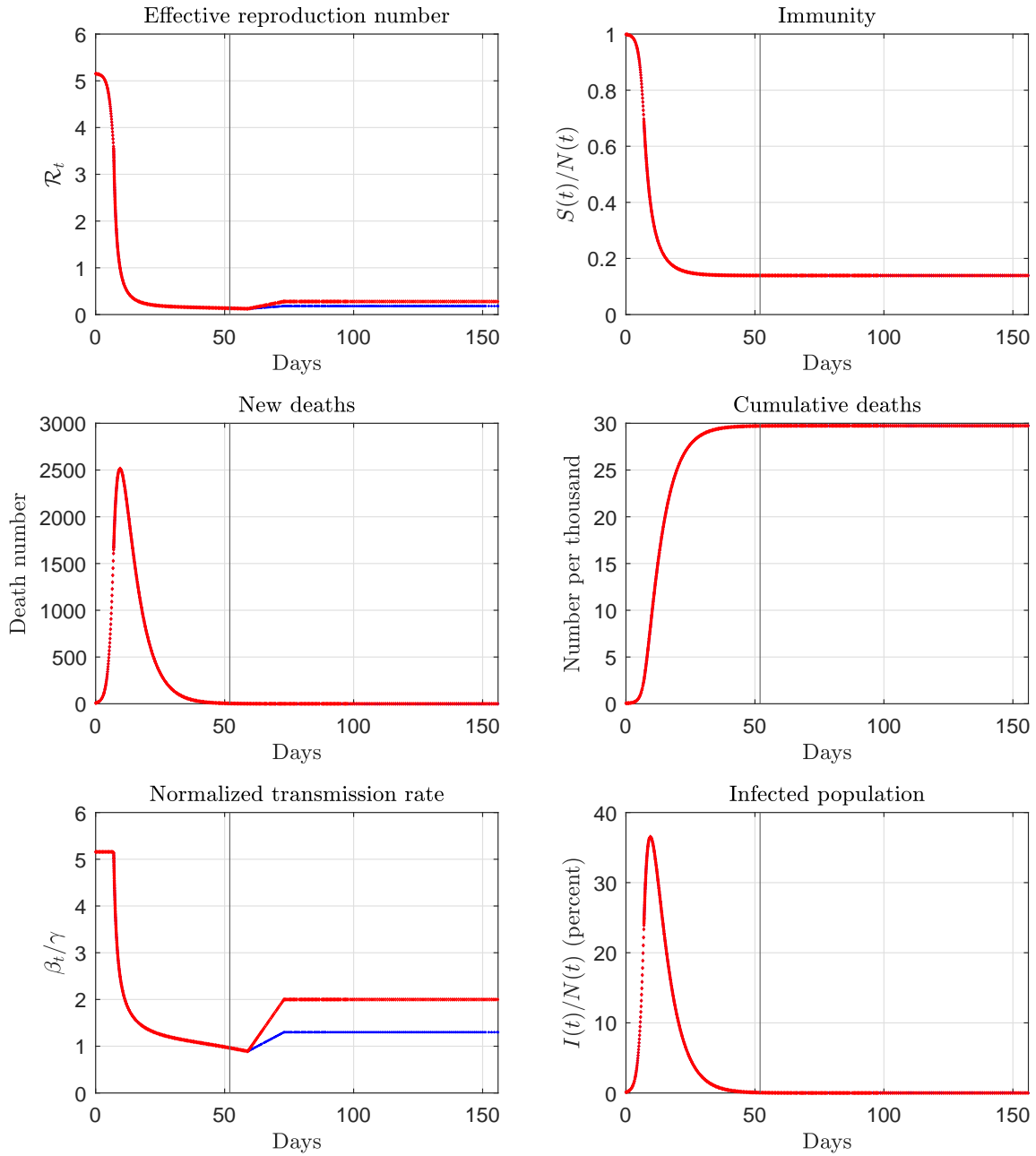
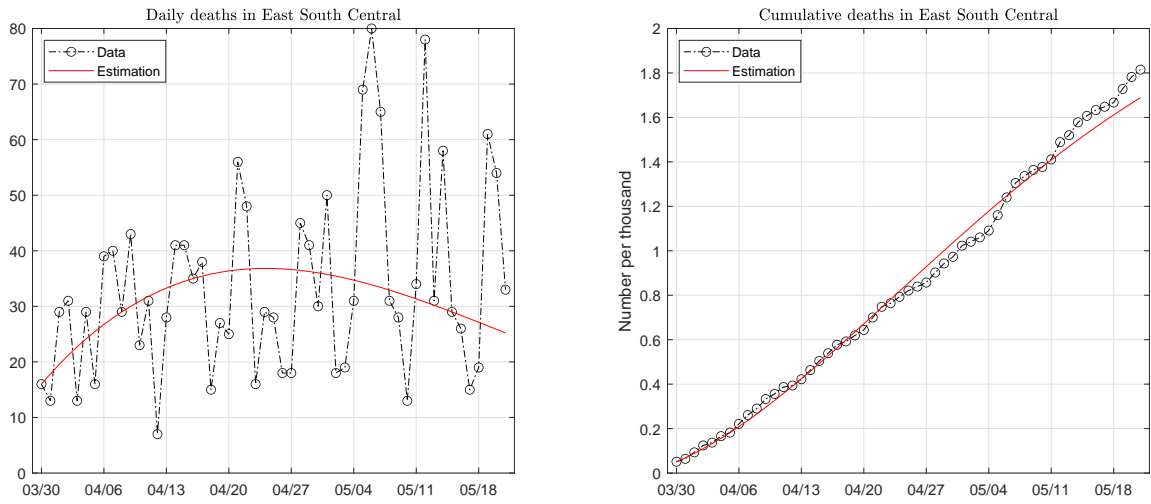**Figure 12:** Counterfactual paths for Massachusetts. The vertical line marks the end of the sample.
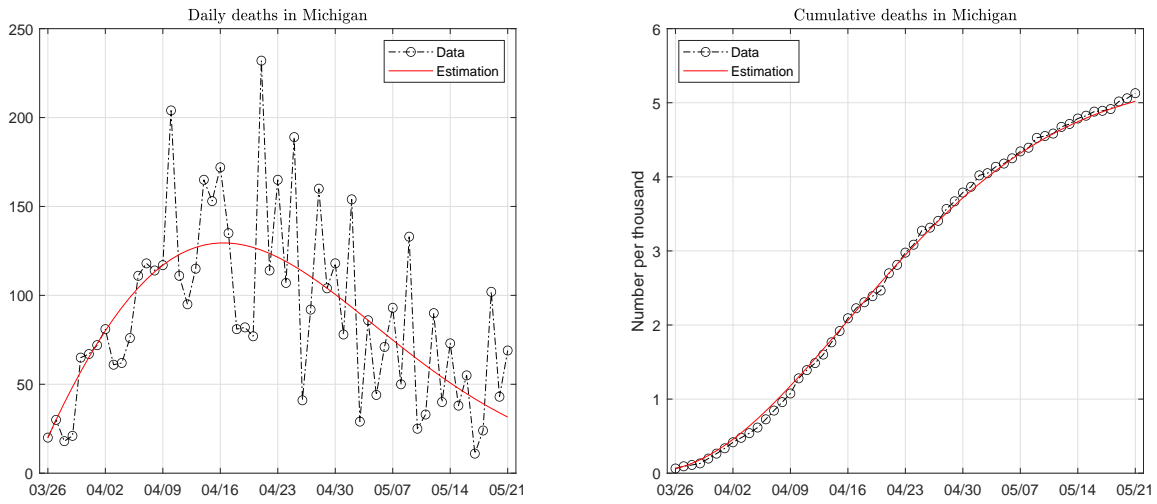
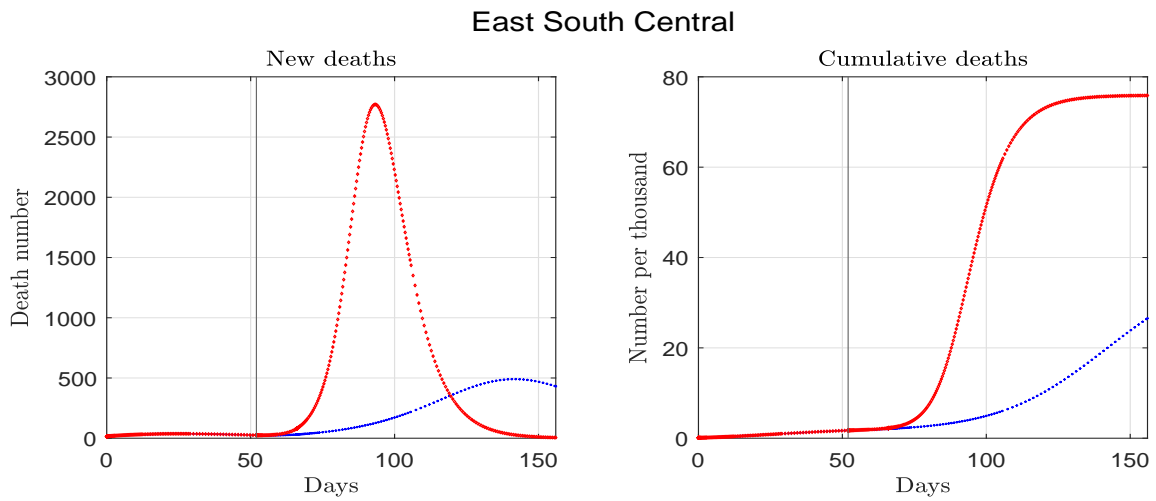**Figure 13:** Data and fitted paths of deaths in Michigan. The death pattern is fitted with one Weibull function.
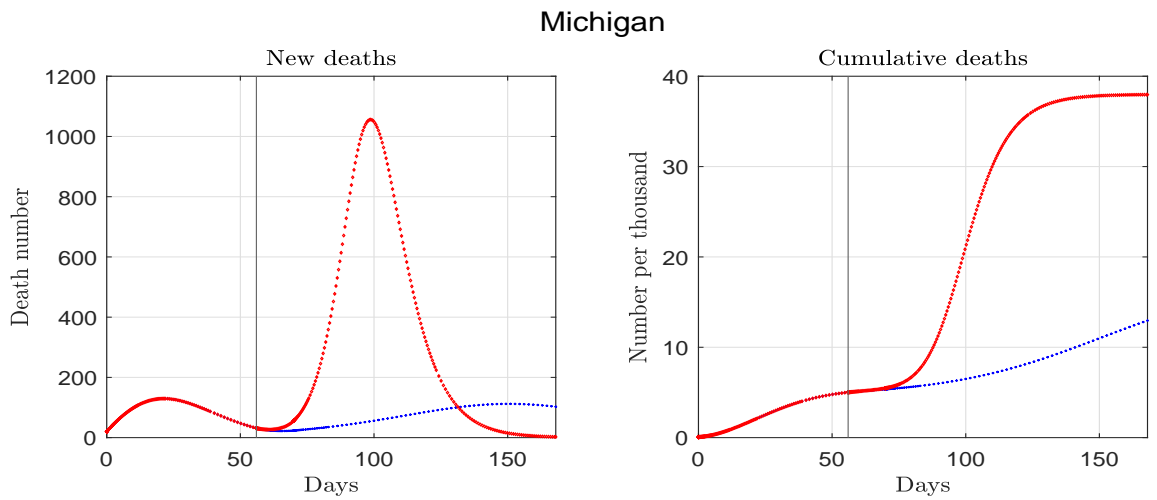
Figure 14: Estimated and forecast deaths for Michigan. The vertical line marks the end of the sample.

46
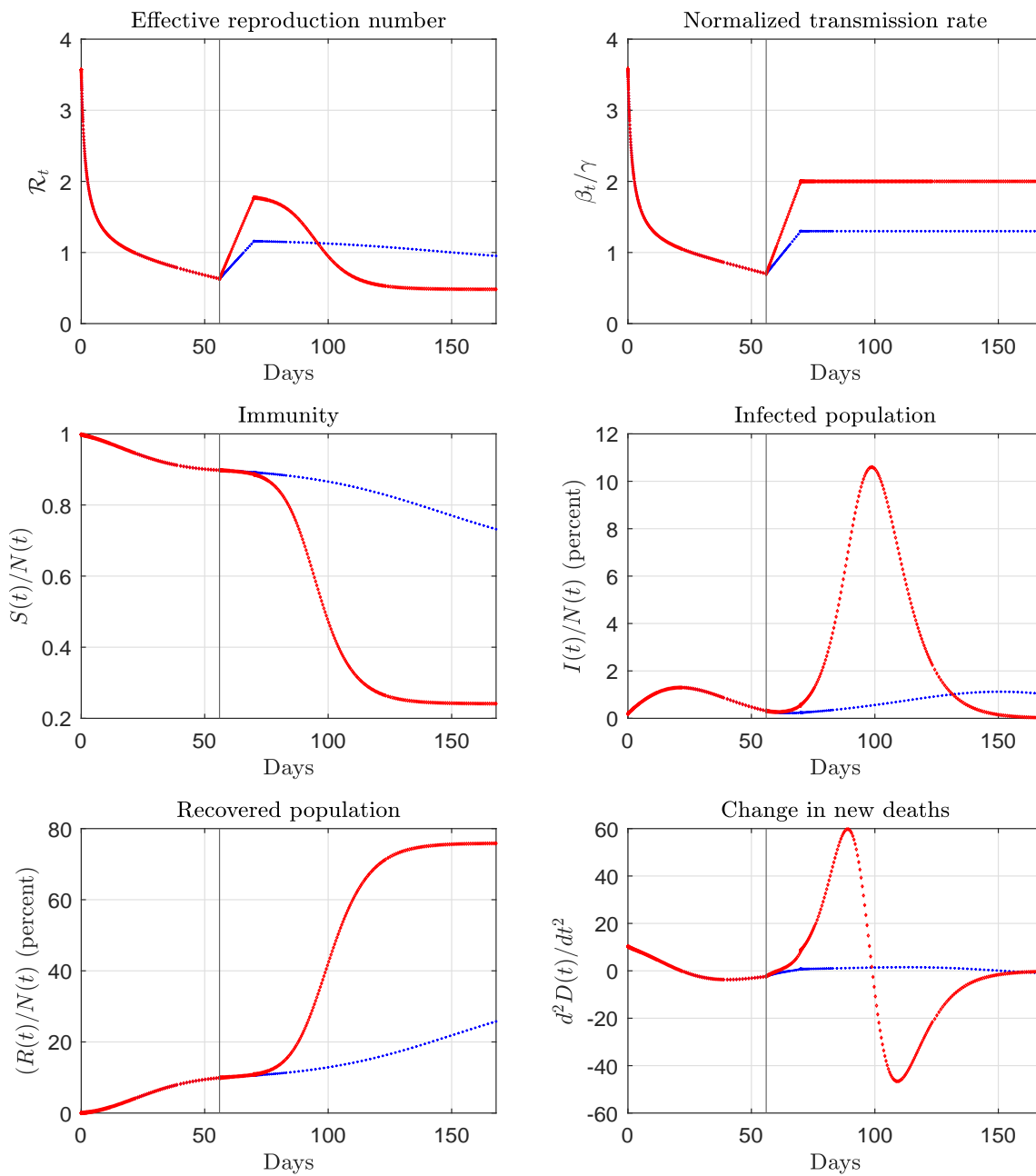
Michigan

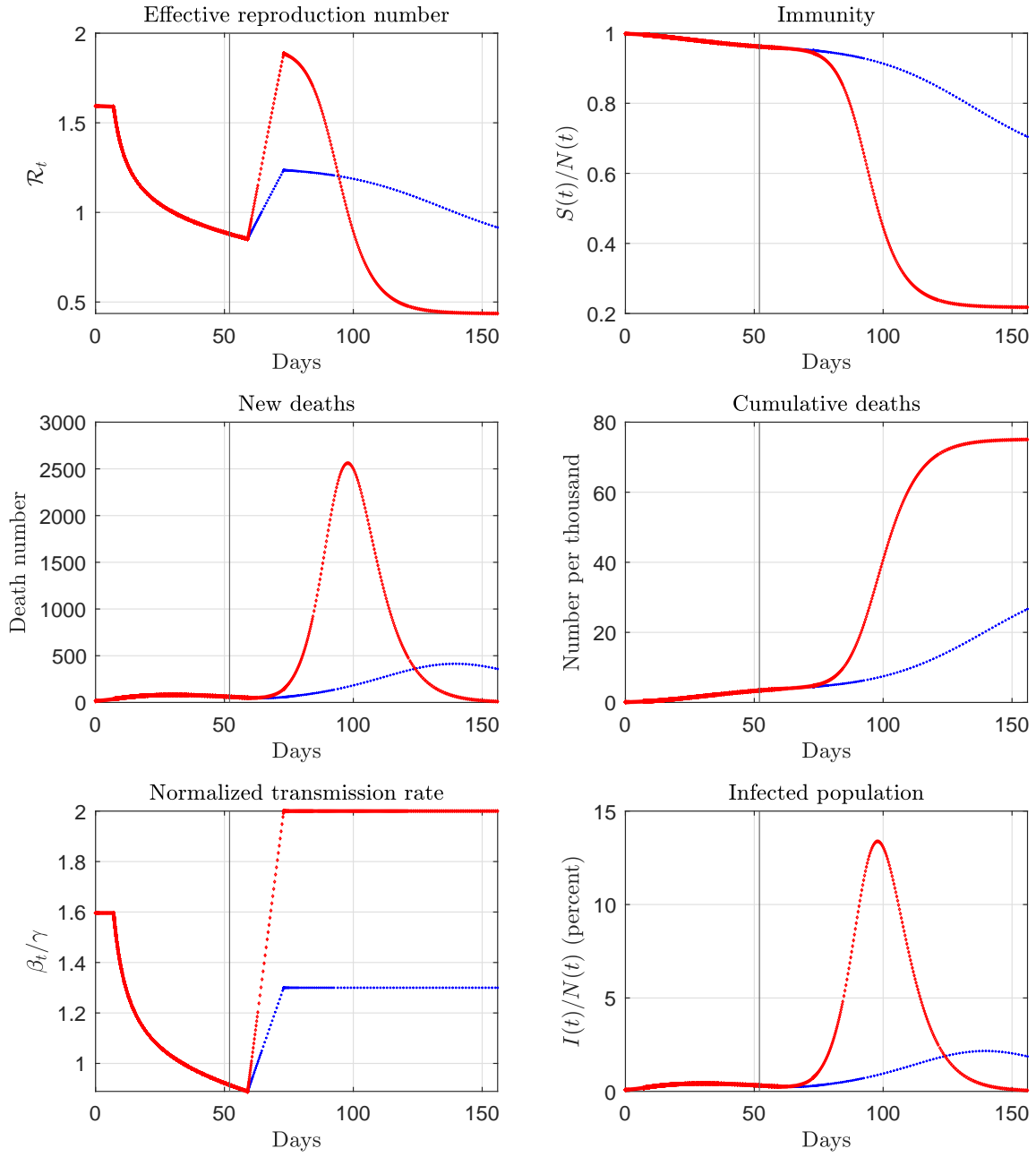**Figure 15:** Estimated and forecast paths for Michigan. The vertical line marks the end of the sample.
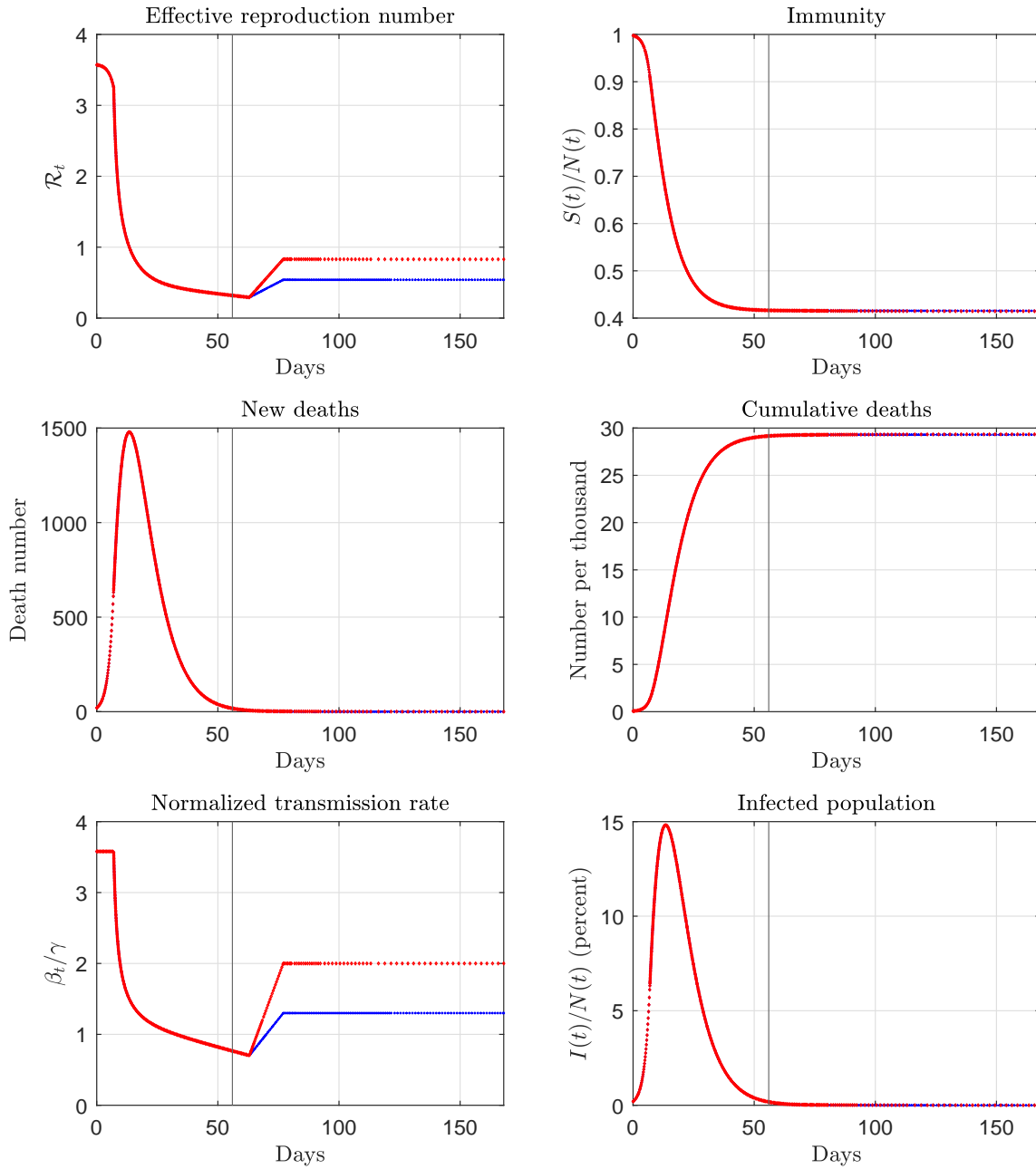
Figure 16: Counterfactual paths for Michigan. The vertical line marks the end of the sample.
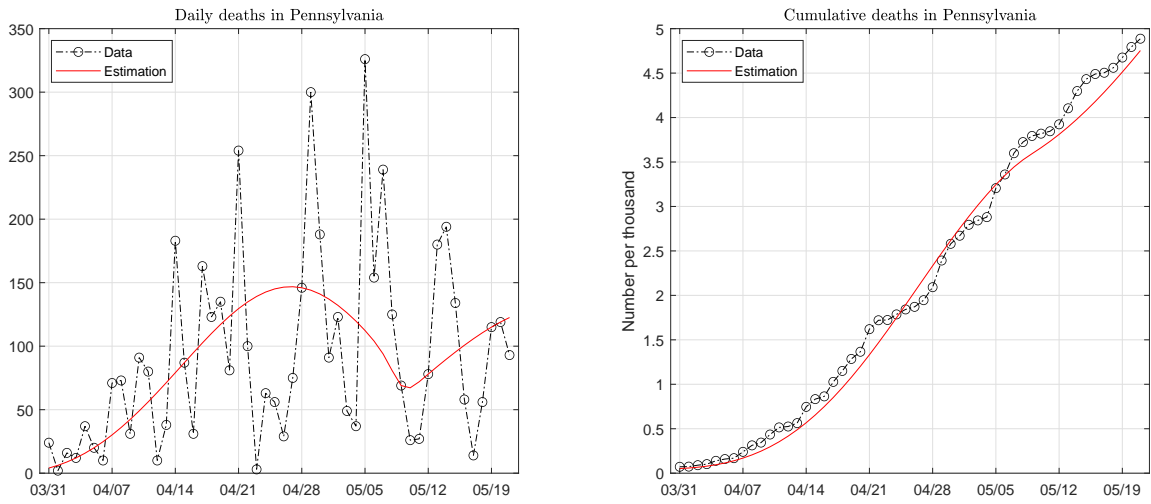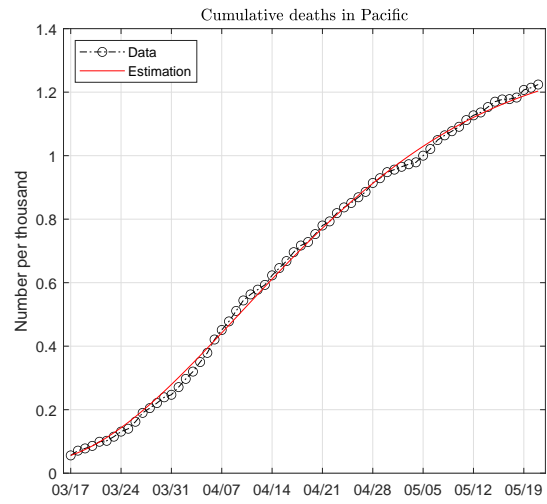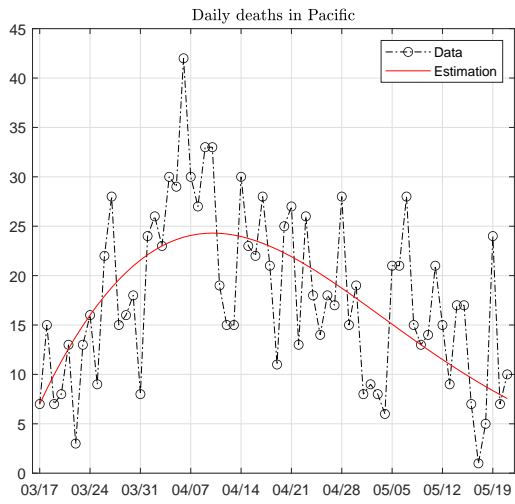
Figure 17: Data and fitted paths of deaths in Pennsylvania. The death pattern is fitted with two Weibull functions.
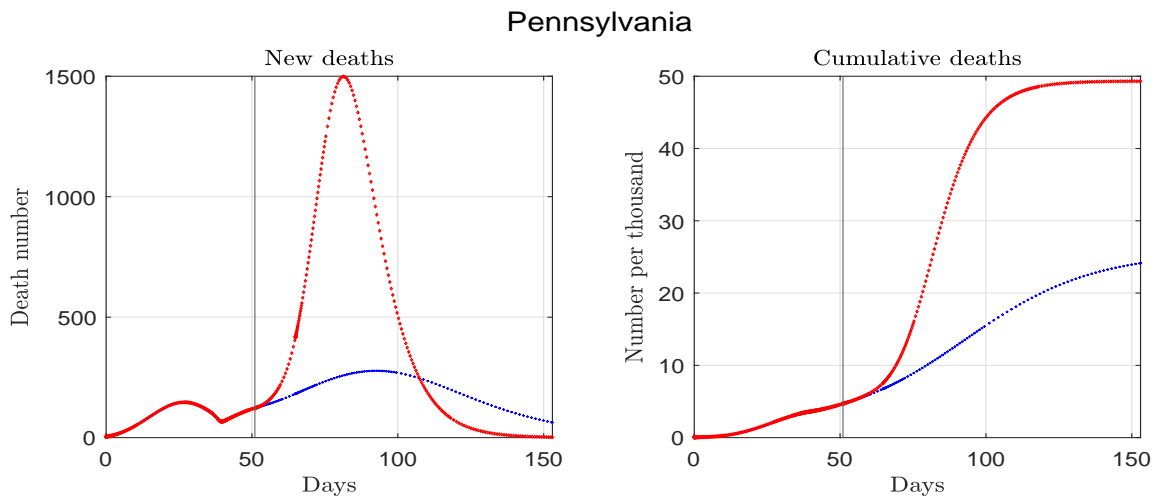
Figure 18: Estimated and forecast deaths for Pennsylvania. The vertical line marks the end of the sample.

Pennsylvania
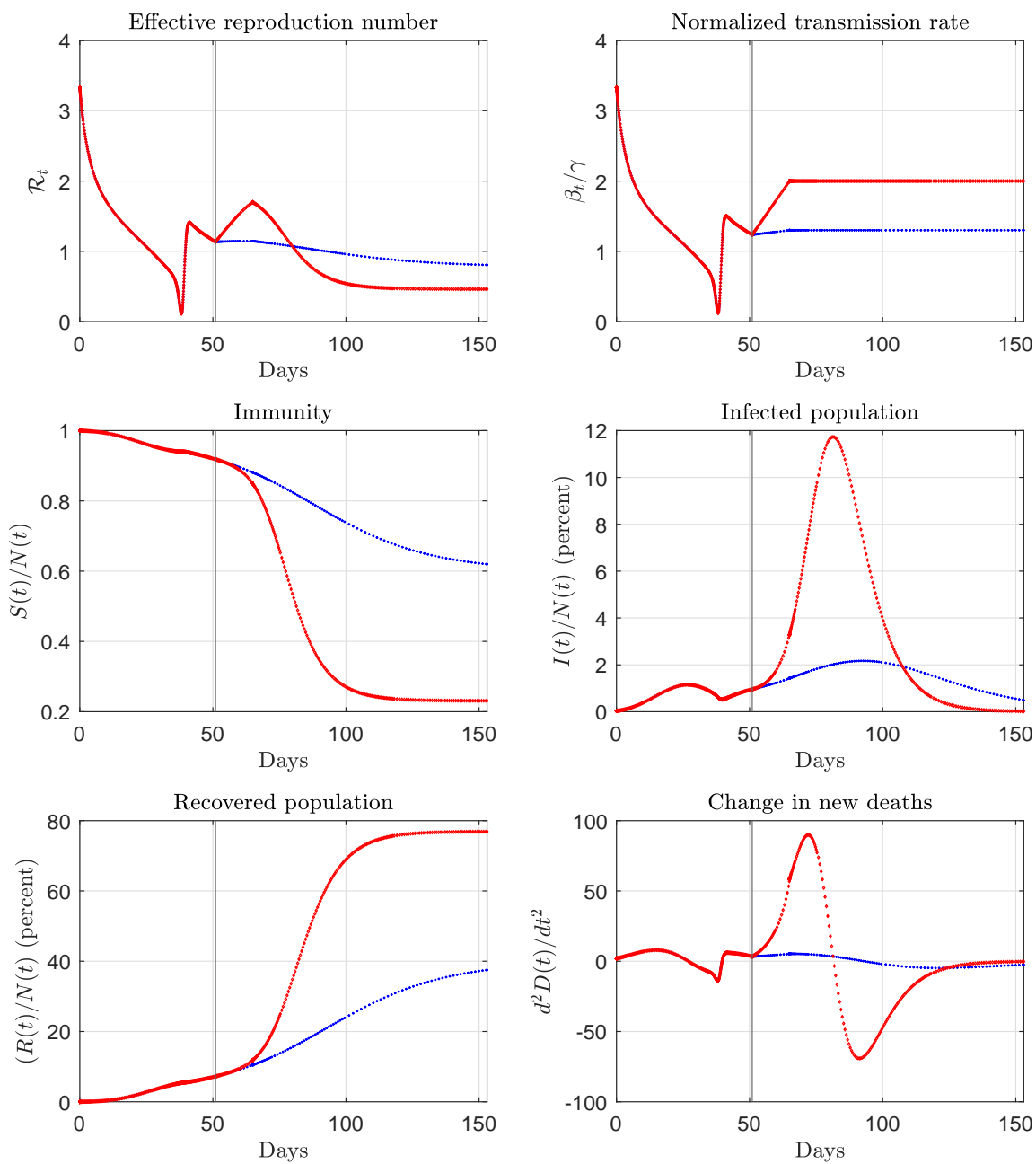
Figure 19: Estimated and forecast paths for Pennsylvania. The vertical line marks the end of the sample.
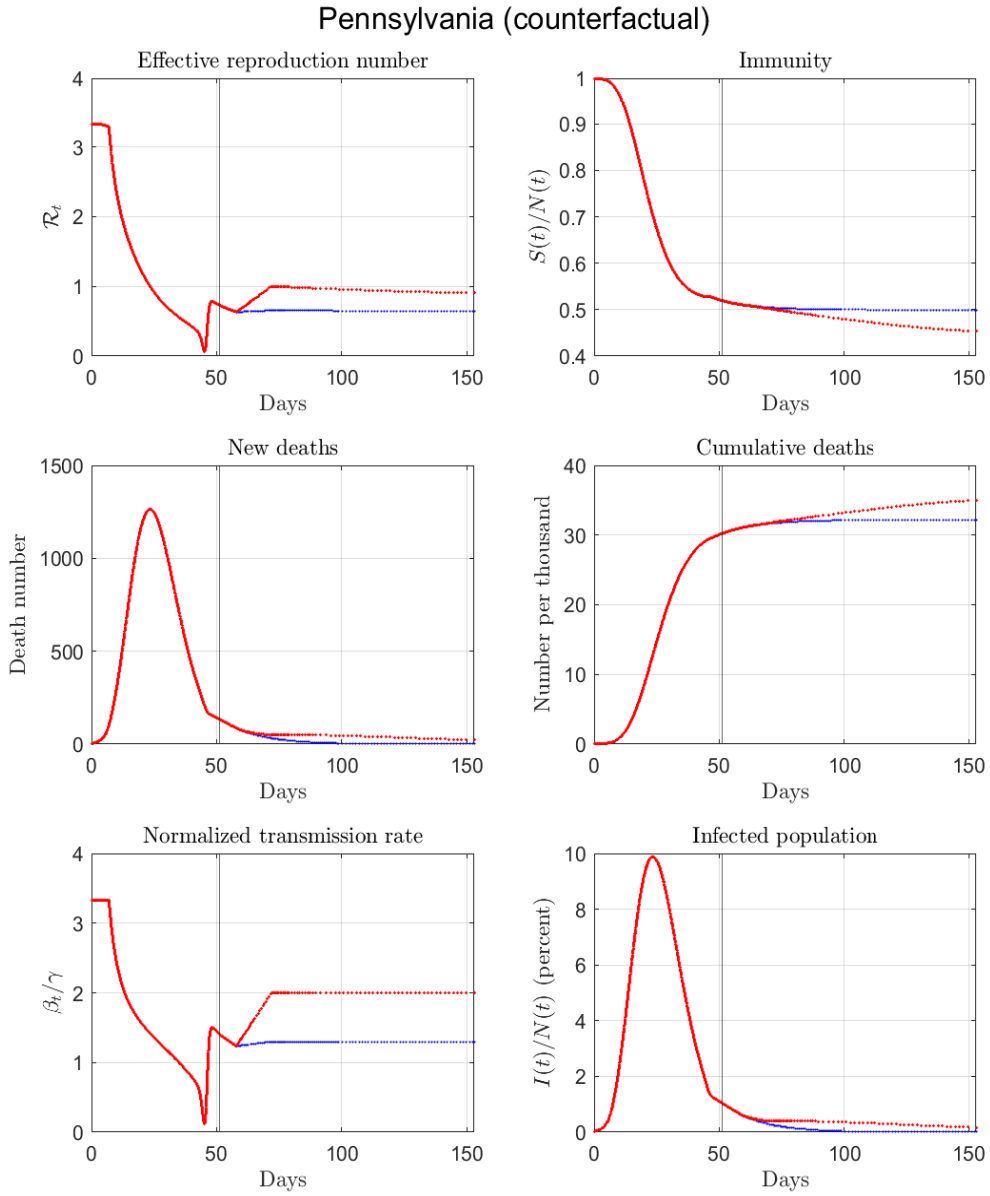
Figure 20: Counterfactual paths for Pennsylvania. The vertical line marks the end of the sample.

51
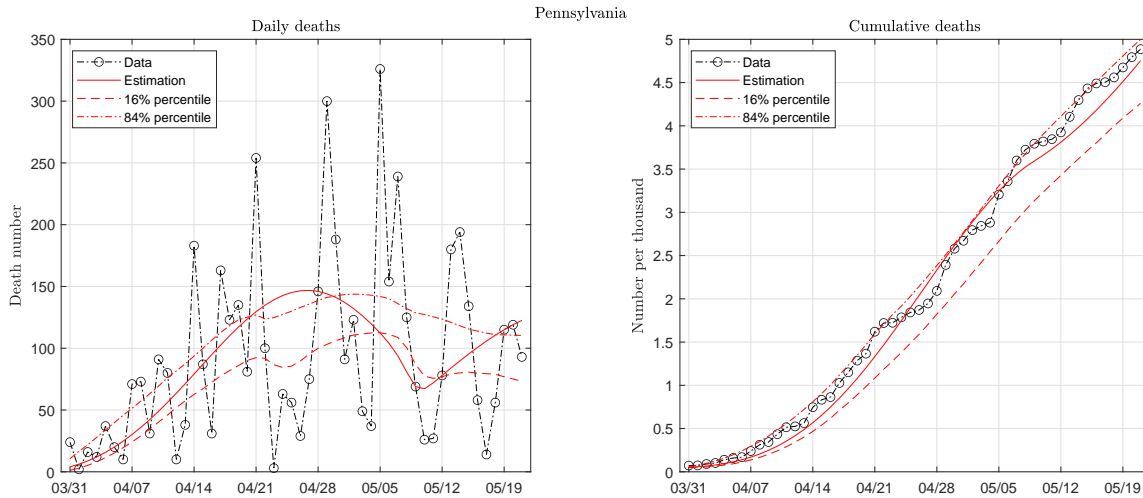
**Figure 21:** Data and fitted paths of deaths in Pennsylvania. The death pattern is fitted with two Weibull functions. The solid curve represents the estimated path at the posterior peak. The 68% probability bands are represented by the dashed curve (the 16% percentile) and the dash-dotted curve (the 84% percentile)

52
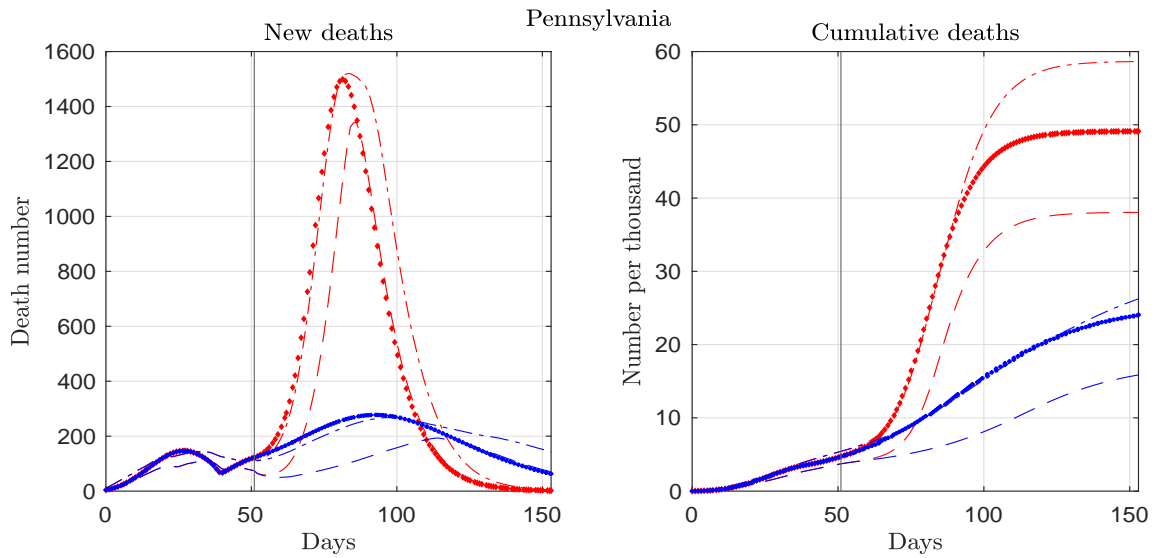
Figure 22: Death paths with uncertainty bands under the two scenarios for the normalized transmission rate during the forecast period. The vertical line marks the end of the sample. The star or diamond curve represents the path estimated at the posterior peak. The 68% probability bands are represented by the dashed curve (the 16% percentile) and the dash-dotted curve (the 84% percentile)
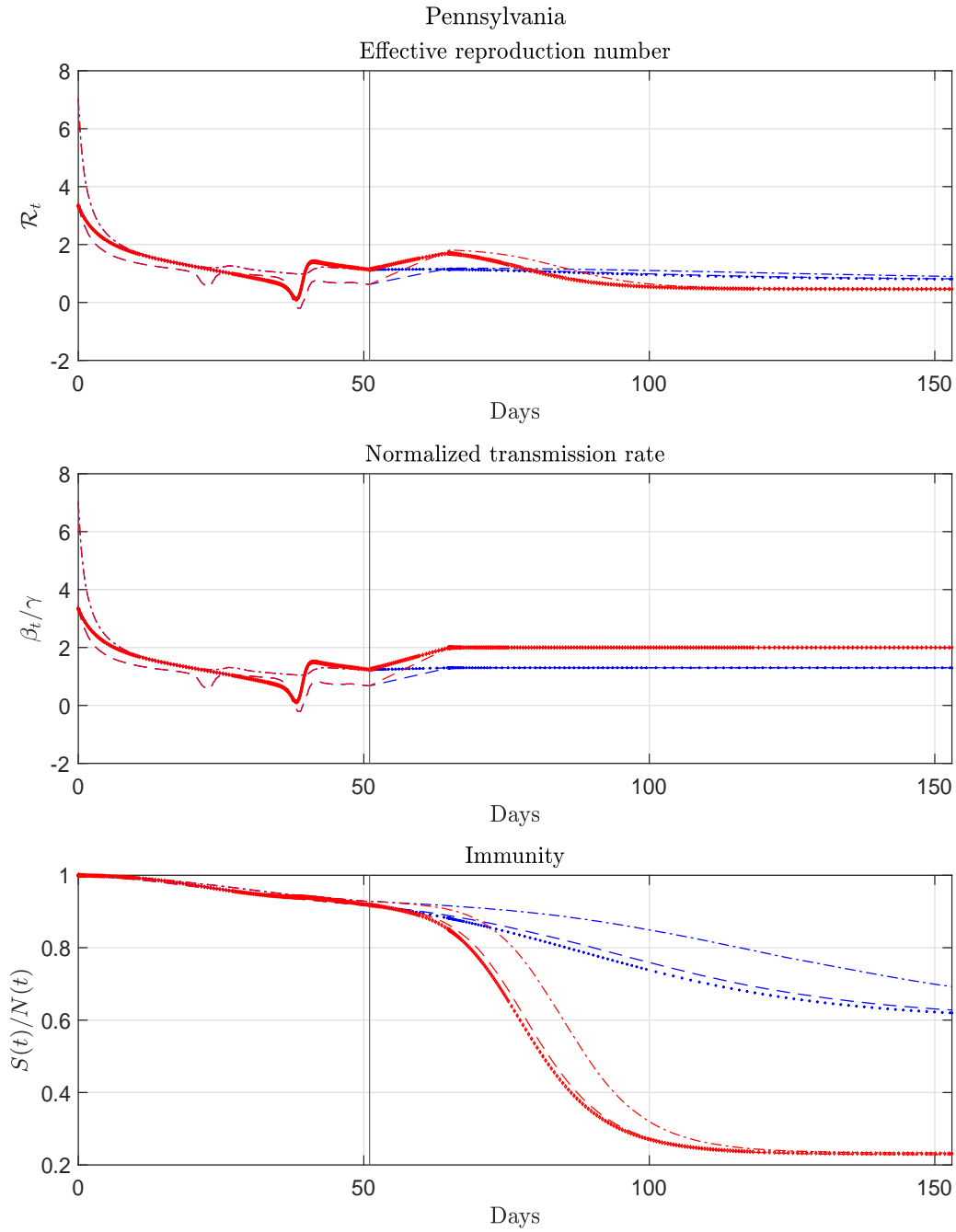
Figure 23: Estimated and forecast paths with uncertainty bands under the two scenarios for the normalized transmission rate during the forecast period. The vertical line marks the end of the sample. The star or diamond curve represents the path estimated at the posterior peak. The 68% probability bands are represented by the dashed curve (the 16% percentile) and the dash-dotted curve (the 84% percentile)
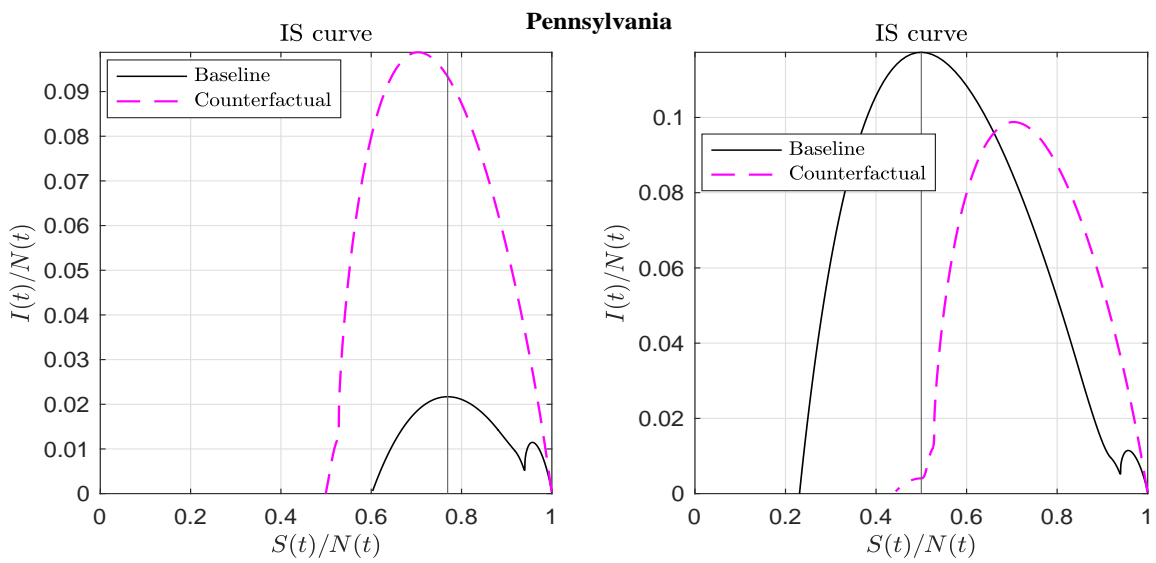
Figure 24: The IS curves under the two forecast scenarios with an initial delay of 7 days.
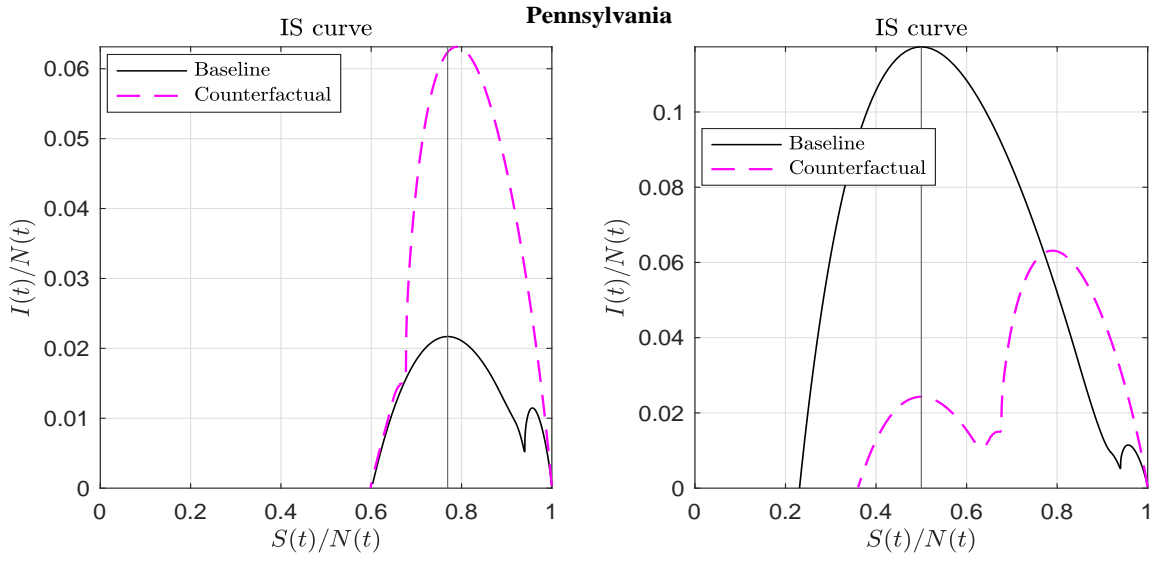
Figure 25: The IS curves under the two forecast scenarios with an initial delay of 5 days.
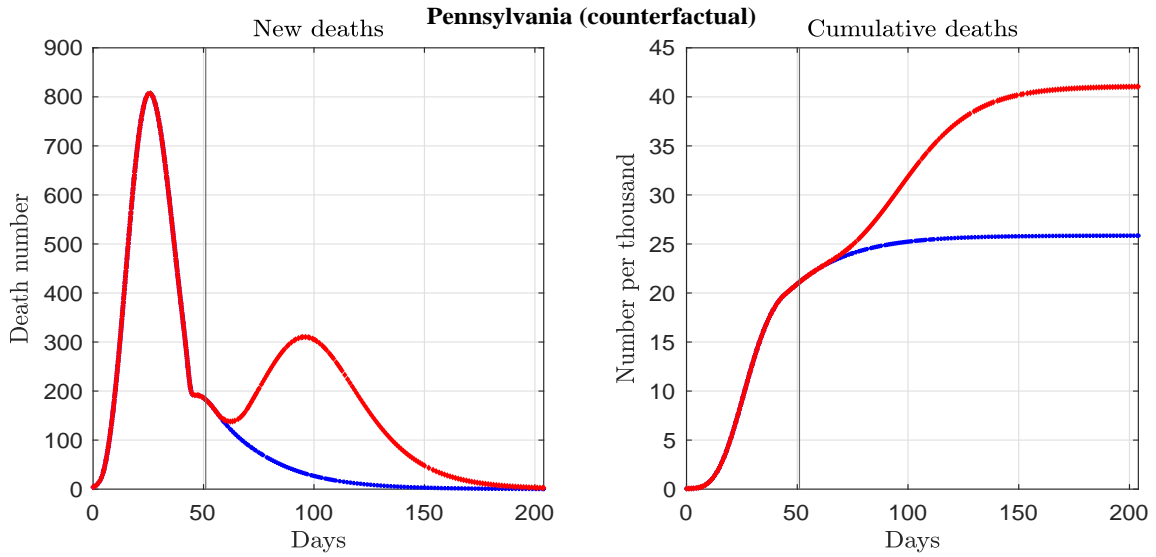
Figure 26: The counterfactual death paths under two forecast scenarios with an initial delay of 5 days. The vertical line marks the end of the sample.
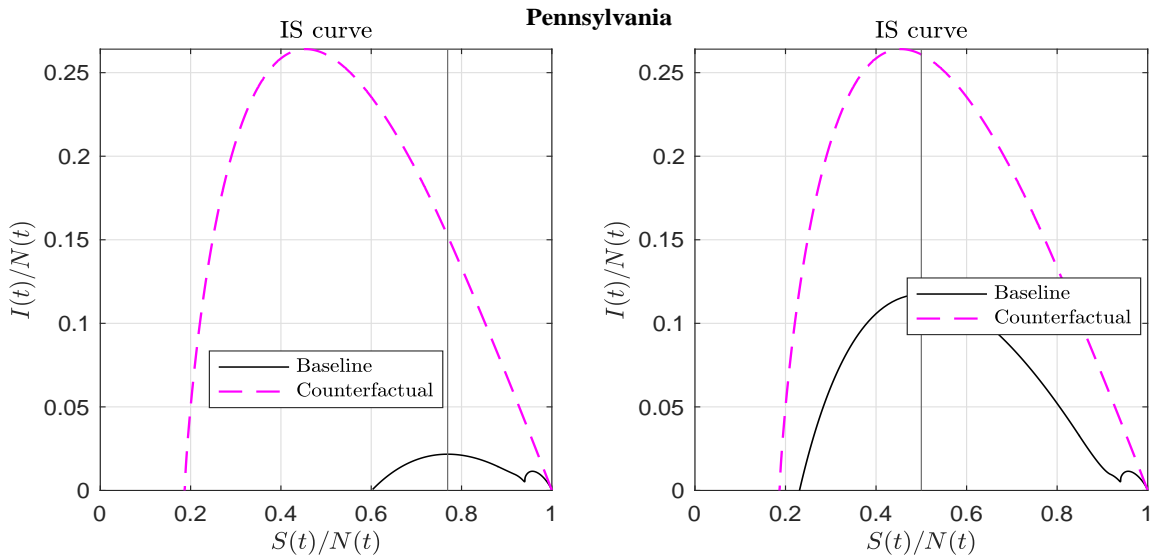
Figure 27: The IS curves under the two forecast scenarios with an initial delay of 14 days.
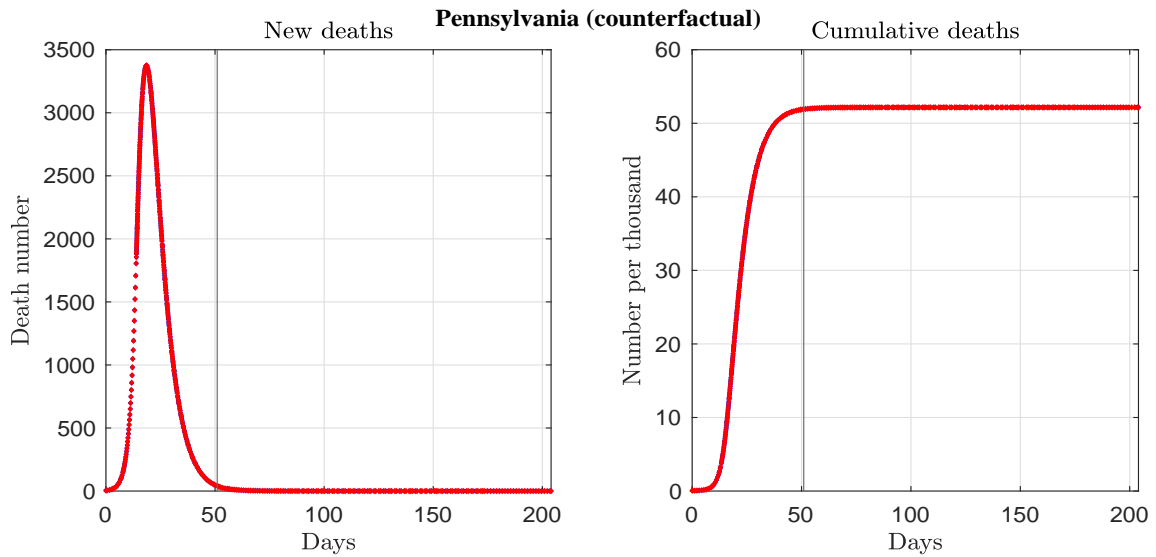
Figure 28: The counterfactual death paths under two forecast scenarios with an initial delay of 14 days. The vertical line marks the end of the sample. The red and blue curves are on top of each other so that it is almost indistinguishable by eye.

57
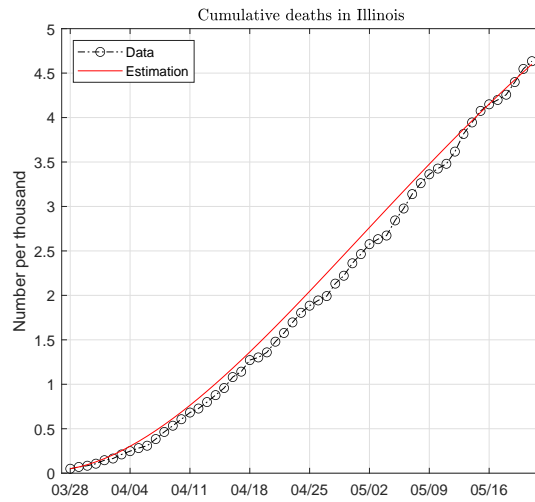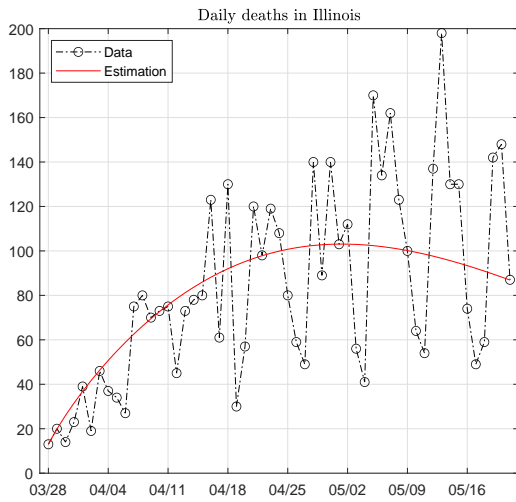
Figure 29: Data and fitted paths of deaths in Illinois. The death pattern is fitted with one Weibull function.
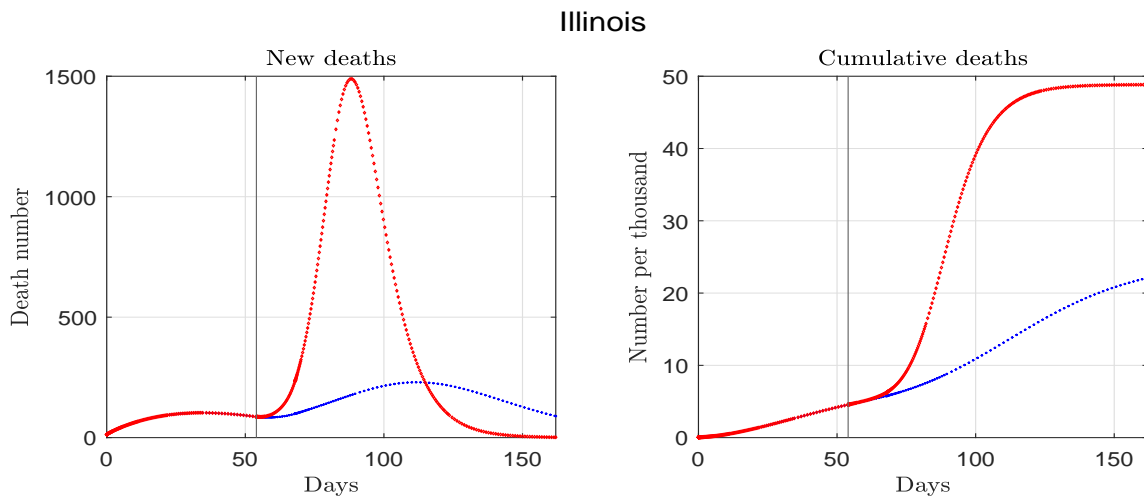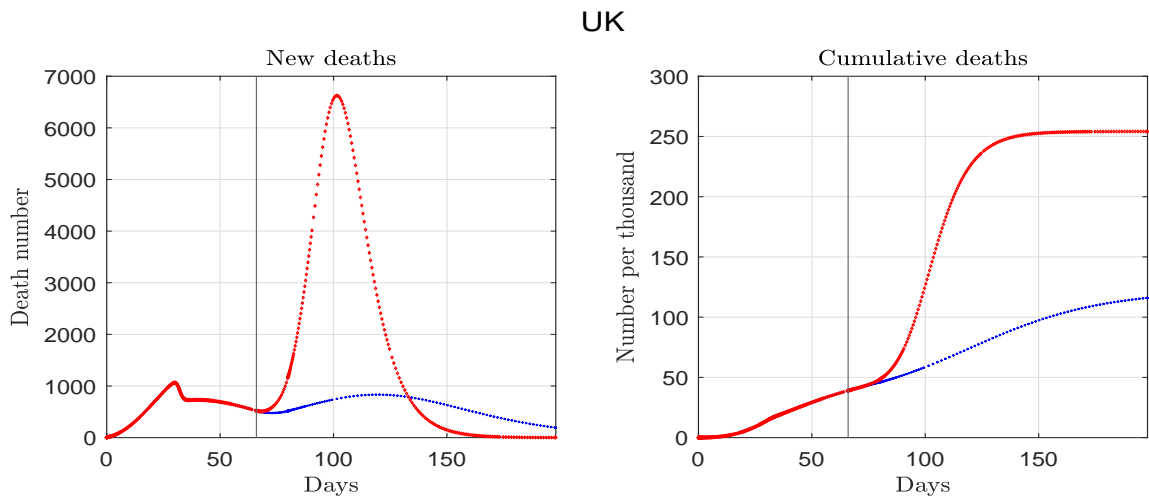

Figure 30: Estimated and forecast deaths for Illinois. The vertical line marks the end of the sample.

Illinois
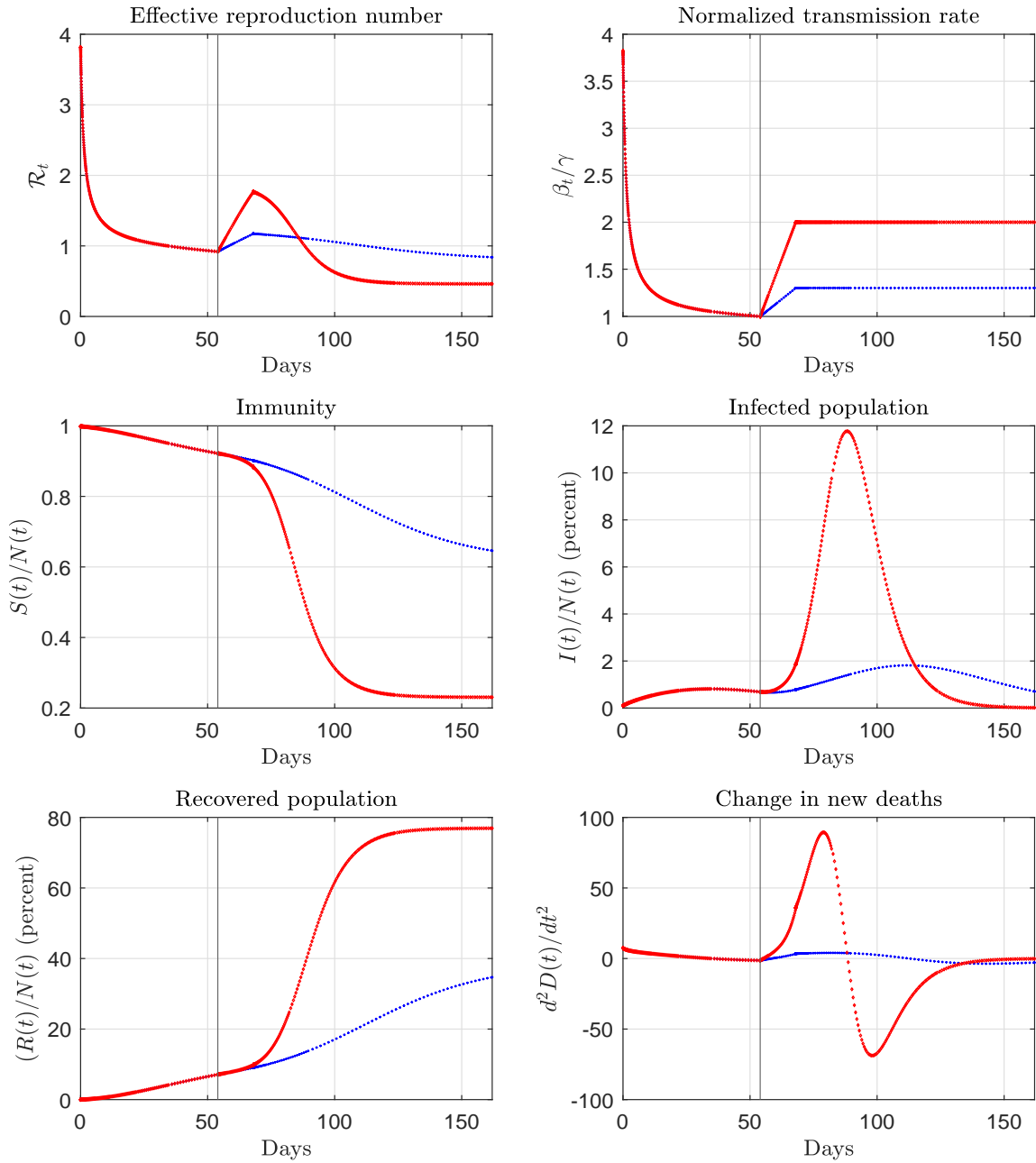
Figure 31: Estimated and forecast paths for Illinois. The vertical line marks the end of the sample.
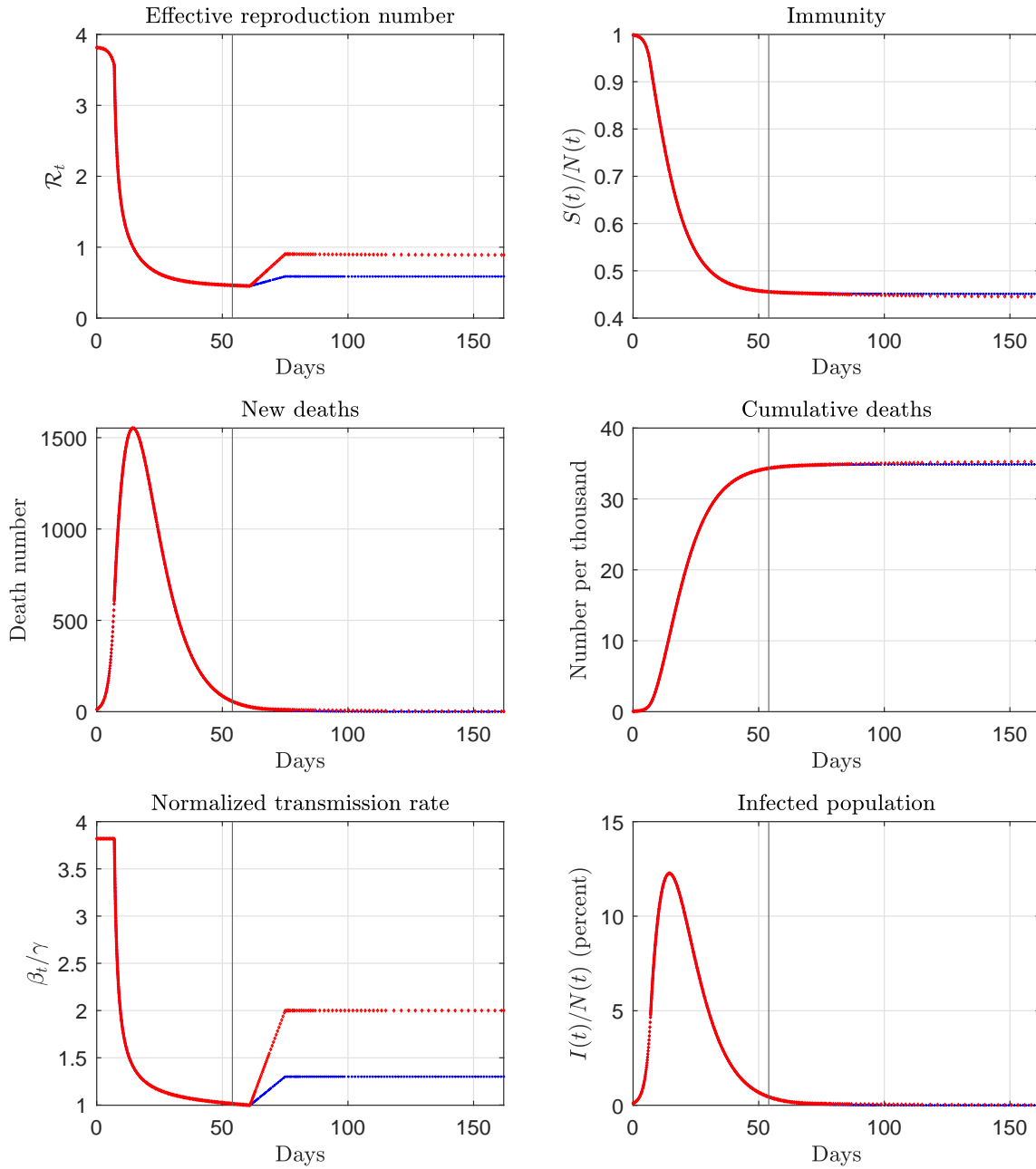
Figure 32: Counterfactual paths for Illinois. The vertical line marks the end of the sample.
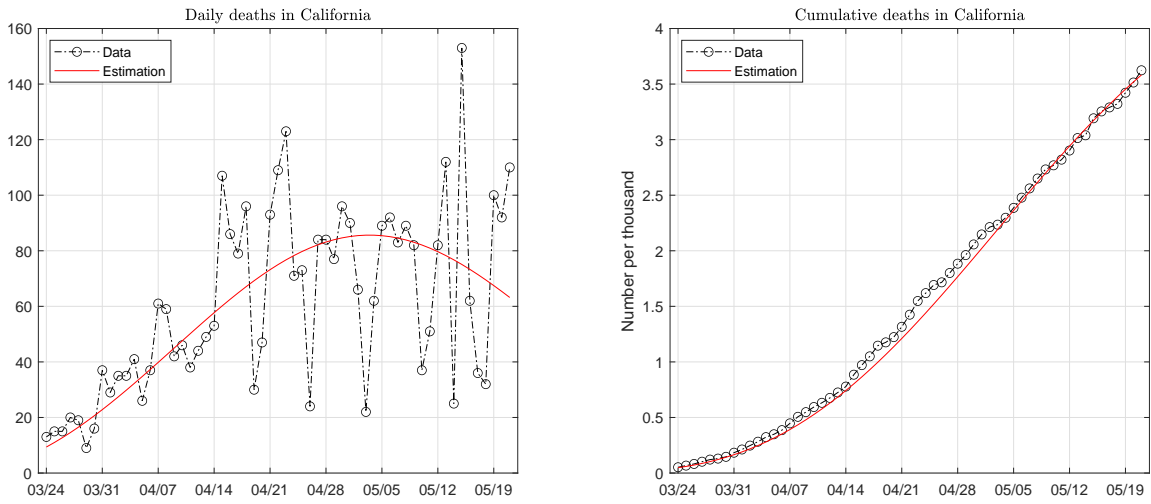
Figure 33: Data and fitted paths of deaths in California. The death pattern is fitted with one Weibull function.
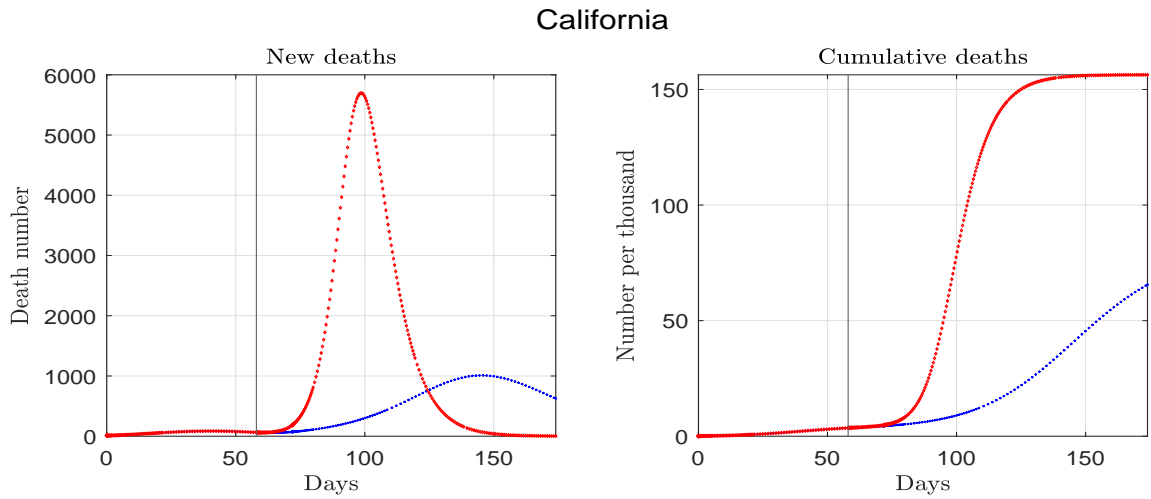
Figure 34: Estimated and forecast deaths for California. The vertical line marks the end of the sample.

California
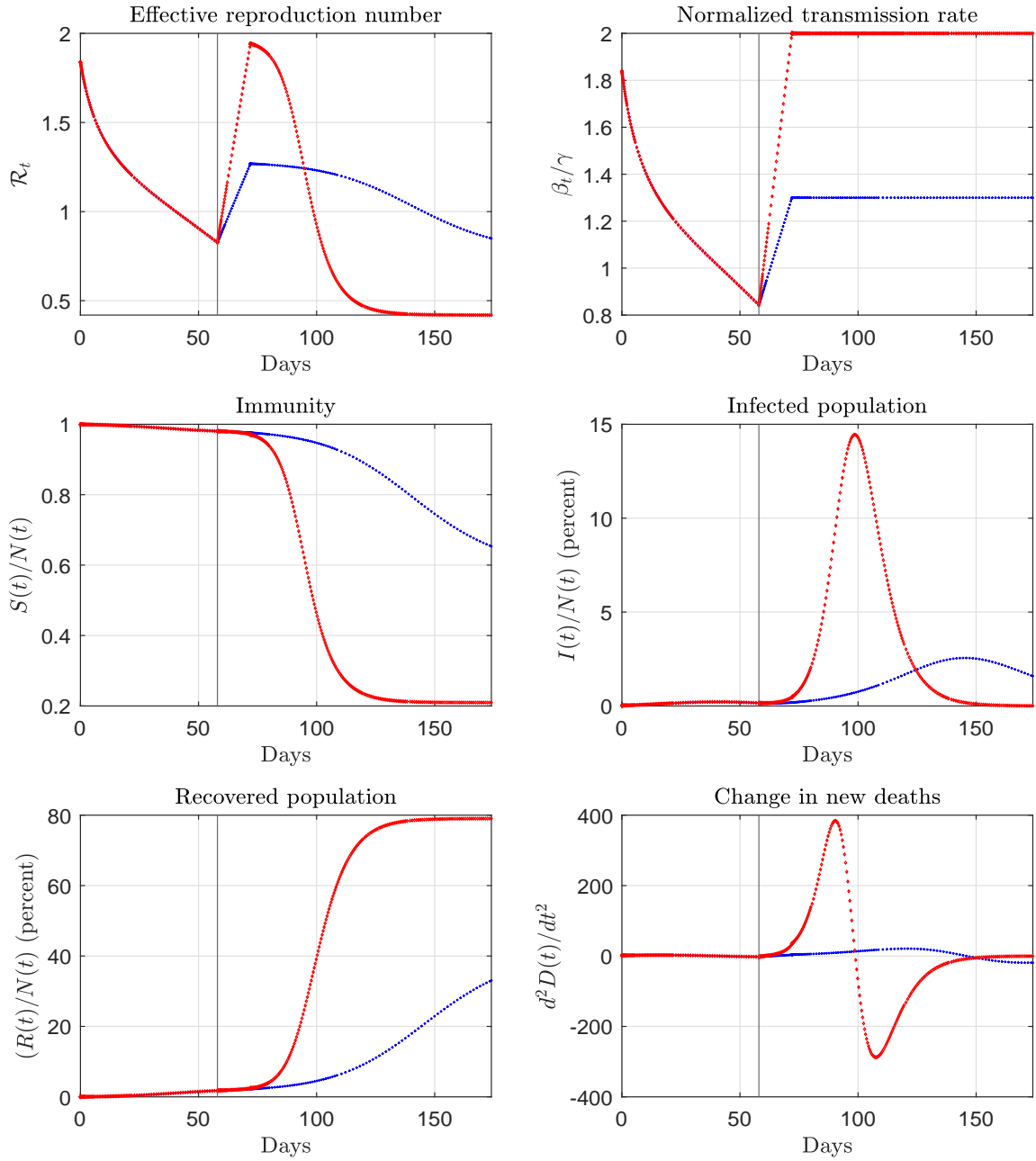
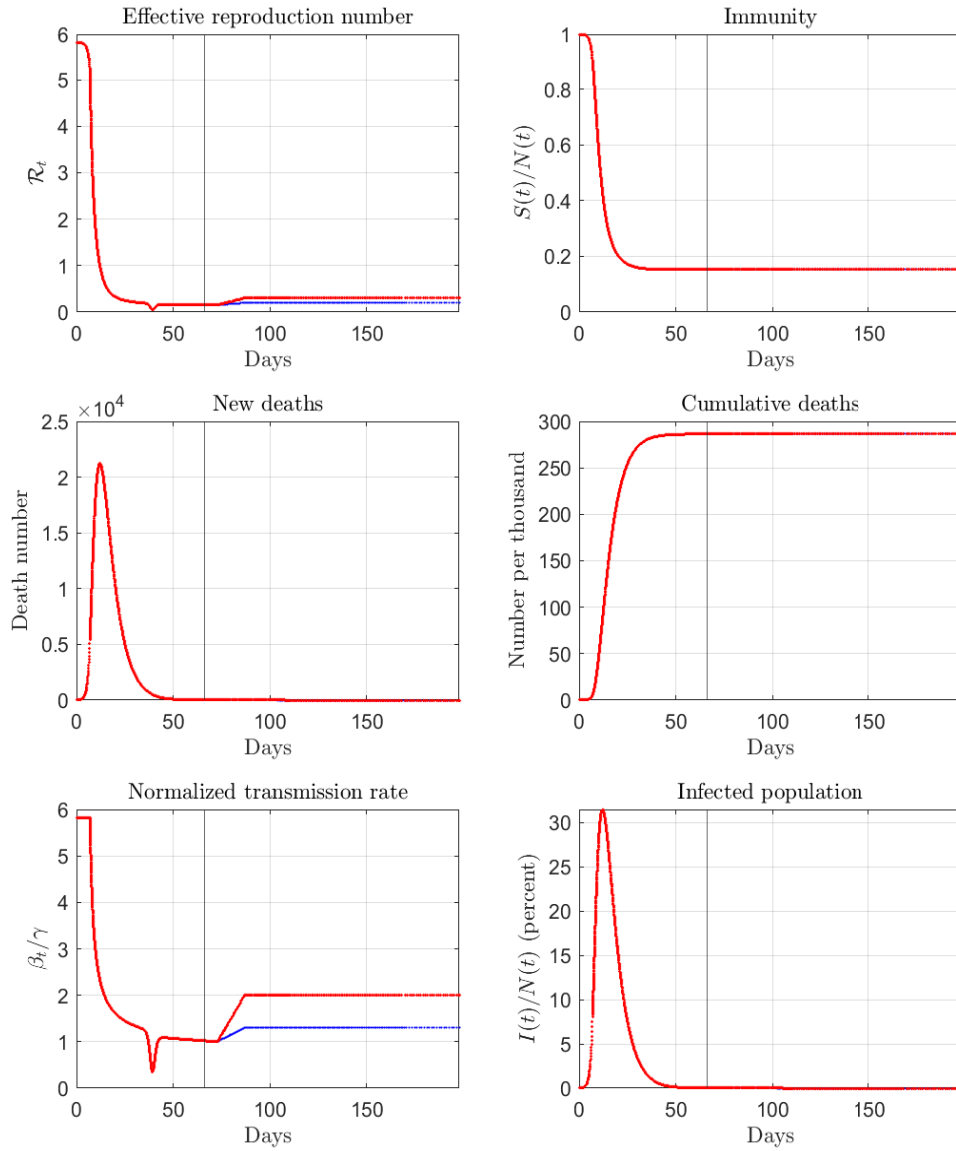**Figure 35:** Estimated and forecast paths for California. The vertical line marks the end of the sample.
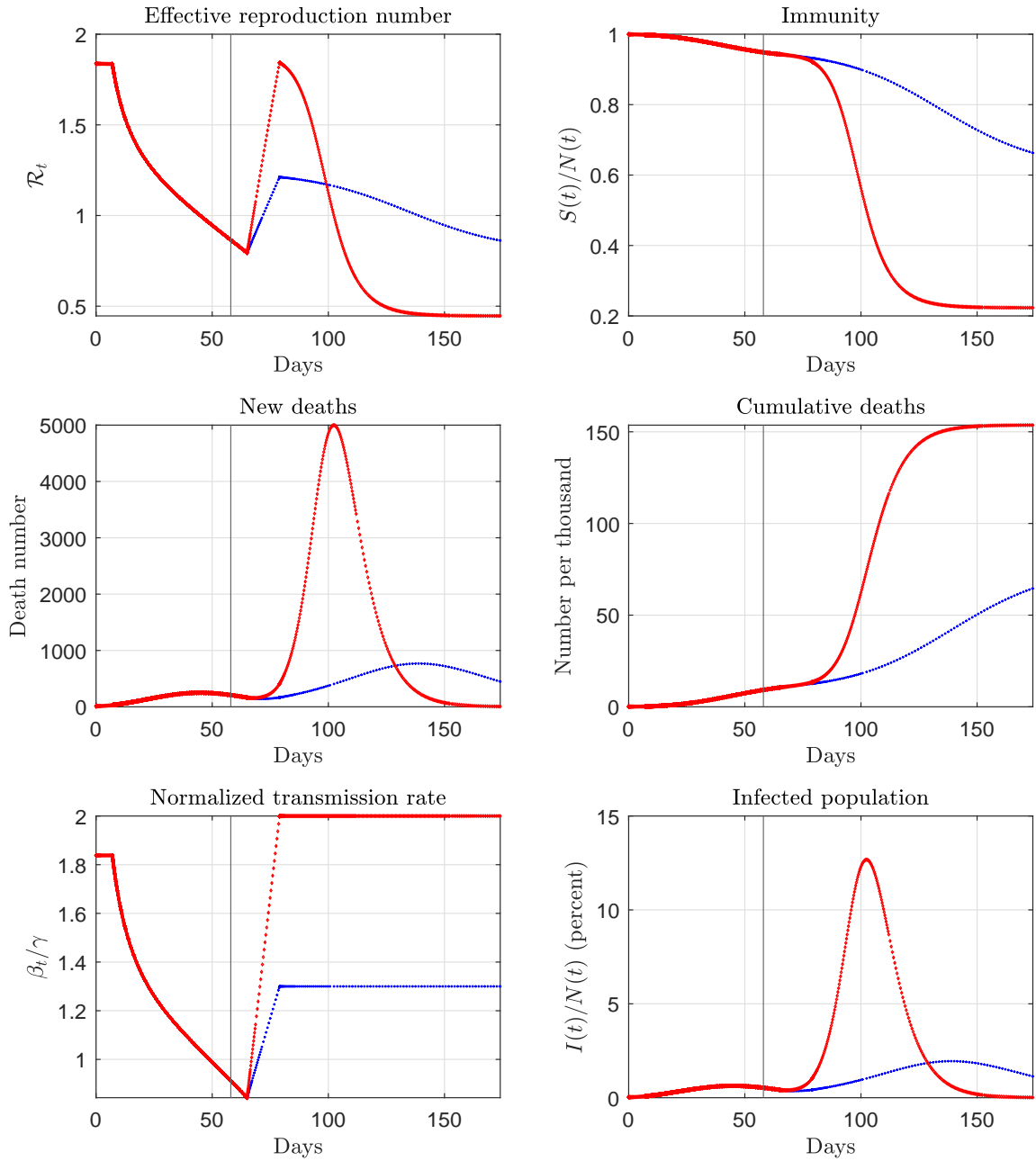
Figure 36: Counterfactual paths for California. The vertical line marks the end of the sample.
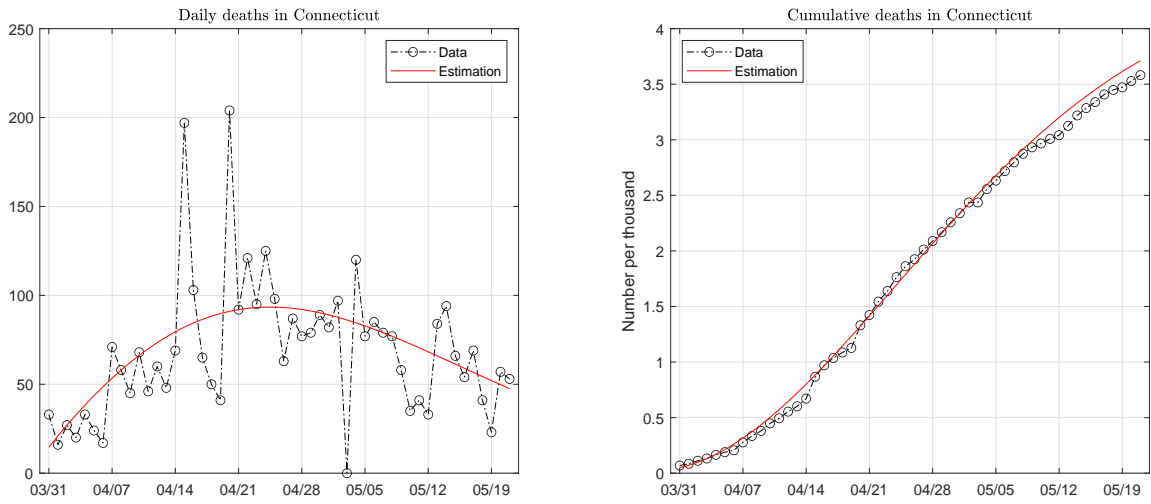
Figure 37: Data and fitted paths of deaths in Connecticut. The death pattern is fitted with one Weibull function.
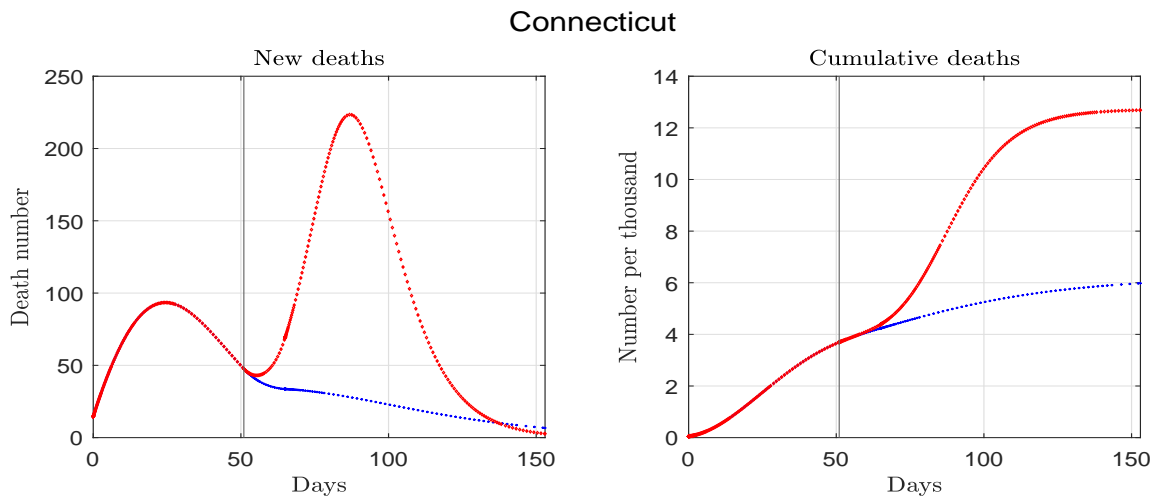
Figure 38: Estimated and forecast deaths for Connecticut. The vertical line marks the end of the sample.

64

Connecticut

Figure 39: Estimated and forecast paths for Connecticut. The vertical line marks the end of the sample.

Connecticut (counterfactual)
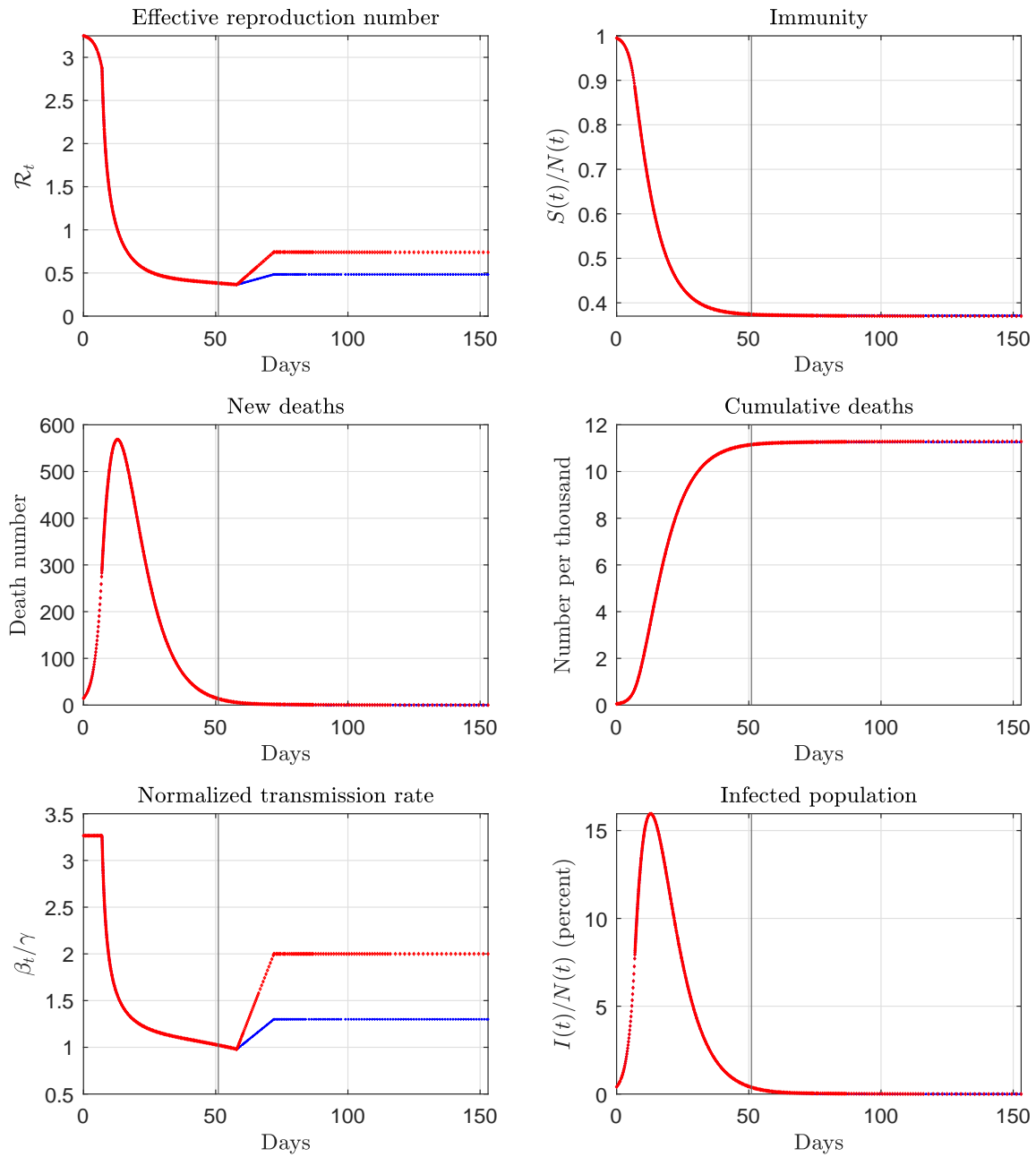
Figure 40: Counterfactual paths for Connecticut. The vertical line marks the end of the sample.
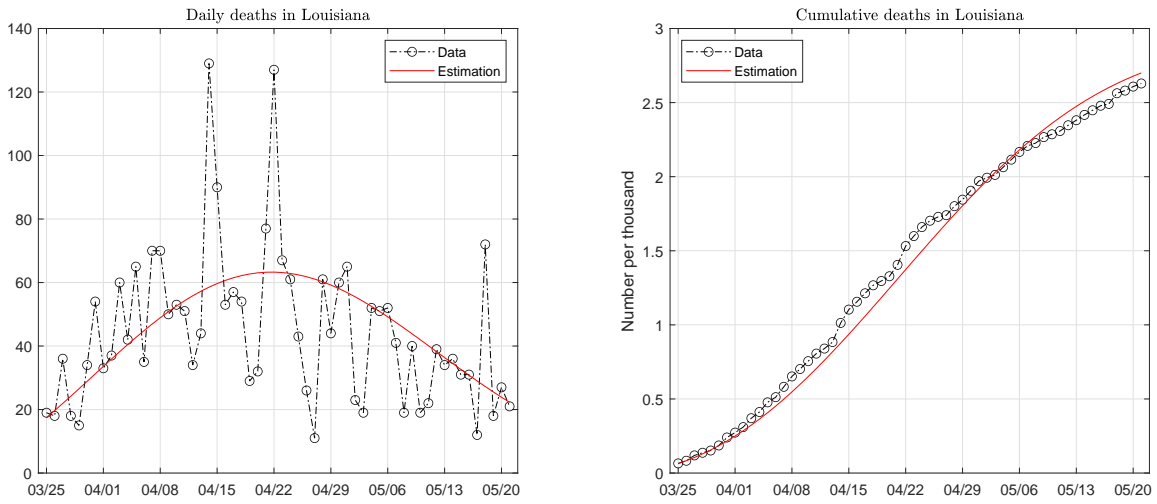
Figure 41: Data and fitted paths of deaths in Louisiana. The death pattern is fitted with one Weibull function.
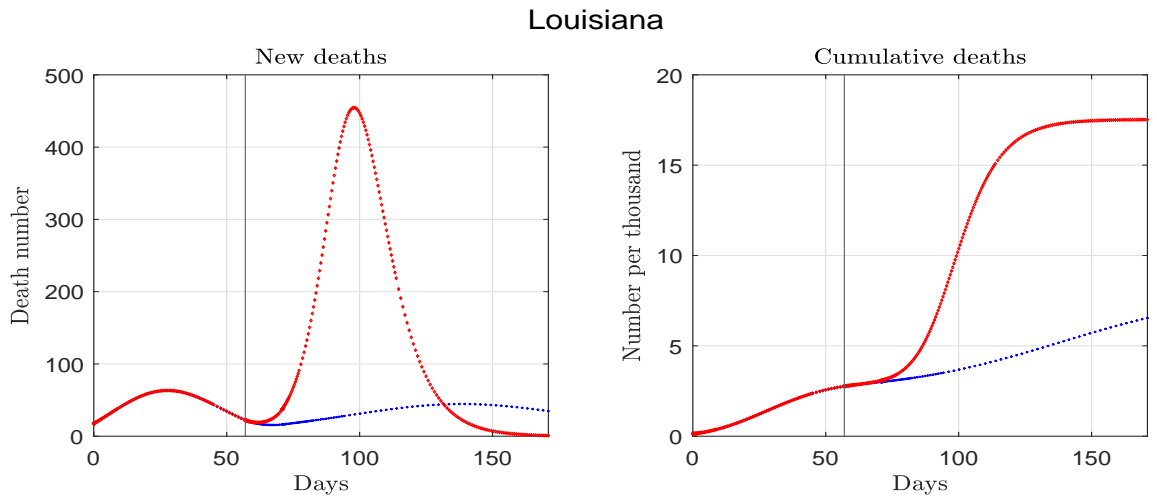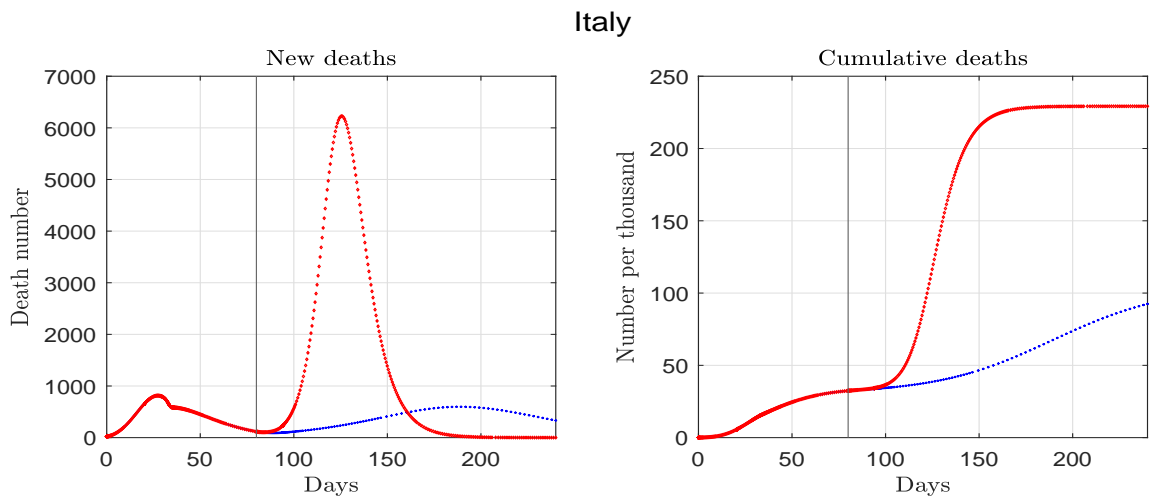

Figure 42: Estimated and forecast deaths for Louisiana. The vertical line marks the end of the sample.
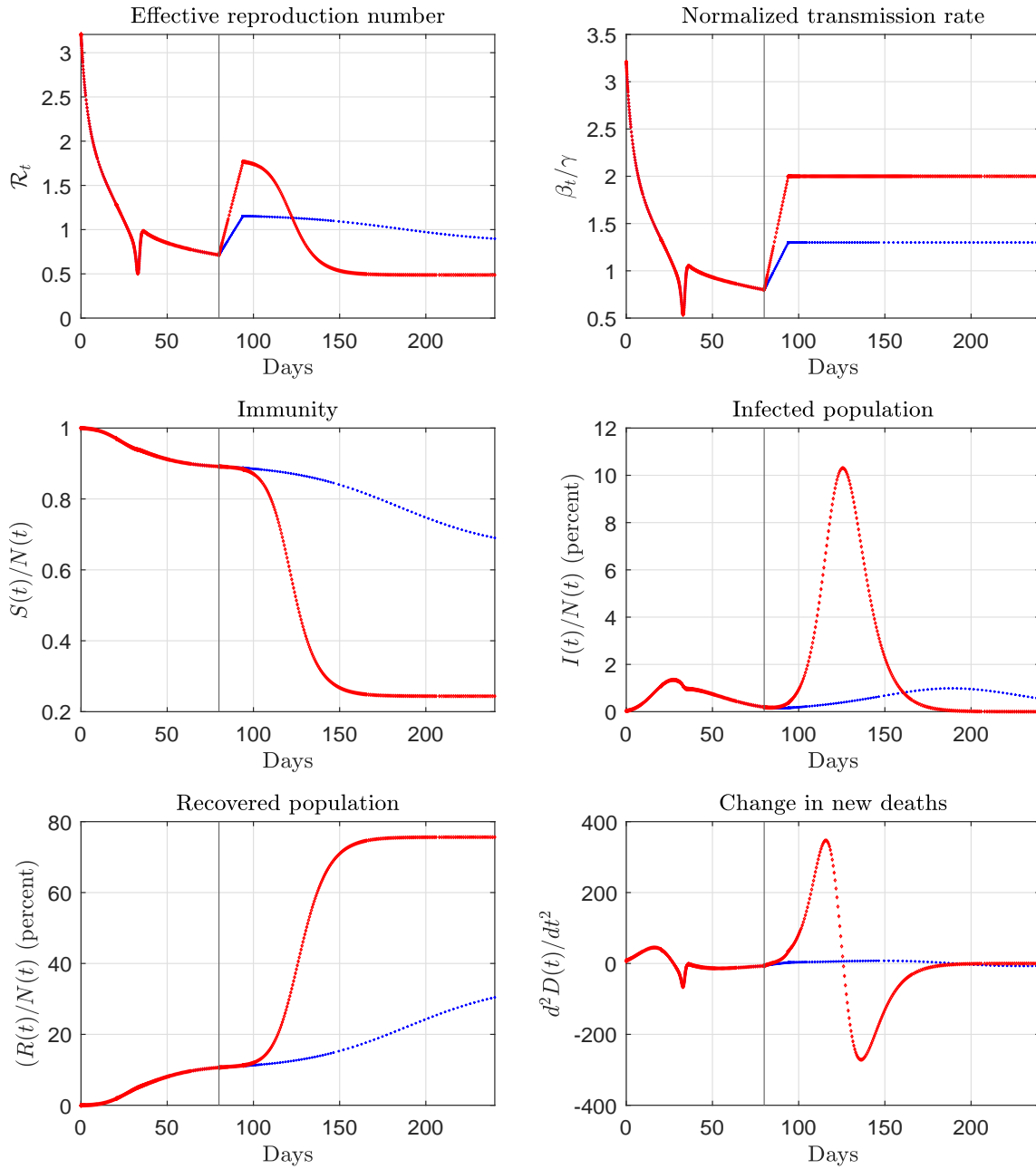
Louisiana
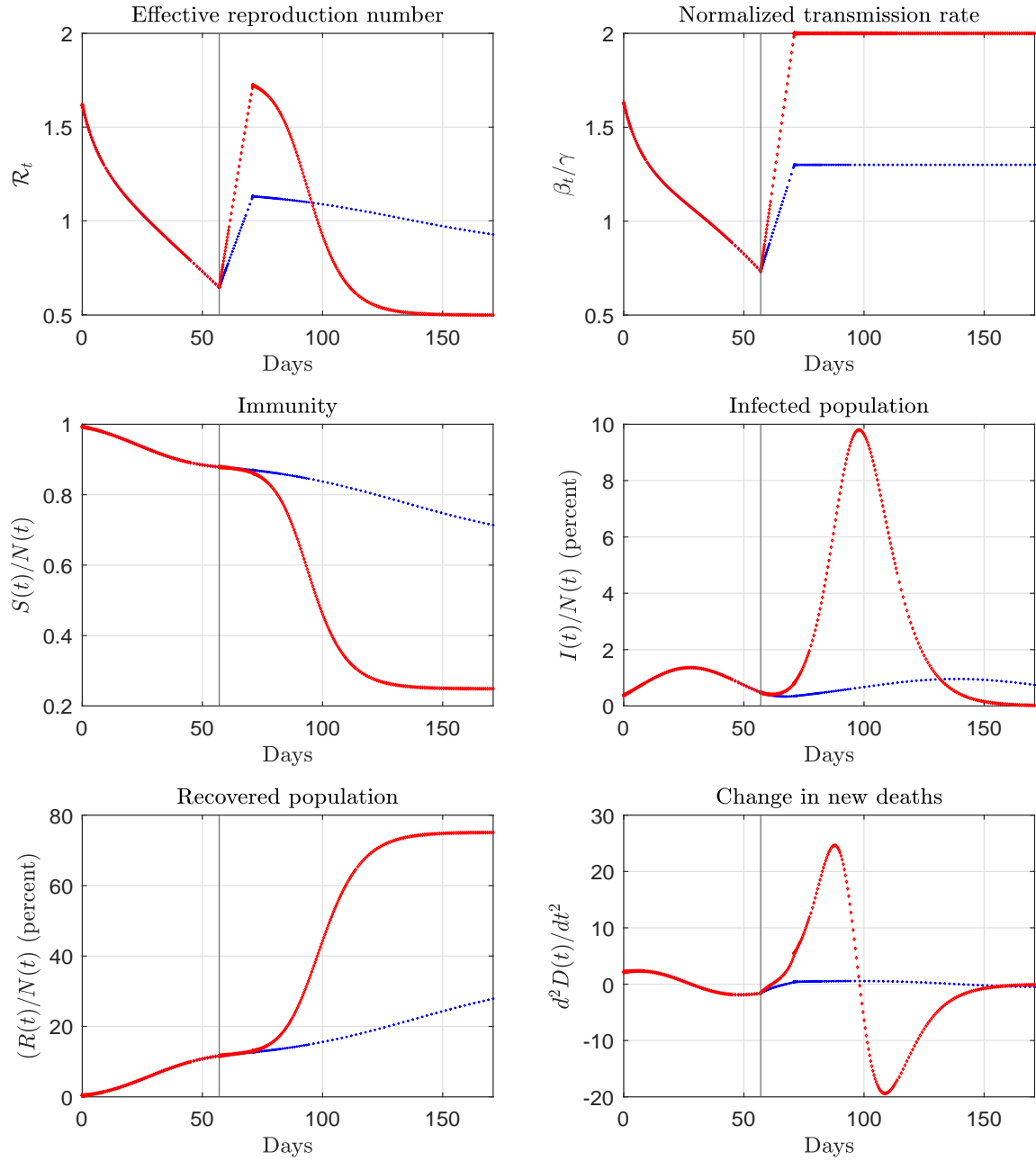
Figure 43: Estimated and forecast paths for Louisiana. The vertical line marks the end of the sample.
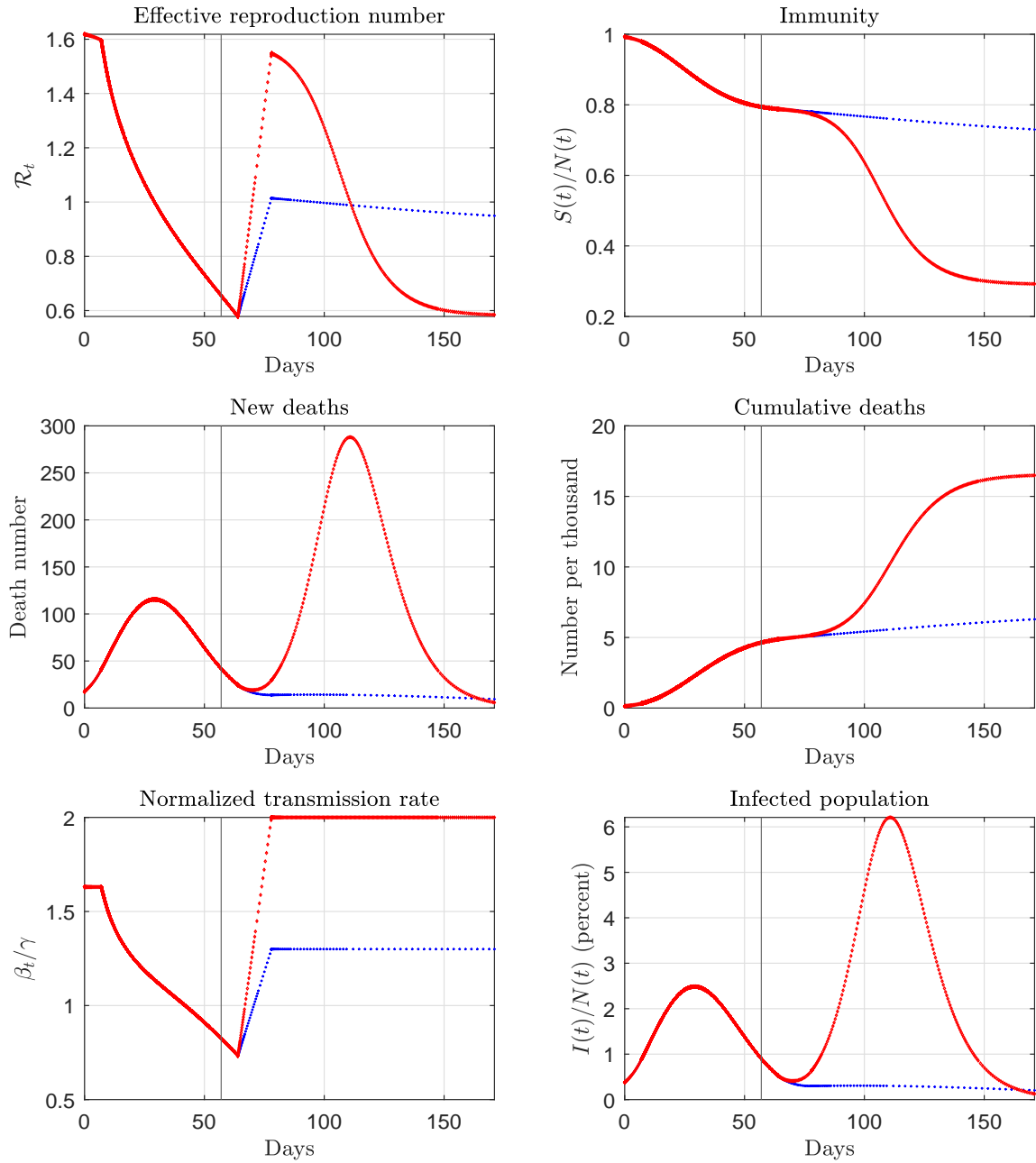
Figure 44: Counterfactual paths for Louisiana. The vertical line marks the end of the sample.

69
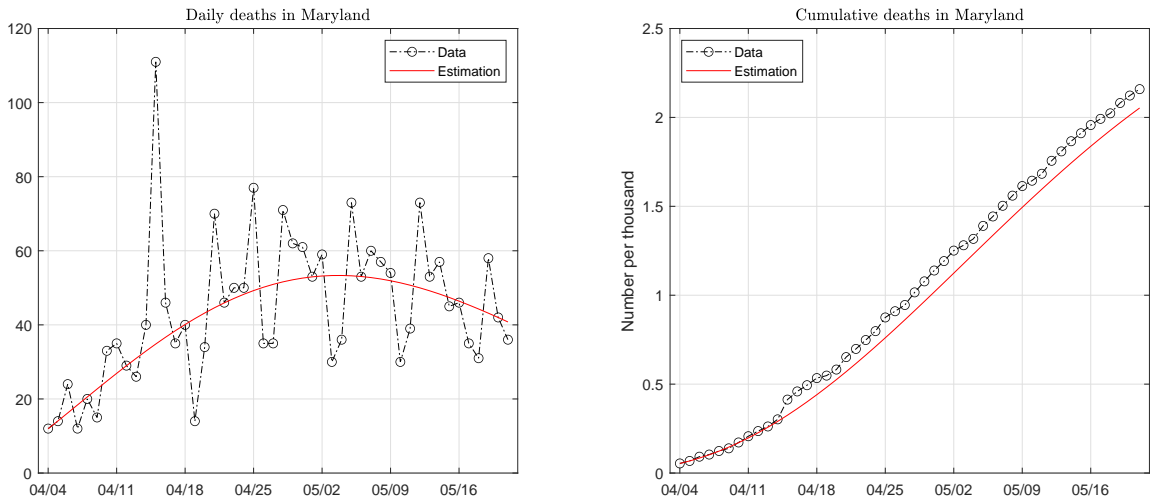
Figure 45: Data and fitted paths of deaths in Maryland. The death pattern is fitted with one Weibull function.
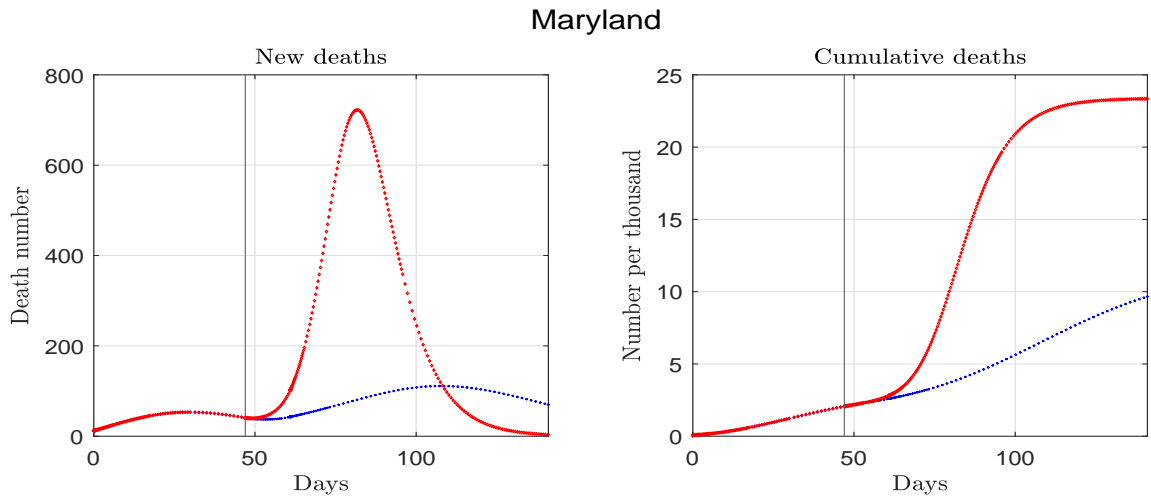
Figure 46: Estimated and forecast deaths for Maryland. The vertical line marks the end of the sample.

70

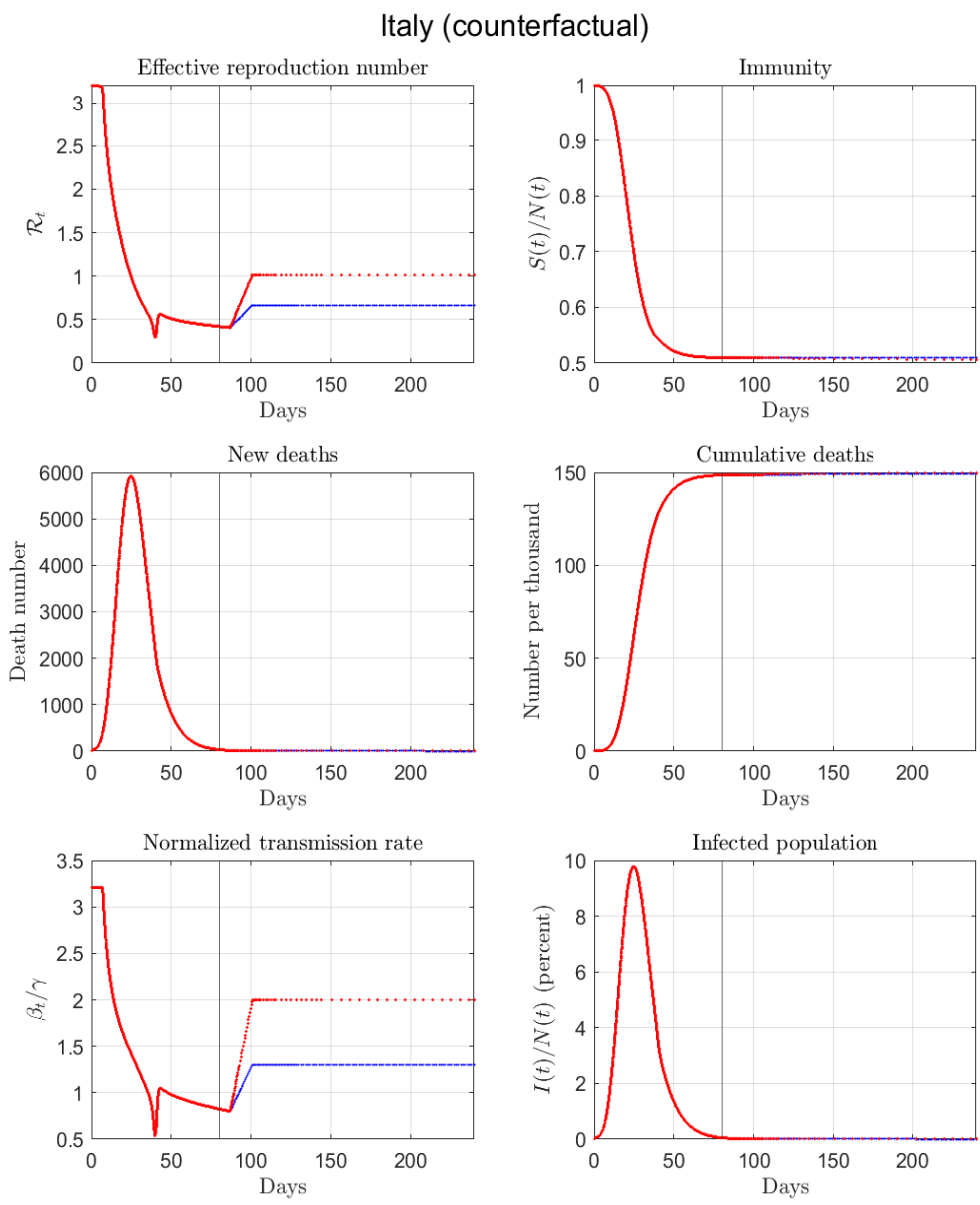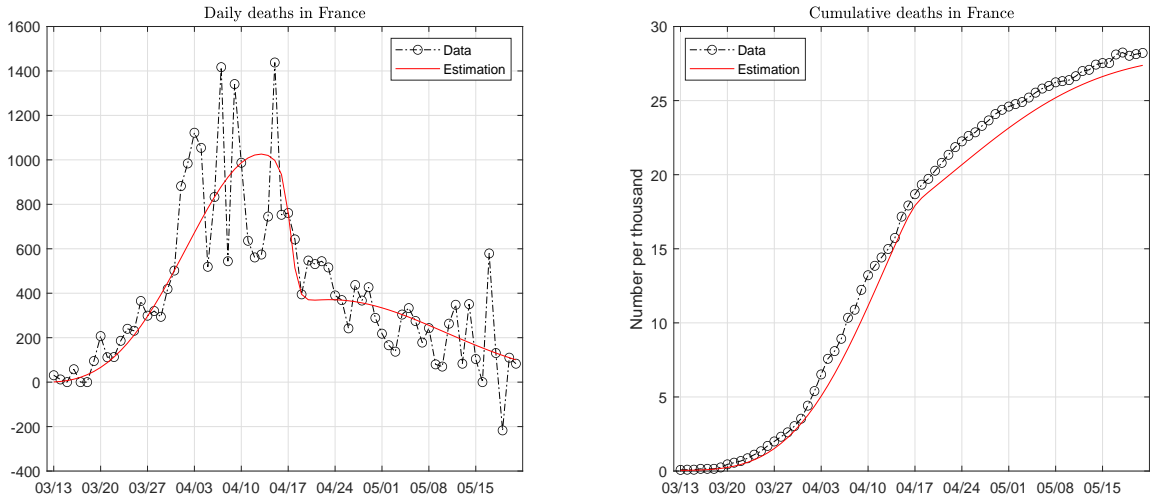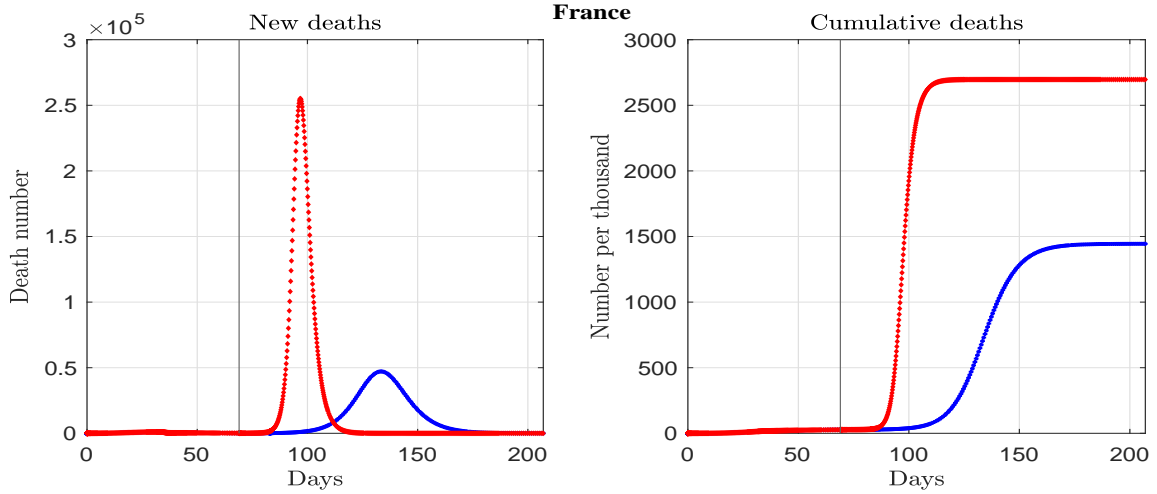**Figure 47:** Estimated and forecast paths for Maryland. The vertical line marks the end of the sample.

Figure 48: Counterfactual paths for Maryland. The vertical line marks the end of the sample.
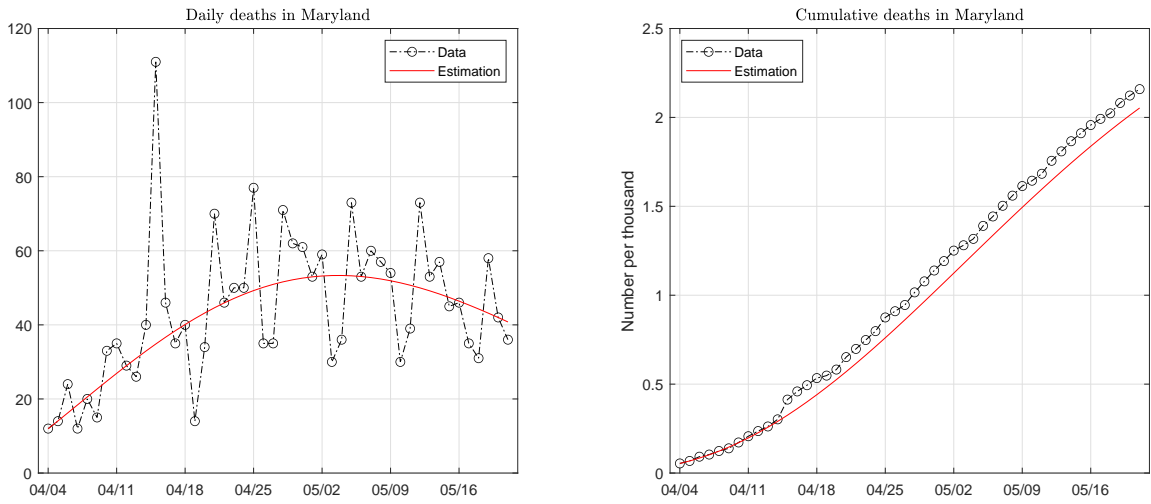
Figure 49: Data and fitted paths of deaths in Maryland. The death pattern is fitted with one Weibull function.
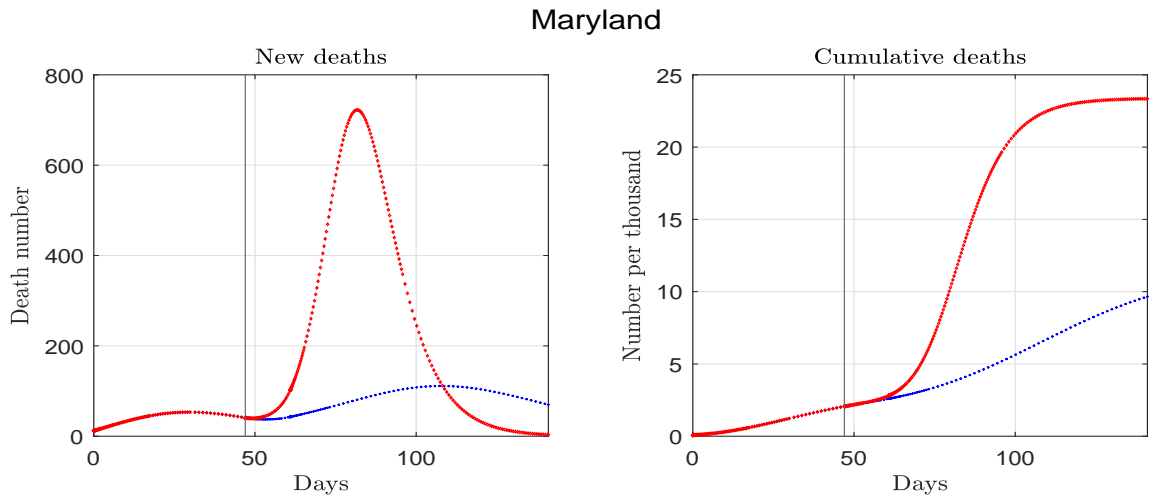
Figure 50: Estimated and forecast deaths for Maryland. The vertical line marks the end of the sample.
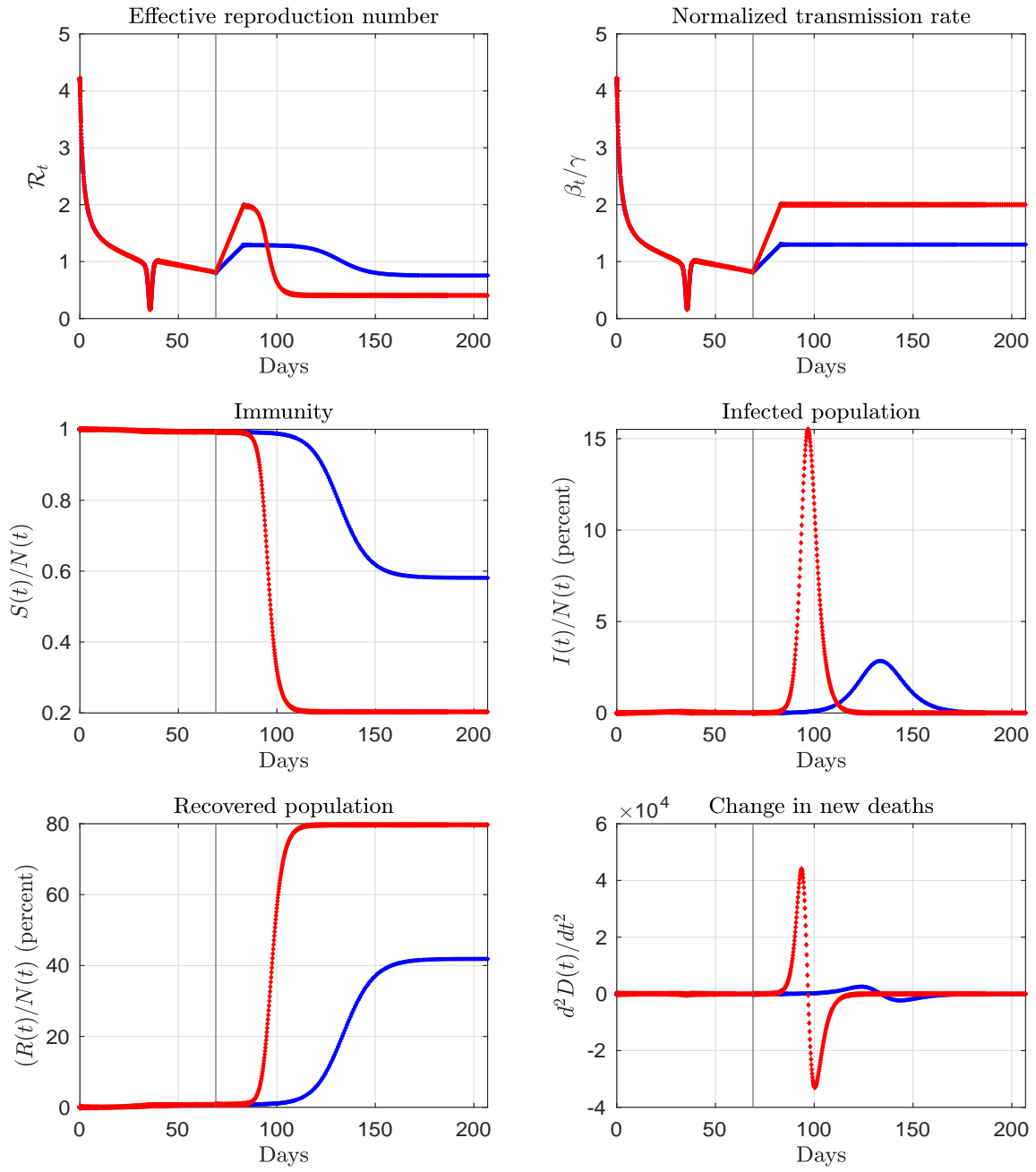
Maryland
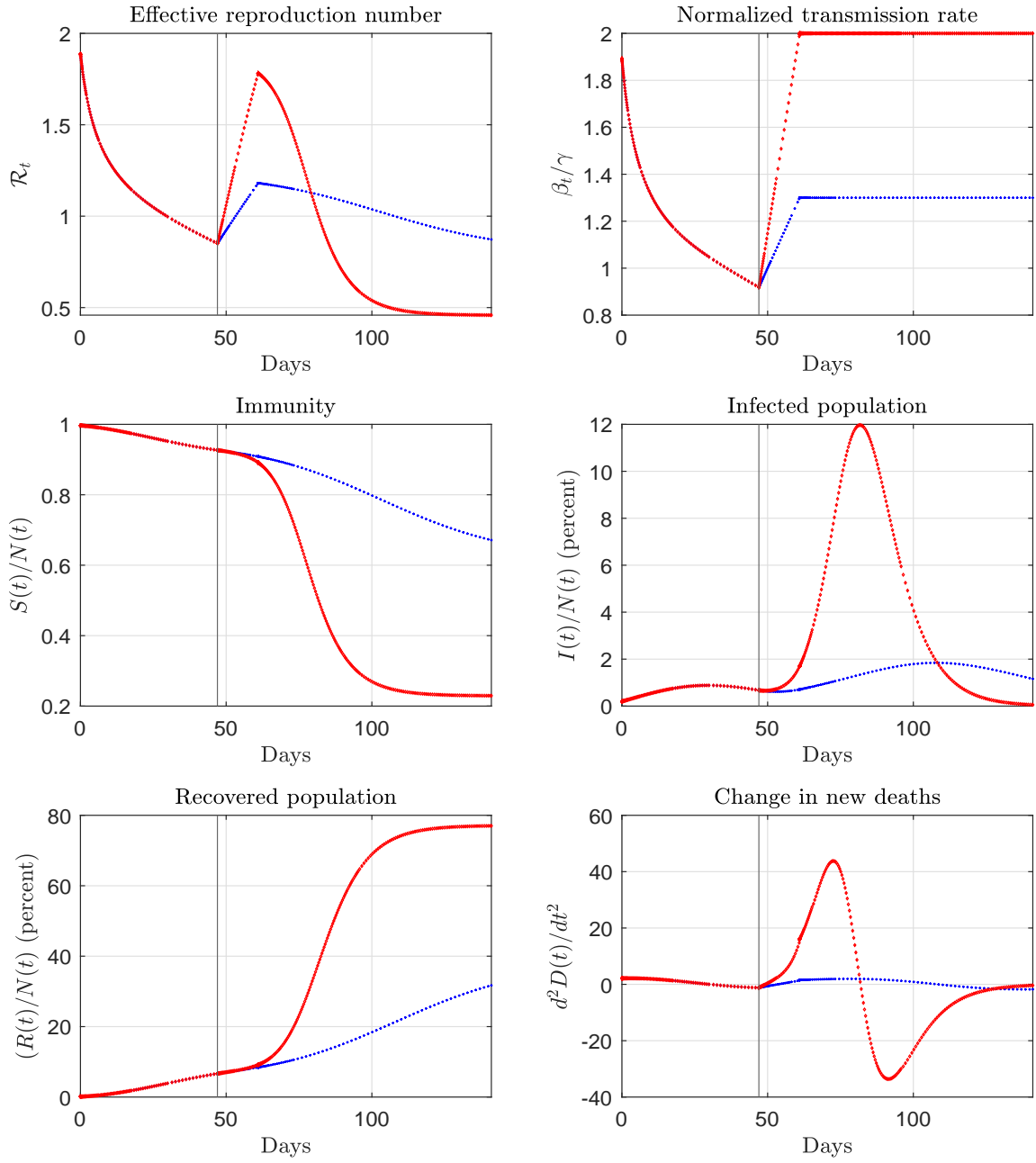
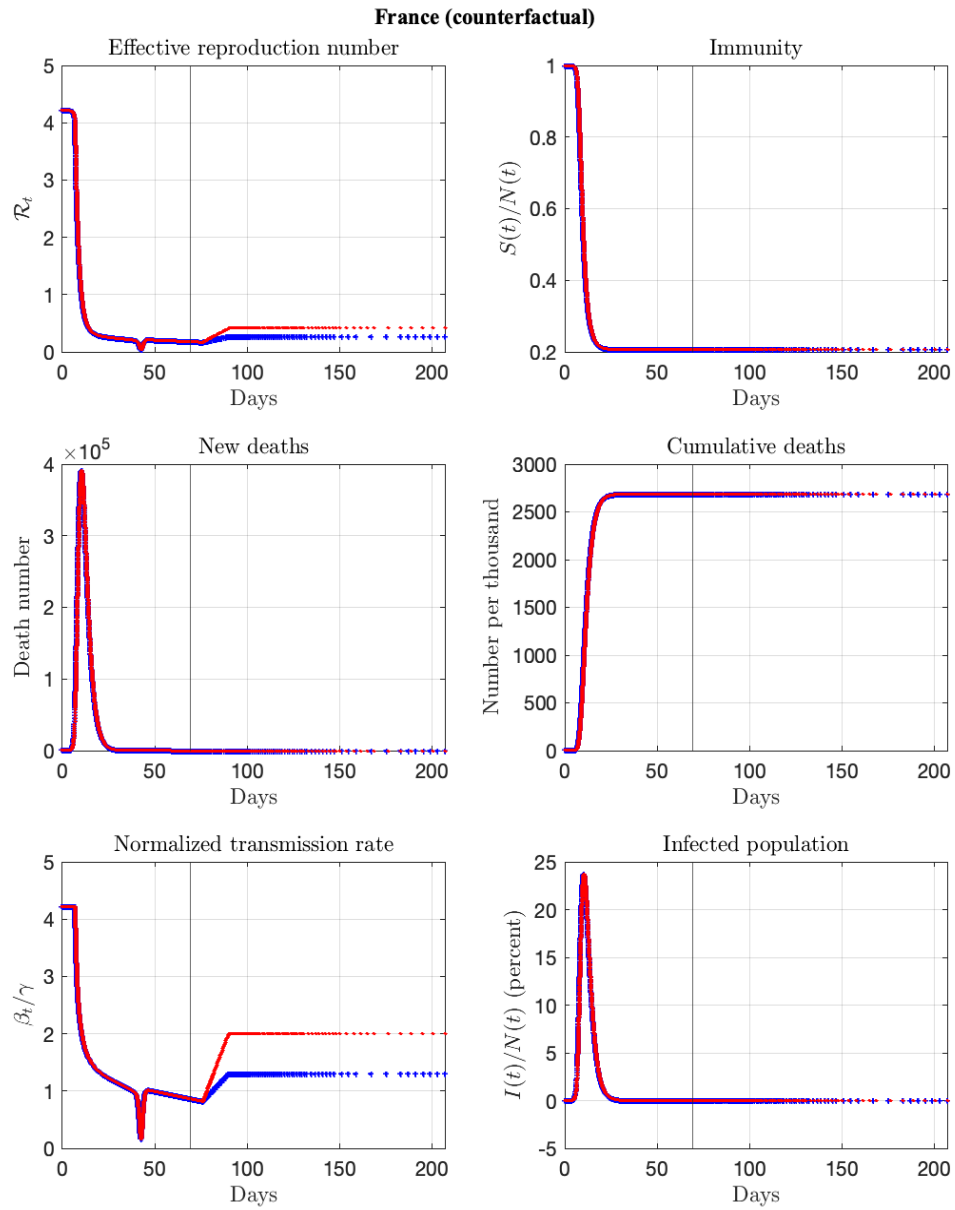**Figure 51:** Estimated and forecast paths for Maryland. The vertical line marks the end of the sample.

74
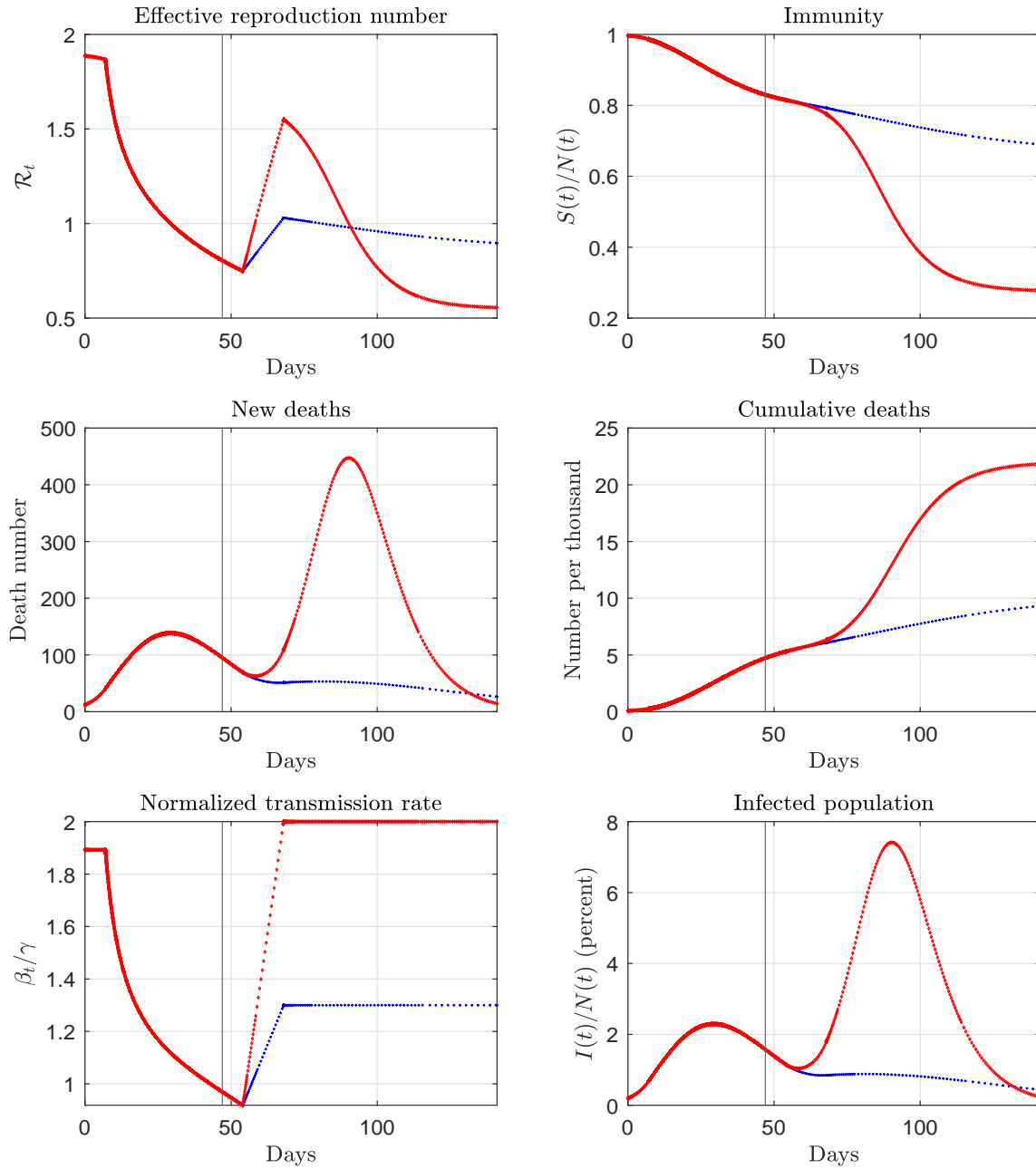
Figure 52: Counterfactual paths for Maryland. The vertical line marks the end of the sample.
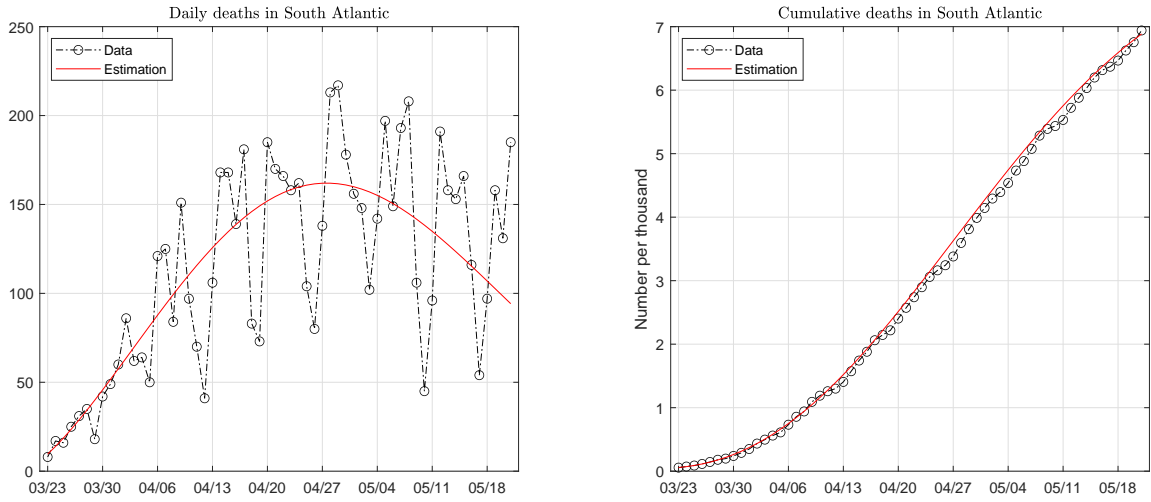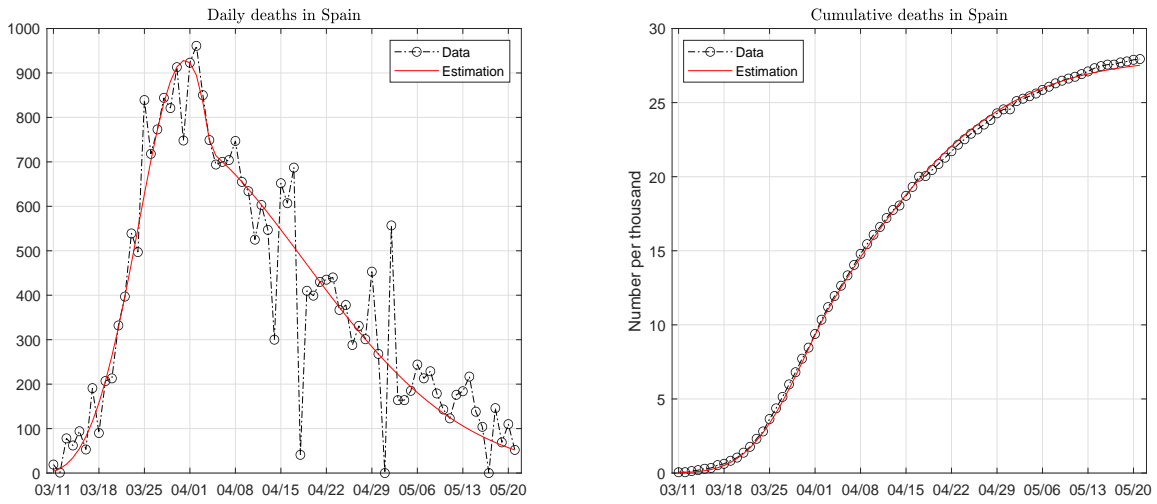
Figure 53: Data and fitted paths of deaths in the South Atlantic region. The death pattern is fitted with one Weibull function.
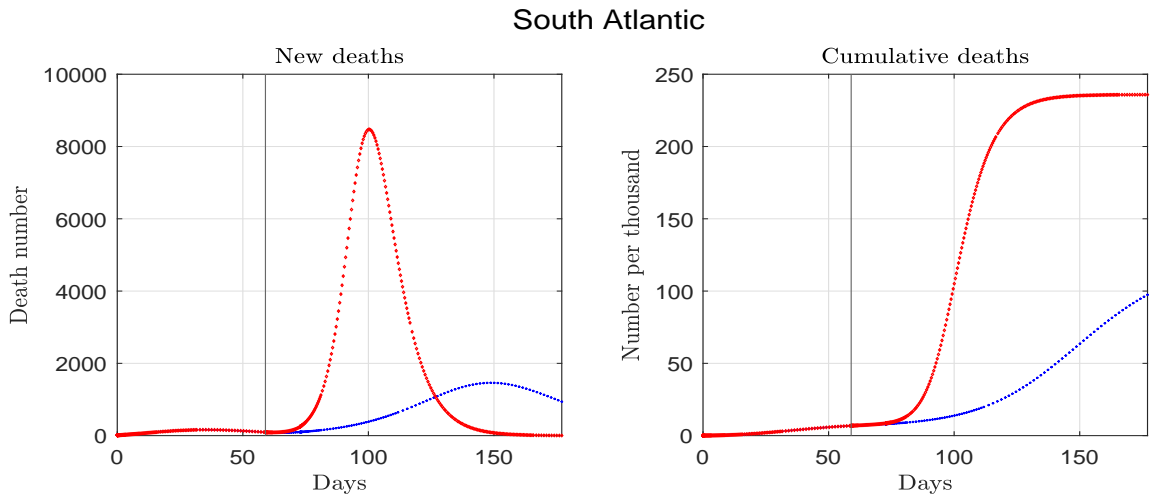
Figure 54: Estimated and forecast deaths for the South Atlantic region. The vertical line marks the end of the sample.

76
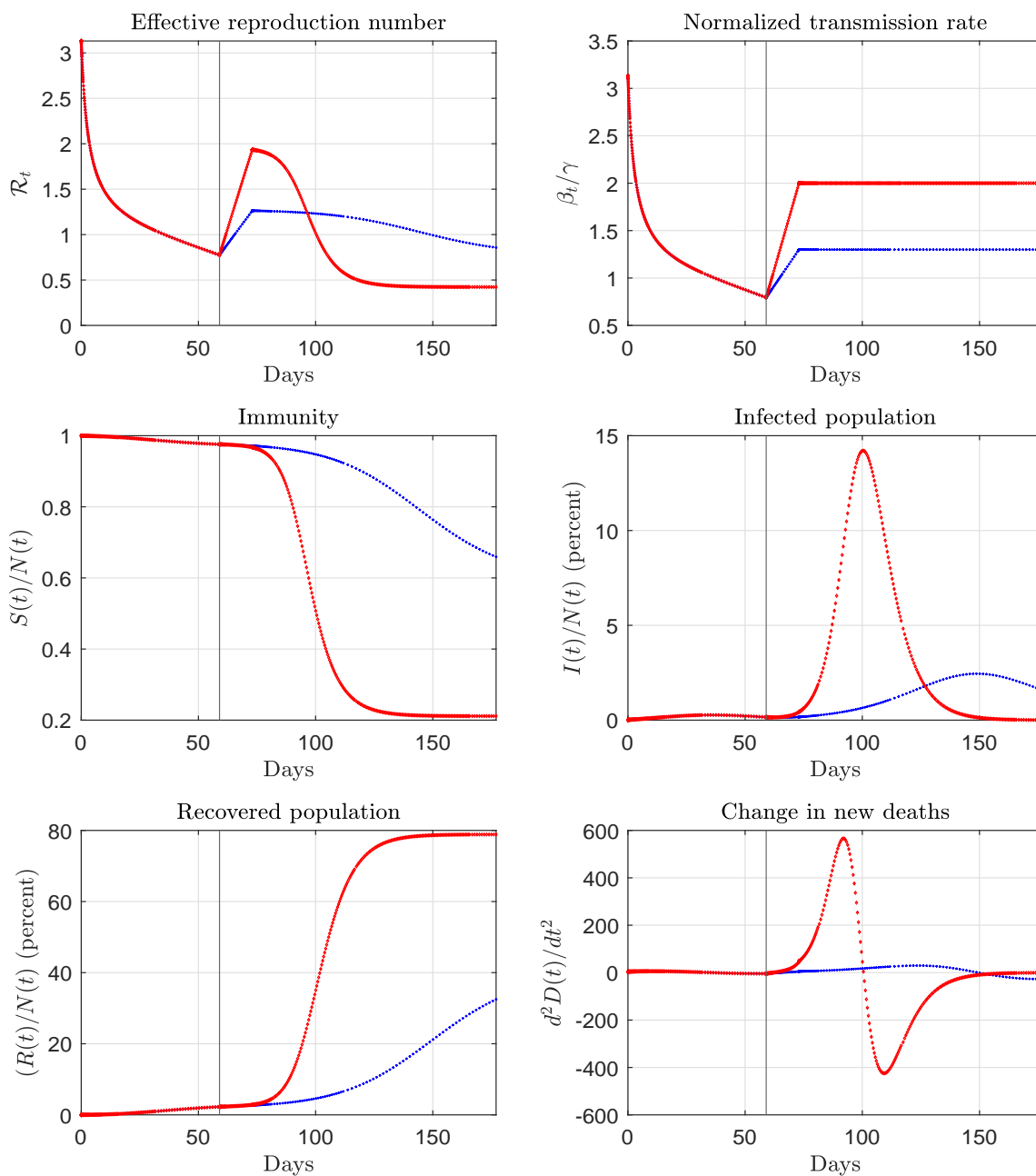
South Atlantic

Figure 55: Estimated and forecast paths for the South Atlantic region. The vertical line marks the end of the sample.
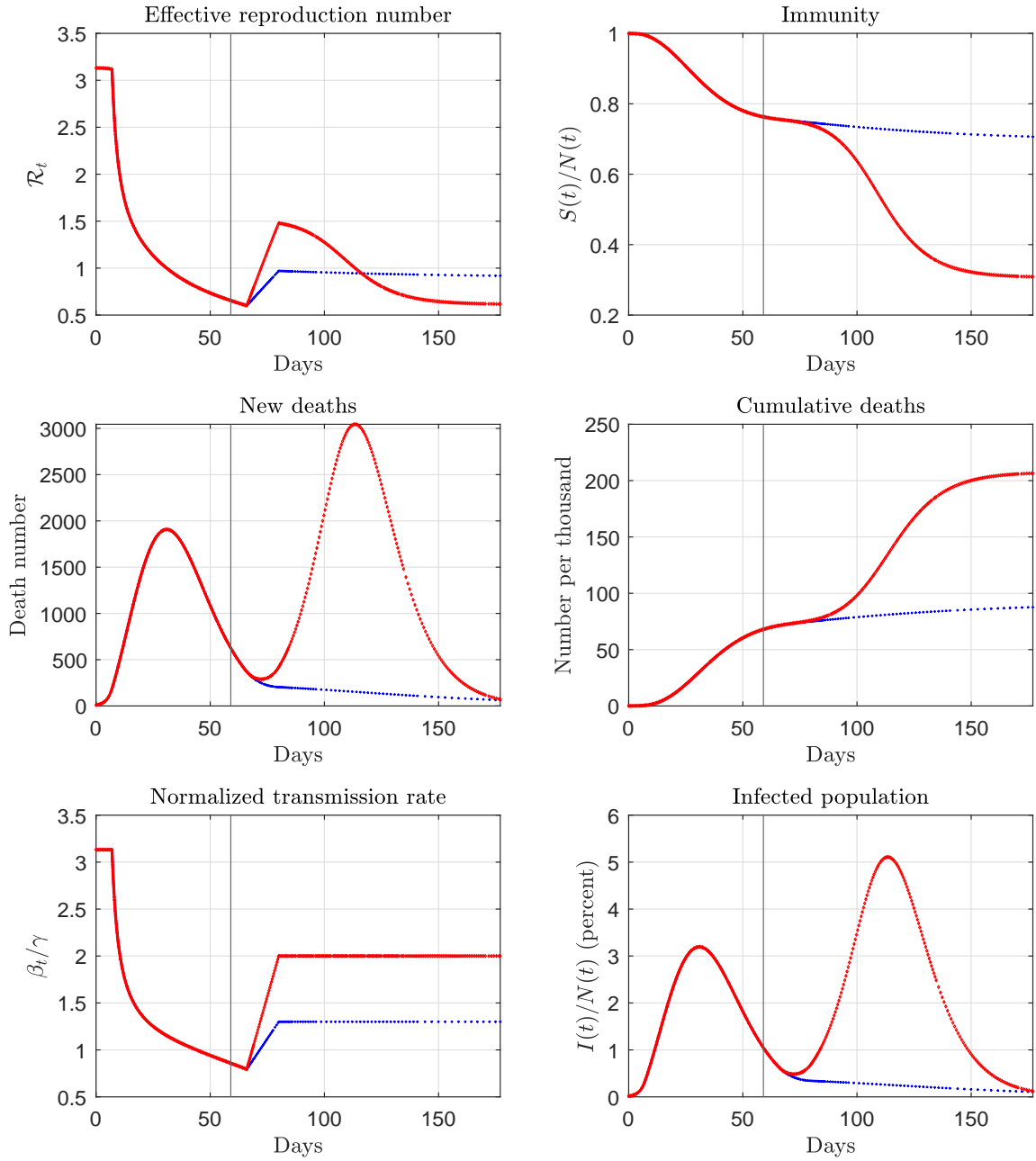
Figure 56: Counterfactual paths for the South Atlantic region. The vertical line marks the end of the sample.
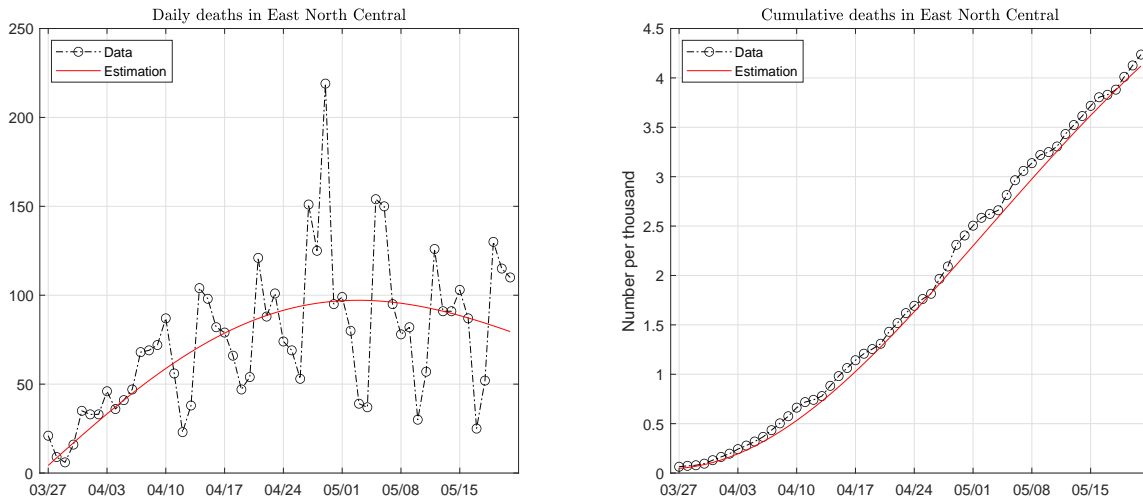
Figure 57: Data and fitted paths of deaths in the East North Central region. The death pattern is fitted with one Weibull function.
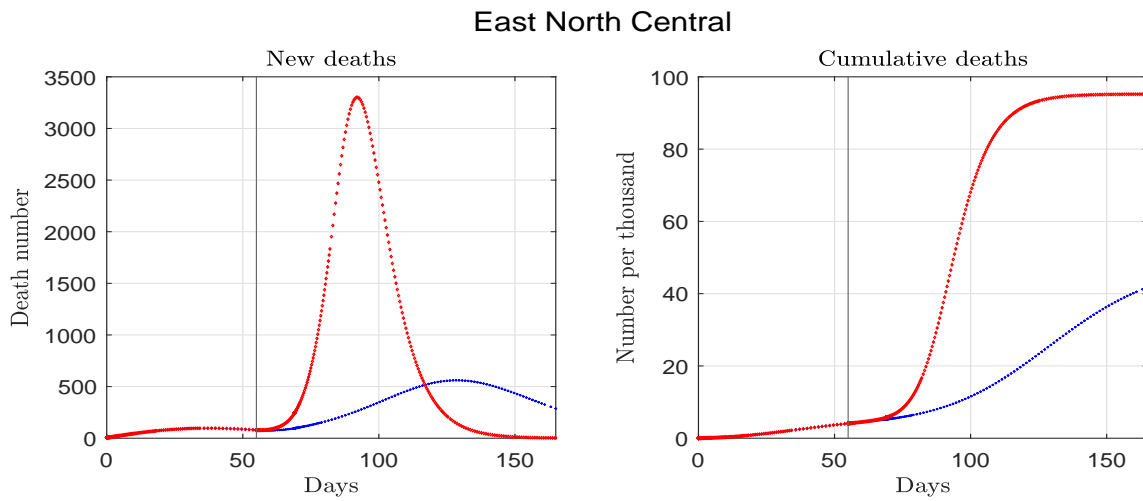
Figure 58: Estimated and forecast deaths for the East North Central region. The vertical line marks the end of the sample.

East North Central
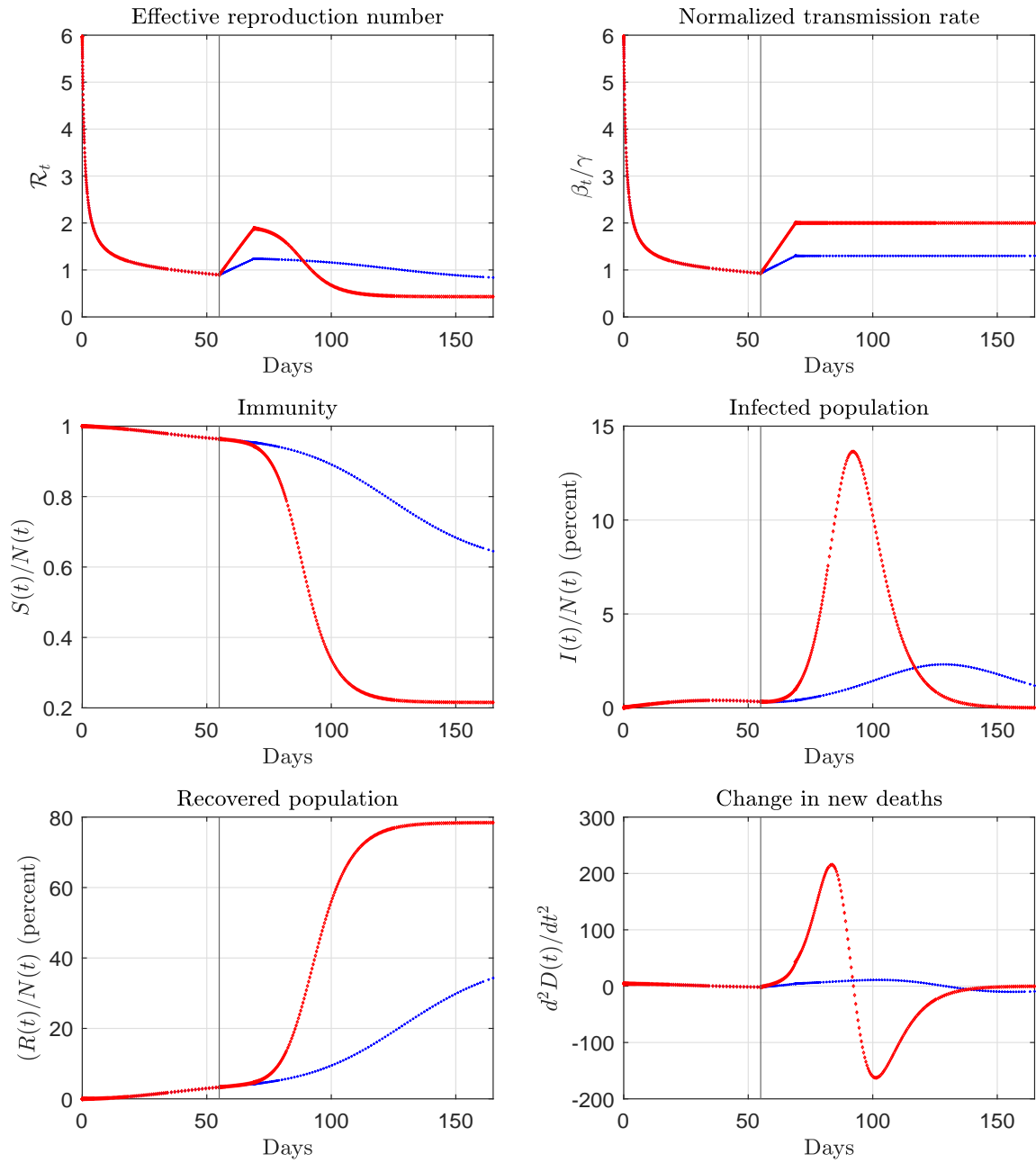
Figure 59: Estimated and forecast paths for the East North Central region. The vertical line marks the end of the sample.

80

East North Central (counterfactual)
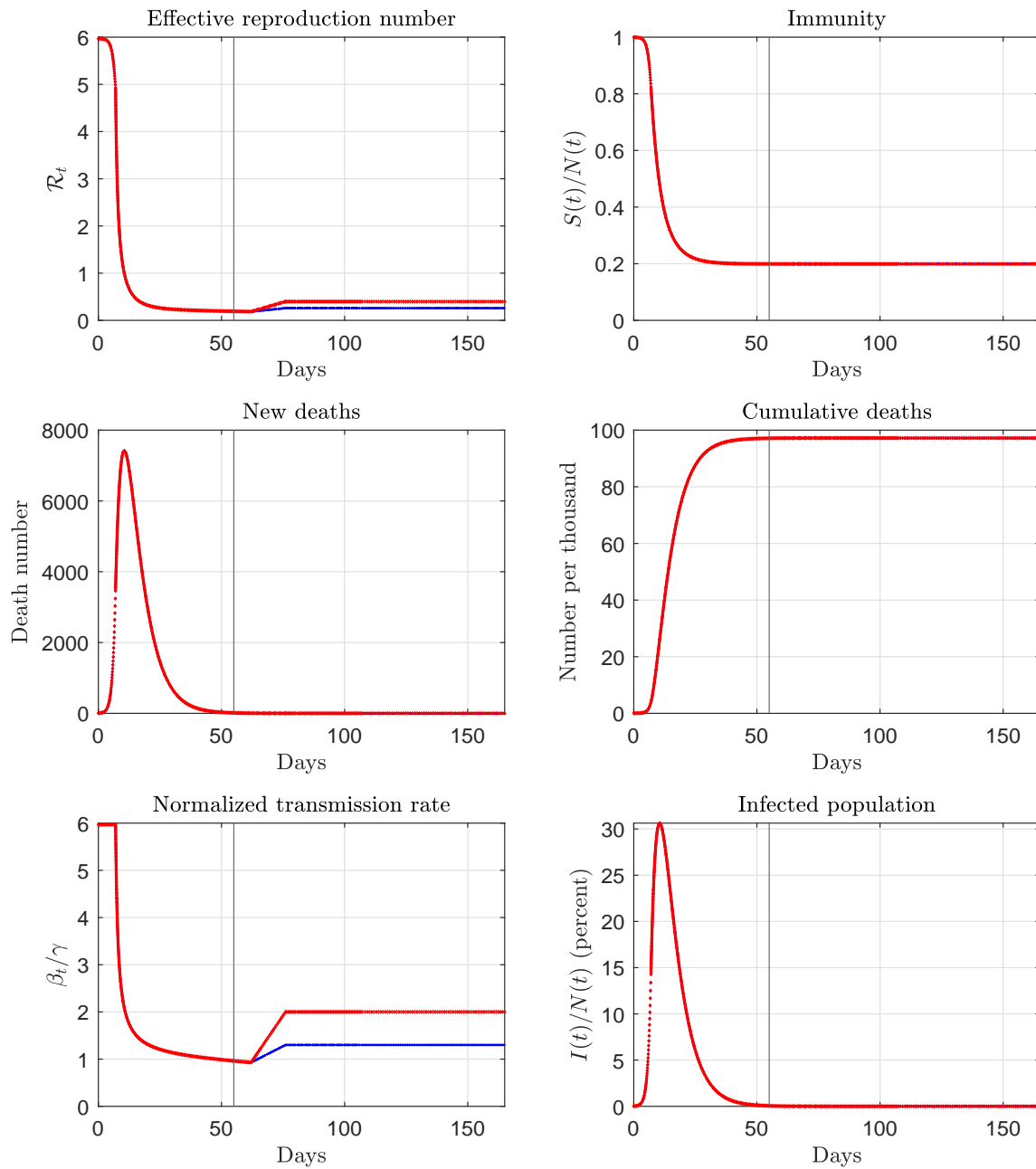
Figure 60: Counterfactual paths for the East North Central region. The vertical line marks the end of the sample.

Figure 61: Data and fitted paths of deaths in the Mountain region. The death pattern is fitted with one Weibull function.
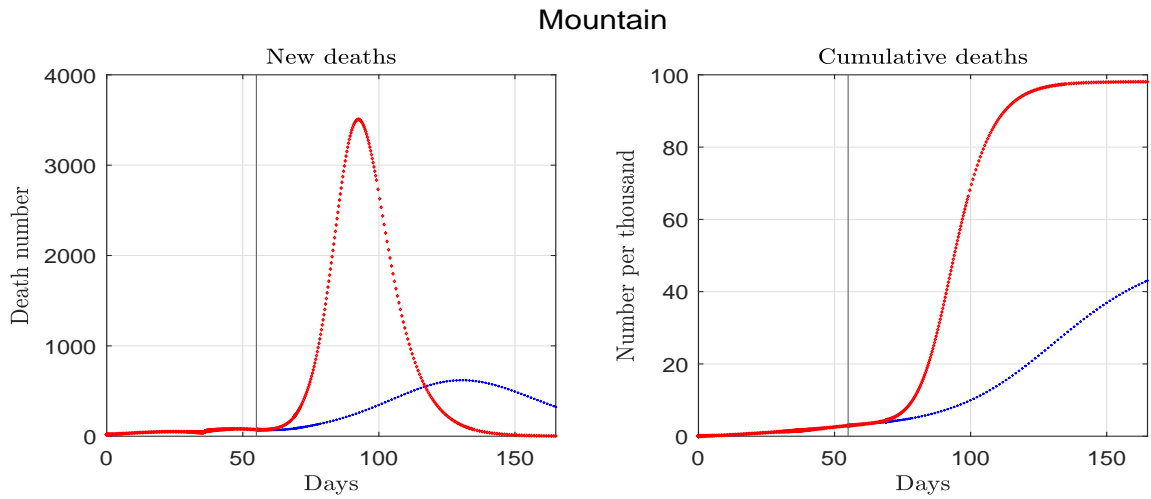
Figure 62: Estimated and forecast deaths for the Mountain region. The vertical line marks the end of the sample.

Figure 63: Estimated and forecast paths for the Mountain region. The vertical line marks the end of the sample.

Figure 64: Counterfactual paths for the Mountain region. The vertical line marks the end of the sample.

Figure 65: Data and fitted paths of deaths in the West North Central region. The death pattern is fitted with one Weibull function.
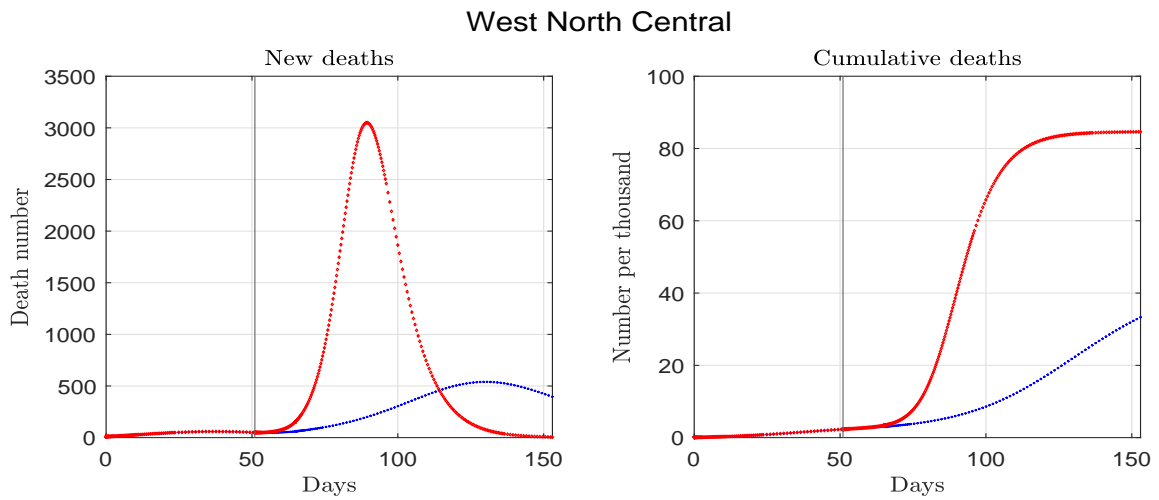
Figure 66: Estimated and forecast deaths for the West North Central region. The vertical line marks the end of the sample.

85
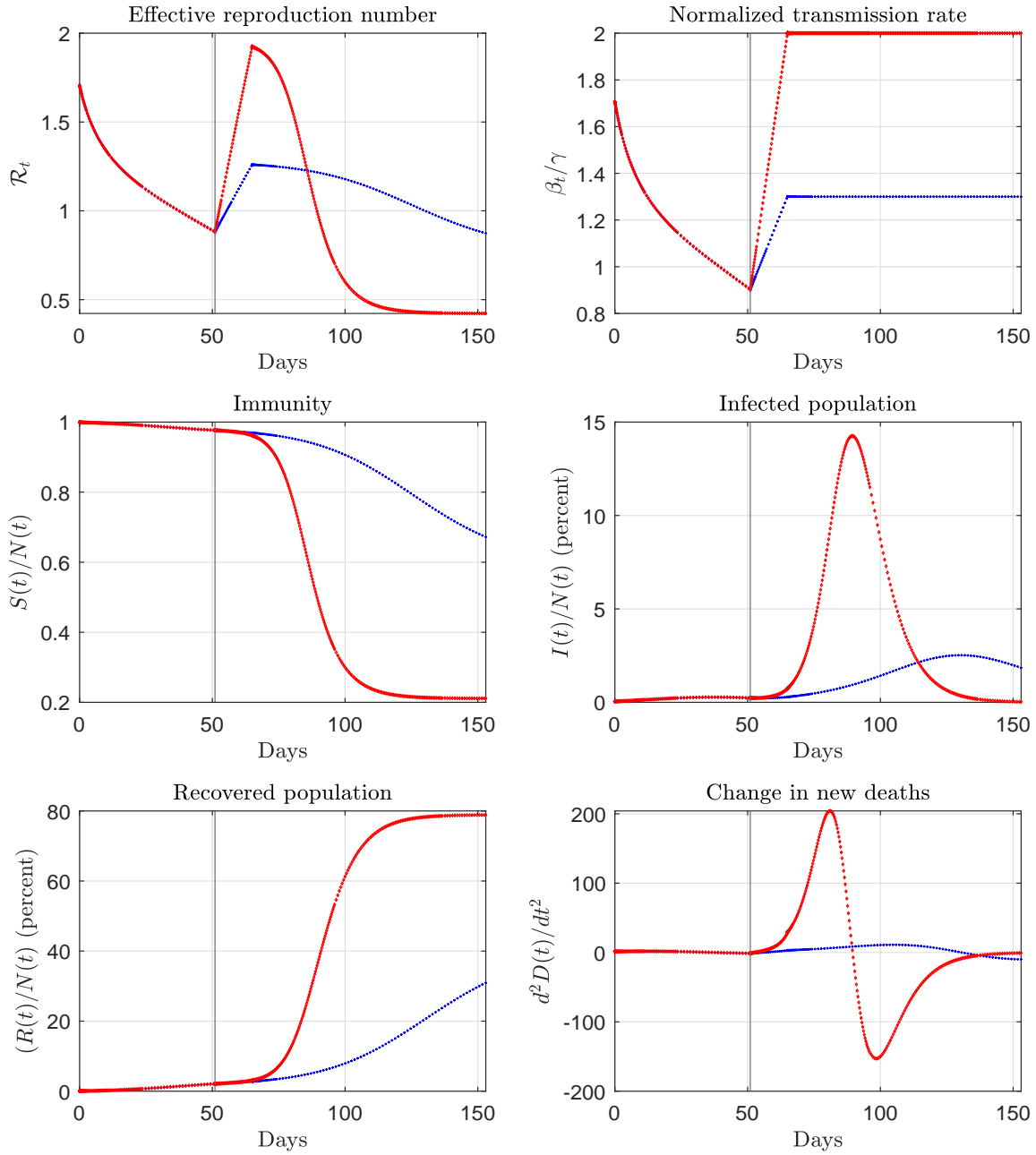
West North Central

Figure 67: Estimated and forecast paths for the West North Central region. The vertical line marks the end of the sample.

Figure 68: Counterfactual paths for the West North Central region. The vertical line marks the end of the sample.

Figure 69: Data and fitted paths of deaths in the West South Central region. The death pattern is fitted with one Weibull function.

Figure 70: Estimated and forecast deaths for the West South Central region. The vertical line marks the end of the sample.

88

West South Central

Figure 71: Estimated and forecast paths for the West South Central region. The vertical line marks the end of the sample.

89

Figure 72: Counterfactual paths for the West South Central region. The vertical line marks the end of the sample.

Figure 73: Data and fitted paths of deaths in the East South Central region. The death pattern is fitted with one Weibull function.

Figure 74: Estimated and forecast deaths for the East South Central region. The vertical line marks the end of the sample.

91
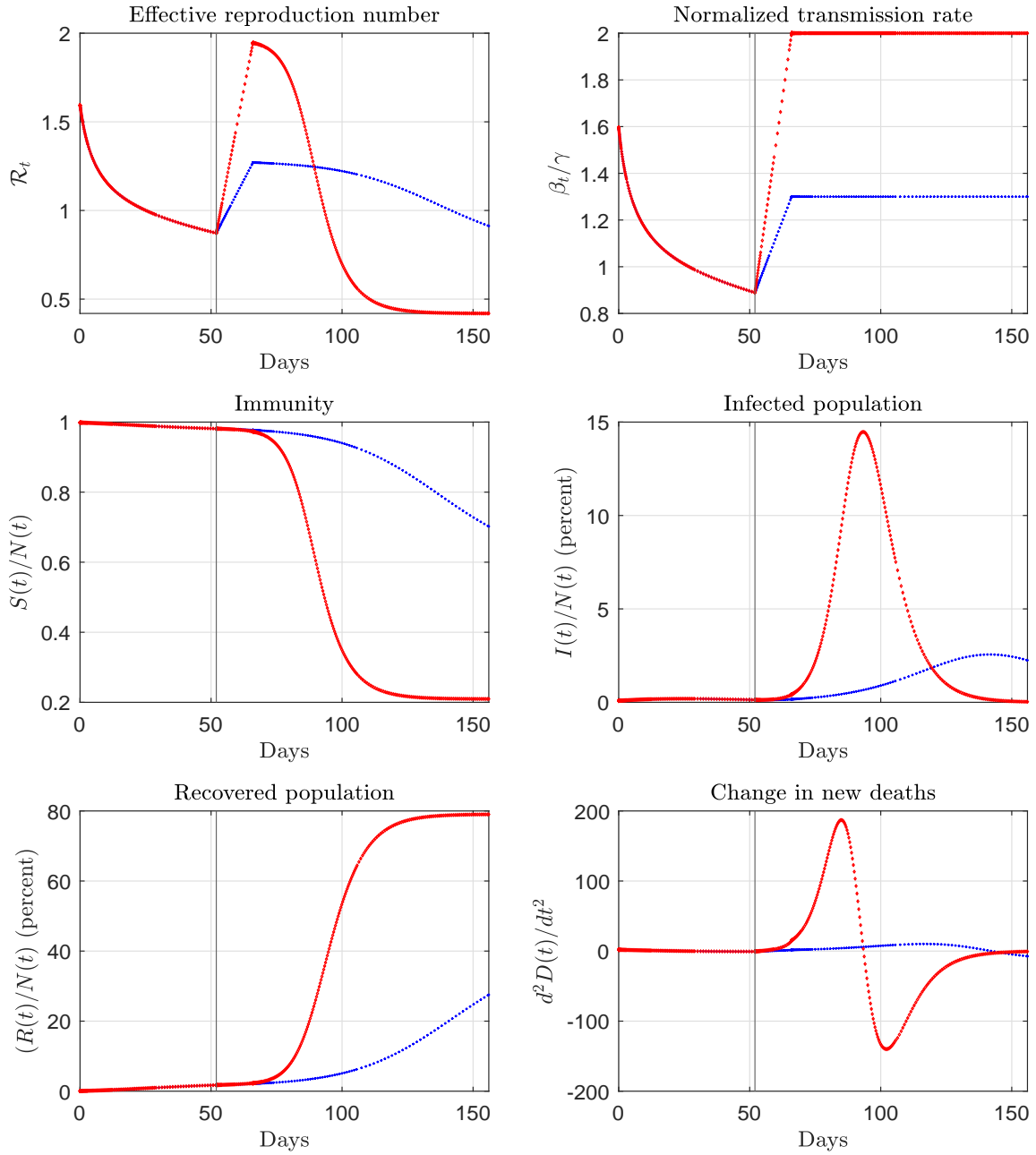
East South Central

Figure 75: Estimated and forecast paths for the East South Central region. The vertical line marks the end of the sample.

Figure 76: Counterfactual paths for the East South Central region. The vertical line marks the end of the sample.

Figure 77: Data and fitted paths of deaths in the Pacific region. The death pattern is fitted with one Weibull function.
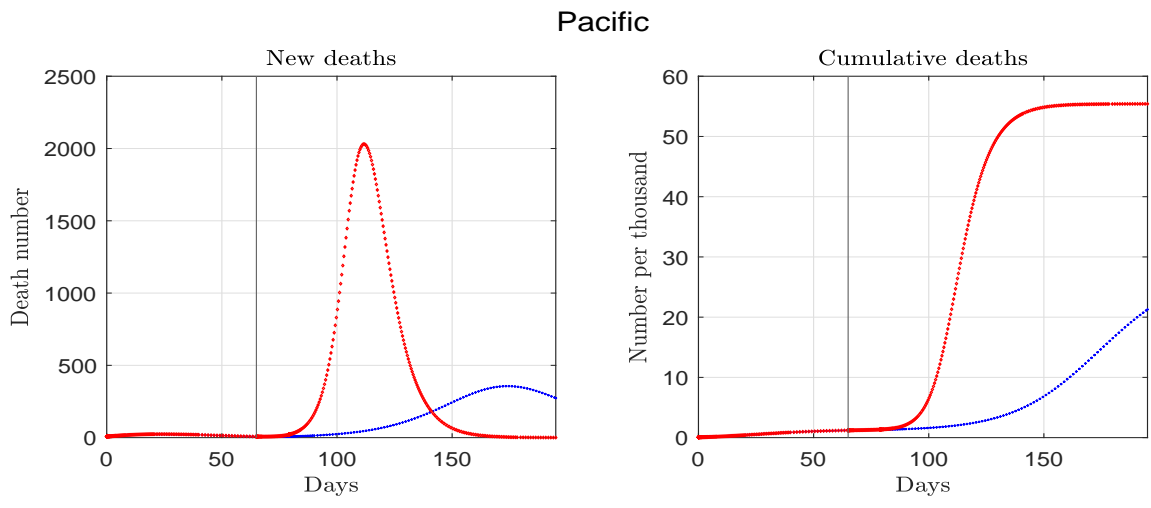
Figure 78: Estimated and forecast deaths for the Pacific region. The vertical line marks the end of the sample.

Pacific
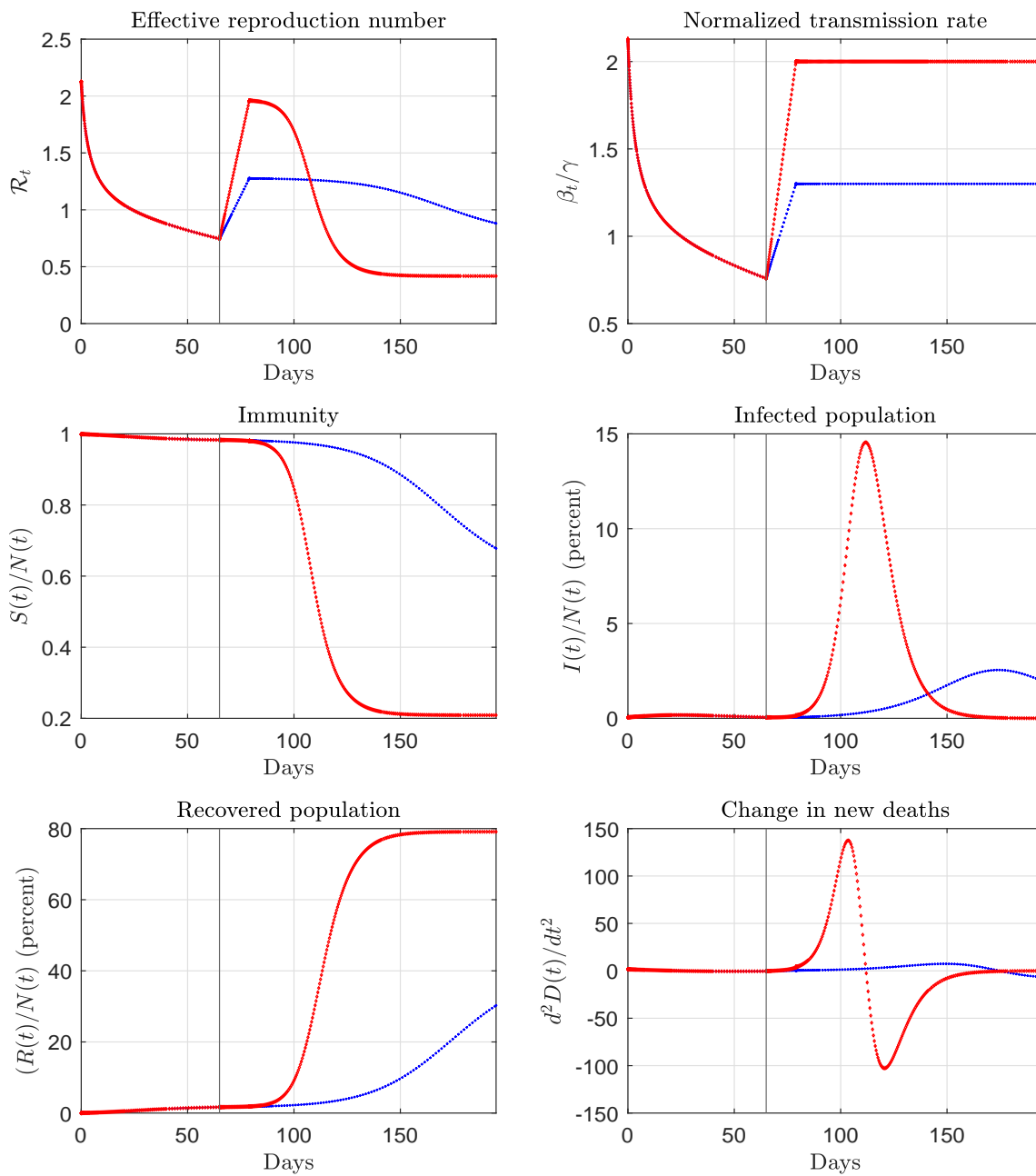
Figure 79: Estimated and forecast paths for the Pacific region. The vertical line marks the end of the sample.
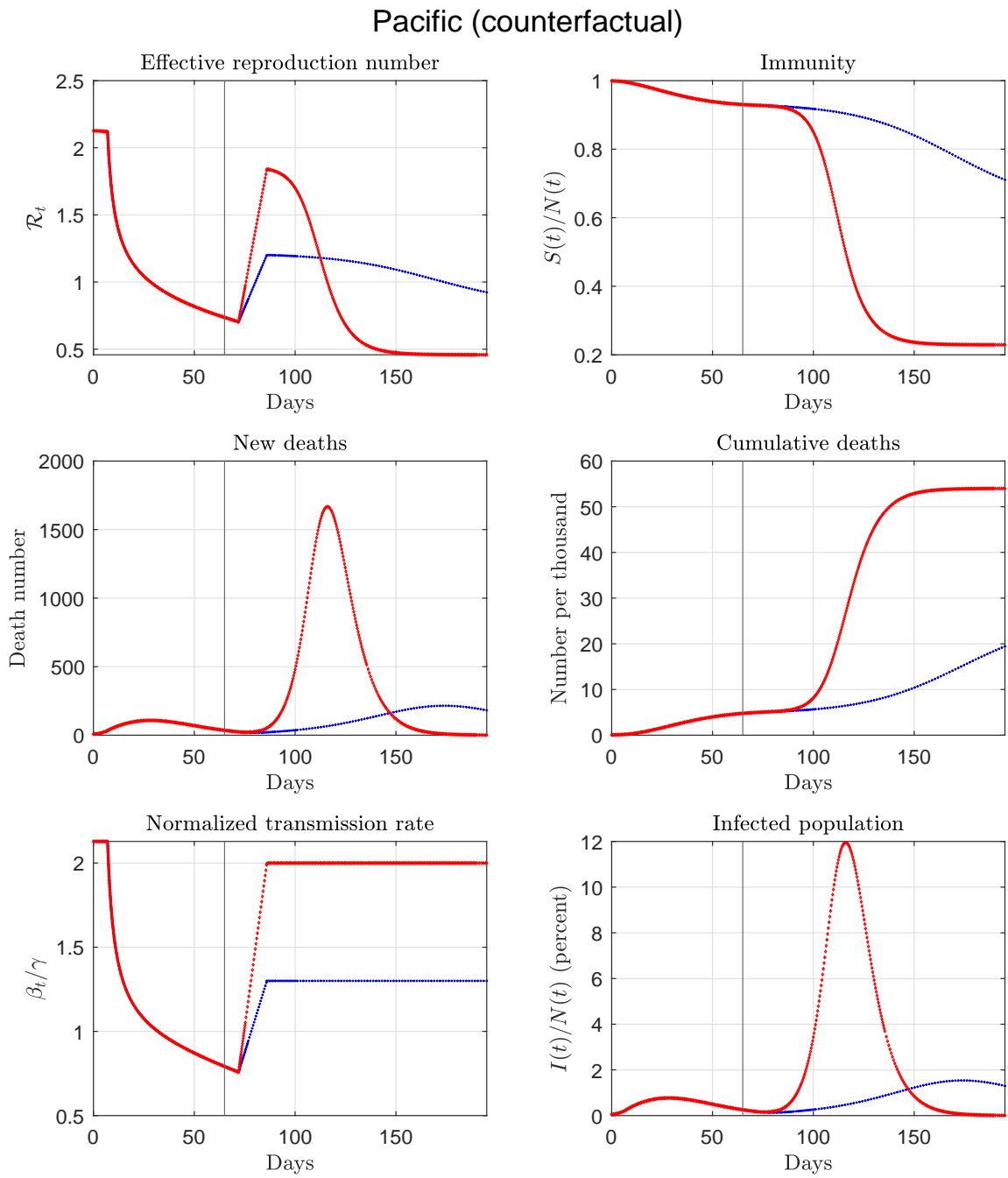
Figure 80: Counterfactual paths for the Pacific region. The vertical line marks the end of the sample.
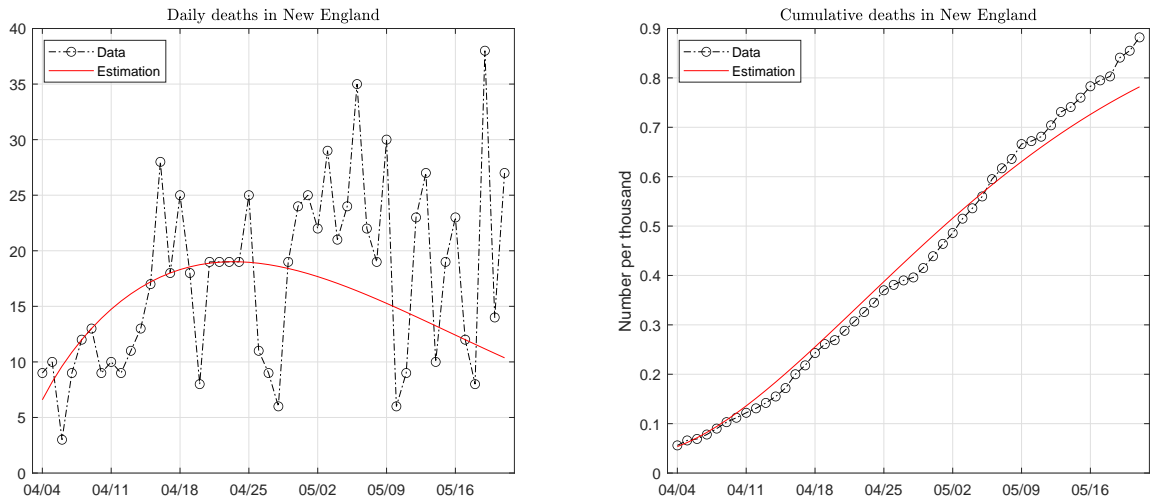
Figure 81: Data and fitted paths of deaths in the New England region. The death pattern is fitted with one Weibull function.
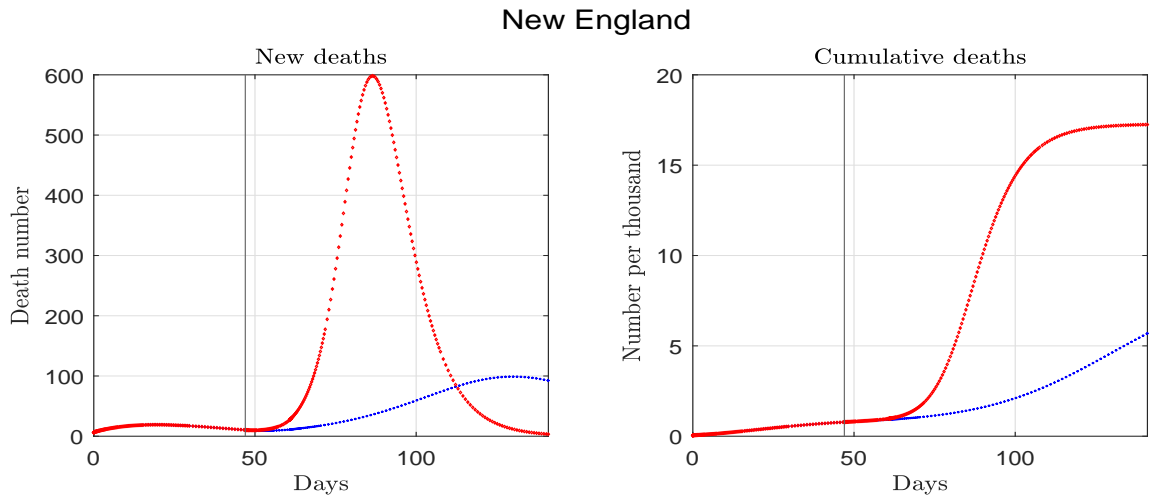
Figure 82: Estimated and forecast deaths for the New England region. The vertical line marks the end of the sample.

97
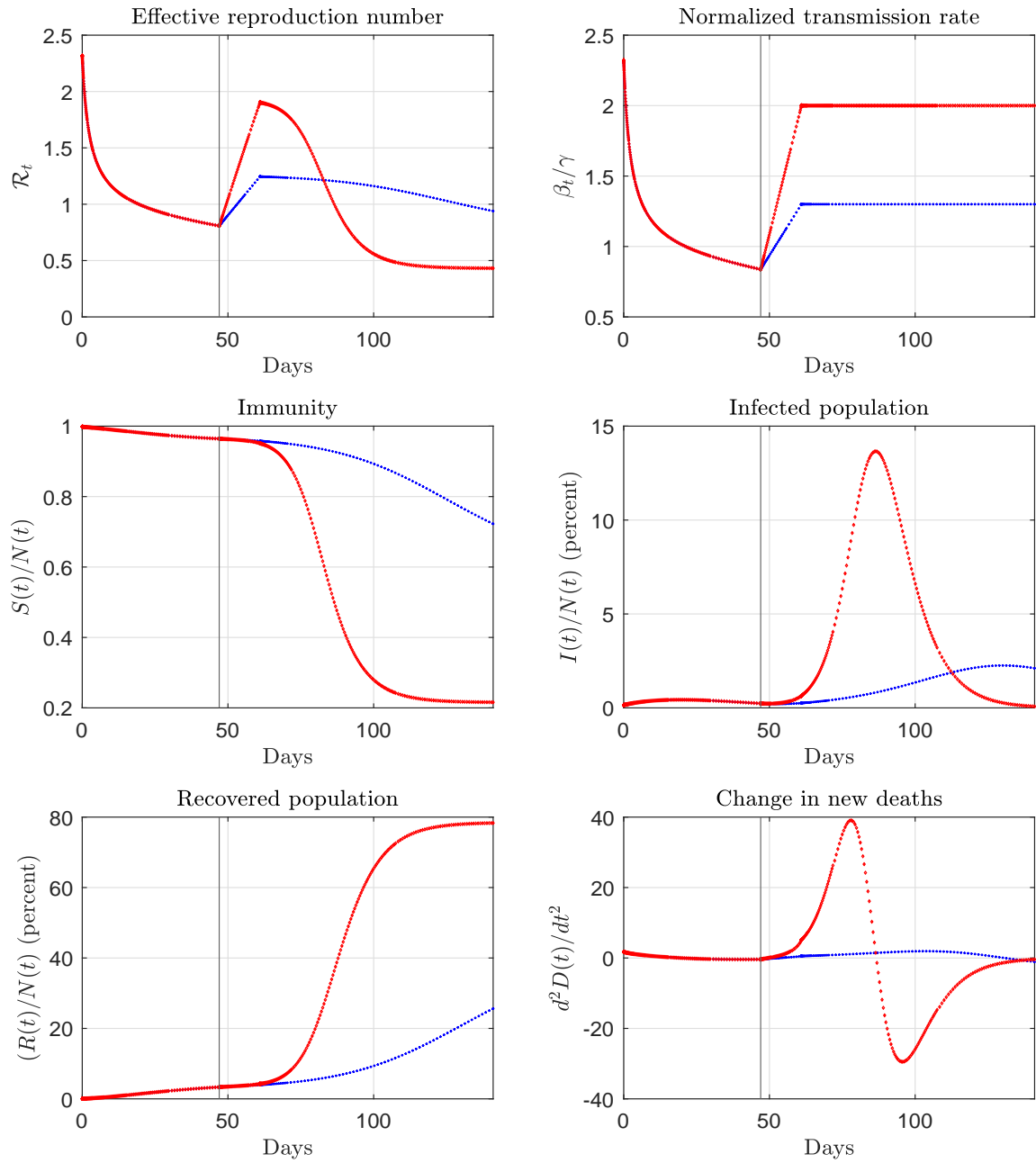
New England

Figure 83: Estimated and forecast paths for the New England region. The vertical line marks the end of the sample.
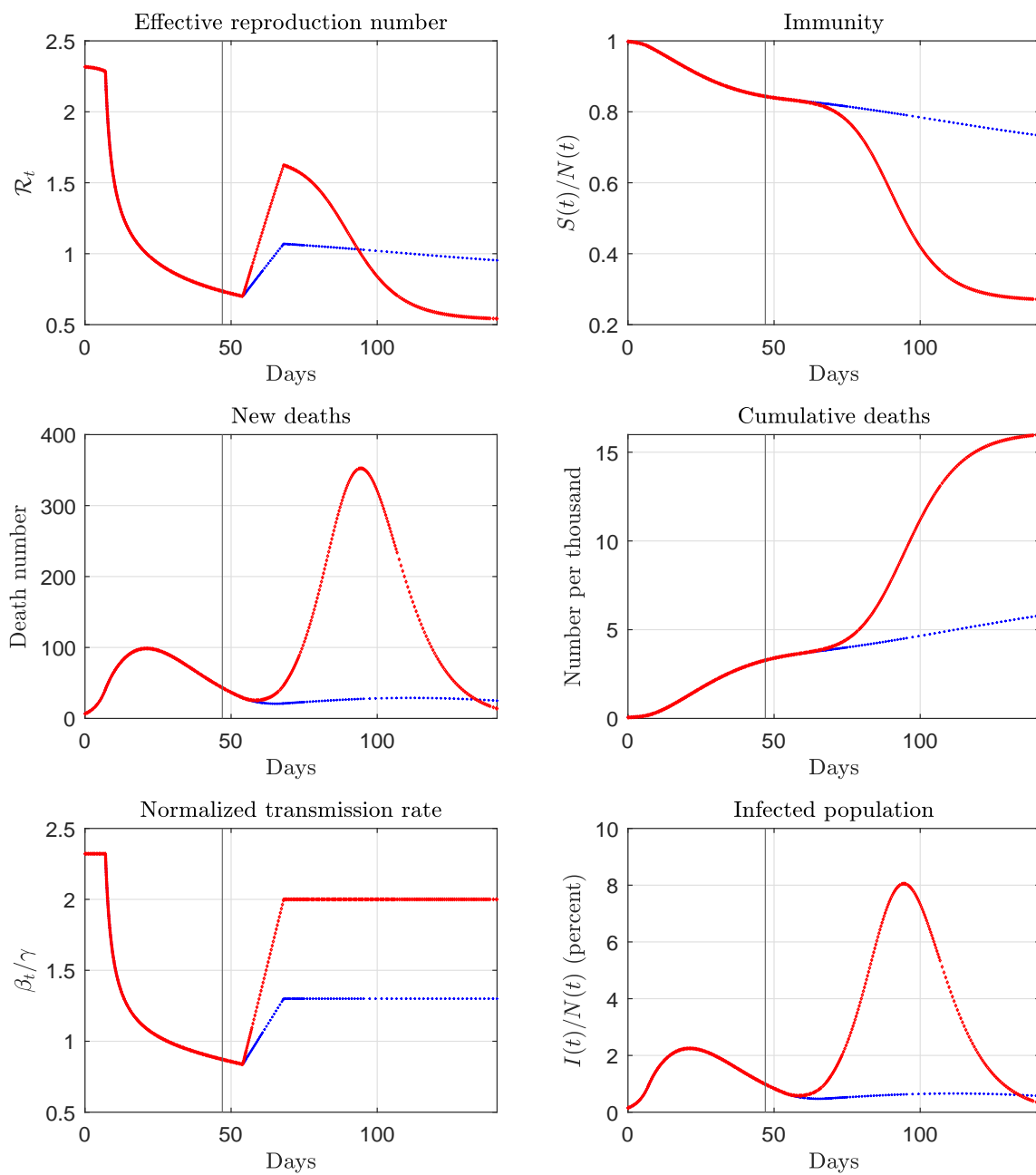
Figure 84: Counterfactual paths for the New England region. The vertical line marks the end of the sample.

A Empirical results for other countries

For all the countries reported below, $\gamma = 0.2$ except for France and Mexico where γ is set to 0.5 to keep β_t positive during the sample period.
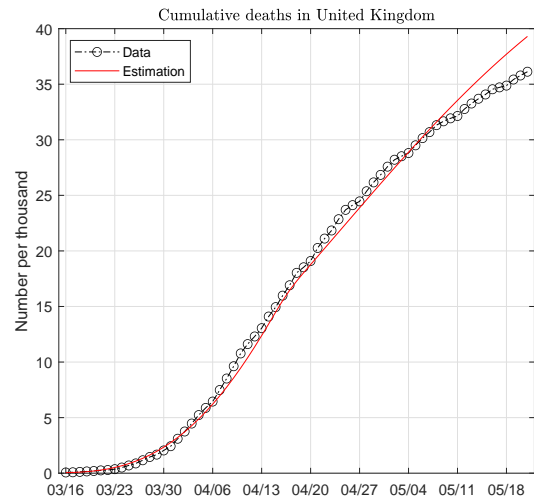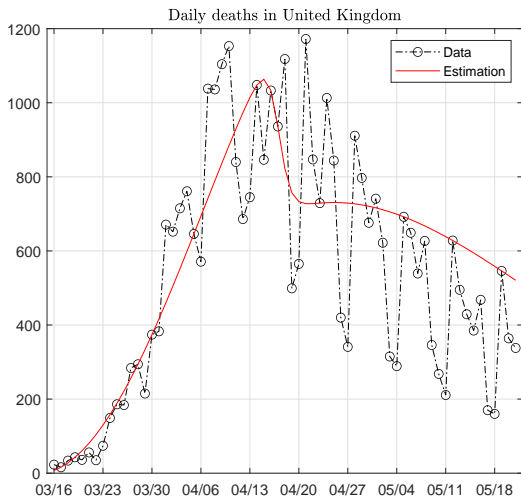
Figure A.1: Data and fitted paths of deaths in United Kingdom. The death pattern is fitted with a mixture of two Weibull functions.

Figure A.2: Estimated and forecast deaths for United Kingdom. The vertical line marks the end of the sample.
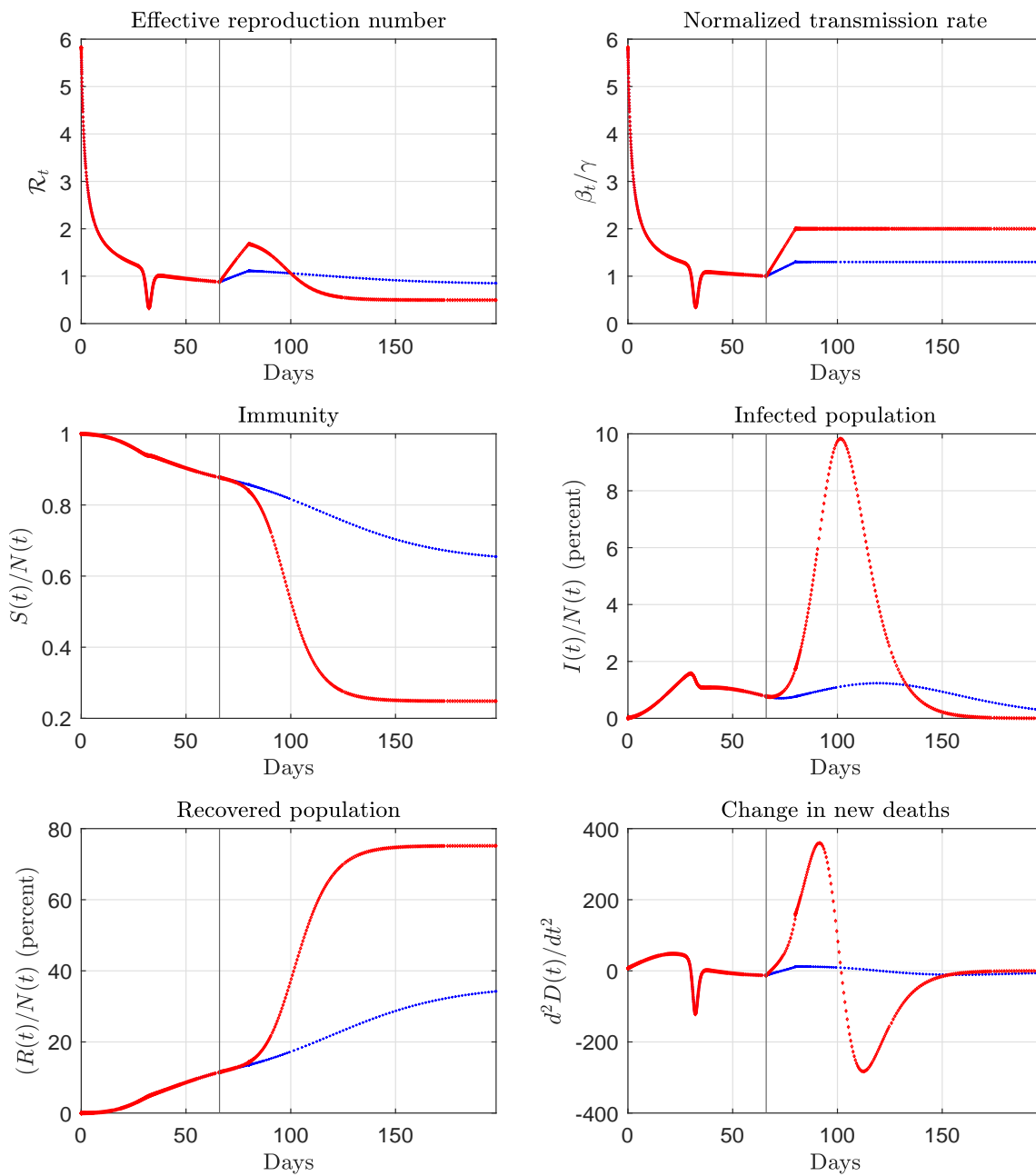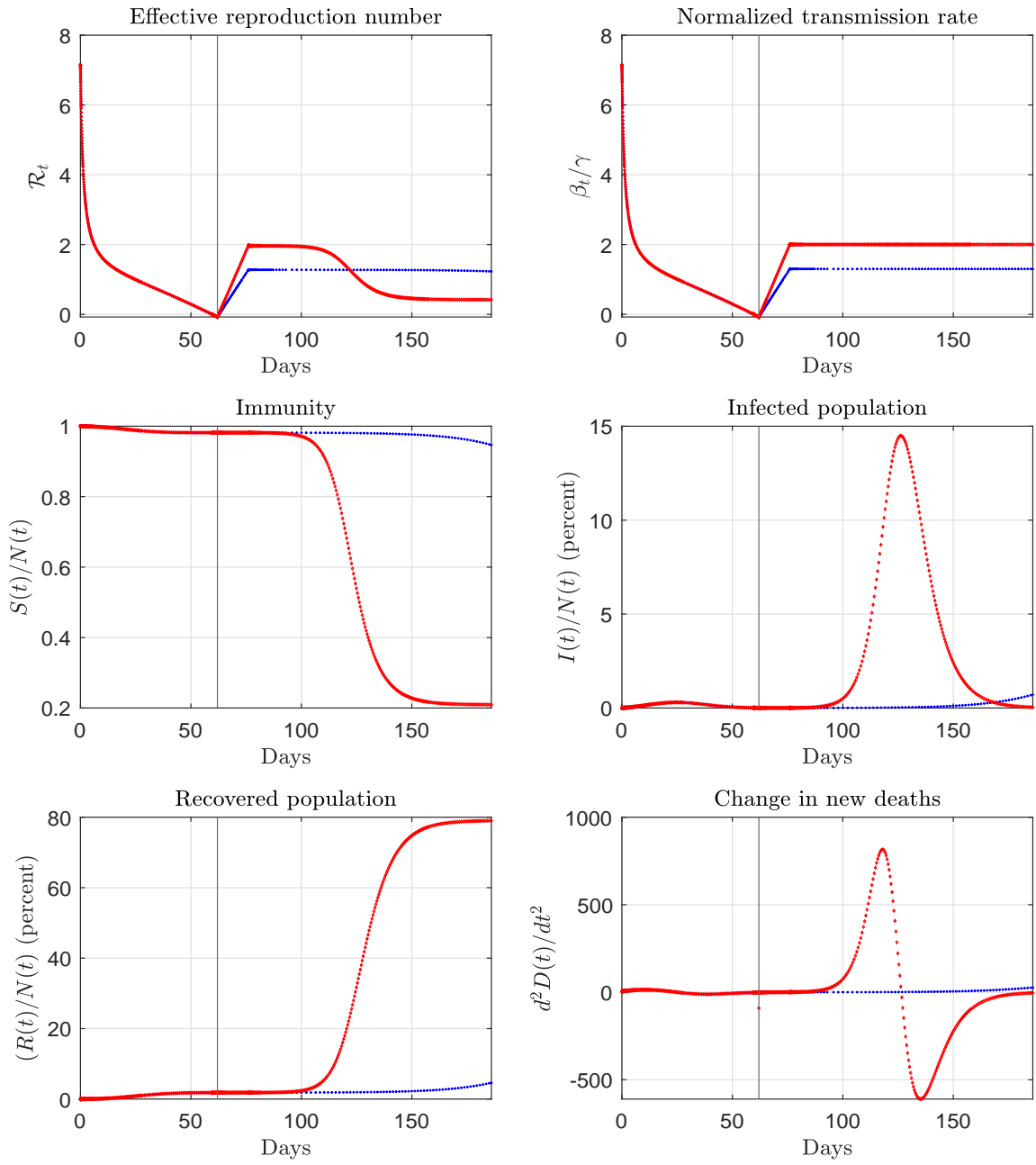
Figure A.3: Estimated and forecast paths for United Kingdom. The vertical line marks the end of the sample.

Figure A.4: Counterfactual paths for United Kingdom. The vertical line marks the end of the sample.
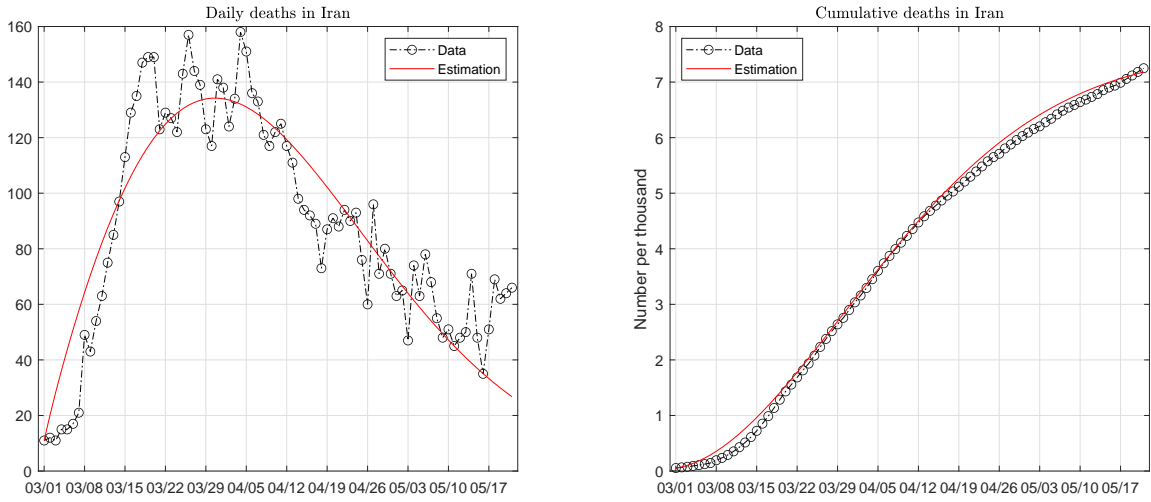
103
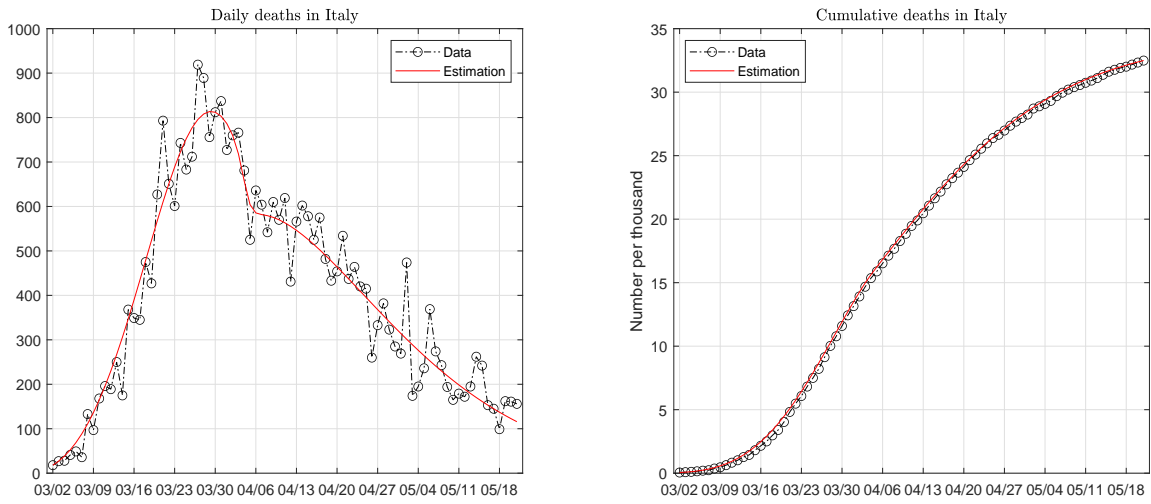
Figure A.5: Data and fitted paths of deaths in Italy. The death pattern is fitted with a mixture of two Weibull functions.
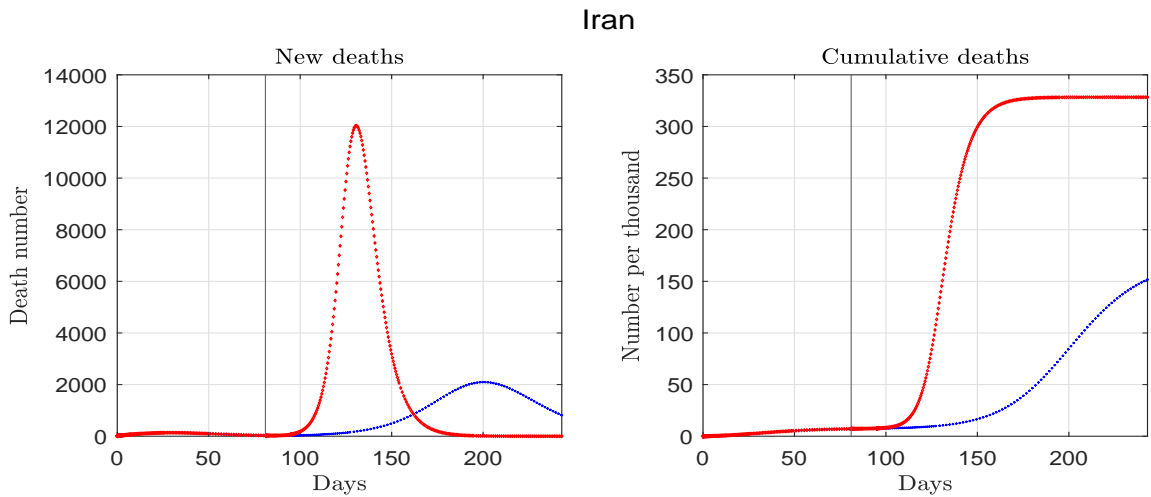

Figure A.6: Estimated and forecast deaths for Italy. The vertical line marks the end of the sample.

104

Italy

Figure A.7: Estimated and forecast paths for Italy. The vertical line marks the end of the sample.

Figure A.8: Counterfactual paths for Italy. The vertical line marks the end of the sample.

Figure A.9: Data and fitted paths of deaths in France. The death pattern is fitted with a mixture of two Weibull functions.

Figure A.10: Estimated and forecast deaths for France. The vertical line marks the end of the sample.
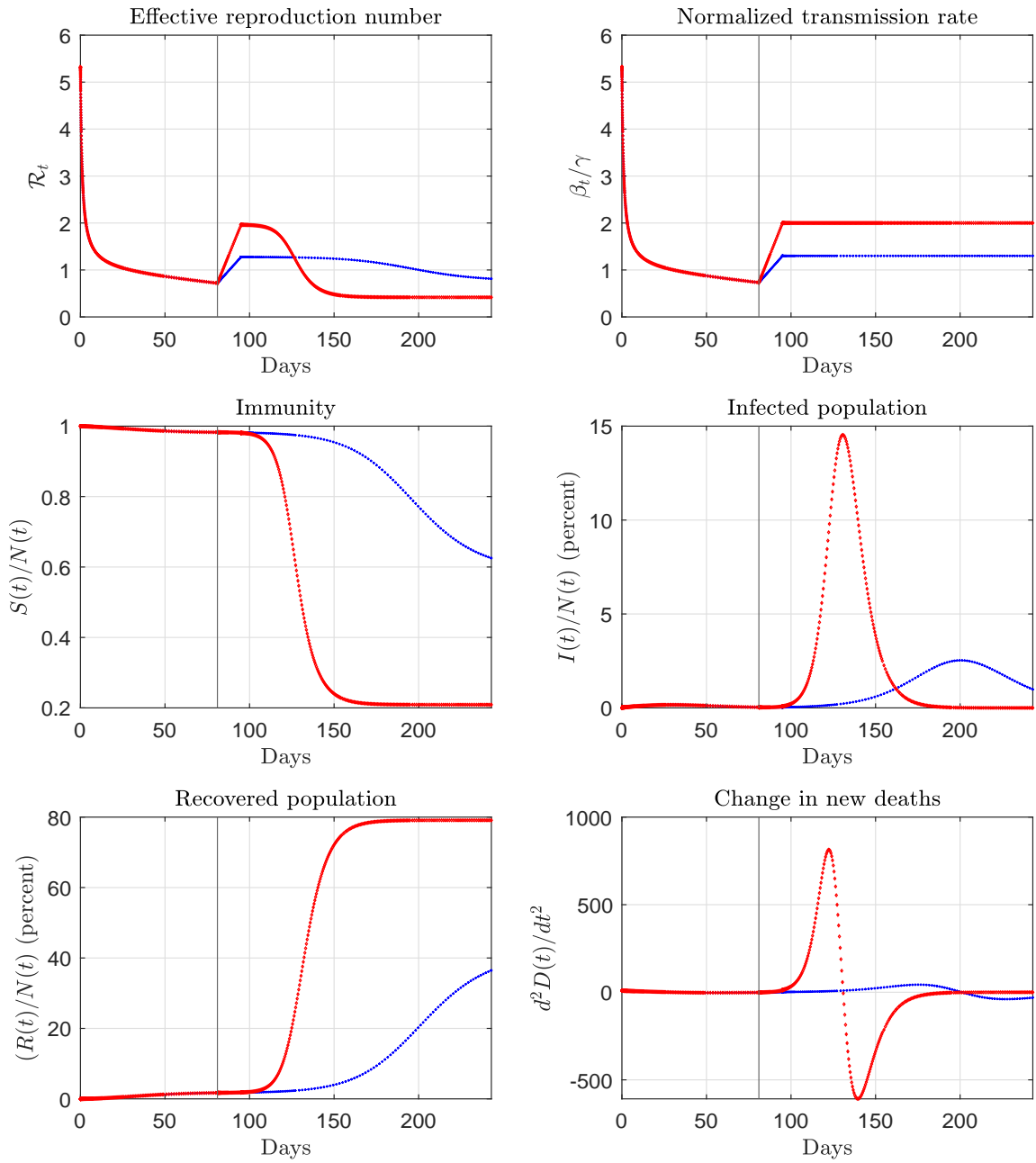
107

France

Figure A.11: Estimated and forecast paths for France. The vertical line marks the end of the sample.
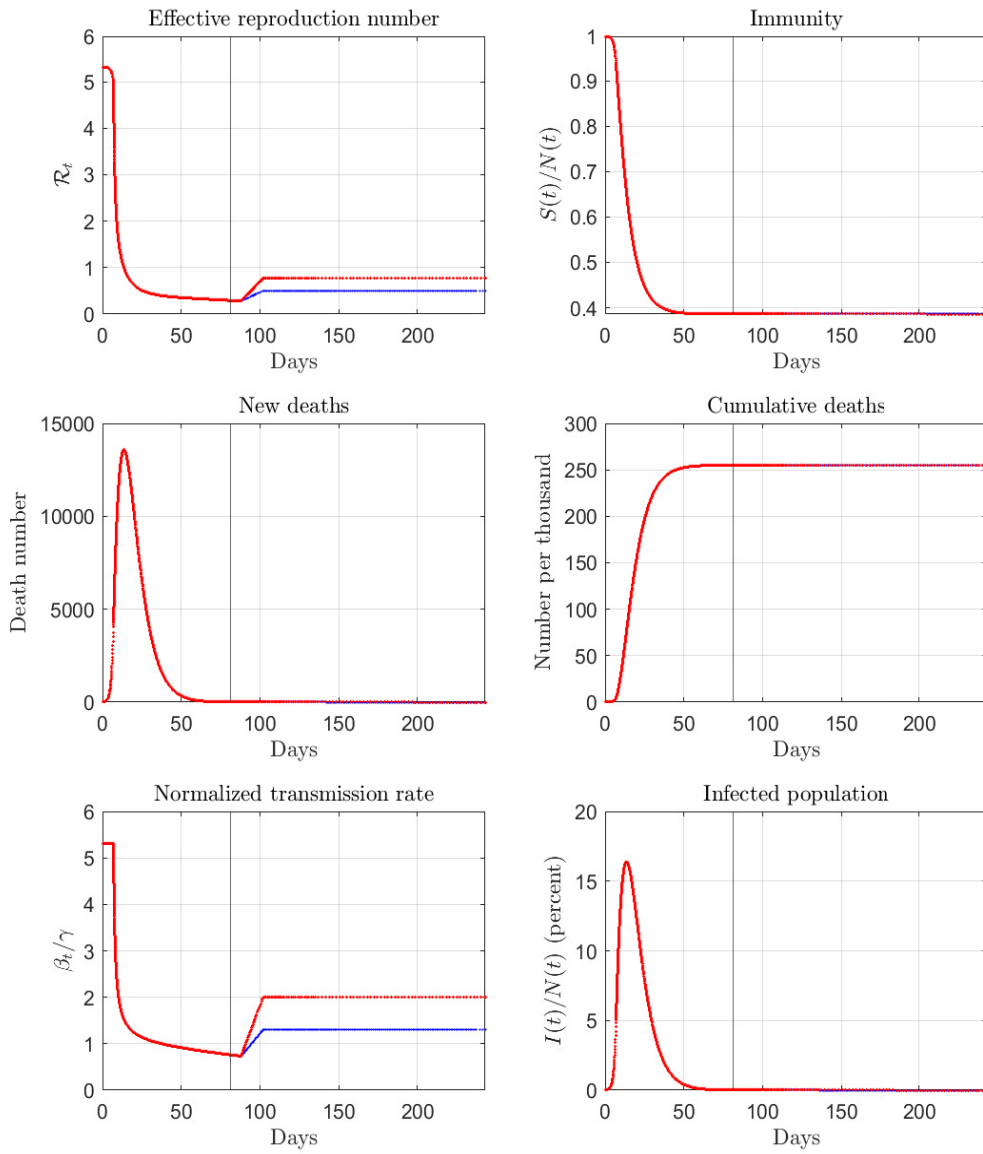
108

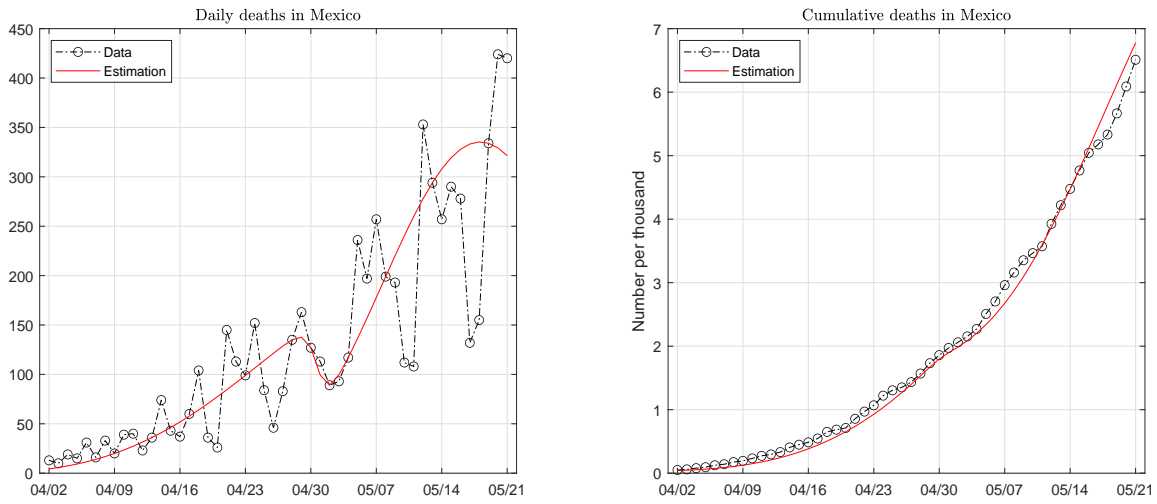**Figure A.12:** Counterfactual paths for France. The vertical line marks the end of the sample.

Figure A.13: Data and fitted paths of deaths in Spain. The death pattern is fitted with a mixture of two Weibull functions.
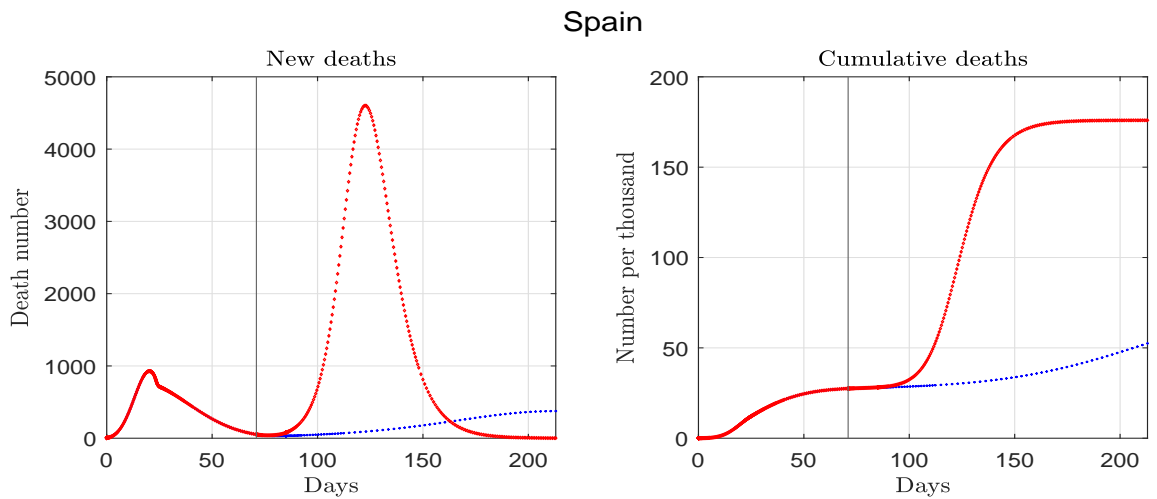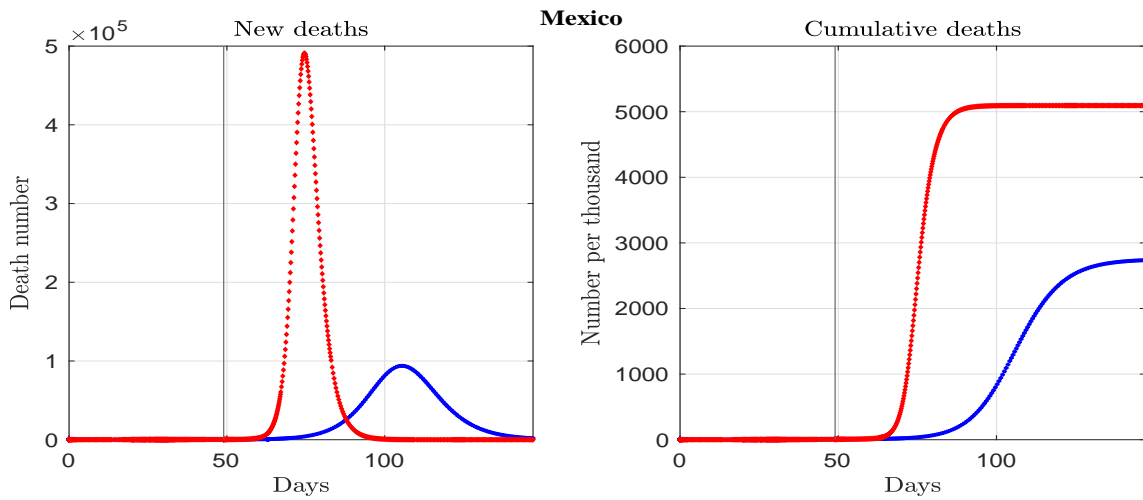

Figure A.14: Estimated and forecast deaths for Spain. The vertical line marks the end of the sample.
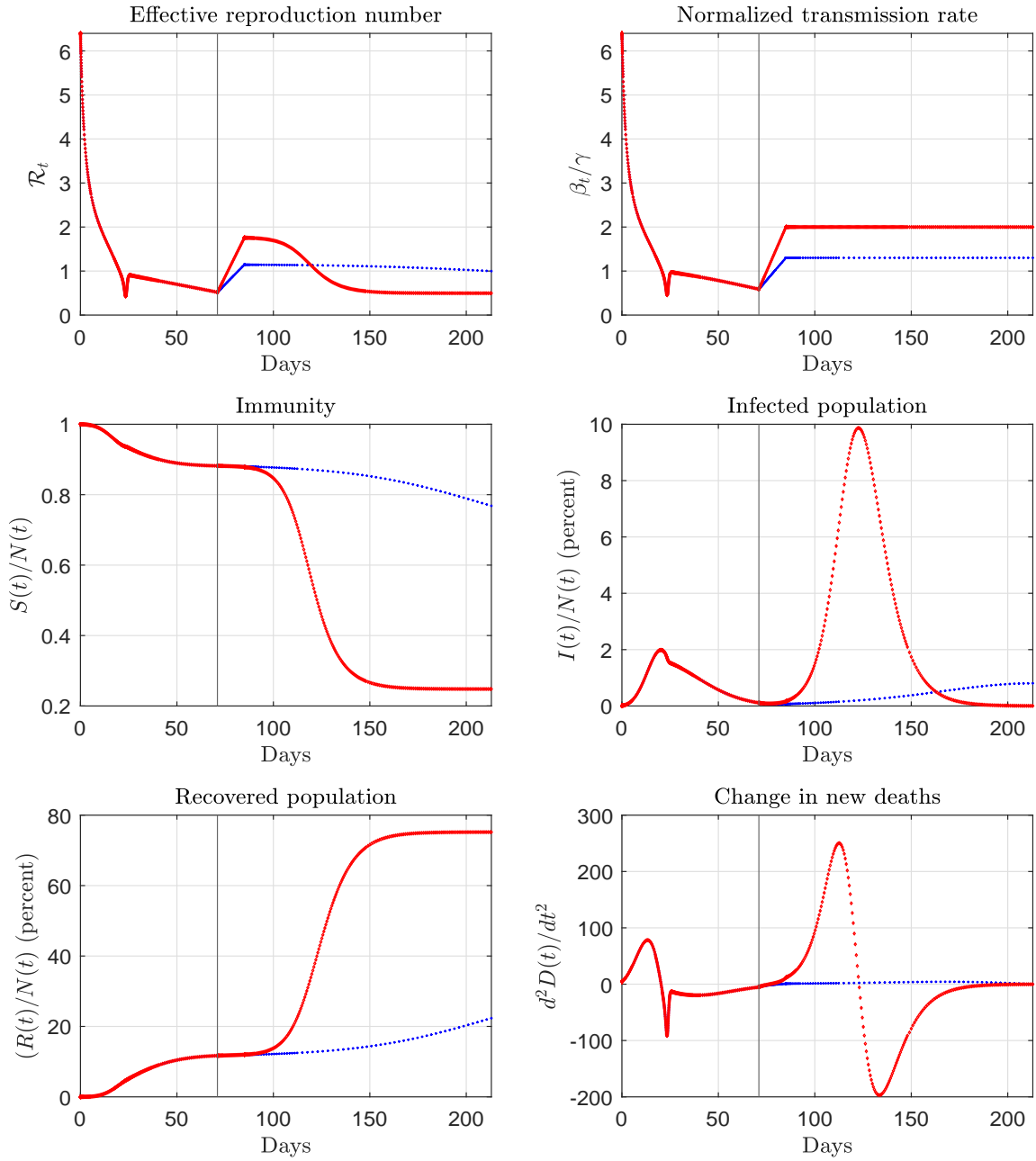
Spain

Figure A.15: Estimated and forecast paths for Spain. The vertical line marks the end of the sample.

Spain (counterfactual)
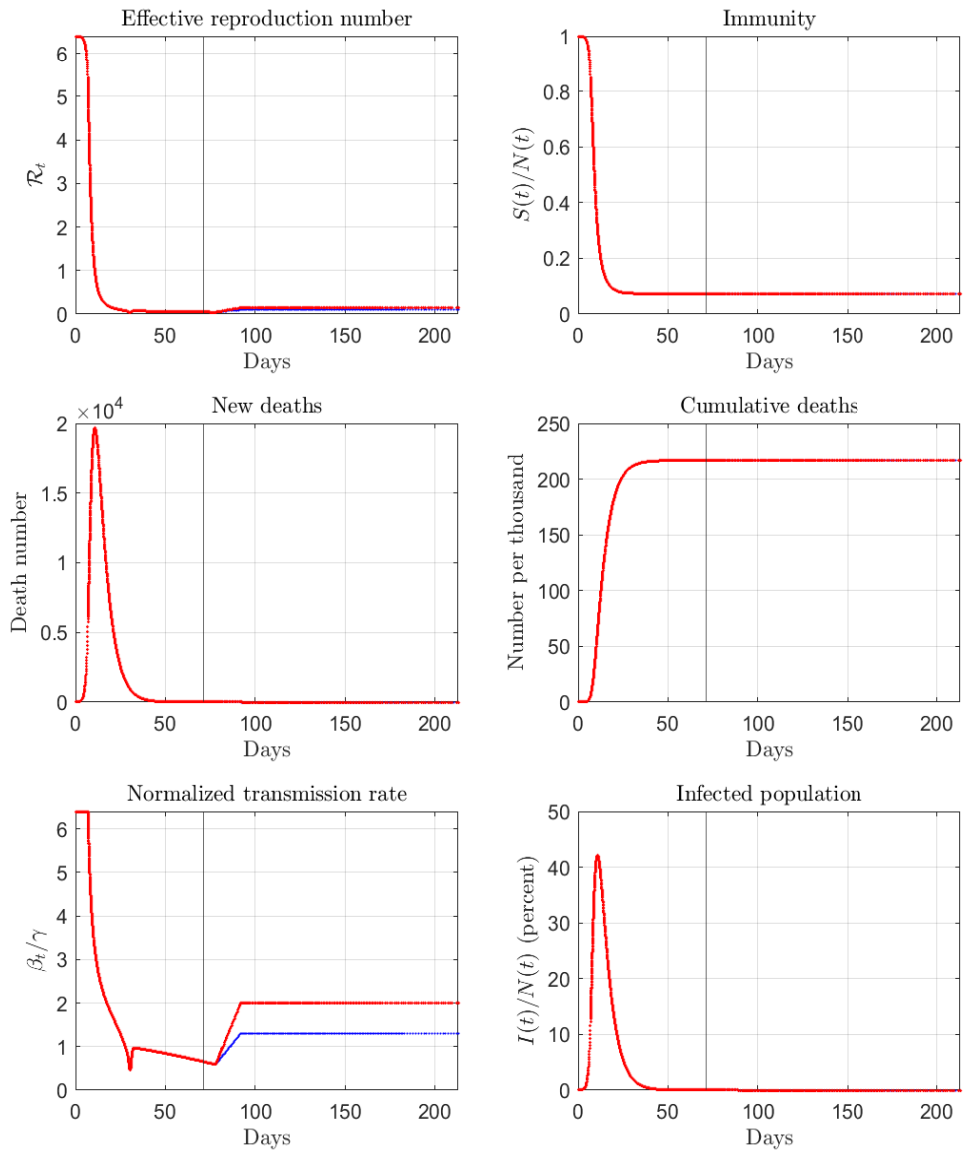
Figure A.16: Counterfactual paths for Spain. The vertical line marks the end of the sample.
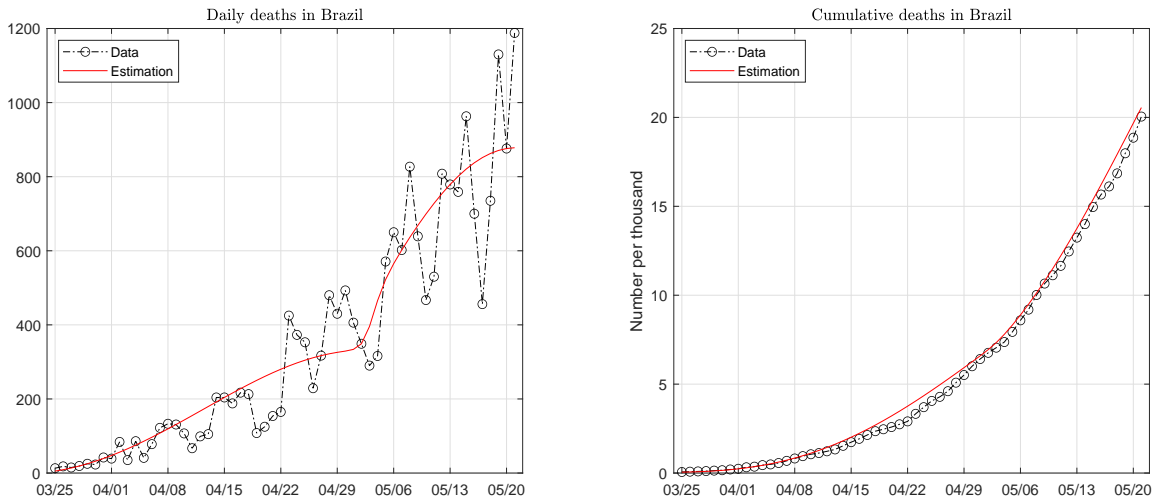
Figure A.17: Data and fitted paths of deaths in Brazil. The death pattern is fitted with a mixture of two Weibull functions.
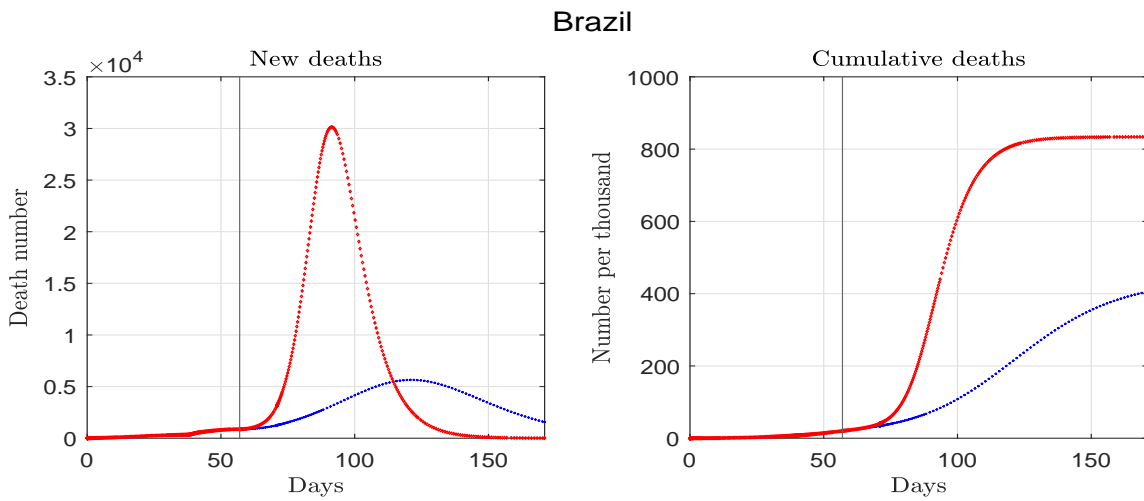
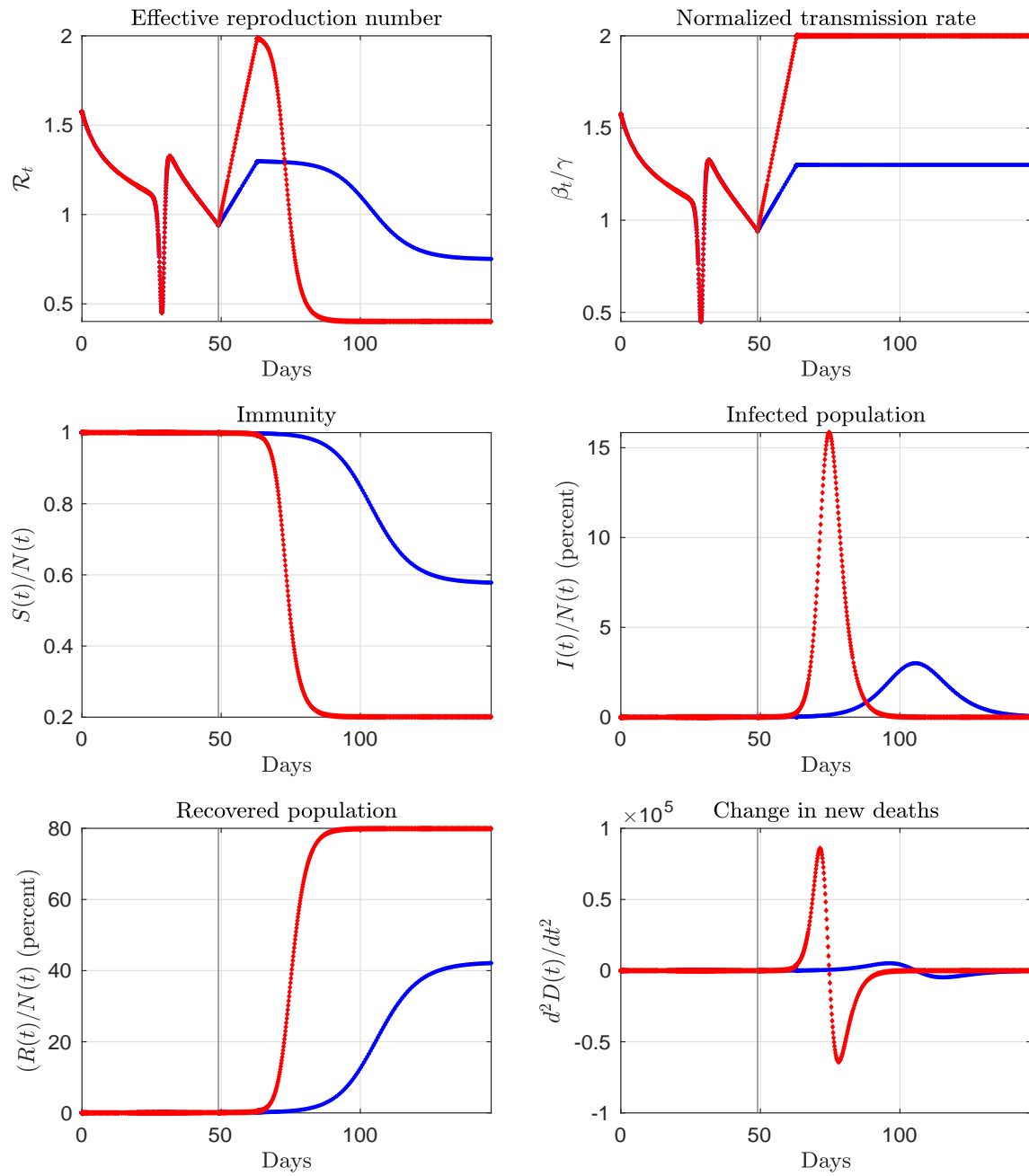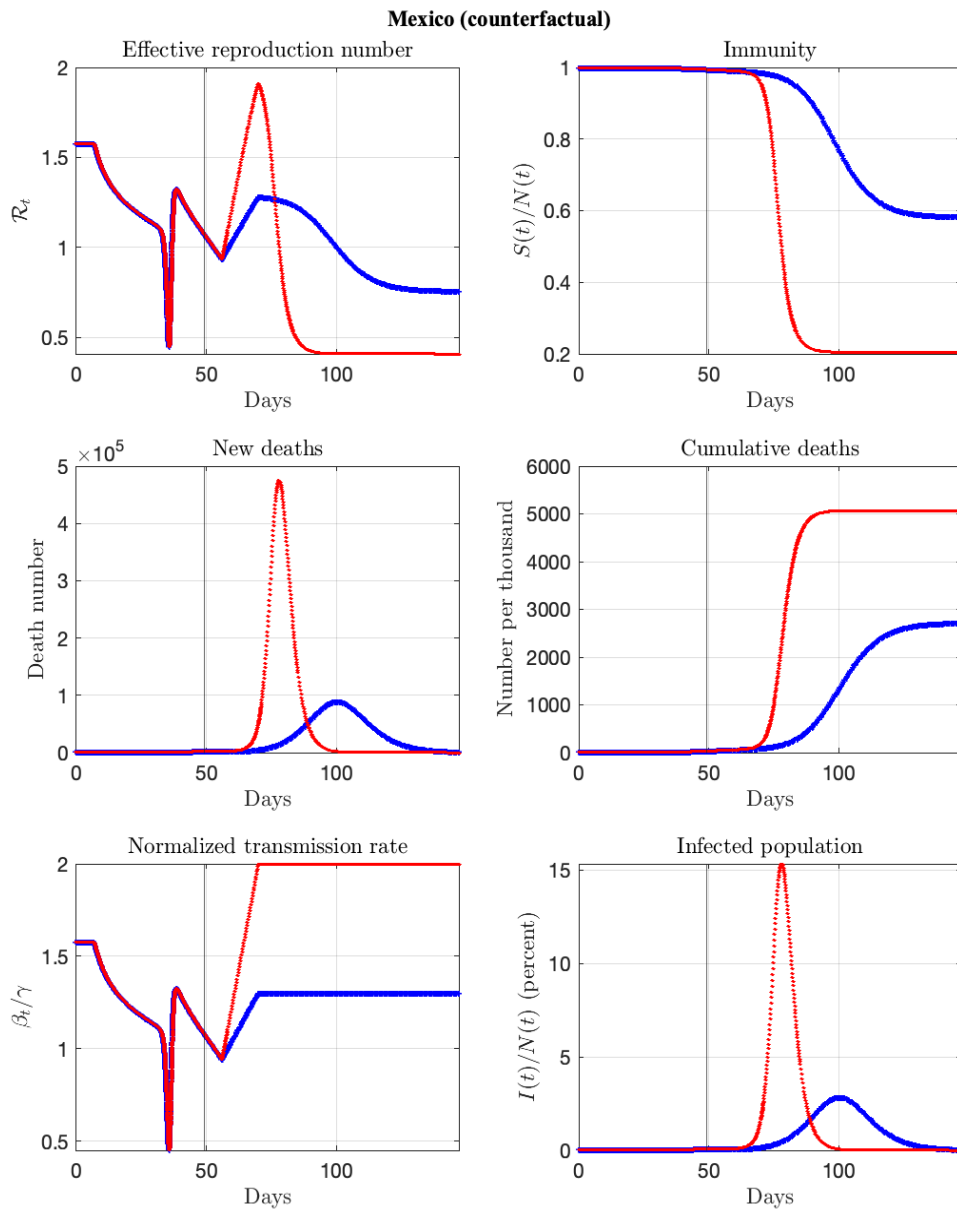**Figure A.18:** Estimated and forecast deaths for Brazil. The vertical line marks the end of the sample.
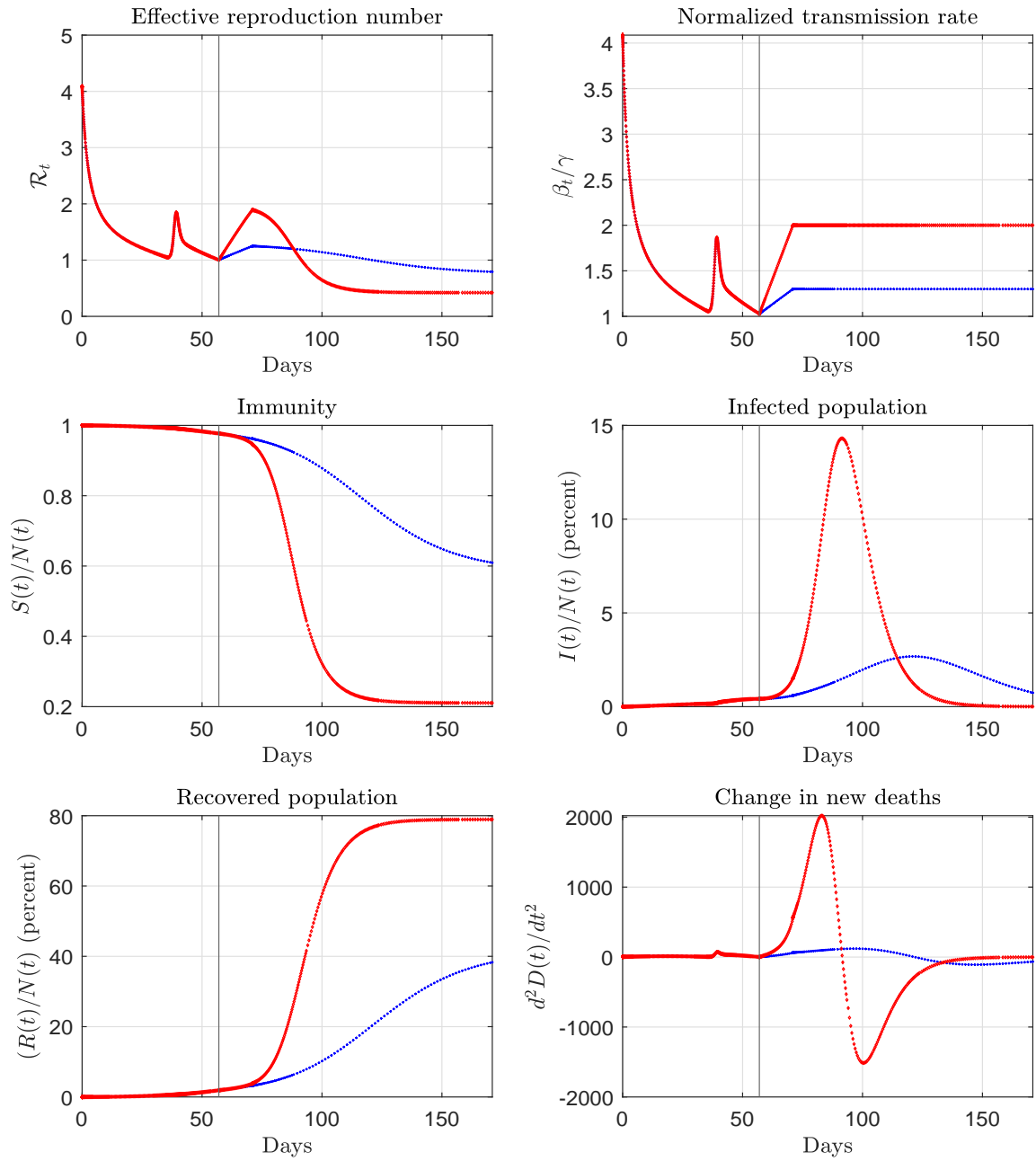
Brazil

Figure A.19: Estimated and forecast paths for Brazil. The vertical line marks the end of the sample.

Brazil (counterfactual)
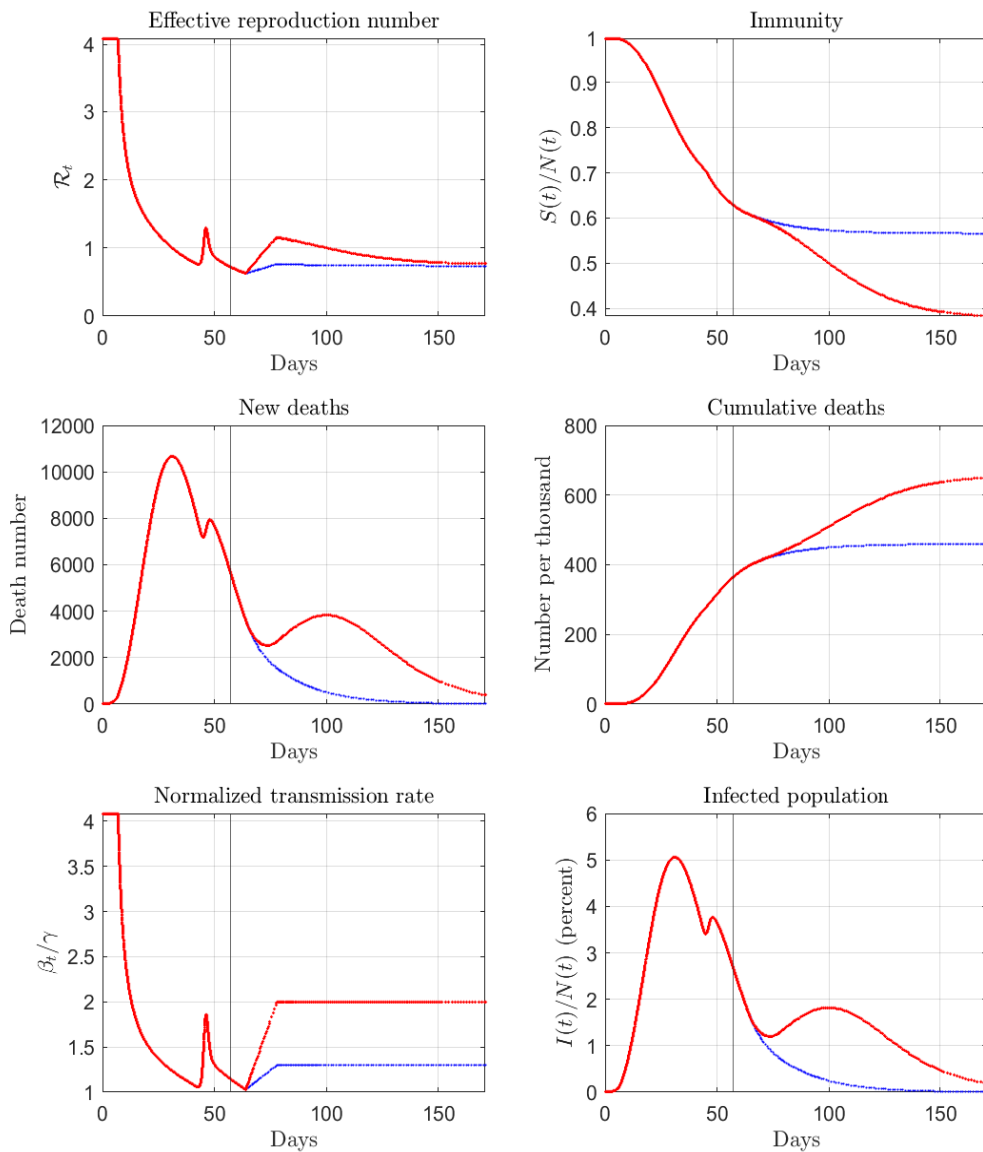
Figure A.20: Counterfactual paths for Brazil. The vertical line marks the end of the sample.
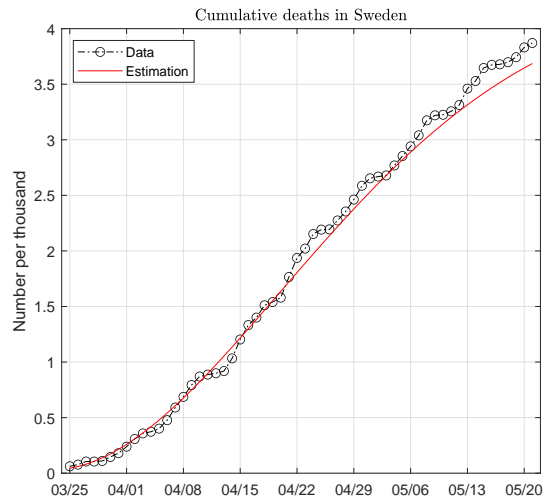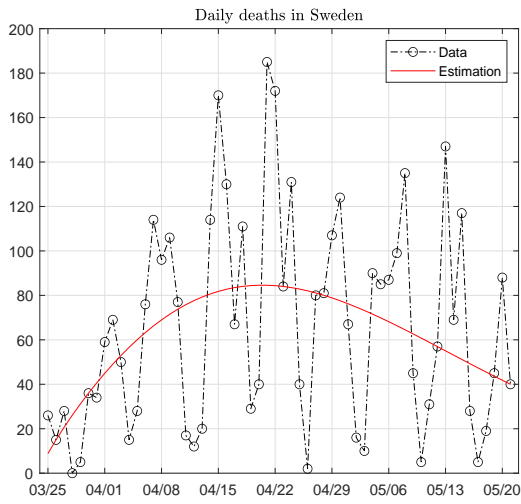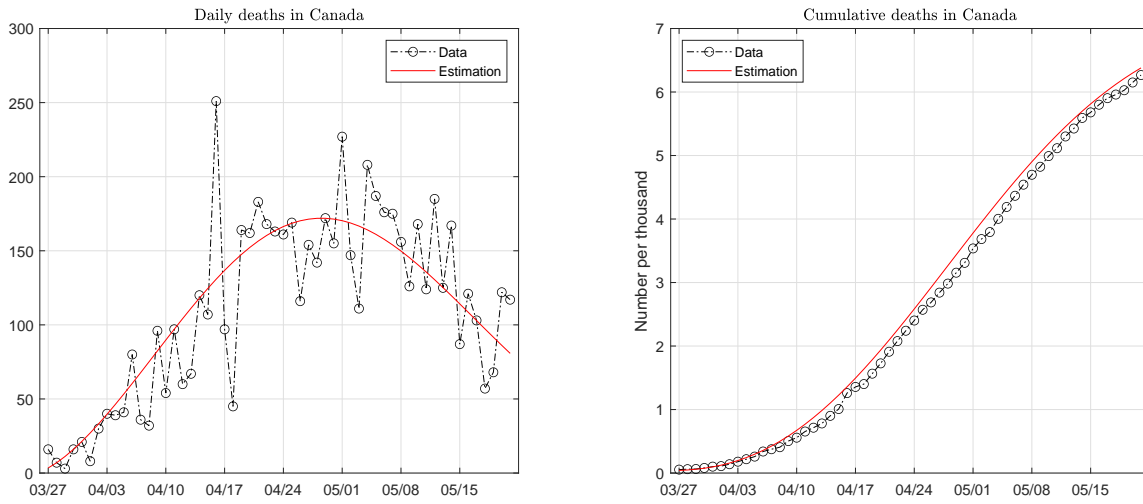
Figure A.21: Data and fitted paths of deaths in Sweden. The death pattern is fitted with a mixture of two Weibull functions.
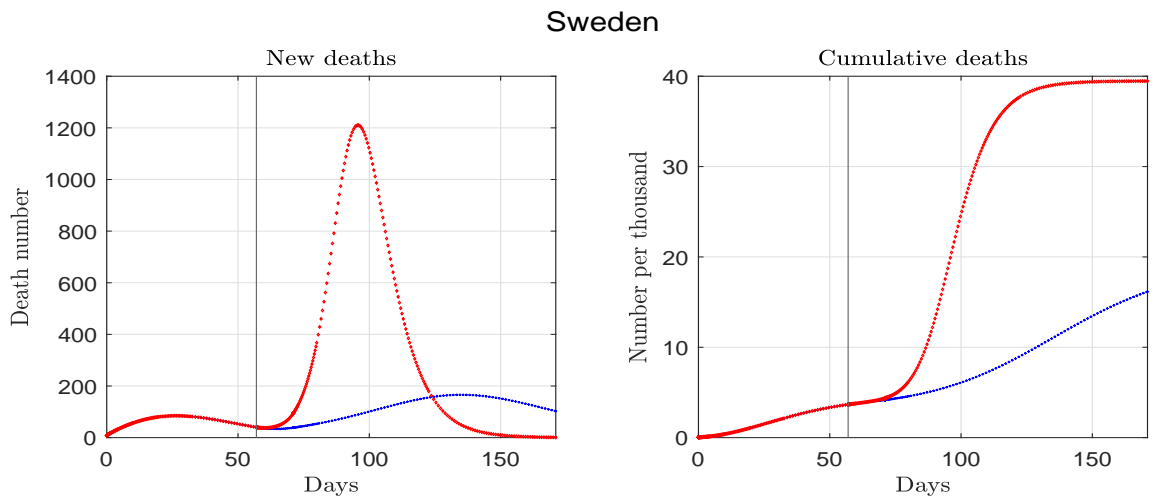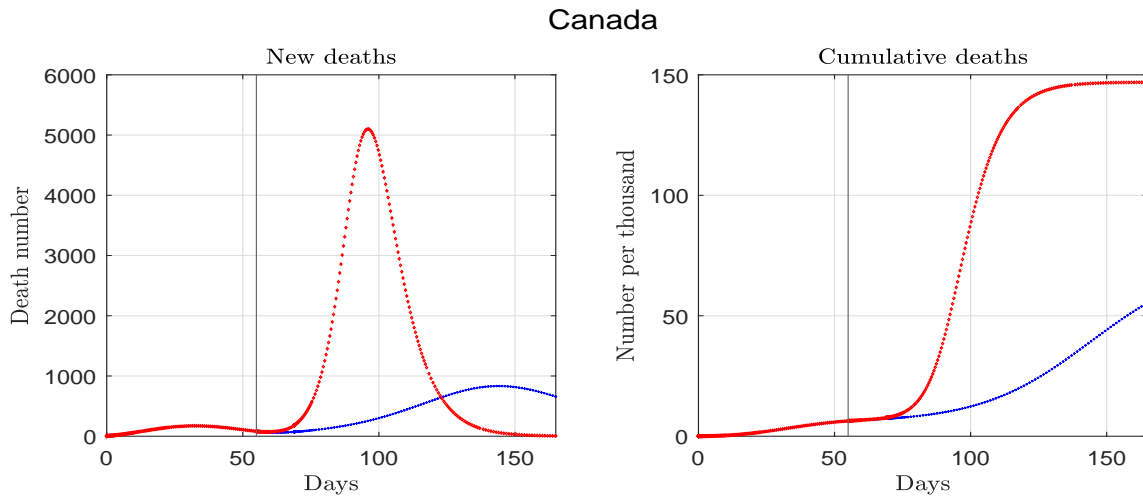

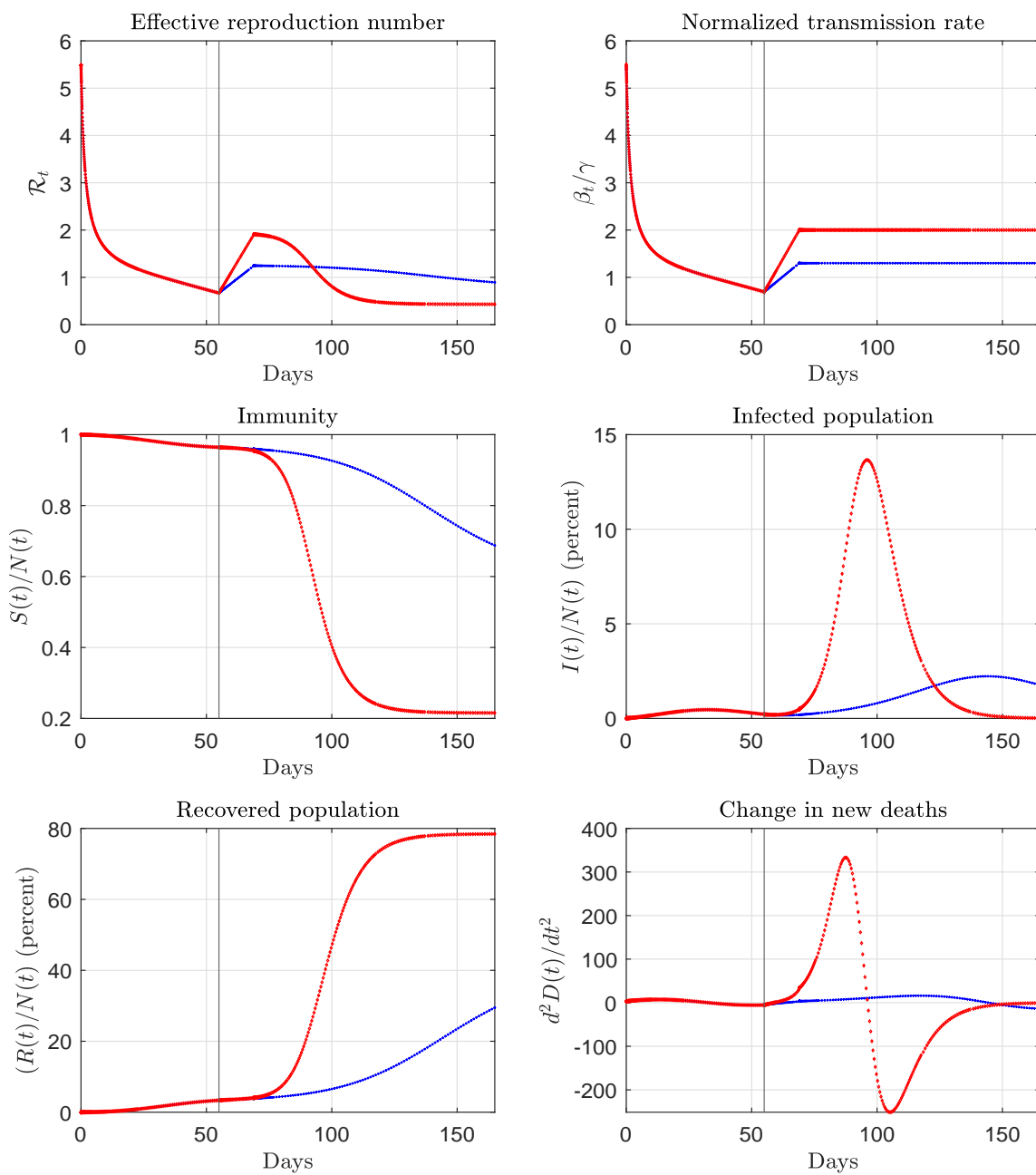**Figure A.22:** Estimated and forecast deaths for Sweden. The vertical line marks the end of the sample.
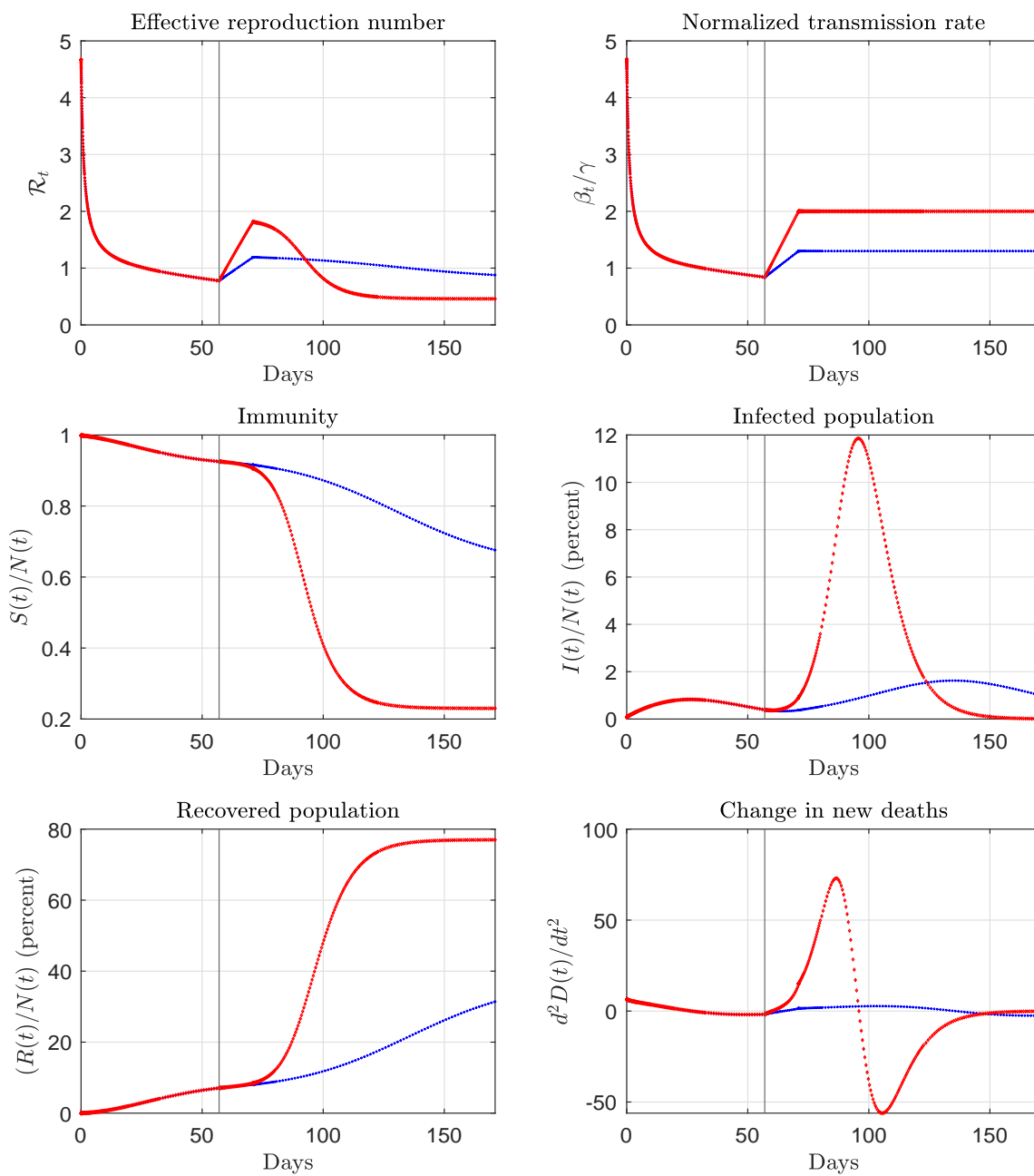
Sweden

Figure A.23: Estimated and forecast paths for Sweden. The vertical line marks the end of the sample.
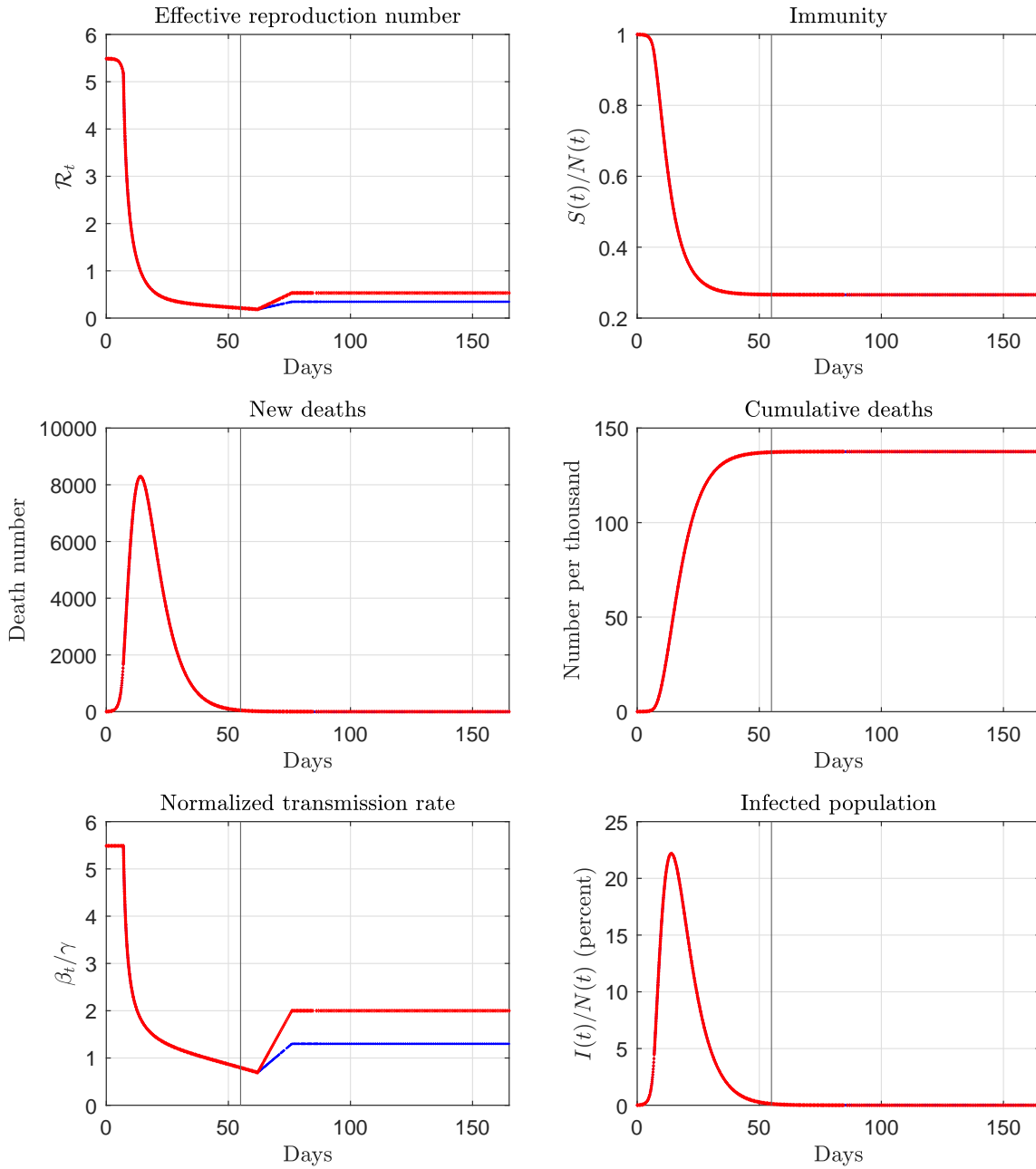
Sweden (counterfactual)
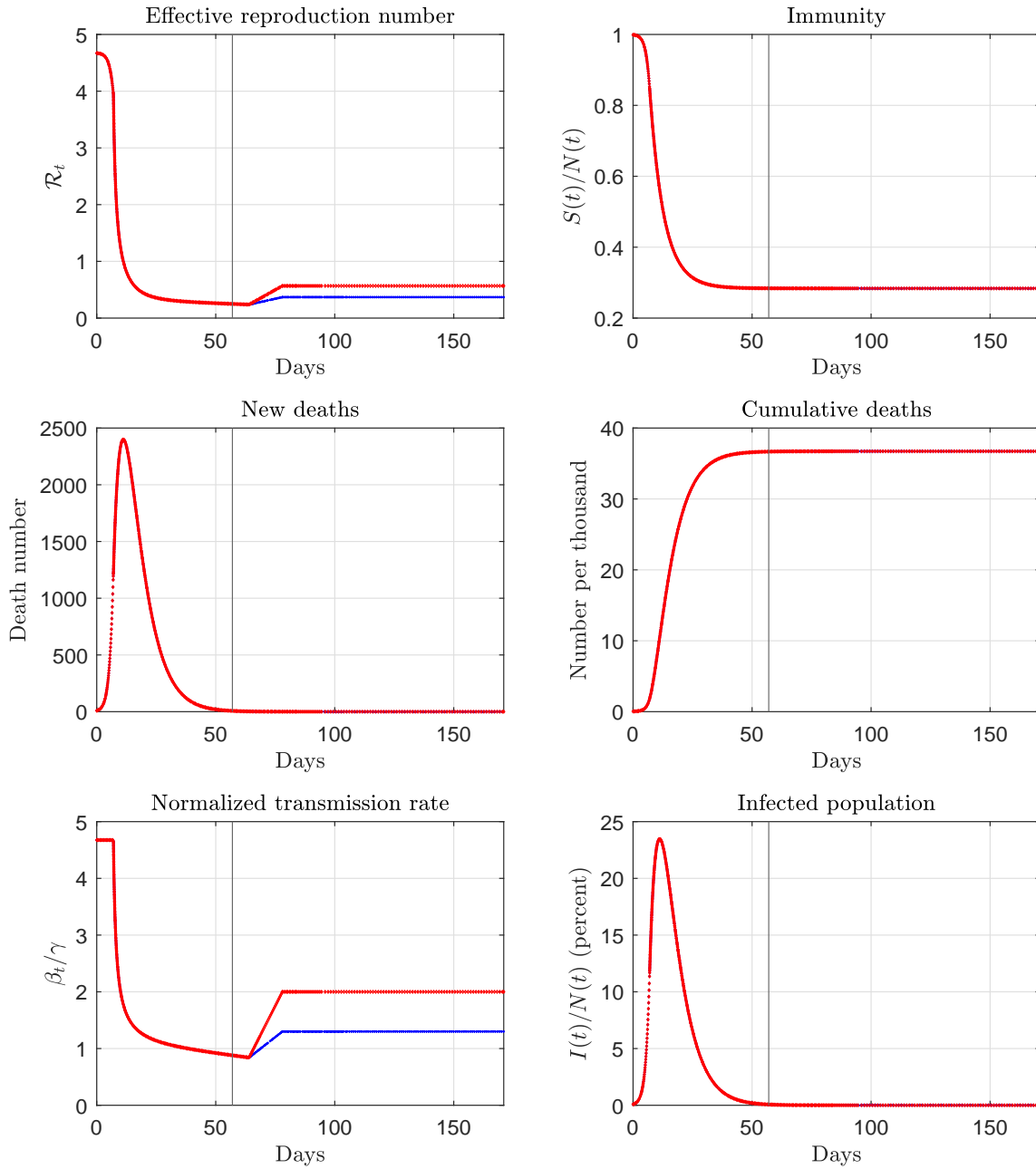
Figure A.24: Counterfactual paths for Sweden. The vertical line marks the end of the sample.

118
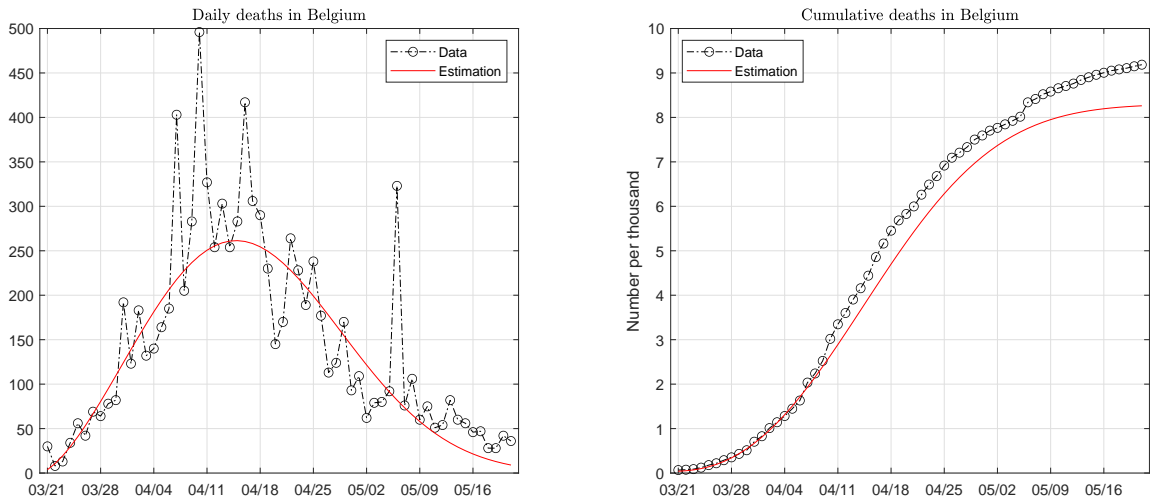
Figure A.25: Data and fitted paths of deaths in Belgium. The death pattern is fitted with a mixture of two Weibull functions.
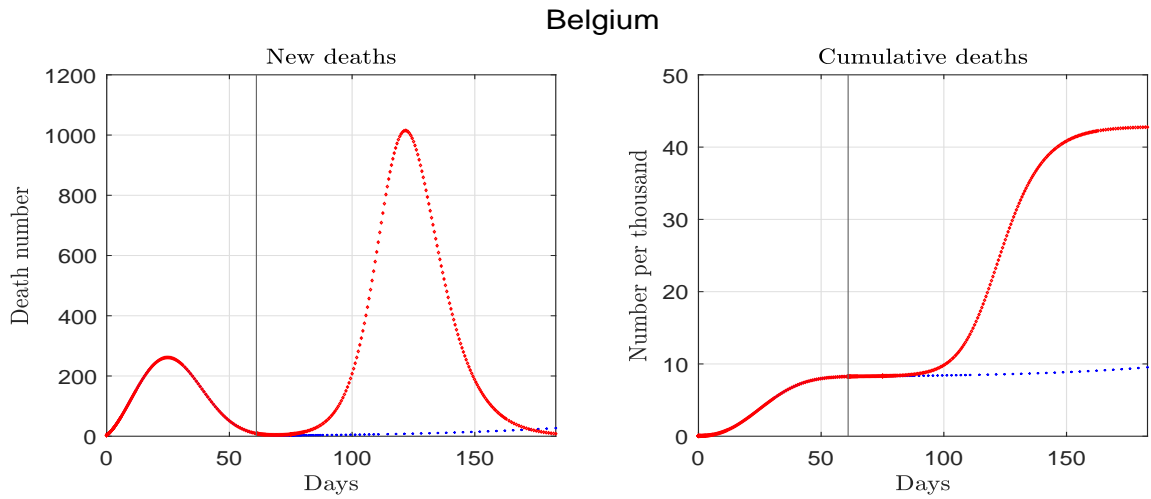
Belgium

Figure A.26: Estimated and forecast deaths for Belgium. The vertical line marks the end of the sample.
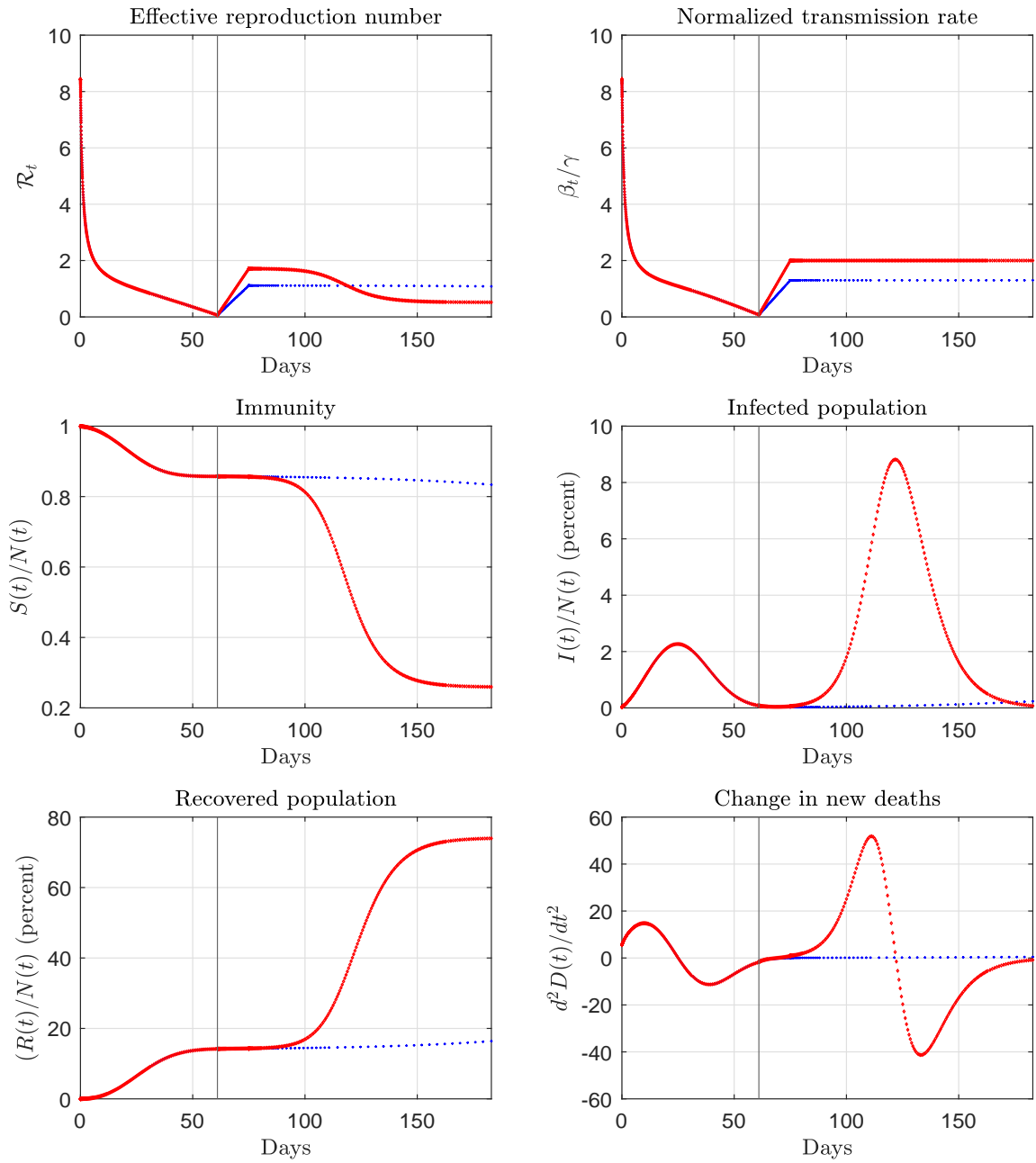
Belgium

Figure A.27: Estimated and forecast paths for Belgium. The vertical line marks the end of the sample.

Belgium (counterfactual)
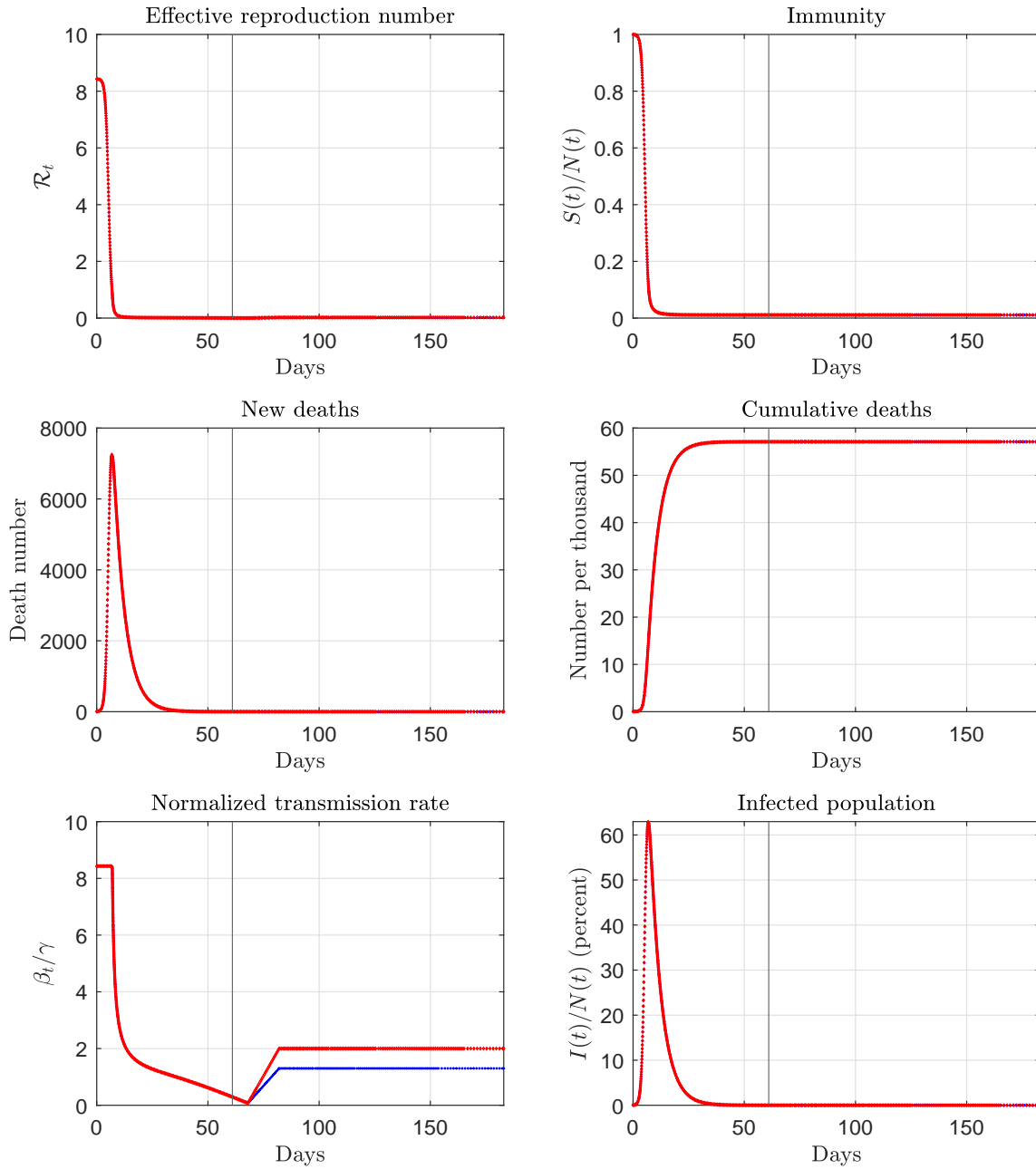
Figure A.28: Counterfactual paths for Belgium. The vertical line marks the end of the sample.
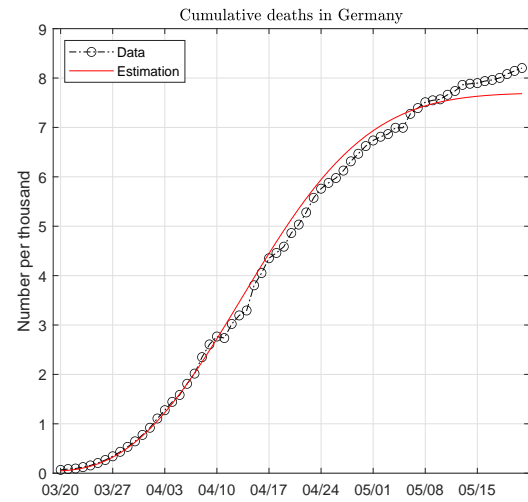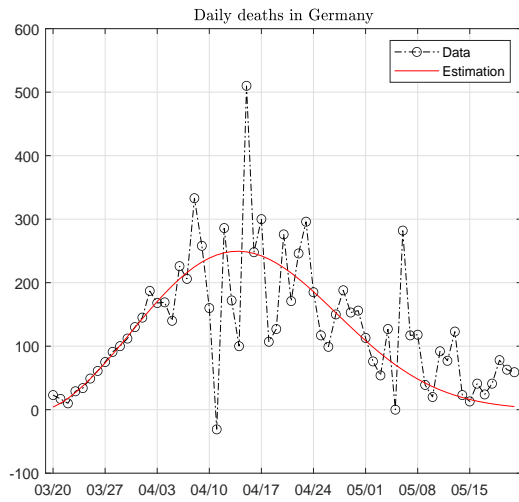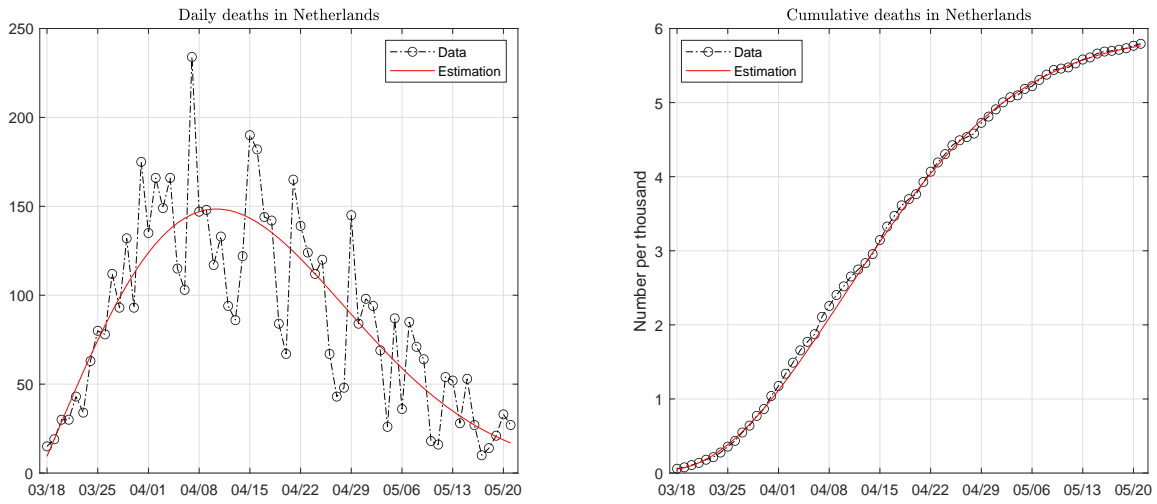
Figure A.29: Data and fitted paths of deaths in Germany. The death pattern is fitted with a mixture of two Weibull functions.
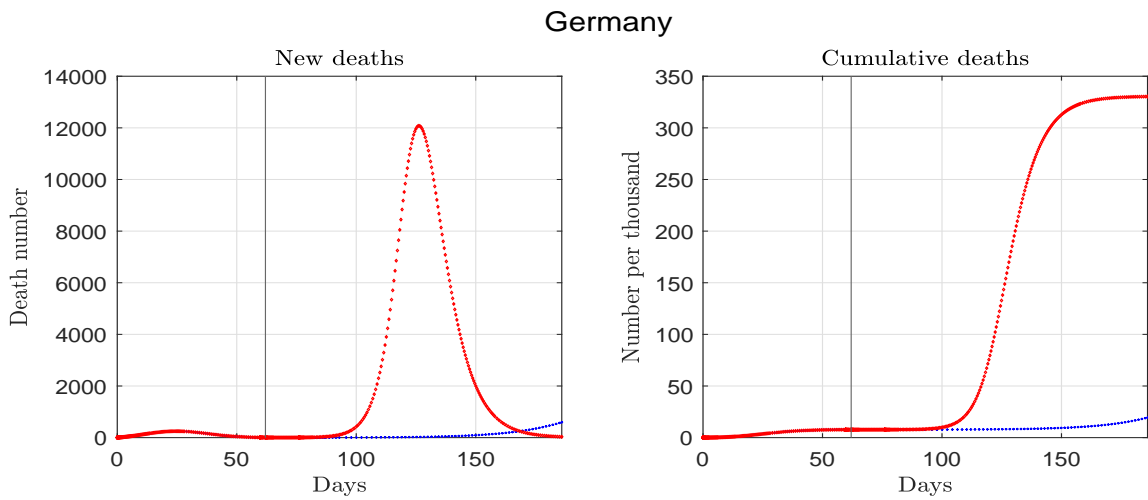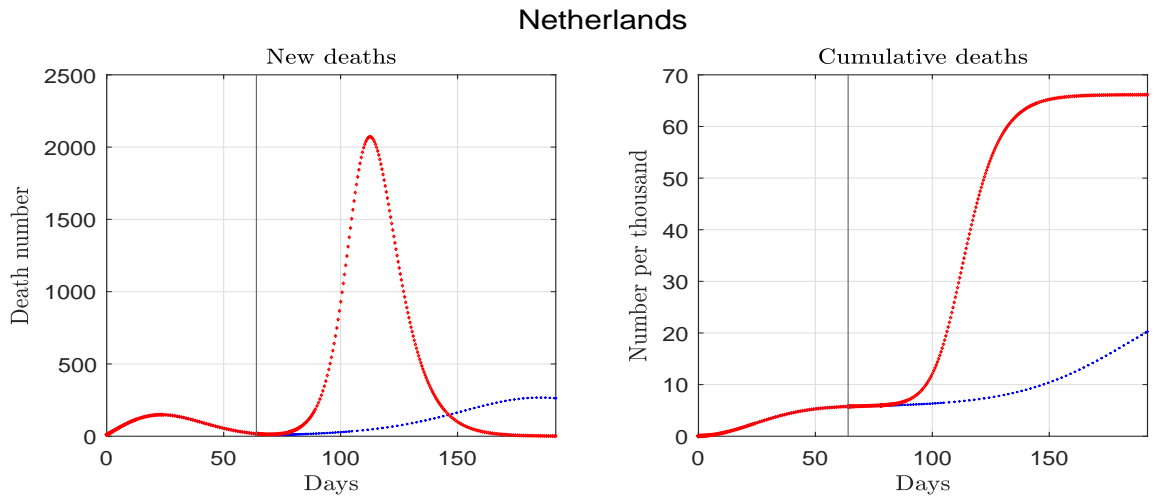

Figure A.30: Estimated and forecast deaths for Germany. The vertical line marks the end of the sample.
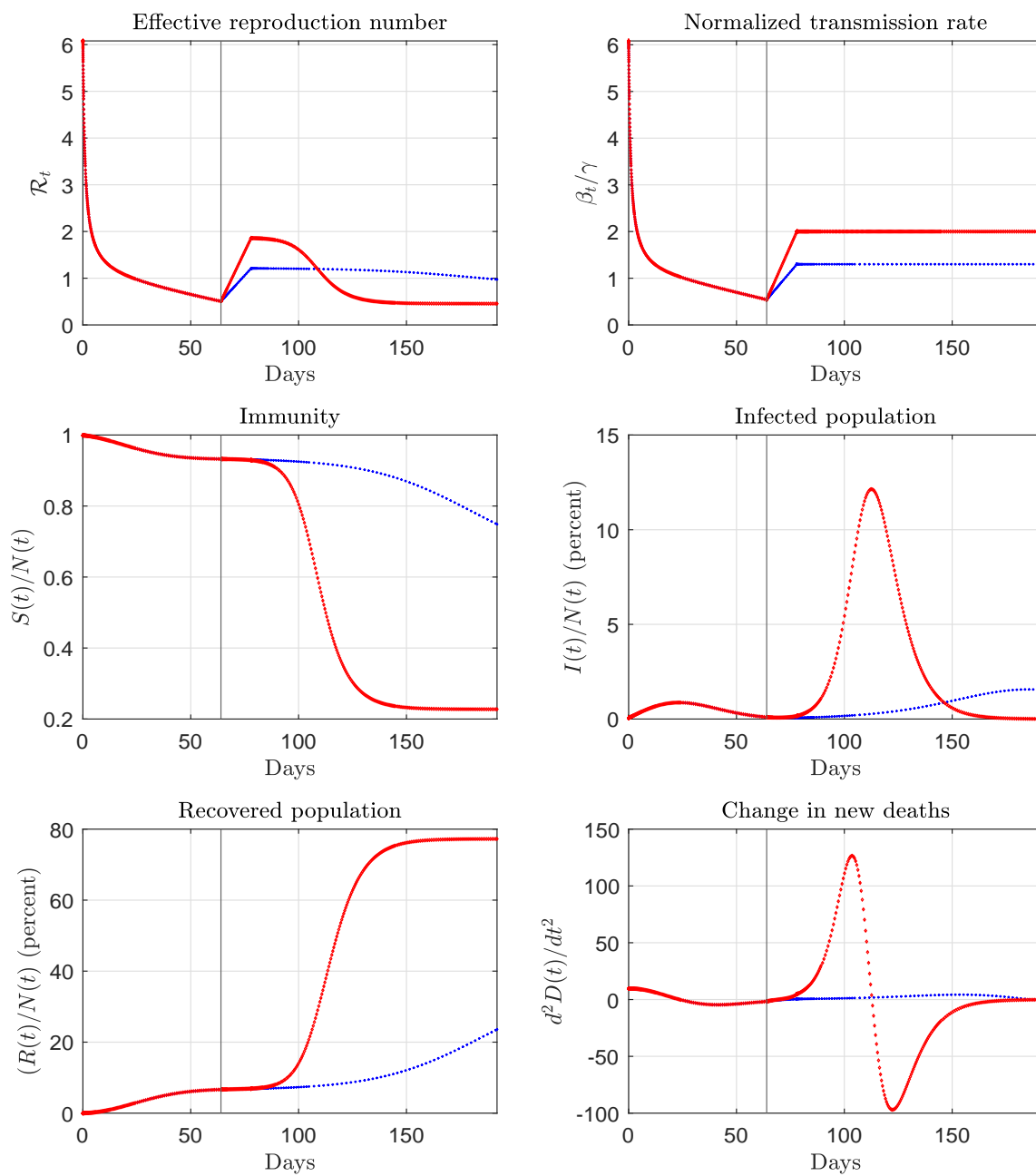
Germany

Figure A.31: Estimated and forecast paths for Germany. The vertical line marks the end of the sample.
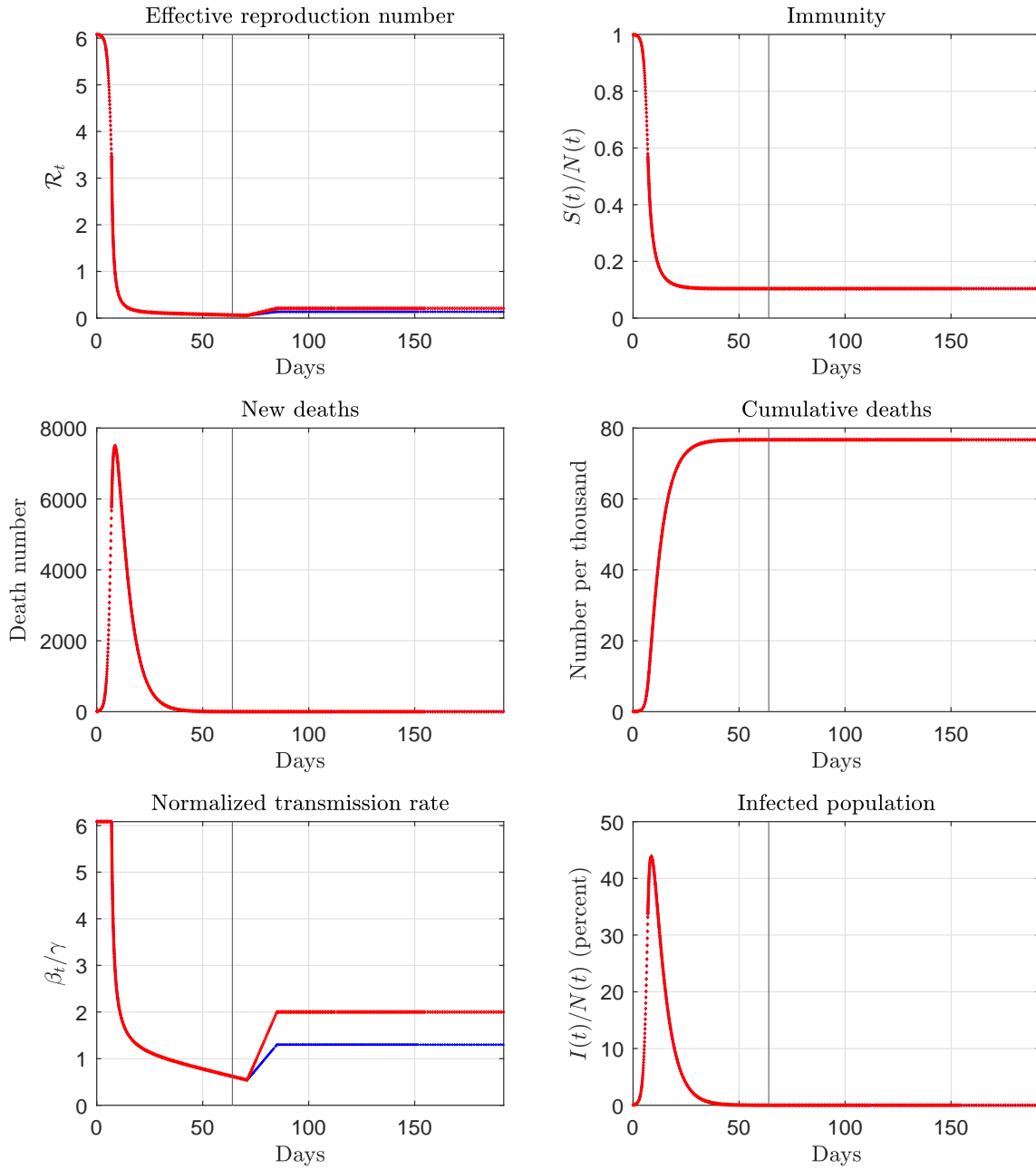
Germany (counterfactual)
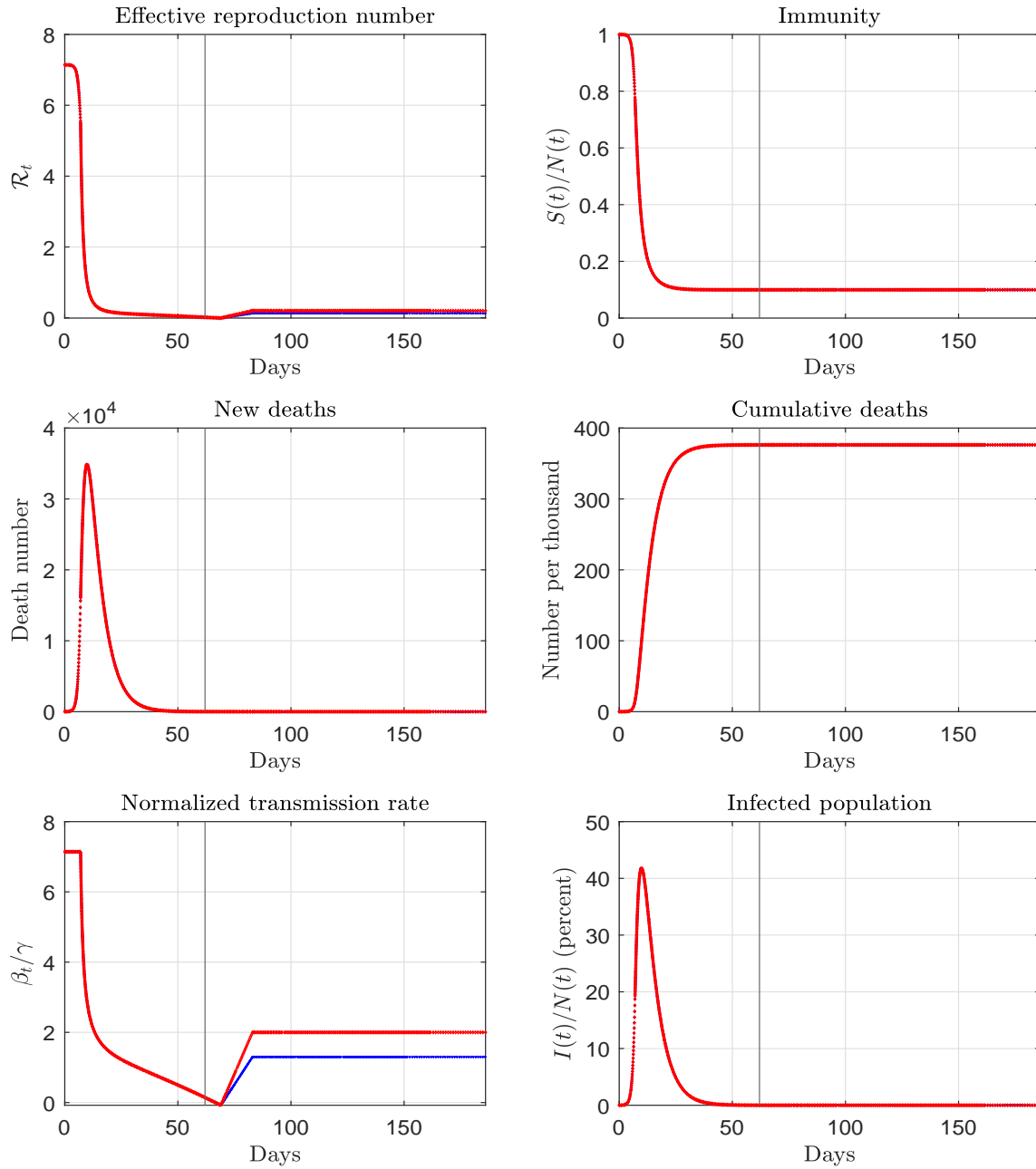
Figure A.32: Counterfactual paths for Germany. The vertical line marks the end of the sample.
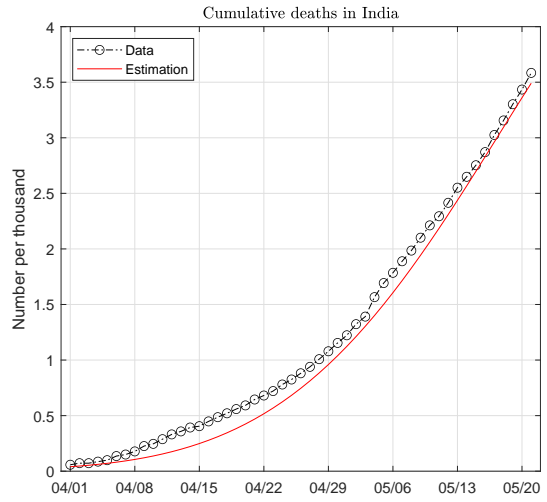
Figure A.33: Data and fitted paths of deaths in Iran. The death pattern is fitted with a mixture of two Weibull functions.

Figure A.34: Estimated and forecast deaths for Iran. The vertical line marks the end of the sample.

Iran

Figure A.35: Estimated and forecast paths for Iran. The vertical line marks the end of the sample.

126

Figure A.36: Counterfactual paths for Iran. The vertical line marks the end of the sample.
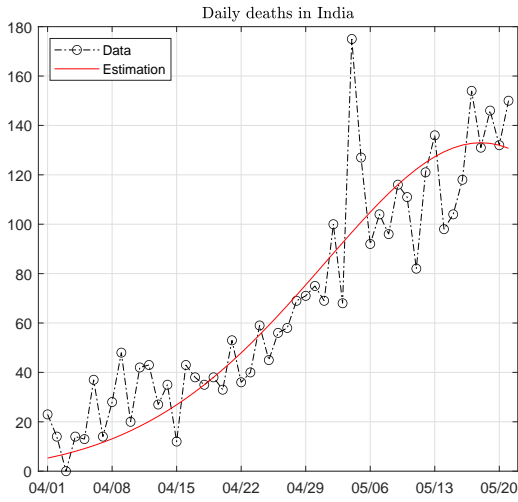
127

Figure A.37: Data and fitted paths of deaths in Mexico. The death pattern is fitted with a mixture of two Weibull functions.

Figure A.38: Estimated and forecast deaths for Mexico. The vertical line marks the end of the sample.

Mexico

Figure A.39: Estimated and forecast paths for Mexico. The vertical line marks the end of the sample.

129

Figure A.40: Counterfactual paths for Mexico. The vertical line marks the end of the sample.

Figure A.41: Data and fitted paths of deaths in Canada. The death pattern is fitted with a mixture of two Weibull functions.
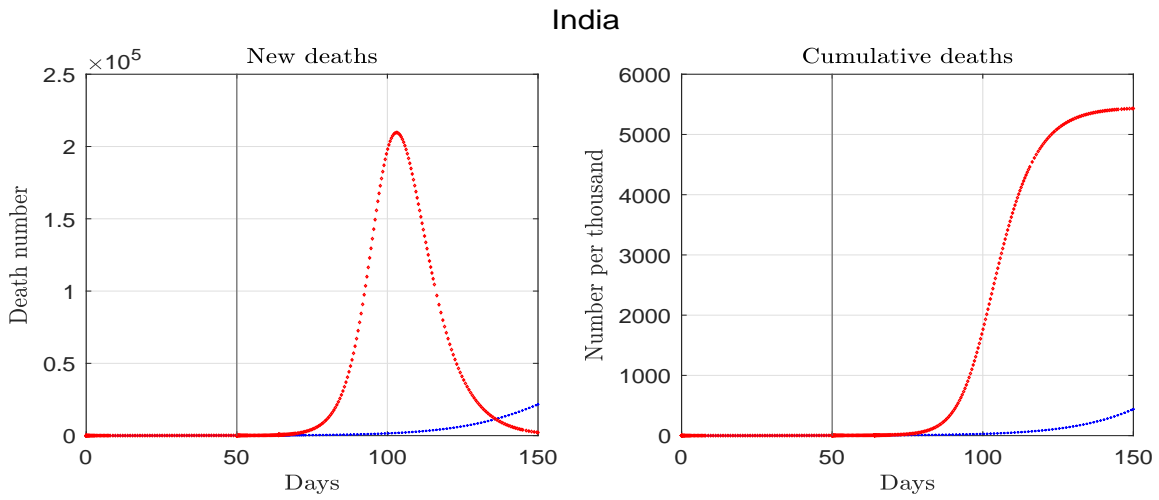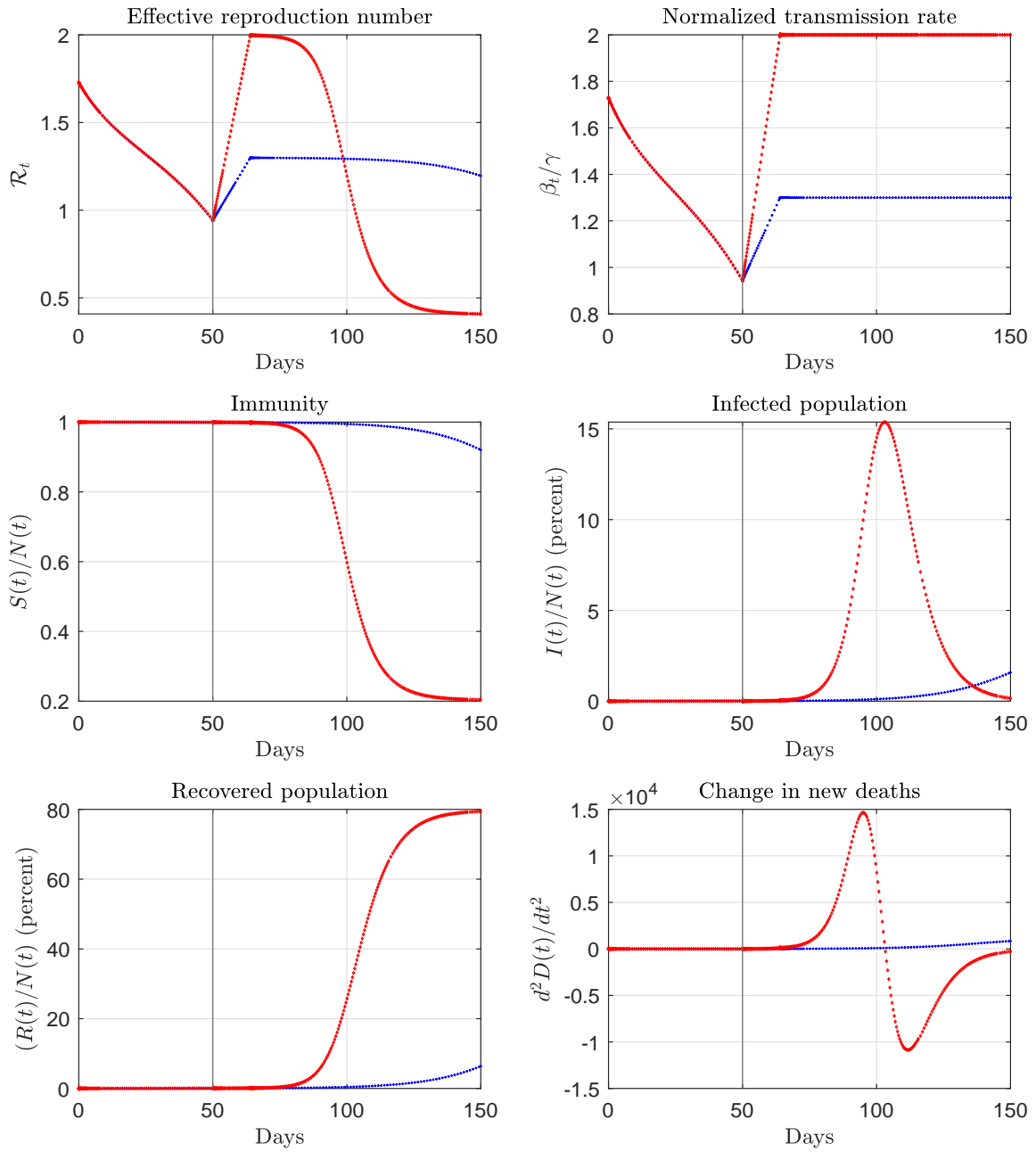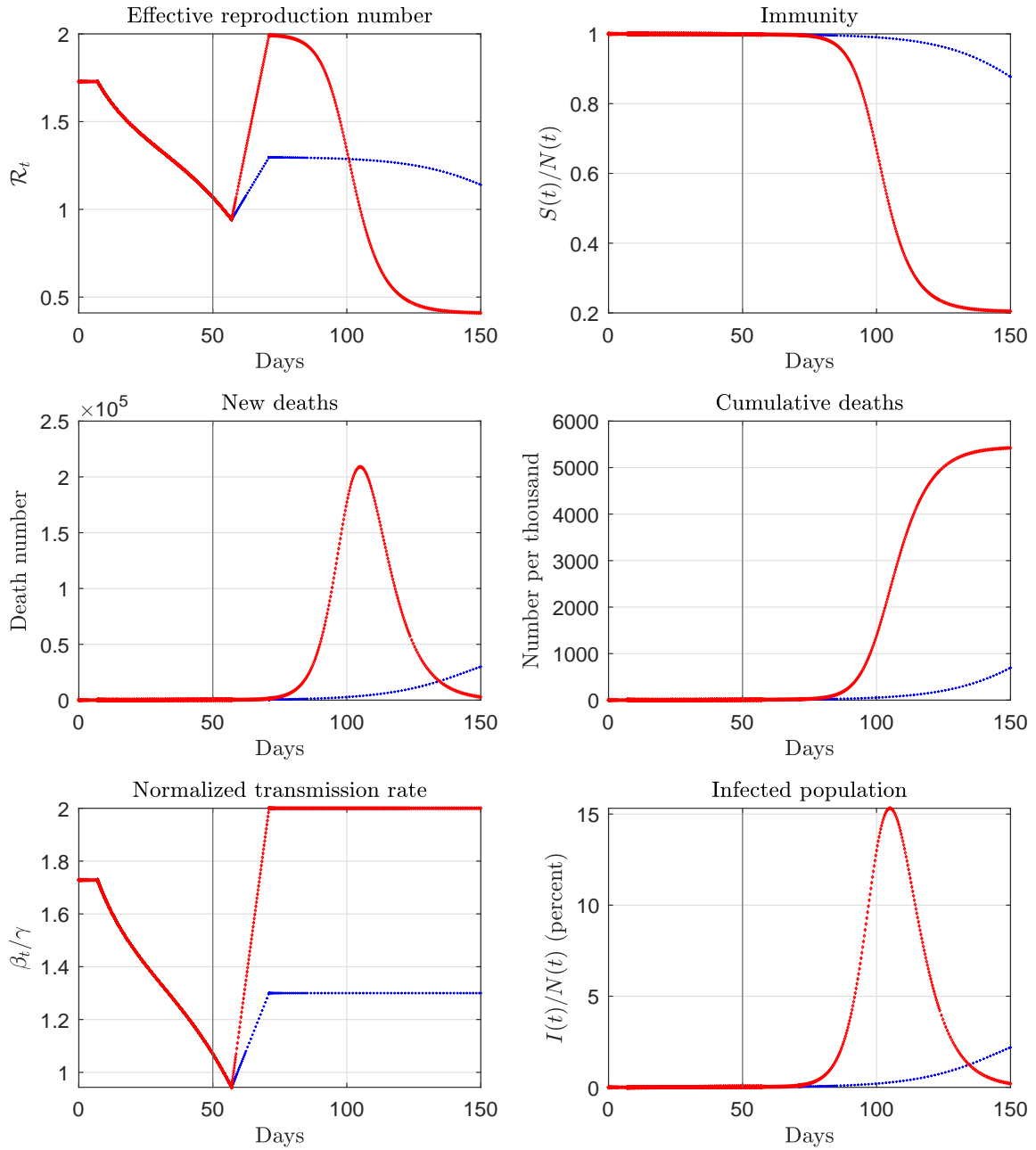

Figure A.42: Estimated and forecast deaths for Canada. The vertical line marks the end of the sample.

131

Canada

Figure A.43: Estimated and forecast paths for Canada. The vertical line marks the end of the sample.

Figure A.44: Counterfactual paths for Canada. The vertical line marks the end of the sample.
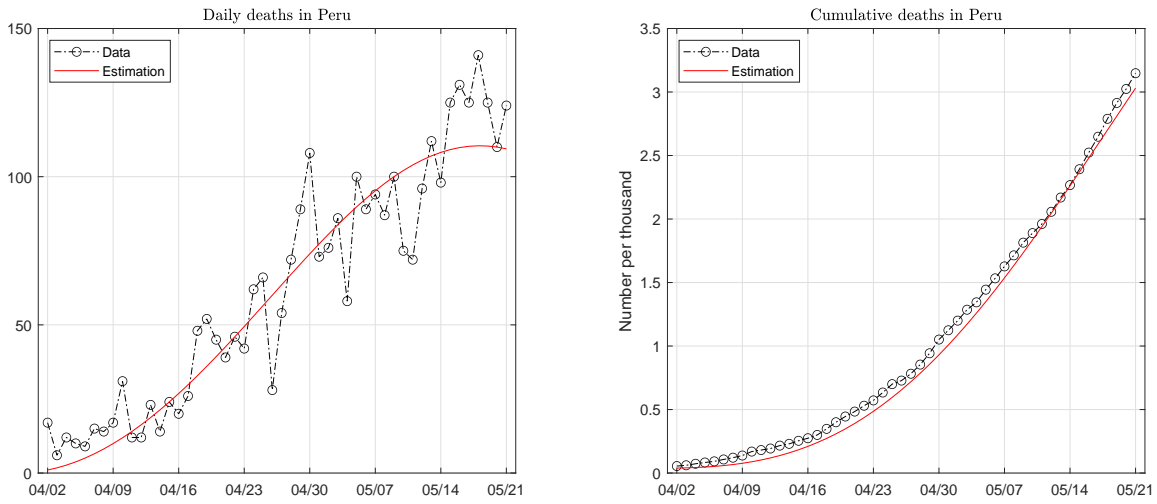
133

Figure A.45: Data and fitted paths of deaths in Netherlands. The death pattern is fitted with a mixture of two Weibull functions.
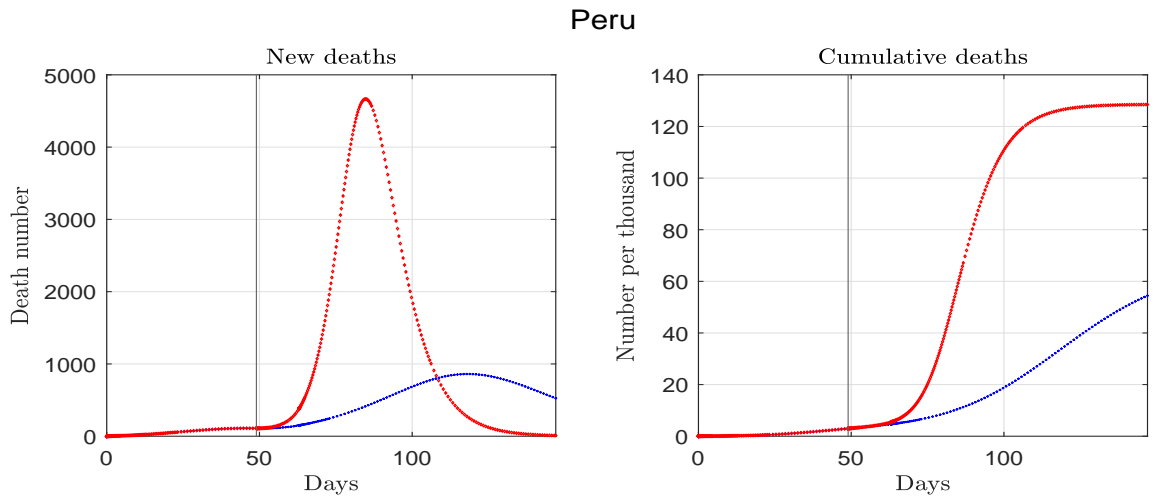

Figure A.46: Estimated and forecast deaths for Netherlands. The vertical line marks the end of the sample.
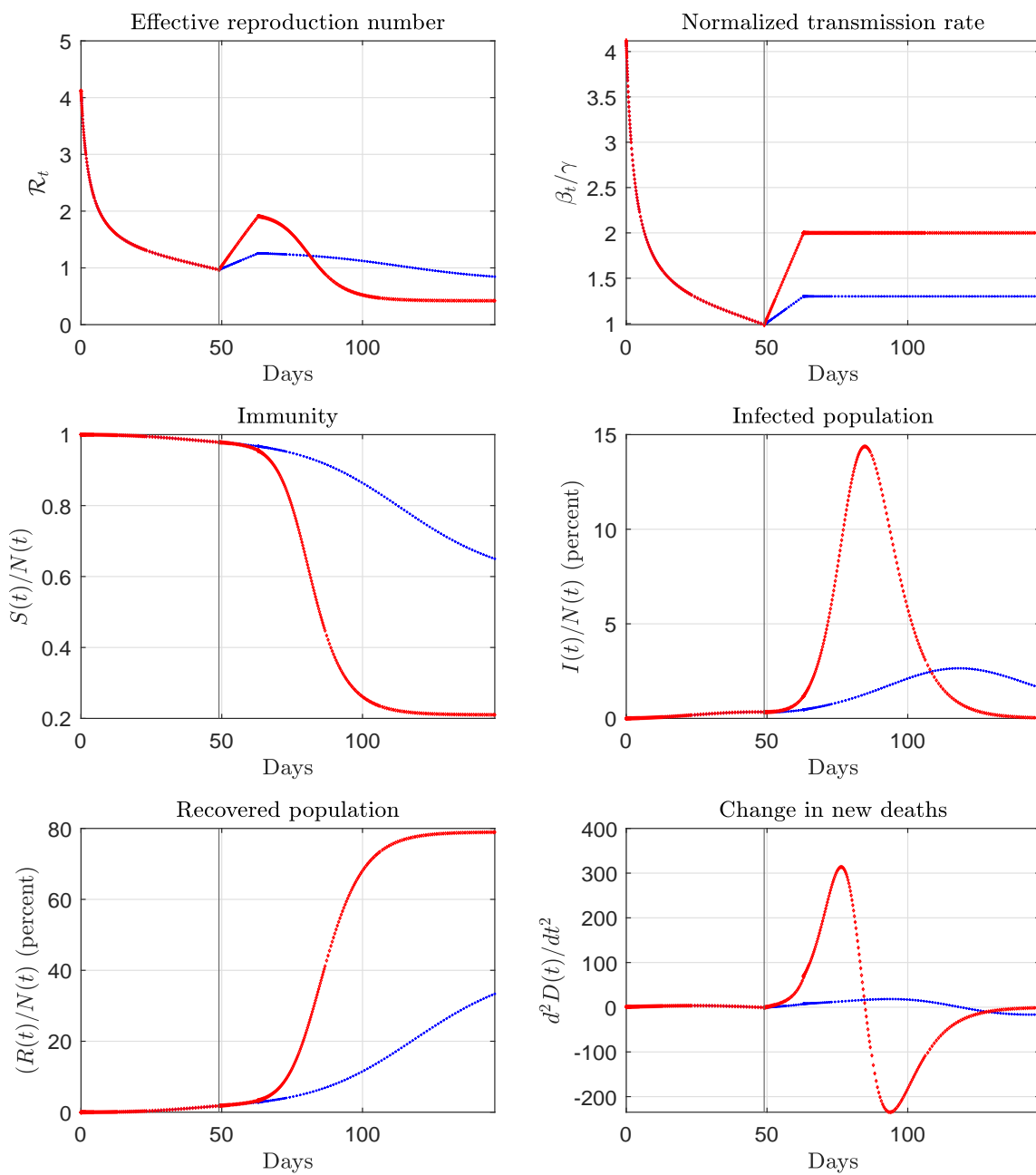
134

Figure A.47: Estimated and forecast paths for Netherlands. The vertical line marks the end of the sample.

135

Netherlands (counterfactual)
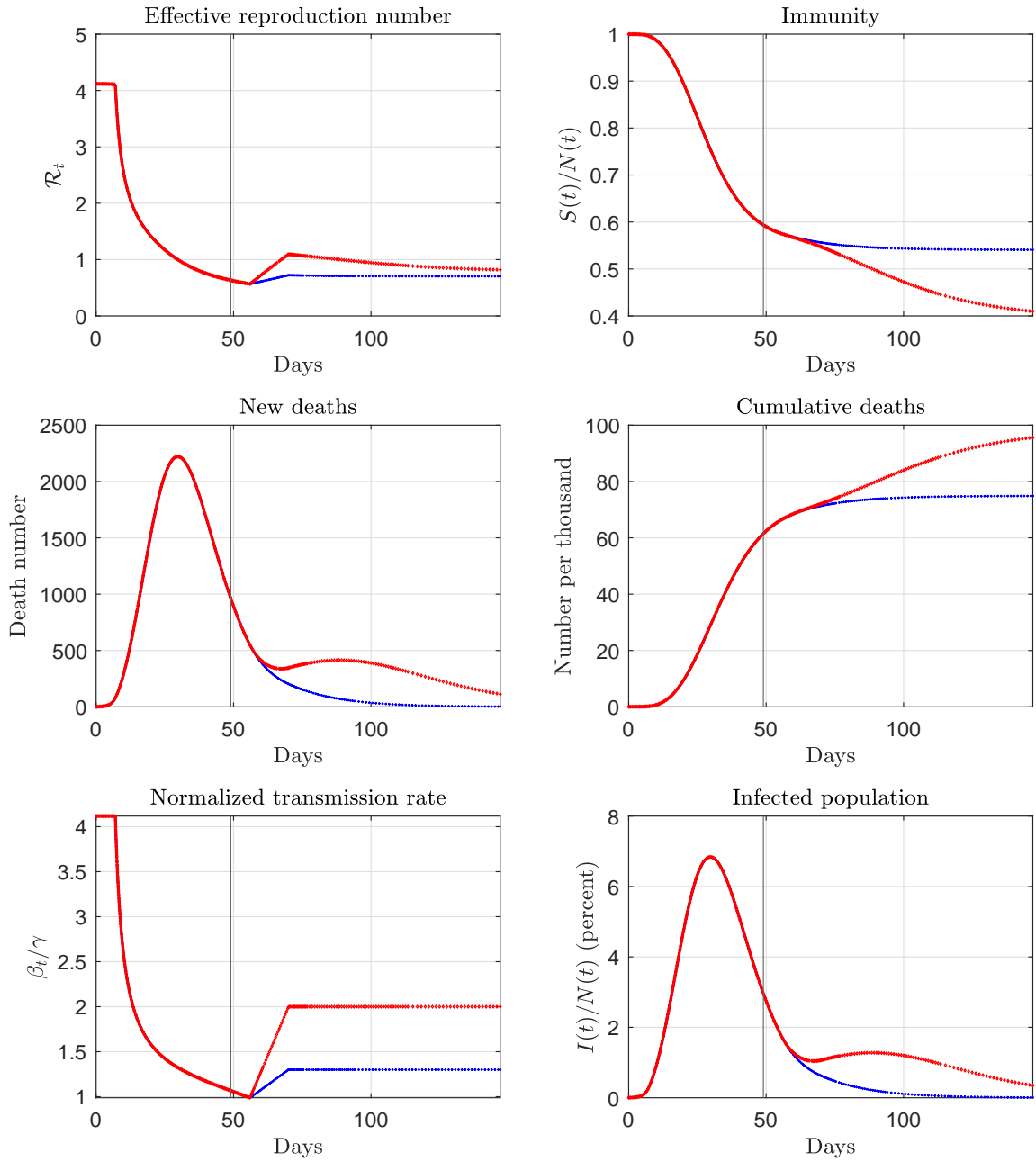

Figure A.48: Counterfactual paths for Netherlands. The vertical line marks the end of the sample.
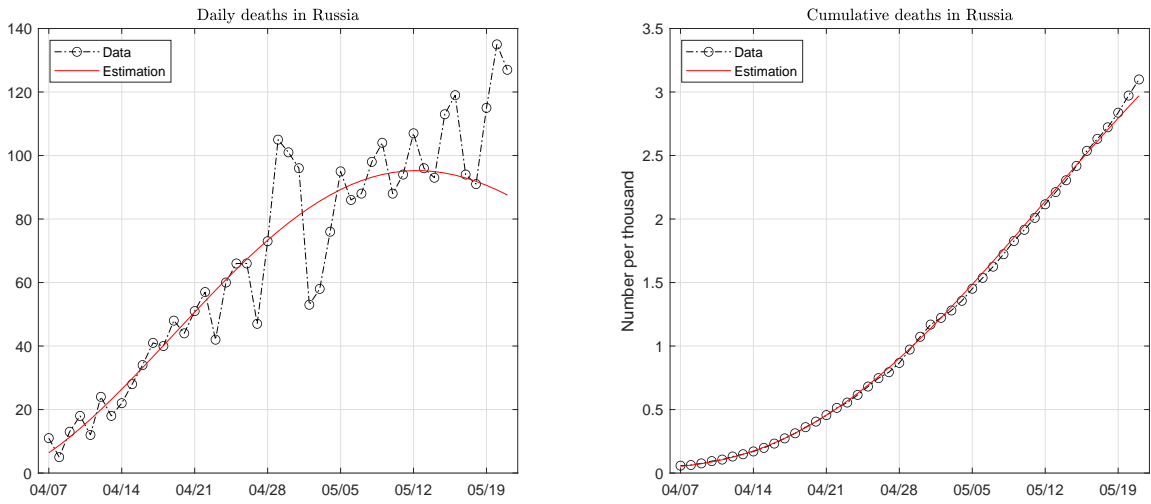
136

Figure A.49: Data and fitted paths of deaths in India. The death pattern is fitted with a mixture of two Weibull functions.

Figure A.50: Estimated and forecast deaths for India. The vertical line marks the end of the sample.

137

Figure A.51: Estimated and forecast paths for India. The vertical line marks the end of the sample.

India (counterfactual)

Figure A.52: Counterfactual paths for India. The vertical line marks the end of the sample.

Figure A.53: Data and fitted paths of deaths in Peru. The death pattern is fitted with a mixture of two Weibull functions.
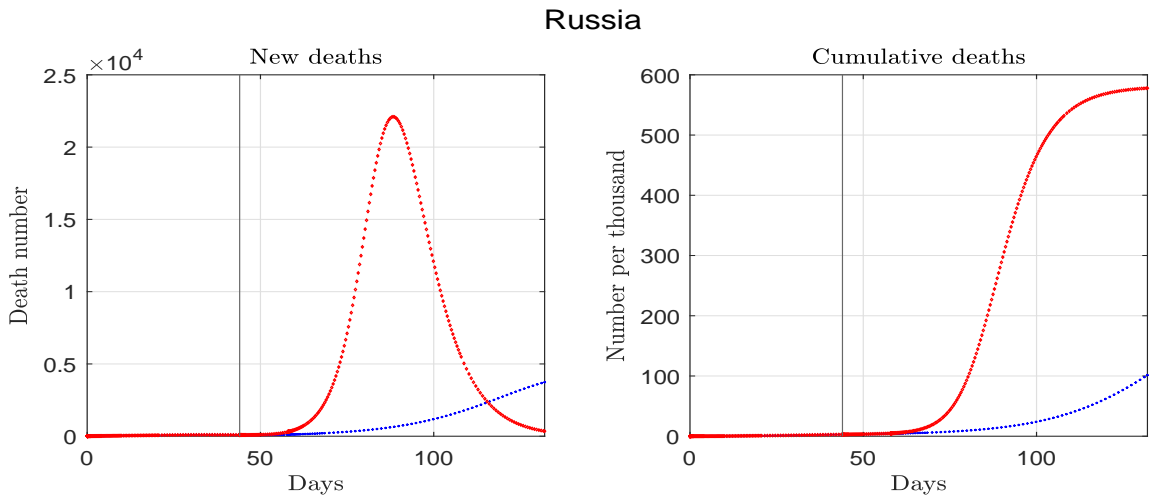

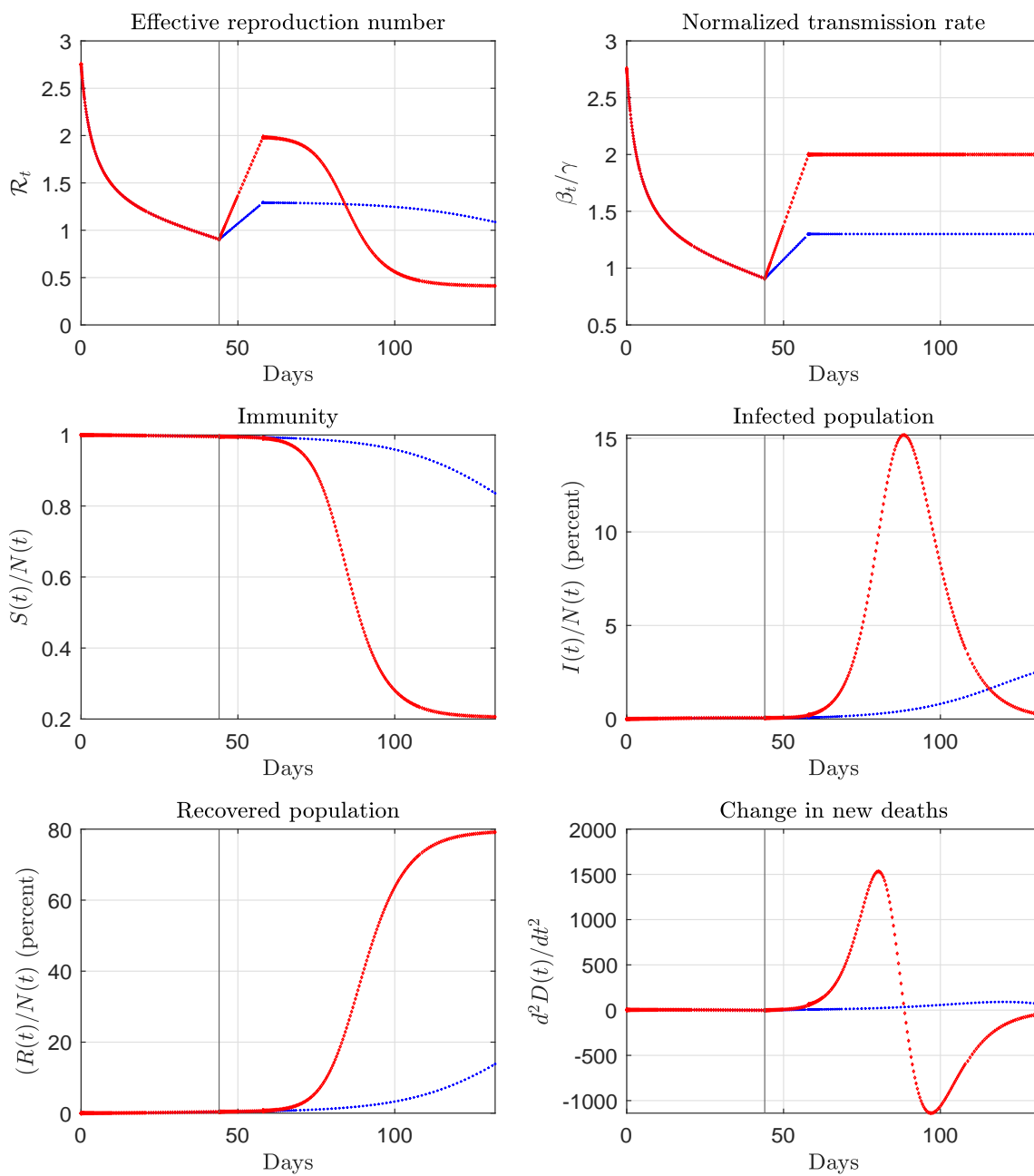**Figure A.54:** Estimated and forecast deaths for Peru. The vertical line marks the end of the sample.

140

Peru

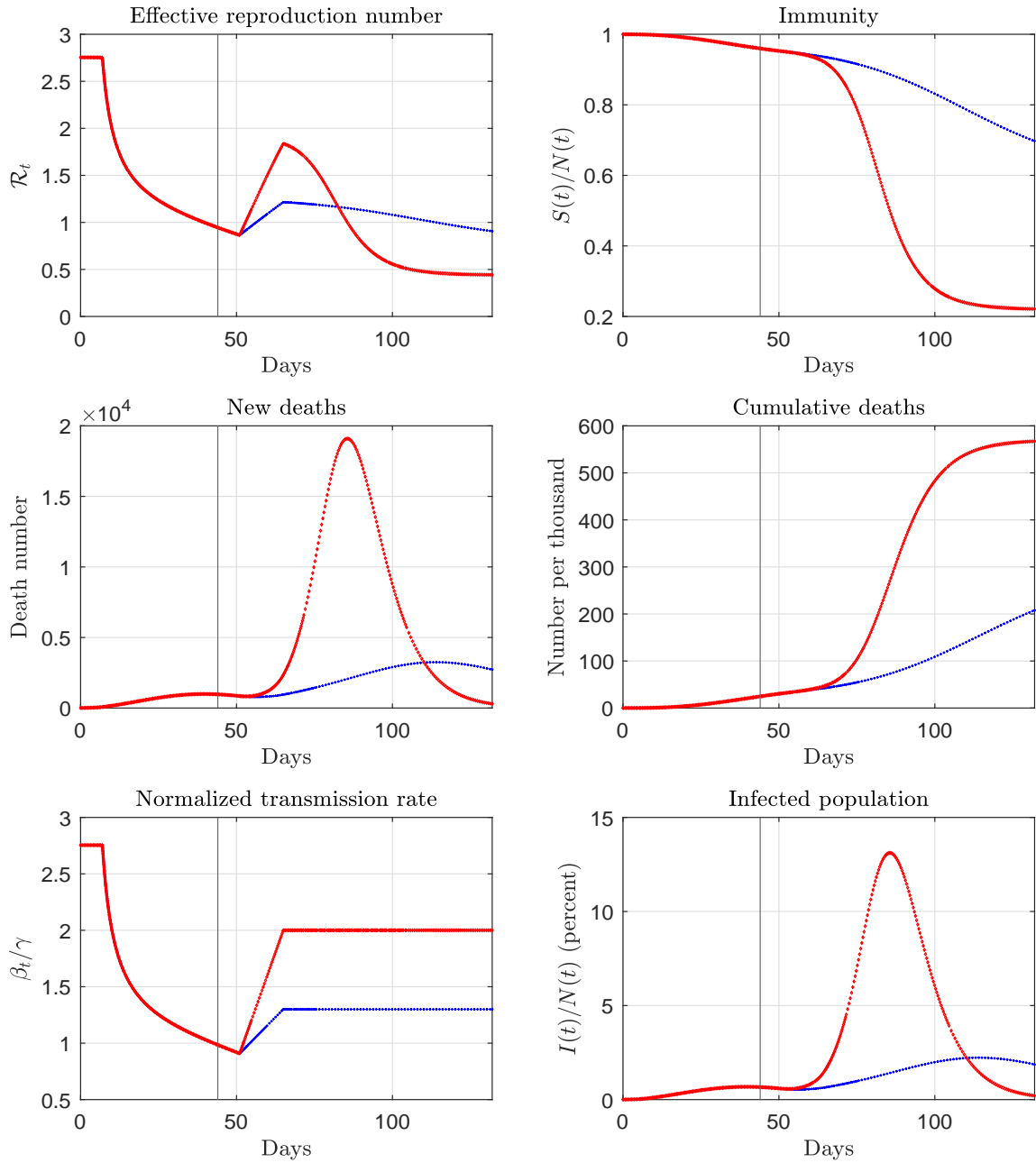**Figure A.55:** Estimated and forecast paths for Peru. The vertical line marks the end of the sample.

Figure A.56: Counterfactual paths for Peru. The vertical line marks the end of the sample.

Figure A.57: Data and fitted paths of deaths in Russia. The death pattern is fitted with a mixture of two Weibull functions.

Figure A.58: Estimated and forecast deaths for Russia. The vertical line marks the end of the sample.

143

Russia

Figure A.59: Estimated and forecast paths for Russia. The vertical line marks the end of the sample.

Russia (counterfactual)

Figure A.60: Counterfactual paths for Russia. The vertical line marks the end of the sample.
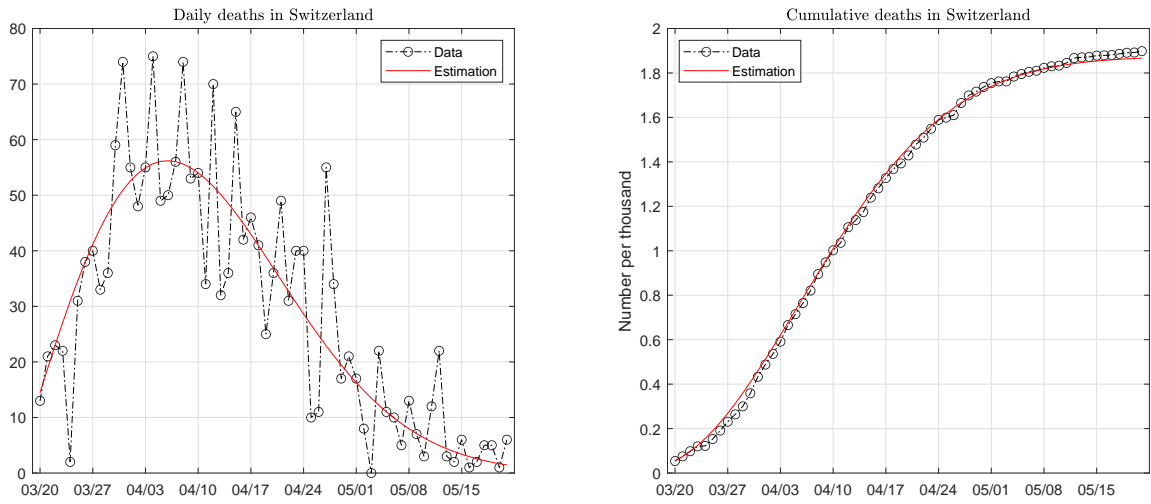
145

Figure A.61: Data and fitted paths of deaths in Switzerland. The death pattern is fitted with a mixture of two Weibull functions.
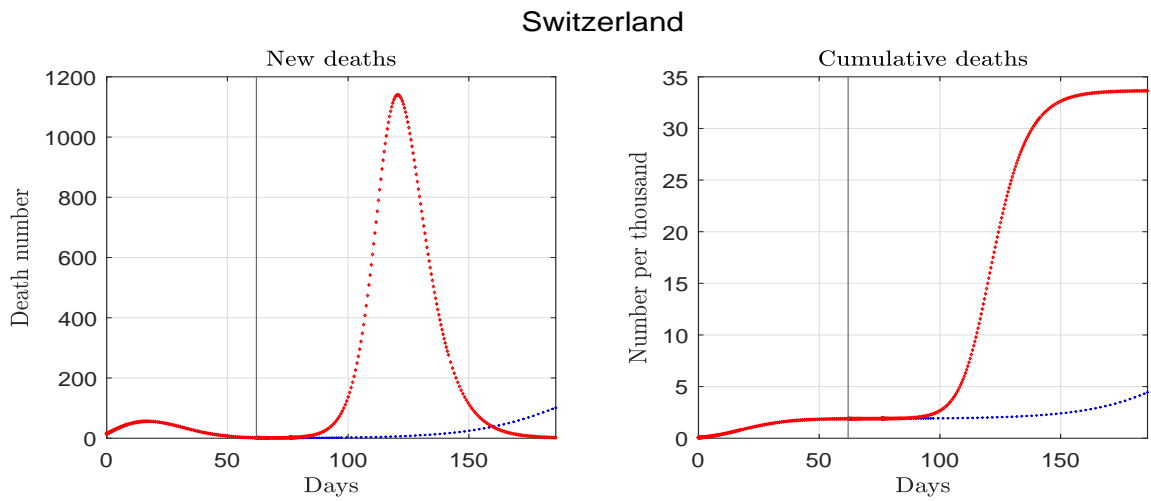

Figure A.62: Estimated and forecast deaths for Switzerland. The vertical line marks the end of the sample.
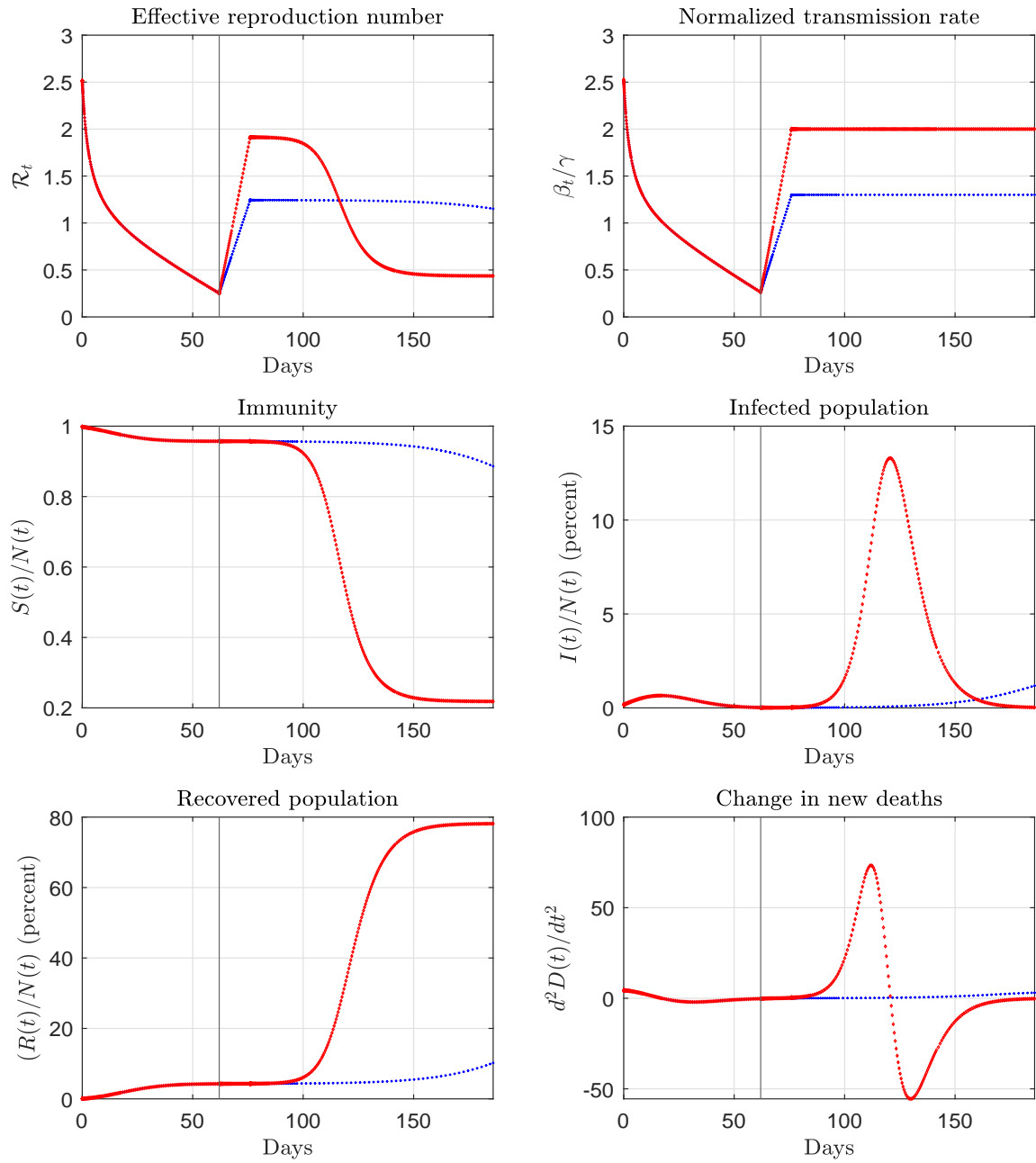
146

Switzerland

Figure A.63: Estimated and forecast paths for Switzerland. The vertical line marks the end of the sample.
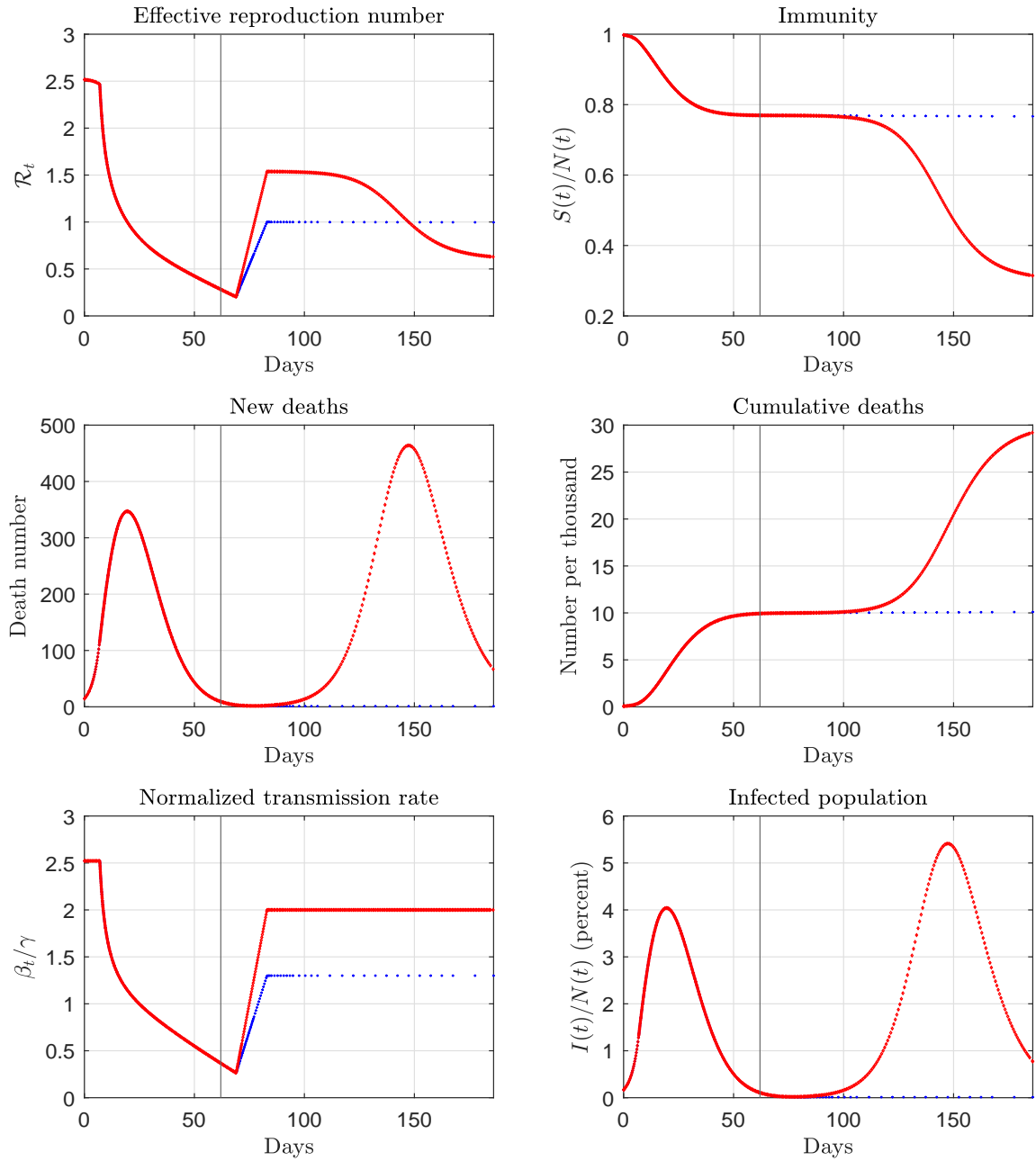
Switzerland (counterfactual)

Figure A.64: Counterfactual paths for Switzerland. The vertical line marks the end of the sample.